mTORC1 Selective Inhibitors for the Treatment of KRAS G12C Mutant Cancers

by

Adele Simone Whaley

A Dissertation

Presented to the Faculty of the Louis V. Gerstner, Jr. Graduate

School of Biomedical Sciences,

Memorial Sloan Kettering Cancer Center

in Partial Fulfillment of the Requirements for the Degree of Doctor of

Philosophy

New York, NY

March 2023

_____ _____

Neal Rosen, MD, PhD Date

Dissertation Mentor

To my family and like-family: Rodney, Bernadette, Jordan, Daniel, Krystal, Angie, Chelsea, CJ, Dillian, Michael, Moriya, Dillon, Jocelyn, Ken, Ava, and Kenny

“Time pushes everything forward. No stunning success and no sorrowful failure lasts forever” – Rapelang Rabana

Abstract

KRAS is the most frequently altered oncogene in lung cancer, with G12C being the most common mutation subtype. Recently developed KRAS G12C inhibitors have shown clinical efficacy in several tumor types, with non-small cell lung cancer patients achieving the highest objective response rate. However, this metric only approaches 40%. Hence, rational combination strategies are required to improve potency. ERK and PI3K are key effectors of RAS. Although dual inhibition of these pathways has demonstrated synergistic effects in preclinical models, toxicity has hindered clinical efficacy. Here, we demonstrate that suppression of mTORC1 substrates correlates with sensitivity to KRAS G12C inhibition. The combination of a novel mTORC1-selective inhibitor with KRAS G12C inhibitors exhibited enhanced effects *in vitro*, and also yielded dramatic tumor regression in KRAS G12C mutant lung cancer PDX models. Notably, the combination did not induce hyperglycemia, a hallmark of mTORC2/AKT inhibition. mTORC1 selective inhibitors promoted KRAS G12C inhibitor-induced cell growth inhibition and death through suppression of Cyclin D1 and other oncogenic targets.

Interestingly, we also discovered that α-Tocopherol, a major component of the natural antioxidant vitamin E, commonly taken as a dietary supplement, directly impedes the activity of KRAS GTP and mTOR bi-steric inhibitors independent of its antioxidant function. While the interference is less durable for KRAS GTP inhibitors, it’s potent, enduring, and dynamic for mTOR bi-steric inhibitors. Furthermore, the remaining seven analogues of vitamin E provoke interference towards RM6, a highly selective mTORC1 inhibitor currently in clinical trials. Given that the drug interaction profile of vitamin E is

predominantly based on its antioxidant and immunomodulatory properties, to our knowledge, this is the first demonstration of the vitamin E family directly interfering with a class of targeted pharmacological inhibitors based solely on its structural features. Collectively, these results demonstrate that the combination of KRAS G12C with mTORC1 inhibition can be a novel therapeutic strategy for KRAS G12C mutant lung cancer, and that vitamin E may have potential to temper both the efficacy and the toxicity of this combination in the clinical setting.

Biographical Sketch

Adele Simone Whaley was born on December 12th, 1989, in Brooklyn, NY. Interested in science from a young age, Adele chose to study Biochemistry at Stony Brook University. While completing her studies, she worked in the medicinal chemistry section of Dr. Iwao Ojima's laboratory. At the time of her enrollment, this sector of the Ojima Lab synthesized potent cytotoxic analogs of natural compounds, constructed anti-cancer drug conjugates for targeted delivery, and determined the efficacy of these agents through collaborative biological analysis. Adele's research focused on synthesizing one of these novel anticancer agents – SB-T-1216 – with the project culminating in a written thesis entitled "Towards the Synthesis and Biological Evaluation of 2nd-Generation Taxoid SB-T-1216," affording her an honorary degree. Adele's experience with the Ojima group exposed her to the field of biomedical research, and she was particularly captivated by clinically translatable projects – from bench to bedside.

Adele chose to briefly exit the sciences and spend time working as a nanny while deciding between attending a PhD program or medical school. Resolving to pursue the former, she first joined the lab of Dr. Ronald Crystal as a research technician at Weill Cornell Medicine to gain additional research experience. Her main project involved assessing the efficacy of an adeno-associated virus (AAV) gene transfer vector encoding human C1 esterase inhibitor in treating genetically engineered knockout mice. These mice clinically and phenotypically recapitulated type I hereditary angioedema, a debilitating, and potentially fatal, disorder. This work was published in the European Academy of Allergy and Clinical Immunology (2019), where Adele is listed as third author.

Adele ultimately decided to pursue a PhD at the Gerstner Sloan Kettering Graduate School of Biomedical Sciences at Memorial Sloan Kettering Cancer Center in New York City. She joined the lab of Neal Rosen, enthralled by the wealth of interesting research, and the inherent translational prospects of a pharmacology lab. Adele worked on several projects in the Rosen Lab, with a common thread being the evaluation of RAS/ERK and PI3K/AKT/mTOR pathway inhibitors in non-small cell lung cancer (NSCLC) and colorectal cancer (CRC) models. With newly developed KRAS G12C inhibitors and mTORC1 selective inhibitors, Adele was afforded the opportunity to evaluate if mTORC1 selective inhibitors would enhance the efficacy of KRAS G12C inhibitors without the toxicity limitations that have plagued conventional PI3K, AKT, and mTOR inhibitors from reaching clinical efficacy. With the combination demonstrating cell death induction and tumor regression in KRAS G12C mutant NSCLC and CRC models, she went on to explore what mechanism(s) of cell death mediated these effects. In doing so, Adele serendipitously discovered that α-Tocopherol considerably impedes the activity of mTORC1 selective inhibitors, a finding that can potentially be leveraged to manage toxicity in the clinical setting.

Acknowledgments

In order of appearance

To my parents: I literally wouldn't be here without you. Thanks for supporting my interests in science, and for listening to me discuss my varied research topics. Even when the details of my work were outside your scope of understanding, you both listened enthusiastically, and encouraged me to continue excelling in my research. Thanks for everything Mommy and Daddy.

To my siblings: Jordan, you've been particularly helpful with your guidance and support, beginning with our joint college years. Daniel, you've been generous with sharing resources that have helped me over the years. Krystal, you've been there to support me during the best of times and the worst of times. Angie, you've also welcomed my tales of grievances and happiness. Collectively you guys have encouraged and supported me in your own ways throughout the years, and you're all the perfect reminder that some of the best things in life are free.

To my aunts and uncles: Thanks for often inquiring about my grad school progress and listening intently when I discussed my ongoing research. It's amazing to have so many engaged aunts and uncles in my life.

To my many cousins: I love that we're always there for each other even if we don't see each other often. You guys have all been a fantastic source of fun and happiness.

To Dillian and the late Vernon: You've been like second parents to me since my days in elementary school, supporting me immensely over the years.

To Suzie and Clarisse: Thanks for entertaining my walls of text during my high moments and low moments, and for being all around amazing friends.

To the TTM folks: We may not spend as much time together now as we did when younger, but when we do get together it's always a blast. You guys have been a great foundation of support in many different ways.

To Jocelyn and Ken: Thanks for being so supportive and accommodating over the years in various ways. I'm grateful to have met you both.

To Michael, Moriya, Dillon, Ava, Kenny, Chelsea, and CJ: You guys are collectively my 'kids,' regardless of our actual relationship and your current ages. You've all brought a considerable amount of happiness to my life, and I'm grateful I had the opportunity to care for all of you and watch you grow into amazing people. I hope the journey of life treats you well, and that you're each able to find your passion and achieve your dreams despite obstacles you may face along the way. By all means seek advice from trusted family members, friends, colleagues, and professionals, but absolutely never let anyone stop you

from pursuing your passions and being true to yourself. It may take time for you to get there, but once you gain confidence in yourself, your interests, your choices, and how you want to live your life, and understand that you don't have to hold yourself to the standards and judgment of others, you become truly, and I mean truly, free. You've literally only got this one life as you are now. So make the most of it, and surround yourself with people who will bring you up rather than put you down. I know it's getting to be increasingly difficult with the extensive prevalence of social media to not compare yourself to the life and standards of others. But really, just live your life for YOU. Have unshakeable faith and pride in yourself as you are and in your choices. In this I have found unparalleled peace and satisfaction. I genuinely hope you all achieve this too.

To the late Amanda: As one of my first 'kids,' you gave me so much joy. We shared our birthdays and our passions for science – me in the biology field and you in the world of physics. You grew into such an amazingly smart, talented, and kind young adult. I know you would have gone on to do great things.

To my Kung Fu classmates: Thanks for serving as my outlet for a different kind of learning and training outside of scientific research.

To Odelya: If it weren't for you encouraging me to pursue graduate school when I started to become complacent, I probably wouldn't be here now.

To Al and Anna: Thank you for being both amazing friends and my source for outdoor engagement, helping me stay balanced between schoolwork, research, and spending time in nature on crazy fun adventures.

To the GSK Graduate School: Thank you for accepting me into the program, and for all the genuine care and support over the years.

To my GSK classmates: You've all been so amazing. Our times spent together have provided me with many wonderful memories that I will cherish.

To Florisela: Some things just happen for a reason. Out of all the graduate programs we could have attended, and the differing times we could have pursued graduate school, we ended up joining the same program at the same time. I'm immensely grateful to have had you not merely as a friend, but also as a classmate going through the same grind as me. With a comparable understanding of the challenges of graduate school at its varied levels, you have been my absolute greatest support. I'm thrilled we joined together, and even more elated that we finished together too.

To the late Jordan Aronowitz: You were such a phenomenally talented, intelligent, kind, funny, and wholesome individual. Losing you merely two years into our graduate program was incredibly devastating. I regret that we didn't spend more time together. I regret the missed photo and video opportunities to capture and physically immortalize the great times we had. I regret the missed opportunities to have connected and spent more time with you

between our similar research interests and hobbies like martial arts and games. But I'll absolutely never regret having met you, and I will forever cherish the wonderful memories we created together. No matter how difficult grad school became, I used your memory as a source of motivation. I wanted to finish on your behalf. I wanted to finish for both of us. I've finished now. It's bittersweet, but we made it.

To Susan and Jeff Aronowitz: In the midst of such a trying and very raw time, I was both amazed and touched by the concern you showed towards me and my classmates. You said you would look forward to us finishing and graduating. Many of us have now done just that. I'm so very grateful for the genuine consideration you've shown throughout the years, and I'm really glad to have met Jordan and you both, despite the devastating circumstances that brought us together.

To Neal: Thank you for accepting me into your lab, and for the immense scientific freedom you afforded me. Surmounting the array of challenges presented by this pervasive independence has been both incredibly instructive and humbling.

To my committee: David Solit and Sarat Chandarlapaty, thank you for being supportive through the years. Also, thank you Sarat for providing me with constructive comments to improve my presentation and reporting skills. I've greatly appreciated this.

To my lab mates: Thank you for making the lab a welcoming, fun, and collaborative place to work. Within my third week of rotating this lab felt like home, and I knew I wanted to

join it in large part because of the then current members who made it such a happy and inviting place. Those who joined with and after me have added to this home-like feeling, and I've had such an amazing time learning from and hanging out with you all. You guys are the absolute best lab mates ever!

To Sandra: As my first hands on mentor in the lab, thank you for taking me under your wing and teaching me not only experimental techniques, but also how to improve my presenting and storytelling skills. You set me up for success, and for that I am truly grateful.

To Hide: Thank you for sharing your project with me. I had a wonderful time working with you, and you've taught me much. I couldn't have made my discoveries without you laying the phenomenal groundwork, so どうもありがとうございます!

To Jake, Radha, and Sunyana: Thank you all for serving as my quasi-mentors throughout my time in the lab. I truly couldn't have achieved this success without the wonderful input, support, and commiseration you each have given me throughout the years. I'm so very happy to have met and learned from you all. I'm truly a better scientist and person because of each of you.

To Margo: Your help over the years has been absolutely invaluable, and I truly mean that!

To Mike Overholtzer: Thank you so much for all the advice and support. Your pragmatic guidance has been greatly appreciated, and it was fantastic collaborating with you.

Table of Contents

List of Tables

List of Figures

List of Abbreviations

14-3-3: Tyrosine 3-monooxygenase/tryptophan 5-monooxygenase activation protein

4EBP: EIF4E Binding Protein

ABCA1: ATP-Binding Cassette Transporter 1

ABCG1: ATB-Binding Cassette Transporter G1

ACSL4: Acyl-CoA Synthetase Long-Chain Family Member 4

ADP: Adenosine Diphosphate

AMP: Adenosine Monophosphate

AMPK: AMP-Activated Protein Kinase

APAF-1: Apoptotic Protease Activating Factor

ApoB: Apolipoprotein B

ATP: Adenosine Triphosphate

BAD: BCL2 Antagonist of Cell Death

BAK: BCL2 Antagonist Killer 1

BAX: BCL2 Associated X Protein

Bcl-2: B-Cell Lymphoma Protein 2

Bcl-w: BCL2 like 2 protein

Bcl-xL: BCL2 Related Protein, Long Isoform

BID: BH3 Interacting Domain Death Agonist

BIM: BCL2 Interacting Protein

Caspase: Cysteinyl Aspartic Acid-Protease

CD36: Scavenger Receptor Cluster of Differentiation 36

CDX: Cell Line Derived Xenograft

CEHCs: Carboxyethyl Hydroxychromans

c-FLIP: FLICE-Inhibitory Protein

CRC: Colorectal Cancer

DAC: Diacylglycerol

DED: Death Effector Domain

DEP: Dishevelled, Egl-10, and Pleckstrin

DEPTOR: DEP Domain-Containing mTOR-Interacting Protein

DFO: Deferoxamine mesylate

DISC: Death Inducing Signaling Complex

DMSO: Dimethyl Sulfoxide

DR: Death Receptor

DUSP: Dual-Specificity Phosphatases

EGF: Epidermal Growth Factor

EGFR: Fibroblast Growth Factor Receptor

eIF: Eukaryotic Initiation Factor

ERK: Extracellular Signal-Regulated Kinase

FADD: Fas-Associated Death Domain

FAS: Fatty Acid Synthetase Receptor

FGF: Fibroblast Growth Factor

FGFR: Epidermal Growth Factor Receptor

FKBP12: FK506 Binding Protein 12

FOXO: Forkhead Box Protein O

FRB: FKBP12 Rapamycin Binding

FSP1: Ferroptosis-Suppressor-Protein 1

FTase: Farnesyltransferase

FTIs: Farnesyltransferase Inhibitors

GAB: GRB-2 Associated Binding

GAP: GTPase-Activating Protein

GATOR: GAP Toward RAGs

GDP: Guanosine Diphosphate

GEF: GTPase Exchange Factor

GGTase-1: Geranylgeranyltransferase Type 1

GLUT: Glucose Transporter

GPCR: G-Protein Coupled Receptor

GPX4: Glutathione Peroxidase 4

GRB: Growth Factor Receptor-Bound Protein

GRD: GAP Related Domain

GSH: Glutathione

GSK3β: Glycogen Synthase Kinase-3 β

GSR: Glutathione–Disulfide Reductase

GTP: Guanosine Triphosphate

HDL: High-Density-Lipoprotein

HIF1α: Hypoxia Inducible Factor 1 α

HO-1: Heme Oxygenase 1

HRAS: Harvey Rat Sarcoma Virus

HtrA2/Omi: High-Temperature Requirement Factor A2

HVR: Hyper Variable Region

IAP: Inhibitor of Apoptosis Proteins

ICMT: Isoprenylcysteine Carboxyl Methyltransferase

IEG: Immediate Early Genes

IGF1R: Insulin-like Growth Factor 1 Receptor

IRS1: Insulin Receptor Substrate 1

KRAS: Kirsten Rat Sarcoma Viral Oncogene Homolog

LDL: Low-Density-Lipoprotein

LDLR: Low-Density-Lipoprotein Receptor

LKBP1: Liver Kinase B1

LOOH: Lipid Hydroperoxides

LOX: Lipoxygenase

LPCAT: Lysophosphatidylcholine Acyltransferase

LPL: Lipoprotein Lipase

Mcl-1: Myeloid Leukemia 1

MDR2: Multidrug Resistance

MEK: Mitogen-Activated Protein Kinase Kinase

mLST8: mTOR Associated Protein, LST8 Homolog

MNK: MAPK Interacting Protein Kinase

mRNA: messenger RNA

MSK: Mitogen and Stress-Activated Protein Kinase

mTOR: Mammalian Target of Rapamycin

mTORC: mTOR Complex

MTTP: Microsomal triglyceride transfer protein

MUFA: Monounsaturated Fatty Acid

NADPH: Nicotinamide Adenine Dinucleotide Phosphate

NF1: Neurofibromin 1

NFκB: Nuclear Factor kappa-Light-Chain-Enhancer of Activated B Cells

NORE1A: Novel RAS Effector 1A

Noxa: Phorbol-12-Myristate-13-Acetate-Induced Protein 1

NPC1L1: Niemann-Pick C1-like 1

NRAS: Neuroblastoma RAS Viral Oncogene Homolog

NRF2: Nuclear factor erythroid 2–related factor 2

NSCLC: Non-Small Cell Lung Cancer

PARP: Poly (ADP-Ribose) Polymerase

PCD: Programmed Cell Death

PDAC: Pancreatic Ductal Adenocarcinoma

PDCD4: Programmed Cell Death 4

PDGFR: Platelet Derived Growth Factor Receptor

PDK1: Pyruvate Dehydrogenase Kinase 1

PD-L1: Programmed Death Ligand 1

PDX: Patient Derived Xenograft

PH: Pleckstrin Homology

PI3K: Phosphatidylinositol-4,5-Bisphosphate 3-Kinase

PIKK: PI3K-Related Protein Kinase

PIP2: Phosphatidylinositol 4,5-Bisphosphate

PIP3: Phosphatidylinositol (3,4,5)-Triphosphate

PKC: Protein Kinase C

PL: Phospholipid

PLC: Phospholipase C

PLOOH: Phospholipid Hydroperoxides

PMA: Phorbol 12-Myristate 13-Acetate

PRAS40: Proline-Rich AKT1 Substrate 1

Protor 1/2: Protein Observed with Rictor-1/2

PTEN: Phosphatase and Tensin Homolog

PUFA: Polyunsaturated Fatty Acid

PUFA-PL: PUFA Phospholipids

Puma: BCL2 Binding Component 3

PXR: Pregnane X Receptor

RA: RAS Association

RAF: Rapidly Accelerated Fibrosarcoma

Raptor: Regulatory Associated Protein of mTOR

RAS: RAT Sarcoma

RBD: RAS Binding Domain

RCD: Regulated Cell Death

RCE1: RAS Converting CaaX Endopeptidase 1

RHEB: RAS Homolog Enriched in Brain

Rictor: Rapamycin-Insensitive Companion of mTOR

RIN1: RAS and RAB Interactor 1

RIP: Receptor-Interacting Protein

RNS: Reactive Nitrogen Species

ROS: Reactive Oxygen Species

RSK: Ribosomal S6 protein kinase

RSL3: RAS-Selective Lethal 3

RTA: Radical Trapping Antioxidant

RTK: Receptor Tyrosine Kinase

S6K: S6 Kinase

SAM: S-adenosylmethionine

SAR: Structure Activity Relationship

SCD1: Stearoyl-Coenzyme A Desaturase

SEC14L: Sec14-like

SH: Src Homology

SHP2: Src Homology Region 2

Sin: Stress-Activated Protein Kinase-Interacting Protein

SMAC/DIABLO: Second Mitochondrial Activator of Caspases/Direct IAP Binding Protein with Low PI

SOS: Son of Sevenless

SPRED: Sprouty-Related, EVH1 Domain-Containing Protein

SR-BI: Scavenger Receptor Class B Type I

SREBP: Sterol Regulatory Element Binding Protein

TAP: Tocopherol-Associated Protein

tBID: Truncated BID

TCF: Ternary Complex Factor

TFEB: Transcription Factor EB

TGF-β: Transforming Growth Factor β

TIAM: T Cell Lymphoma Invasion and Metastasis-Inducing Protein

TME: Tumor Microenvironment

TNFR1: Tumor Necrosis Factor Receptor 1

TNF-α: Tumor Necrosis Factor α

Toc: Tocopherol

TRADD: TNF Receptor-Associated Death Domain

TRAF: TNF Receptor Associated Factor

TRAIL: Tumor Necrosis Factor-Related Apoptosis-Inducing Ligand

TSC: Tuberous Sclerosis Complex

TT: Tocotrienol

TXNDR1: Thioredoxin Reductase 1

UPS: Ubiquitin-Proteasome System

UTR: Untranslated Region

VEGF: Vascular Endothelial Growth Factor

VEGFR: Vascular Endothelial Growth Factor Receptor

VLDL: Very Low-Density-Lipoprotein

WNT: Wingless/Integrated

WT: Wild-Type

xCT: Cystine/Glutamate Antiporter SLC7A11

XIAP: X-linked Inhibitor of Apoptosis

α-TTP: α-Tocopherol Transfer Protein

Chapter 1: Introduction

The mitogen activated protein kinase (MAPK) cascades are highly conserved signal transduction networks that control an extensive array of fundamental cellular processes through the relay of signals from upstream extracellular stimuli to varied downstream cytoplasmic and nuclear effectors. Among the initiating stimuli are a diverse complement of mitogens, growth factors, cytokines, and stress factors. Each cascade consists of three core kinases that propagate signaling through sequential phosphorylation and activation of the subsequent kinase, eventually converging on the phosphorylation of target regulatory proteins by the terminal MAPK constituent (Raman et al. 2007). Mammalian genomes encode fourteen distinct MAPKs, which are classified as conventional or atypical based on their sequence and mechanism of activation. The most well characterized MAPK cascades in mammalian cells are from the conventional class – extracellular signal regulated kinase-1/2 (ERK1/2), c-Jun N-terminal kinase (JNK), p38, and ERK5 – denominated by their utmost kinase (Plotnikov et al. 2011).

The RAS-RAF-MEK-ERK Signaling Pathway

The ERK1/2 signaling pathway, also known as the classical MAPK cascade, facilitates a multitude of cellular functions, including growth, proliferation, survival, differentiation, and motility. Signaling begins with activation of cell-surface receptors, mainly receptor tyrosine kinases (RTKs), by cognate ligands such as epidermal growth factor (EGF), fibroblast growth factor (FGF), and insulin-like growth factor 1 (IGF1) (McCain 2013). Binding of the initiating element leads to receptor dimerization, with subsequent formation and activation of complexes that contain adaptors, such as SH2-containing (SHC) factors. Proteins containing SH2 domains are recruited to specific

phospho-tyrosine residues. Among the SH2 class are growth-factor-receptor bound protein 2 (GRB2) and GRB-2 associated binding (GAB) protein. Adaptor proteins associated with the intracellular domains of phosphorylated RTKs can recruit guanine nucleotide exchange factors (GEFs) to the cell membrane. GRB2 constitutively binds to the guanine nucleotide exchange factor (GEF) SOS, a prime activator of RAS that increases the level of RAS bound to guanosine triphosphate (GTP) (Bos et al. 2007).

RAS-GTP directly binds to the serine/threonine kinase RAF, leading to its plasma membrane recruitment, dimerization, and allosteric transactivation. The three isoforms of RAF – ARAF, BRAF, and CRAF/RAF-1 – share a high degree of similarity in their domain organization and can form homo- and hetero-dimers (Matallanas et al. 2011, Stephen et al. 2014). Inactive RAF exists in an autoinhibited state whereby its N-terminal region contacts and represses its catalytic site. Phosphorylation of serine 259 (S259) within CRAF's conserved region 2 (CR2) domain, or serine 365 (S365) in BRAF's equivalent site, also helps to suppress catalytic activity. Phosphorylation of these residues enables binding of 14-3-3 proteins to their motifs within RAF, likely stabilizing the inhibitory interaction between the N terminal region and the catalytic site. Apart from membrane recruitment, which is essential to RAF activation, RAS activity also promotes the dephosphorylation of the inhibitory 14-3-3 binding sites, mediated by protein phosphatase 2A (PP2A) and PP1 (Lavoie and Therrien 2015).

Activated RAF phosphorylates and activates the tyrosine and serine/threonine dual-specificity mitogen-activated protein kinase kinase-1/2 (MEK1/2) by phosphorylating S218 and S222 within the activation segment of MEK1/2. In turn, MEK1/2 transduces the signal to the serine/threonine kinase ERK1/2 (**Figure 1.1**). Although RAF is one of many

factors that can activate MEK1/2, MEK1 and MEK2 are exclusive activators of ERK1/2 (Lavoie et al. 2020). ERK1 (p44) and ERK2 (p42) are proteins encoded by two splice variants of the same gene. Inactive ERK1/2 is associated with microtubules in the cytoplasm. Upon phosphorylation by MEK1/2 at positions threonine (T202) and tyrosine (Y204) for ERK1, and T173 and Y185 for ERK2, they activate a compendium of cytoplasmic and nuclear targets, thereby regulating an extensive array of cellular events (Ünal et al. 2017, Ullah et al. 2022). Unless otherwise specified, for simplicity, the term 'ERK' is used hereafter to designate both ERK1 and ERK2. The same simplification is applied to other proteins that have multiple isoforms, such as RAS, RAF, and MEK.

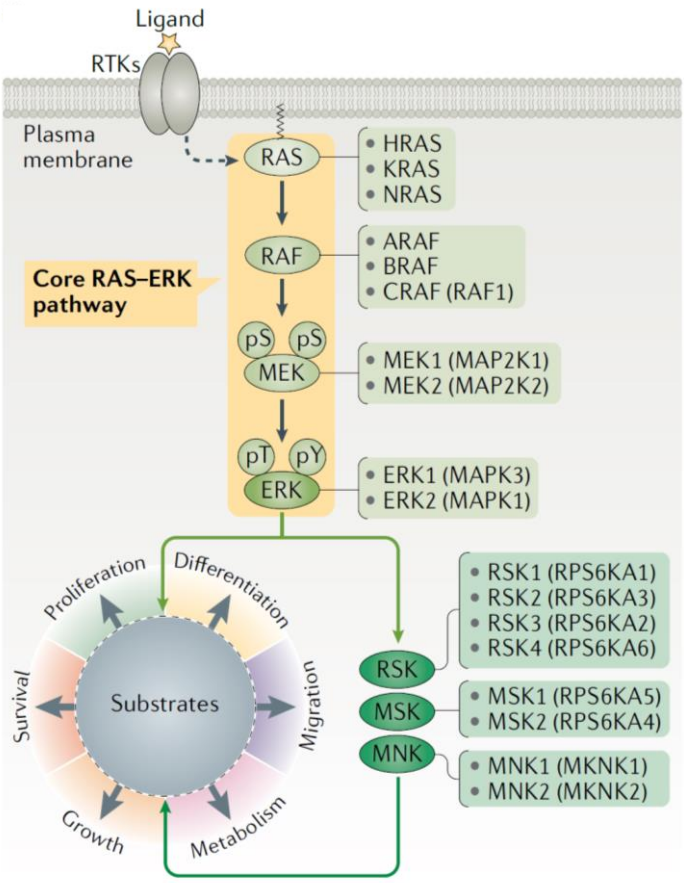

Figure 1.1 The RAS-RAF-MEK-ERK Signaling Cascade.

Modified from Lavoie et al., *Nat Rev Mol Cell Biol.* (2020)

Activated ERK phosphorylates various cytoplasmic signaling proteins, including MNK (MAPK-interacting kinase), MSK (mitogen- and stress-activated protein kinase), and p90 ribosomal S6 kinase (RSK), all of which play roles in regulating mRNA translation, as well as nuclear end-point effectors, such as transcription factors. Among the ERK nuclear targets is the ternary complex factor (TCF) transcription factors, such as ELK-1, which play a major role in promoting expression of the immediate early genes (IEGs). IEGs do not necessitate *de novo* synthesis to be transcriptionally induced. Products of IEGs, including c-Fos and c-Myc, induce late-response genes that promote cell survival, proliferation, and motility. The target specificity of activated ERK is controlled by substrate availability, which itself is determined by cell type, cell cycle phase, the extracellular environment, ERK scaffolding, and subcellular localization. Scaffolding proteins tether MEK and ERK to specific substrates and subcellular locales, and they're required for ERK phosphorylation of correspondingly bound or local substrates (McCain 2013, Lavoie et al. 2020).

The ERK cascade is under extensive homeostatic control by feedback loops, which can broadly be divided into two categories: rapid-short term effects and delayed long-term effects. Rapid feedback mechanisms include ERK mediated direct inhibition of the pathway by phosphorylating negative regulatory sites on RAF, MEK, RTKs, and indirectly on SOS through its target RSK, which dampens signal propagation to maintain stable cellular functions. Delayed feedback mechanisms stem from ERK mediated *de novo* transcription of negative regulators, including the dual specificity phosphatase (DUSP) proteins, which modulate ERK activity by dephosphorylation, and Sprouty (SPRY), which inhibits RTKs and SOS (Lito et al. 2013, Liu et al. 2018) (**Figure 1.2**).

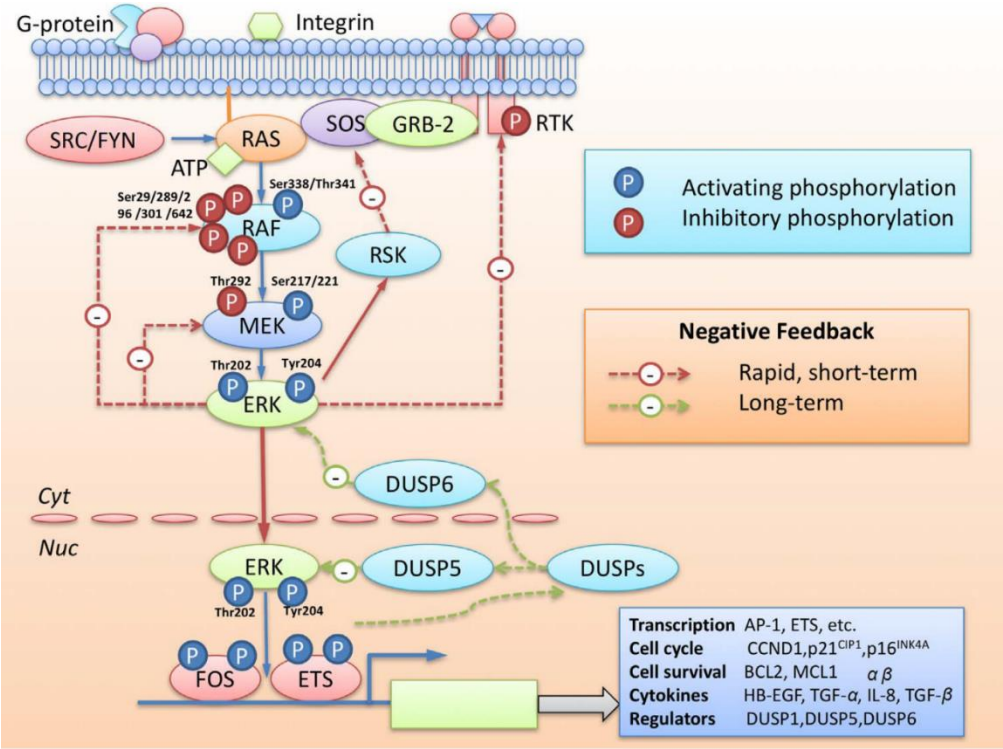

Figure 1.2 Physiological Role of ERK1/2 Target Genes and Mechanisms of ERK1/2 Mediated Feedback Inhibition of the Pathway.

From Liu et al. *Acta Pharm Sin B.* (2018)

RAS

RAS is among the more than 150 members belonging to the GTPase superfamily. First identified in the 1960s, the RAS family is composed of five members – RAS, RAB, RHO, ARF, and RAN. The RAS family itself can be further divided into 6 subfamilies – RAS, RAL, RAP, RAD, RHEB, and RIT. Of these, RAS is the most frequently studied, and there exists a compendium of data providing insight into its regulation and vast biological functions (Liu et al. 2018, Singh et al. 2023). In humans, there are four canonical RAS proteins encoded by three genes – Harvey rat sarcoma viral oncogene homolog (*HRAS*) encoding HRAS, neuroblastoma rat sarcoma viral oncogene homolog (*NRAS*)

encoding NRAS, and Kirsten rat sarcoma viral oncogene homolog (*KRAS*) encoding two isoforms, KRAS4A and KRAS4B, from alternative mRNA splicing. Although KRAS4B is the predominant splice variant expressed in many tissues, and hence has garnered greater focus, there is significant KRAS4A expression in some tissues, particularly of cancer lineage (Hobbs et al., 2016). The N-terminal 164 residues comprise the GTPase-(G)-domain, which is involved in GTP binding and hydrolysis. The four RAS isoforms contain identical residues in the first half of the G-domain (termed the effector lobe, aa 1-86), sharing 82% sequence identity in the second half (termed the allosteric lobe, aa 87-166). The last 19-20 amino acids located at the C-terminal end exhibit significant sequence diversity among the RAS isoforms, constituting what's termed the "hypervariable region" (HVR) (Hobbs et al. 2016, Simanshu et al. 2017).

The subcellular localization of RAS proteins is determined by their specific lipid modification, the composition of local membranes, and the electrostatic nature of the isoform specific HVRs (Abankwa et al. 2010). Association with membranes is essential for activating downstream signaling pathways, and this is facilitated by prenylation and palmitoylation of cysteine residues located in the HVR. Prenylation of RAS proteins involves farnesylation of the cysteine residue present in the C-terminal CaaX motif by farnesyltransferase (FTase). The CaaX motif is a tetrapeptide sequence having an invariant cysteine (C), two aliphatic amino acids (a1 and a2), and one of several amino acids in the terminal position (X). Subsequently, the CaaX motif undergoes cleavage of the -aaX residues by RAS converting CaaX endopeptidase 1 (RCE1), followed by carboxymethylation of the farnesylated cysteine residue by isoprenylcysteine carboxyl methyltransferase (ICMT). Aside from KRAS4B, which contains a polybasic region in the

HVR that facilitates its membrane association, the remaining three RAS isoforms undergo palmitoylation that enables their full association with the plasma membrane (Simanshu et al. 2017).

Role in Physiology

RAS proteins function as obligate GTP-GDP binary on/off switches. This switch mechanism has been highly conserved among diverse GTP/GDP binding proteins that regulate a multiplicity of biological functions. RAS cycling between its active GTP bound state and inactive GDP bound state is mediated by GEFs (e.g., SOS1), which catalyze the release of bound GDP to be replaced by the more abundant GTP, and guanine nucleotide activating proteins (GAPs, e.g., NF1), which catalyze the intrinsic GTP hydrolysis rate of RAS proteins (Bos et al. 2007). The reliance of RAS and other GTPases on GEFs and GAPs to switch them on/off enables these processes to be highly regulated and responsive to multiple signaling inputs. The driving force behind this tight control is translocation. All RAS biology occurs in membranes. In addition to the plasma membrane, RAS signaling also takes place on intracellular membranes such as endosomes, the endoplasmic reticulum (ER), the Golgi apparatus, and mitochondria (Baines et al. 2011). GEFs and GAPs act on RAS when they are recruited to the plasma membrane and placed in direct proximity to it. This proximal positioning, as modeled in a 2D surface setting, is equivalent to five orders of magnitude increase in the binding constant relative to free solution. RAS-GTP subsequently activates effectors by recruiting them to the plasma membrane (Simanshu et al. 2017).

When activated, RAS preferentially binds to downstream effectors containing a RAS-binding-domain (RBD) or RAS-association (RA)-domain. While the RBD and RA domains are distinct in their respective primary sequence, they are structurally related, sharing the topology of the ubiquitin superfold. Ubiquitin-like domains are a feature of many multi-domain proteins involved in various signal transduction processes. The ubiquitin superfold, featuring an α/β roll (e.g., ββαββαβ), serves as a stable scaffold on which diverse binding epitopes can mediate specific interactions with proteins and their intramolecular domains (Kiel and Serrano 2006, Singh and Smith 2020) (**Figure 1.3A**). There are over seven unique RAS effector families, each of which activates a distinct protein signaling cascade involved in vital cellular processes such as growth, proliferation, differentiation, adhesion, motility, and survival (**Figure 1.3B**). In addition to the most well characterized effectors, RAF and phosphatidylinositol-3-kinase (PI3K), are RalGDS, novel RAS effector 1A (NORE1A), AF6, phospholipase C (PLC), RAS and RAB interactor 1 (RIN1), T cell lymphoma invasion and metastasis-inducing protein (TIAM), and growth factor receptor bound protein 14 (GRB14) (Gimple and Wang 2019).

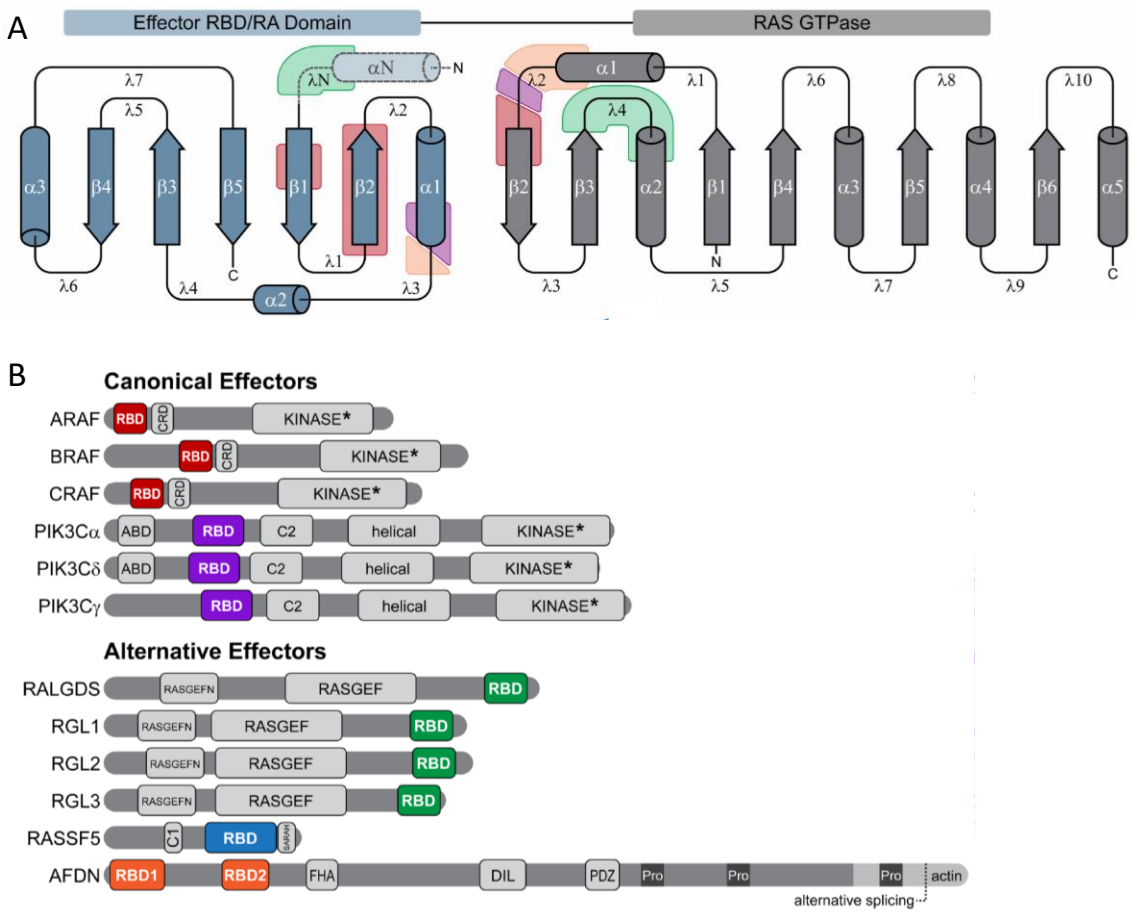

Figure 1.3 Domain Architecture of RAS and Key Domains of Select RAS Effectors.

(A) 2D topology of a typical RBD/RA domain (blue) and an activated RAS GTPase (grey). **(B)** Domain architecture of canonical and alternative RAS effectors

Modified from Singh and Smith. *Biochem Soc Trans.* (2020)

The crystal structure of the G-domain of HRAS in complex with GppNHp, a non-hydrolyzable GTP analog, provided initial insights into how RAS functions as a binary switch. Further structural studies of RAS in complex with domains of various GAP and GEF regulators, as well as RBD effectors, revealed two highly dynamic regions – termed switch-I (aa 30-38) and switch-II (aa 59-76) – and their critical role in protein-protein interactions (**Figure 1.4**). In response to nucleotide binding, these switch regions undergo a conformational change between GDP- and GTP-bound states, described as a loaded

spring mechanism. In the GTP-bound state, T35 acting on switch-I, and G60, acting on switch-II, form hydrogen bonds with the γ-phosphate that hold them open in the active conformation. Upon GTP hydrolysis, the γ-phosphate is released, and both switch regions return to the flexible position in the GDP-bound state (Pai et al. 1989, Milburn et al. 1990, Wittinghofer et al. 1993, Pacold et al. 2000, Hall et al. 2002, Simanshu et al. 2017).

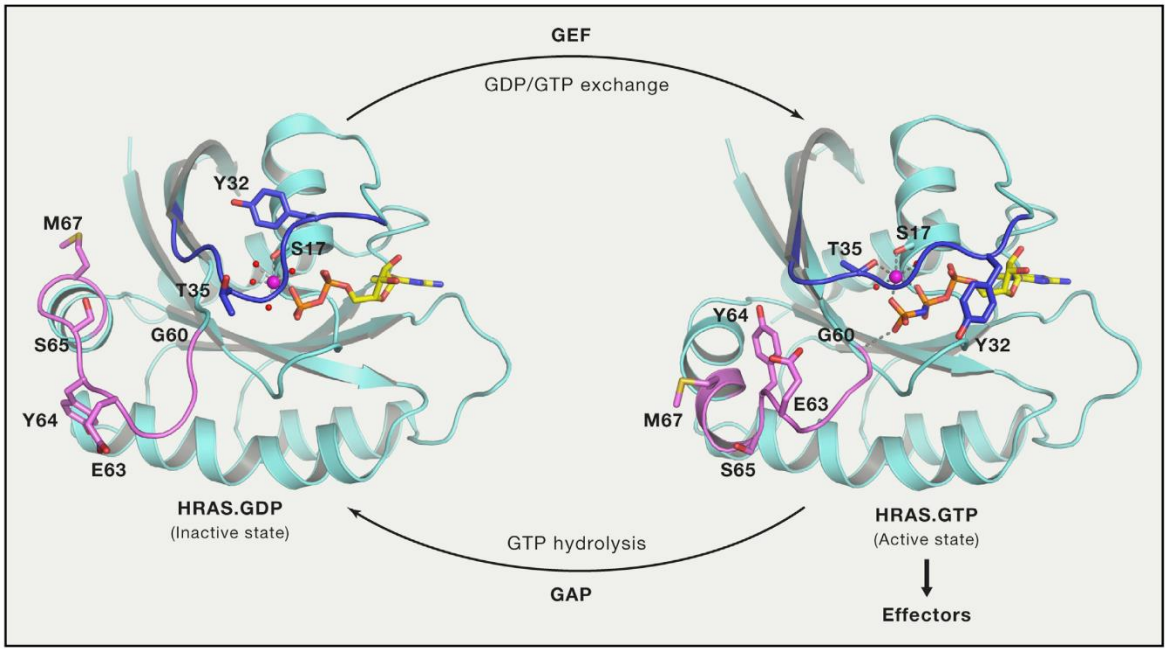

Figure 1.4 Conformational Changes in the Switch-I and Switch-II Regions of RAS During Transitions from Inactive GDP- and Active GTP-Bound States.

From Simanshu et al. *Cell.* (2017)

The very slow off-rate for GDP ($t_{1/2}$ = 6 minutes, k_{off} = 2 x 10^{-3} s^{-1} at 20°C) allows RAS proteins to remain in their inactive state until a signaling impetus provokes GDP/GTP exchange. This requires GEF activity to facilitate the reaction by a several orders of magnitude increase in GDP's off-rate (Hunter et al. 2015). GEF binding to RAS results in conformational changes in the switch-I region and P loop (aa 10-17) that weakens its affinity for GDP, leading to GDP release and exchange (Boriack-Sjodin et al. 1998).

Although the affinity of RAS for GDP and GTP is similar, and GEFs do not favor rebinding of GTP over GDP or vice versa, increased levels of RAS GTP mainly occur due to the ~10-fold higher cellular concentration of GTP compared to GDP. Binding of GTP dissociates the GEF and leads to the formation of an active GTP-bound RAS that can interact freely with effectors until a signaling impetus provokes GAP activity (Simanshu et al. 2017).

Since the intrinsic GTP hydrolysis rate of RAS proteins is quite slow – $t_{1/2}$ = 16 minutes, $k_{off} = 6 \times 10^{-4}\ s^{-1}$ – efficient hydrolysis necessitates the interaction of RAS with GAP proteins that accelerate the cleavage step by several orders of magnitude (Hunter et al. 2015). Initial insights on how GAP stimulates GTP hydrolysis stemmed from structural studies on GDP and AlF3 bound HRAS in complex with the GTPase activating domain – typically referred to as the GAP-related domain (GRD, aa 718–1037) – of RASA1/p120GAP (Scheffzek et al. 1997). Interaction of GAP proteins with the switch-II region of HRAS stabilizes the position of Q61, which then coordinates the catalytic H_20 molecule. Residue R789 of RASA1, called the arginine finger, also protrudes into the active site of HRAS and interacts with the α- and β-phosphate groups of GDP and AlF3, stabilizing the transition state by neutralizing a negative charge at the γ-phosphate (Ahmadian et al. 1997). The interaction of Q61 with the catalytic H_20 molecule and the main chain carbonyl group of the arginine finger enables it to extract a hydrogen atom from the attacking water molecule. This induces the formation of a negatively charged hydroxyl ion that attacks the γ-phosphate of GTP to carry out the hydrolysis reaction.

While the GRDs of RAS GAPs are highly conserved (Ahmadian et al. 1997), RAS GAPs diverge dramatically outside of the GRDs, reflecting distinct roles in signal transduction and RAS regulation (Bos et al. 2007). For example, the RASA1/p120 GAP

contains SH2 and SH3 domains that bind to activated receptors, such as platelet derived growth factor receptor (PDGFR). This is thought to enable its downregulation of RAS activity appropriately during signaling. Alternatively, NF1 is conserved in organisms that lack RTK signaling, such as *S. cerevisiae*, and likely regulates RAS in response to different signals, the nature of which are unknown. In mammalian cells, NF1 depends on SPRED proteins to recruit it to RAS, but the signals governing this critical interaction remain to be identified (Simanshu et al. 2017).

Role in Cancer

Mutations in *RAS* were first reported in cancer over 30 years ago. Since then, numerous studies have validated mutant RAS as a driver of tumor initiation and maintenance. RAS is mutationally active in approximately one-third of all cancers, with pancreas (90%), colon (50%), thyroid (50%), lung (30%), and melanoma (25%) demonstrating high-ranking prevalence (Liu et al. 2018). Notably, there are striking cancer-type-specific mutational profiles of *RAS* isoforms, suggesting tissue-distinct roles for RAS in driving oncogenesis. For example, KRAS is almost exclusively altered in pancreatic ductal, lung, and colorectal carcinoma, NRAS is the predominant isoform mutated in cutaneous melanoma, and HRAS alterations prevail in head and neck squamous cell carcinoma (**Figure 1.5A**) (Hobbs et al. 2016).

Studies seeking to address the issue of why specific RAS gene isoforms are preferentially mutated in certain cancers has begun to shed light on this phenomenon. In one carcinogenesis study, the KRAS G12D, but not NRAS G12D, mutation promoted colon cancer development in Apc-deficient mice, supporting the ability of KRAS to initiate

the formation of colon cancer, and the failure of NRAS to achieve the same in this setting (Haigis et al. 2008). A subsequent murine carcinogenesis study challenged the broad suggestions put forth by Haigis et al. by demonstrating that the preferential basis for KRAS mutations in lung cancer were due to the distinct expressional regulation of the RAS gene isoforms, rather than to unique functional differences between them (Westcott et al. 2015). Thus, whether a specific RAS gene is required for cancer development arising from different tissues remains to be resolved.

RAS alterations predominantly encode mutant proteins harboring single amino acid substitutions primarily at glycine 12 (G12) and glycine 13 (G13) in exon 2, as well as glutamate 16 (Q61) in exon 3 – well regarded hot spot regions at which 98% of mutations occur. Broadly speaking, many of these alterations disrupt GTP hydrolysis (e.g., by precipitating GAP insensitivity) and/or enhance nucleotide exchange, leading to proteins more readily bound to GTP, and a subsequent increase in, and sustainment of, signaling output (Hobbs et al. 2016, Liu et al. 2018, Zhu et al. 2021). In addition to differences in cancer-type occurrence, *RAS* isoforms are also distinguished by their marked divergence in mutation frequency at these hotspot sites (**Figure 1.5B**). G12 mutations predominate in KRAS, comprising 83% of its mutation profile, while G13 alterations account for 14%, and Q61 mutations constitute a modest 2%. In contrast, Q61 is the principally mutated hotspot in NRAS, followed by G12 and G13. HRAS presents an intermediate pattern, with comparable mutation frequencies across these three positions. Adding to the complexity, the mutation frequency of any given RAS isoform can exhibit significant differences between cancer types. NRAS Q61 mutations dominate in melanoma, with G12 alterations being a rare occurrence. Conversely, NRAS G12 mutations are readily observed in acute

myeloid leukemia (AML). KRAS mutations in pancreatic ductal adenocarcinoma (PDAC) are dominated by G12 alterations, whereas aberrations in G13 and Q61 are rare. On the other hand, G13 mutations occur at a relatively high frequency in colorectal adenocarcinoma (COAD). These patterns suggest that the diverse array of RAS mutations may provoke varied functional consequences, with the properties crucial for their oncogenic activity potentially fluctuating depending on the tissue of origin (Hobbs et al. 2016, Murugan et al. 2019).

Although studies on HRAS G12V have contributed much to the current dogma on the consequences of missense mutations on RAS function, there is growing evidence and appreciation for the different structural, biological, and functional outcomes stemming from varied mutations at amino acid positions 12, 13, and 61. Biochemical studies have demonstrated that the G12V mutation leads to a loss of GAP sensitivity, while the Q61L alteration reduces RAS intrinsic GTP hydrolysis and GAP sensitivity, in addition to increasing the intrinsic nucleotide exchange rate. The G13D mutant has decreased GAP-mediated hydrolysis, and a substantially increased rate of intrinsic nucleotide exchange compared to that of wild-type (WT) RAS (Smith et al., 2013). Structural studies of several G12 mutant crystals have demonstrated that, of the complement of these mutations, only G12R alters the structure of RAS relative to WT. The structural perturbation within switch-II appears to be the result of the arginine side chain displacing the glutamate residue at position 61 in the nucleotide binding site, a residue crucial for GTP hydrolysis (Hobbs et al. 2016, Murugan et al. 2019).

While six possible single-base-change missense mutations can occur at the codons for G12, G13 and Q61, their frequencies are not uniform. At G12, aspartic acid (G12D) is

the predominant KRAS (41%) and NRAS (52%) substitution, while valine (G12V) prevails in HRAS (57%). At G13, aspartic acid (G13D) again is the most frequent substitution for KRAS (89%) and NRAS (50%), but is rarely observed in HRAS (3%), where arginine (G13R) dominates instead (85%). At Q61, histidine (Q61H) is the prevalent KRAS alteration (58%), occurring less frequently in both NRAS (6%) and HRAS (5%), where arginine (Q61R) is the chief substituent (47% and 43%, respectably) (**Figure 1.5C**). Compounding the complexity of cancer-type differences in the predominance of the mutant RAS isoforms are the variations in substitutions occurring at a given RAS residue. For example, the predominant substitution for KRAS G12 is aspartic acid (G12D) in PDAC, followed by valine (G12V). In contrast, in lung adenocarcinoma (LAC), the main substitution is cysteine (G12C), which is rare in PDAC (3%). These differences call forth the possibility that distinct substitutions at any one position may have disparate biological outcomes, and further suggests that the same mutation may have varied consequences for each RAS isoform (Hobbs et al. 2016, Murugan et al. 2019).

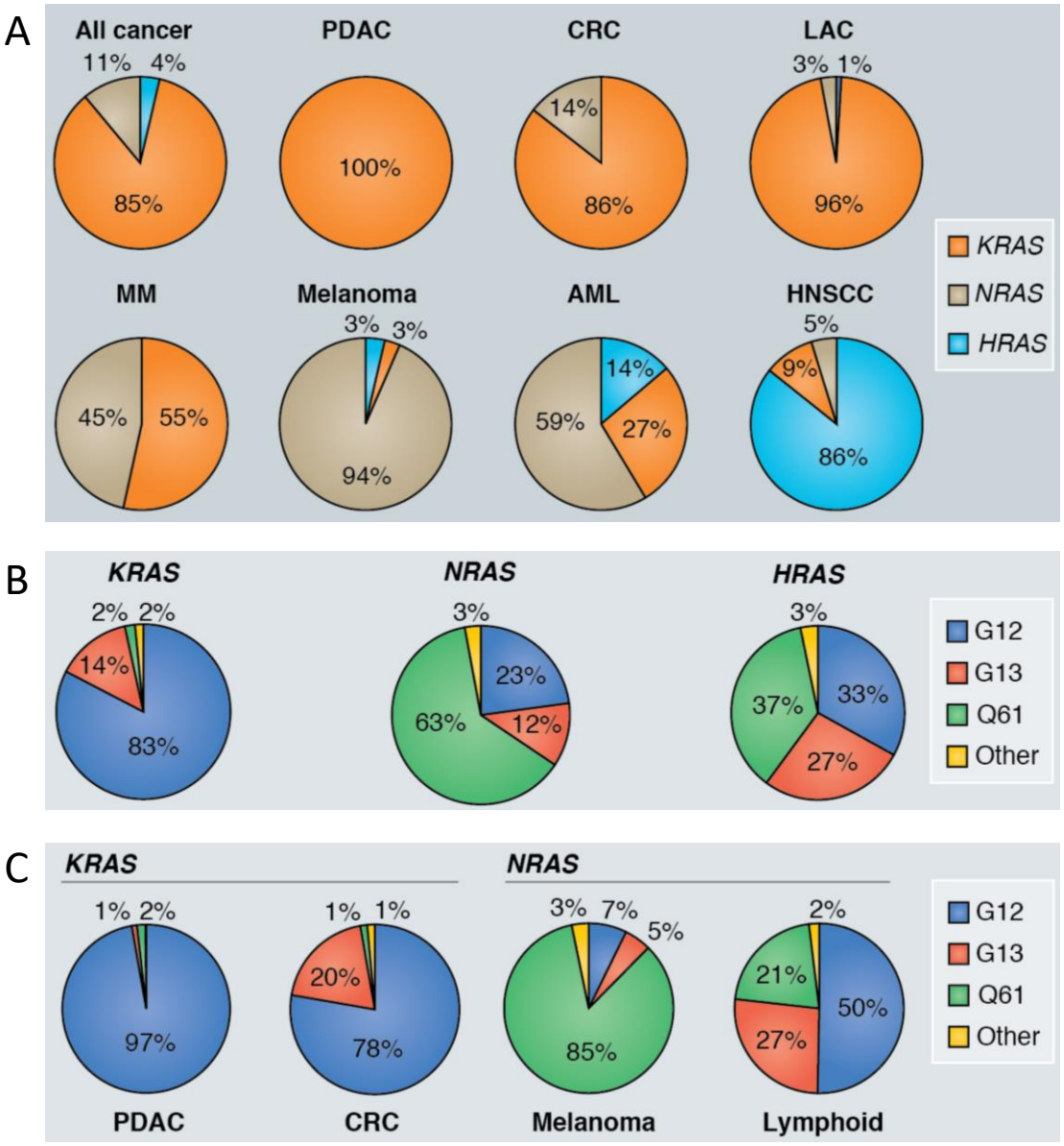

Figure 1.5 RAS Mutation Frequency in All Cancers and Cancer Subtypes.

(A) Prevalence of RAS isoforms mutated in various cancers. **(B)** Occurrence of hotspot mutations within each RAS isoform. **(C)** Frequency of hotspot mutations in the major mutant RAS isoform for select tumor types. AML: acute myeloid leukemia; CRC: colorectal cancer; HNSCC: head and neck squamous cell carcinoma; LAC: lung adenocarcinoma; MM: multiple myeloma; PDAC: pancreatic ductal adenocarcinoma.

Modified from Hobbs et al. *J Cell Sci.* (2016)

Given that the vast complement of *RAS* alterations precipitates a higher prevalence of activated RAS, this results in dysregulated signaling output. Of the RAS effector families, four members – RAF, PI3K, RalGEF, and TIAM1 – have driving roles in oncogenesis due to their regulation of an array of cellular processes that, when aberrated, can readily lead to transformation and subsequent tumor maintenance (Hobbs et al. 2016, Simanshu et al. 2017). Emerging evidence also suggests that there are mutation-specific consequences on effector signaling. A comparison of KRAS G12C, G12V, and G12D alterations in non-small cell lung cancer (NSCLC) cell lines revealed distinct effector preferences between the three mutational substituents. In the case of G12D, higher levels of phosphorylated AKT were observed, while G12C mutant models instead demonstrated increased levels of RAL-GTP (Ihle et al. 2012). In a similar study conducted in CRC comparing KRAS G12 and KRAS G13 mutants, the colon cancer stem cell marker DCLK1 and the RTK MET were upregulated in G12-mutant-expressing cells, while the tight-junction protein ZO-2 was upregulated in G13D-expressing cells compared to parental controls (Hammond et al. 2015). These studies indicate that distinct RAS mutants can vary in their modulation of signaling through their unique effector preferences.

Therapeutic Targeting

The causal role of RAS in human cancers has inspired numerous attempts to generate targeted inhibitors of the protein. The development of inhibitors that compete with ATP binding to the kinase domain has been the most readily successful approach to impeding oncogenic kinases. However, the binding of GTP to RAS proteins is a thousandfold tighter than that of ATP to other kinases. Thus, for decades RAS was thought

to be undruggable due to its picomolar affinity for GTP, compounded by the smooth and floppy nature of its tertiary structure, making both orthosteric and allosteric small molecule inhibitors an unlikely option. While this is no longer the case with the recent advent of novel inhibitors that can indeed directly inhibit RAS, historically, initial efforts focused on indirect approaches in the realm of inhibiting its membrane association, protein expression, and downstream effectors (Simanshu et al. 2017, Liu et al. 2018).

The importance of membrane association for RAS function led to the rational strategy of inhibiting this process at varying nodes towards blocking aberrant RAS activity. As such, numerous farnesyltransferase inhibitors (FTIs) were developed, including CaaX peptidomimetics, nonapeptide peptidomimetics, farnesyl diphosphate analogs, and bisubstrate inhibitors. These FTIs showed potent selectivity for FTase and not the closely related geranylgeranyltransferase type 1 (GGTase-1). Like FTase, GGTase-1 recognizes the CaaX motif, however, it does so preferentially towards motifs where the terminal X is leucine, whereas FTase trends towards motifs where the utmost X is methionine, alanine, serine, or glutamate. Several of these FTIs advanced to clinical testing, either alone or in combination with conventional cytotoxic agents. Although FTIs showed impressive efficacy in preclinical models of HRAS driven tumors, they failed to effectively block NRAS and KRAS prenylation, membrane association, and transforming activity. Unlike HRAS, NRAS and KRAS can serve us substrates for GGTase-1 when FTase is blocked. Hence, these agents did not achieve clinical efficacy, and their use was discontinued (Baines et al. 2011, Liu et al. 2018).

Another early approach at targeting RAS more directly aimed at suppressing its protein expression through the utilization of antisense oligonucleotides, which bind to their

complimentary mRNAs at a specific strand, thereby inhibiting translation and terminal synthesis of the designated protein. One such compound, ISIS 2503, targeted the 5'-untranslated region (UTR) of human HRAS, and demonstrated good tolerability in a phase I clinical trial assessing patients bearing solid tumors, and a phase II clinical trial evaluating patients with refractory CRC. However, patients failed to achieve an objective response when treated with ISIS as a single agent, as well as in subsequent phase I (patients with advanced tumors) and phase II (patients with unresectable metastatic PDAC) clinical trials when combined with gemcitabine. Given its limited clinical efficacy, further development of this agent was discontinued (Uprety and Adjei 2020).

Oncogenic RAS mutations are resistant to therapies targeting upstream signaling elements like RTKs, given that these alterations enable RAS to signal in the absence of an appropriate stimulus. However, RAS-driven cancers retain varying degrees of dependence on upstream signaling and on WT RAS. RTKs recruit and activate GEFs that increase GTP-loading on WT HRAS, NRAS, and KRAS, as well as on other members of the RAS subfamily that can contribute to overall signaling output. In cells in which RAS does not effectively activate PI3K, growth factors can facilitate this function, increasing signaling that may be essential for proliferation and survival (Simanshu et al. 2017). Additionally, RTKs activate PLCγ, leading to mobilization of calcium, diacylglycerol (DAC), and activation of protein kinase C (PKC). The polybasic region of KRAS4B can be phosphorylated at S181 by PKC, resulting in modulation of its localization and function. PKC can also activate RAF. Calcium/calmodulin, in conjunction with PDEδ, can also modify the affinity of KRAS4B for the plasma membrane and redistribute it to endo-membranes (Hobbs et al. 2016, Simanshu et al. 2017). While RTK inhibition alone is

ineffective for RAS-driven tumors, rational combination strategies targeting both upstream regulators and downstream effectors can prove more efficacious than downstream inhibition alone for tumor cells that are reliant on upstream inputs.

Targeting downstream of RAS began with efforts to inhibit RAF. Unexpectedly, the first inhibitor of RAF to enter clinical trials, sorafenib, demonstrated no benefit in KRAS driven tumors. Instead, small skin lesions, termed keratoacanthomas, were observed during these studies. A subsequent trial evaluating vemurafenib, a more potent RAF inhibitor, exacerbated the occurrence of these lesions while remaining ineffective (Simanshu et al. 2017, Uprety and Adjei 2020). We now understand mechanistically the reason for these keratoacanthomas and the lack of clinical efficacy of BRAF inhibitors in KRAS mutant cancers. BRAF inhibition paradoxically activates ERK signaling in WT BRAF cells (Poulikakos et al. 2010), as well as upstream signaling elements in KRAS mutant cells, leading to ERK activation through alternative pathways (Hatzivassiliou et al. 2010).

Focus subsequently shifted to MEK inhibitors. However, these agents likewise yielded disappointing results in several clinical trials across various tumor types. Combination studies of MEK inhibitors with inhibitors of EGF receptor (EGFR) and chemotherapy also failed to demonstrate clinical efficacy (Uprety and Adjei, 2020). MEK inhibition relieves feedback suppression of upstream signaling, leading to increased RTK activity, and lowers the expression of DUSPS, consequently permitting increased ERK activity. These repercussions can dampen the effects of MEK inhibition (Lito et al. 2013). As the terminal kinase, it has been hypothesized that ERK inhibition may be effective in RAS driven tumors. Preclinical data has demonstrated positive results, and several

candidates are in early clinical development as single agents or in combination with chemotherapeutic agents (Uprety and Adjei 2020). However, it should be noted that ERK inhibition is also subject to relief of negative feedback suppression of the pathway, such that positive effects mediated by ERK inhibition may potentially be attenuated by the same (Lito et al. 2013).

Apart from the core canonical MAPK constituents, targeting other downstream regulators of RAS has also been put forth. In KRAS mutant cancers, a SOS-1 inhibitor developed by Boehringer-Ingelheim, BI-3406, has been shown to reduce GTP loading, as well as tumor cell proliferation. This agent also attenuates feedback reactivation induced by MEK inhibition, enhancing sensitivity of KRAS-dependent cancers to MEK suppression (Hofmann et al. 2021). The ubiquitously expressed Src homology 2 containing protein tyrosine phosphatase (SHP2) relays stimulatory signals from various membrane RTKs to the MAPK pathway. SHP2 inhibitors have demonstrated antitumor activity in RTK-driven cancers, and potent synergy with MEK inhibitors in preclinical KRAS mutant models (Uprety and Adjei 2020).

The decades long belief that RAS was undruggable has been rendered null by Kevan Shokat and colleagues in their seminal study. Taking advantage of the nucleophilicity of cysteine thiols, they isolated and developed a series of cysteine-reactive small molecules against the KRAS G12C mutation using a disulphide-fragment based screening approach termed tethering. These electrostatic compounds selectively interacted with KRAS G12C in the GDP-bound, but not GTP-bound state, binding to a previously unrecognized pocket beneath the effector binding switch-II region. As a result, these agents disrupt switch-I and switch-II, preventing the interaction of KRAS with both GEFs and

effectors. Because these compounds rely on the mutant cysteine substitution for their reactivity, they do not affect WT KRAS (Ostrem et al. 2013, Kim et al. 2020).

This groundbreaking work prompted the development of agents that would translate to more clinically efficacious inhibitors. ARS-853 was the first reported compound to demonstrate improvement over the original KRAS G12C small molecules reported by Ostrem et al. Developed through iterative structure activity relationship (SAR) studies to maximize the biochemical and cellular engagement of KRAS G12C, ARS-853 demonstrated enhanced potency compared to previous KRAS G12C inhibitors. ARS-853 markedly reduced the levels of GTP-bound KRAS, activation of effectors, and proliferation, while inducing apoptosis only in KRAS G12C mutant cells, sparing other RAS-mutant and RAS WT cell lines (Lito et al. 2016, Patricelli et al. 2016).

While targeting RAS mutants in their GDP-bound state would seem counterintuitive, given that many of these alterations enhance the degree of KRAS in its active, GTP-bound form, KRAS G12C mutants are unique. Among the oncogenic RAS alterations, G12C has the highest intrinsic GTP hydrolysis rate, cycling to the GDP-bound state with a half-life of ~12 minutes (Hunter et al. 2015, Zuberi et al. 2020). This property allows for binding of the G12C reactive compounds in the switch-II pocket, followed by nucleophilic attack of cysteine 12. Drug-bound KRAS G12C is insusceptible to nucleotide exchange factors and thus trapped in its inactive state. Mutants lacking GTPase activity, and those prompting exchange, reduce the potency of these agents. Furthermore, suppressing nucleotide cycling downstream of RTKs enhances the potency of these inhibitors, while potentiating RTK/GEF activity attenuates their efficacy (Lito et al. 2016).

Although promising in preclinical cell-based models, the inherent poor chemical and metabolic stability of ARS-853 made it unsuitable for *in vivo* studies, prompting efforts to overcome this dilemma. ARS-1620 was subsequently developed through optimization efforts, consisting of a quinazoline core scaffold combined with the acrylamide warhead of ARS-853. ARS-1620 demonstrated superior pharmacokinetics and selectivity for KRAS G12C. Furthermore, it exhibited satisfactory covalent target occupancy in KRAS G12C mutant patient derived xenografts (PDX) *in vivo*, providing the first evidence that KRAS G12C inhibitors could be a viable therapeutic approach for patients with this mutation (Janes et al. 2018, Kim et al. 2020, Zuberi et al. 2020).

Further refinement of these encouraging, preclinical compounds led to the first direct RAS inhibitor to reach clinical trials, AMG510, also known as sotorasib. Developed by Amgen, AMG510 has improved binding to KRAS G12C through interaction with a cryptic groove that extends the switch-II binding pocket and involves interaction of its unique aromatic rings with histidine 95, an amino-acid specific to KRAS. This modification improved both potency and selectivity ~10-fold over ARS-1620, inhibited signaling and growth of KRAS G12C mutant cell line models, and precipitated tumor regression in cell line derived xenograft (CDX) and PDX murine models. Furthermore, AMG510 demonstrated clinical activity in lung cancer patients in the first-in-human dose-escalation study (Canon et al. 2019, Kim et al. 2020, Zuberi et al. 2020).

Like Amgen, Mirati Therapeutics also identified a potent and selective covalent KRAS G12C inhibitor, MRTX849, also known as adagrasib, which likewise modified the mutant cysteine 12 in the inactive GDP-bound state. Treatment with this agent resulted in significant tumor regression in preclinical CDX and PDX models (Fell et al. 2020, Hallin

et al. 2020). KRAS mutant cancers are characterized by an increased production of immune-suppressive cytokines and an upregulation of programmed death-ligand 1 (PD-L1) (Coelho et al. 2017). Both AMG510 and MRTX849 demonstrated positive immune responses that altered the immunosuppressive tumor microenvironment (TME) to a more favorable, anti-tumor one. AMG510 lead to increased T-cell infiltration and an inflamed TME (Canon et al. 2019), while MRTX849 increased pro-inflammatory cytokines, shifted macrophage polarization from M2 (anti-inflammatory) to M1 (pro-inflammatory), and reduced myeloid-derived suppressor cells (Briere et al. 2021).

Revolution Medicines (RM) has also developed a series of RAS inhibitors. Unlike the classical agents that target KRAS G12C in its inactive, GDP-bound state, termed RAS (OFF)/KRAS G12C (OFF) inhibitors, they've generated inhibitors that target the mutant protein in its active, GTP-bound state, termed RAS (ON)/KRAS G12C (ON) inhibitors. These compounds bind to the highly abundant cellular chaperone protein cyclophilin A, creating a binary complex that presents a unique surface capable of engaging not only KRAS G12C, but other RAS mutations. In this tertiary complex, the inhibitor is sandwiched in an induced binding pocket at the interface between both proteins. The tri-complex is fastened by chemical interactions between cyclophilin A and the targeted mutant, along with chemical interactions between the compound and each of the two proteins. In some cases, these inhibitors can form a covalent bond with the RAS mutant, as is the case for the KRAS G12C (ON) inhibitor. To date, RM has also developed RAS(ON) inhibitors for KRAS G12D and KRAS G13C, as well as a multi-RAS inhibitor (Revolution Medicines 2023).

The PI3K-AKT-mTOR Pathway

PI3K is another well described effector of RAS that can play a role in RAS-driven tumorigenesis and maintenance. The PI3K/AKT/mechanistic target of Rapamycin (mTOR) pathway regulates cell growth, proliferation, differentiation, motility, angiogenesis, metabolism, and survival (**Figure 1.6**). Activation of the PI3K/AKT/mTOR axis is controlled by four principal sensors - RTKs, which sample for growth factors, the cytokine-coupled receptors (interleukin family, TNF, TGF-β superfamily, etc.), the G-protein coupled receptors (GPCRs; endothelin receptor, adrenergic receptor, estrogen receptor, angiotensin II receptor, etc.), that are activated by a wide array of ligands (e.g. estrogen, androgen, endothelin, bradykinin, glutamate, etc.), and integrins, which sense cell–cell and cell–matrix adhesions (Fruman et al. 2017).

Human cells express three classes of PI3K enzymes, allocated on the basis of their structure, regulation, and function. Members of class I are designated RAS effectors. Class I PI3Ks are obligate heterodimers composed of a regulatory and catalytic subunit. The four catalytic isoforms – p110α, p110β, p110δ, and p110γ – are encoded by PIK3CA, PIK3CB, PIK3CD, and PIK3CG, respectively. The α and β isoforms are expressed ubiquitously, while their γ and δ counterparts are enriched in immune cells (Vanhaesebroeck and Waterfield 1999, Cantley 2002). p110α, β, and δ (Class IA subgroup) can associate with five regulatory subunits: p85α, p85β, p55α, p50α, and p55γ, with p85α dominating. Each subunit contains two SH2 domains (N-terminal SH2, C-terminal SH2) flanking a coiled-coil region, known as the inter-SH2 (iSH2) domain. The catalytic and regulatory subunits make several contacts that keep the enzyme in a low activity state under basal conditions. Binding of the regulatory subunit's SH2 domains to phosphotyrosine residues on activated

growth factor receptors or adaptor proteins relieves these inhibitory contacts, positioning the dimer near the membrane where it can access substrates and receive further inputs from signaling components (Yu et al. 1998, Fruman et al. 2017).

Activated PI3K catalyzes the phosphorylation of phosphatidylinositol-4,5-bisphosphate (PIP2) to generate phosphatidylinositol-3,4,5-trisphosphate (PIP3). PIP3 acts as a second messenger, and its accumulation at the cell membrane leads to the recruitment of cytoplasmic proteins containing pleckstrin homology (PH) domains. The serine-threonine kinases phosphoinositide-dependent kinase-1 (PDK1) and AKT, along with mTOR complex 2 (mTORC2), are three such factors recruited to PIP3 sites. PDK1 phosphorylates AKT on T308, a residue within its activation loop. Although AKT phosphorylation on T308 is both necessary and sufficient to mediate many downstream events, additional phosphorylation sites control substrate selectivity, stability, and possibly subcellular localization. Hence, a second phosphorylation step, catalyzed by mTORC2 on S473, a residue within its hydrophobic motif, precipitates maximally activated AKT. S473 phosphorylation is particularly important for a subset of targets, including the forkhead box subgroup O (FOXO) transcription factors (Manning and Toker 2017).

AKT activates a multitude of downstream targets, with over 100 substrates identified to date, thereby modifying a wide array of cellular functions. The most prominent AKT targets, particularly as they relate to cancer pathogenesis and progression, include the TSC1/2 complex, BAD, caspase 9, various FOXO proteins, GSK3β, and MDM2. AKT inhibits the proapoptotic factor BAD, the FOXO transcription factors, which regulate expression of genes involved in apoptosis, cell-cycle progression, metabolism, and oxidative stress programs, and GSK3β, a constitutively active kinase that acts as a negative

regulator in the hormonal control of glucose homeostasis, WNT signaling, transcription factor expression, and microtubule control. AKT also increases cytoplasmic availability of MDM2, the negative regulator of p53, and phosphorylates the apoptotic factor caspase 9, reducing its apoptotic activity. Collectively, these modulations promote cell growth, proliferation, and survival (Danielsen et al. 2015, Manning and Toker 2017).

By inhibiting the TSC1/2 complex, AKT leads to the activation of mTORC1. Specifically, AKT phosphorylates and inactivates TSC2, which suppresses the activity of RAS homologue enriched in brain (RHEB)-GTPase, an activator of mTORC1. AKT can also directly activate mTORC1 through phosphorylation of PRAS40, a component of the mTORC1 complex. mTORC1 phosphorylates numerous substrates that promote anabolic metabolism to support cell growth and proliferation (Memmott and Dennis 2009). mTOR will be discussed in more detail in the following section. Briefly, the mTORC1 substrate p70S6 kinase 1 (S6K1) contributes to metabolic reprogramming by increasing glycolysis, as well as protein, lipid, and nucleotide biosynthesis. Phosphorylation of eukaryotic initiation factor-4E (eIF4E)-binding protein (4EBP) by mTORC1 inhibits its binding to eIF4E, allowing the latter to assemble with eIF4G and eIF4A to form the active, cap-binding translation initiation complex eIF4F (Musa et al. 2016, Qin et al. 2016).

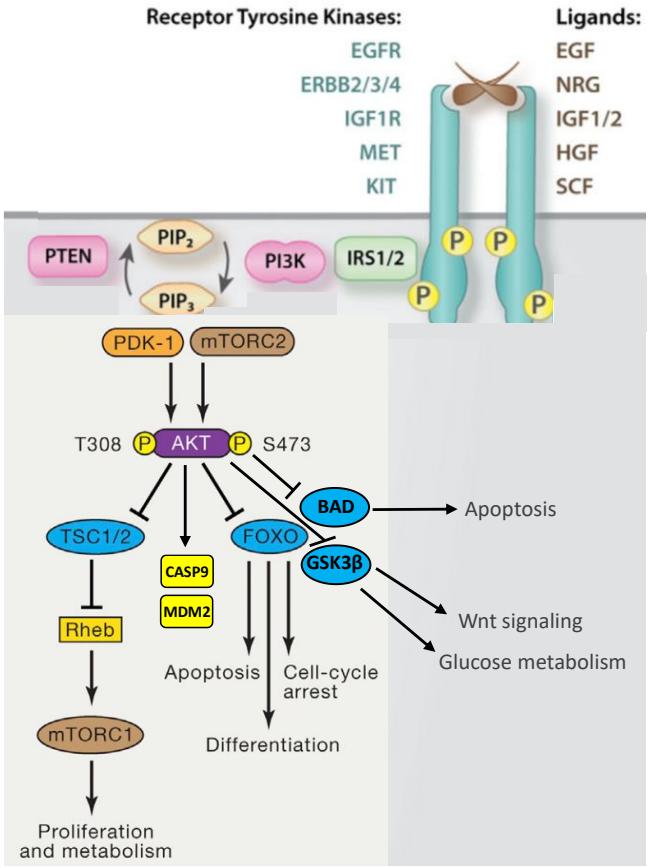

Figure 1.6 The PI3K-AKT-mTOR Signaling Pathway.

Modified from Fruman, et al. *Cell*. (2017) and Danielsen et al. *Biochim Biophys Acta*. (2015)

In normal cells, PIP3 activation is transient, and appropriately tempered through rapid metabolism by lipid phosphatases. The tumor suppressor phosphatase and tensin homolog (PTEN) acts as a negative regulator for PI3K, terminating signaling via removal of the 3'-phosphate from PIP3, yielding PIP2. Two other phosphatases, PHLPP1/2 and PP2A, dephosphorylate AKT at S473 and T308, respectively. These factors work in concert to counteract the action of PI3K, balancing pathway activity. Activated mTORC1 also generates powerful negative feedback regulation of growth factor receptor signaling,

notably towards insulin growth factor 1 receptor (IGF1R), by placing multiple inhibitory phosphorylation marks on insulin receptor substrate 1 (IRS1), both directly and through S6K. mTORC1 also directly phosphorylates and activates growth factor receptor-bound protein 10 (GRB10), a negative regulator of insulin/IGF1 signaling. Thus, mTORC1 downregulates PI3K signaling to dampen mTORC2 activity. S6K also phosphorylates Rictor on T1135 and mSin1 on T86/T398, destabilizing mTORC2 (Fruman et al. 2017, Manning and Toker 2017). PI3K activation also increases the expression of PTEN through mTOR/4EBP1-dependent control of its translation, thereby limiting the duration of the signal and the degree of pathway output (Mukherjee et al. 2021).

mTOR

mTOR is a serine/threonine kinase belonging to the PI3K-related protein kinase (PIKK) family. As its name implies, mTOR was identified as a target of Rapamycin, an antifungal produced by the bacterium *Streptomyces hygroscopicus*. Rapamycin binds to FK506-binding protein of 12 kDa (FKBP12) and interferes with the FKBP12-Rapamycin binding (FRB) domain of mTOR. In mammalian cells, mTOR nucleates two protein complexes – mTOR complex 1 (mTORC1) and 2 (mTORC2) – each with distinct inputs and outputs (**Figure 1.7A**). Shared among these complexes are mLST8 (mammalian lethal with Sec13 protein 8, also known as GβL) and DEPTOR (Dishevelled, Egl-10, and Pleckstrin [DEP] domain containing mTOR interacting protein). Unique to mTORC1 is Raptor (regulatory protein associated with mTOR) and PRAS40 (proline-rich AKT substrate of 40 kDa) (**Figure 1.7B**), while the exclusive components of mTORC2 are Rictor (Rapamycin insensitive companion of mTOR), mSin1 (mammalian stress-activated

protein kinase [SAPK] interacting protein 1), which contains the PH domain responsible for PIP3 binding and subsequent activation, and Protor1/2 (protein observed with rictor-1/2) (**Figure 1.7C**) (Yang et al. 2013, Caron et al. 2015, Liu et al. 2015, Saxton and Sabatini 2017).

Raptor facilitates substrate recruitment to mTORC1 by binding to the TOR signaling (TOS) motif found on several canonical mTORC1 substrates, and it's also required for the appropriate subcellular localization of mTORC1 (Hara et al. 2002, Kim et al. 2002). mLST8 associates with the catalytic domain of mTORC1, likely playing a role in the stabilization of the kinase activation loop. DEPTOR is an inhibitory subunit that suppresses the activity of both complexes and promotes growth factor signaling by blocking the negative feedback loops from mTOR to PI3K (Caron et al., 2015; Saxton and Sabatini, 2017). PRAS40 is another inhibitory subunit of mTORC1. The role of Rictor in mTORC2 has not been fully elucidated, but it likely serves a similar role to Raptor in this complex, though the two proteins themselves are not related. mSin1 and Protor-1/2 are regulatory subunits. Although the composition of mTOR containing complexes varies across organisms, mTOR kinase itself is a highly conserved regulator of anabolic metabolism in eukaryotes (Saxton and Sabatini 2017).

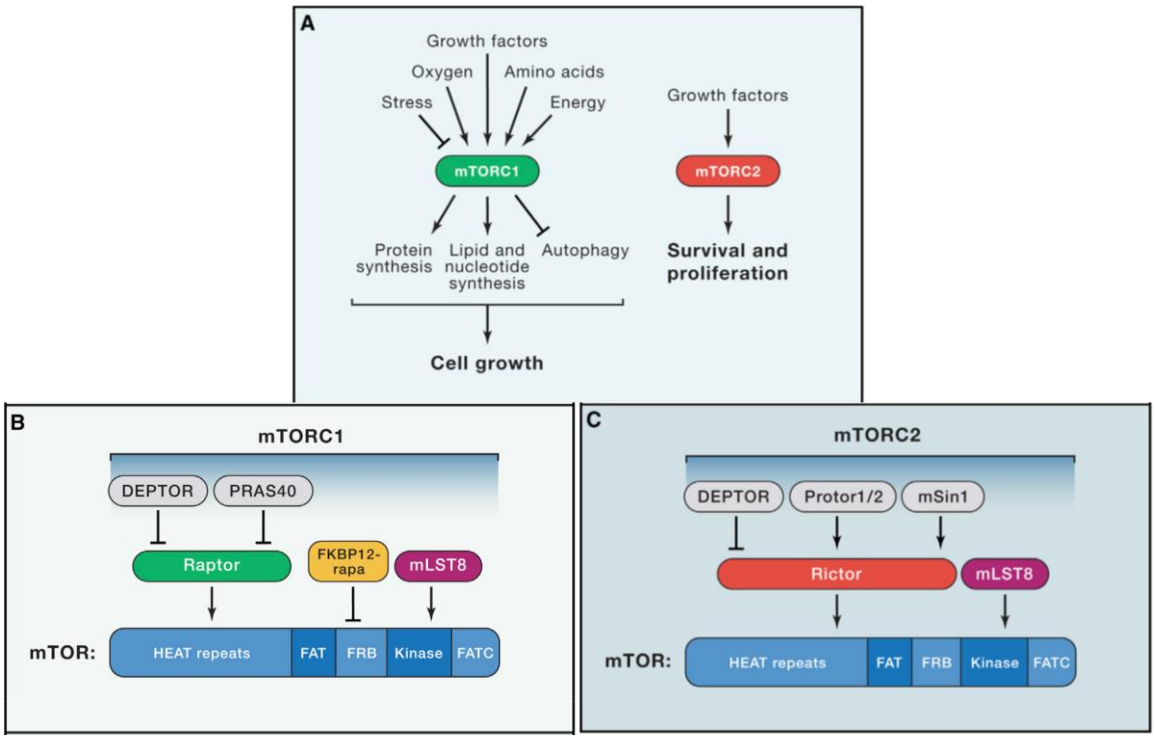

Figure 1.7 Upstream Inputs and Downstream Outputs of mTORC1/2 and the Molecular Components Constituting Each Complex.

(A) Stimulatory inputs and regulatory outputs of mTORC1 and mTORC2. **(B)** mTORC1 subunits and respective binding sites on mTOR. **(C)** mTORC2 subunits and respective binding sites on mTOR.

Modified from Saxton and Sabatini. *Cell*. (2020)

Role in Physiology

Cell growth and proliferation necessitates production of proteins, lipids, and nucleotides, as well as suppression of catabolic pathways such as autophagy. mTORC1 plays a central role in regulating these processes, thereby controlling the balance between catabolism and anabolism, integrating signals from growth factors, amino acids, energy levels, stress, and oxygen to regulate protein synthesis, lipid metabolism, lysosome and mitochondrial biogenesis, energy metabolism, and autophagy (Caron et al. 2015). The

major upstream regulatory inputs of mTORC1 are schematized in **Figure 1.8**, along with the primary downstream targets it phosphorylates.

Under nutrient replete conditions, mTORC1 promotes protein synthesis through two key effectors – S6K1 and 4EBP. mTORC1 directly phosphorylates S6K1 at T389, enabling its ensuing phosphorylation and activation by PDK1. S6K1 subsequently phosphorylates and activates several substrates that promote mRNA translation initiation, including eIF4B, a positive regulator of the eIF4F complex (Holz et al. 2005). It also promotes the degradation of programmed cell death 4 (PDCD4), an inhibitor of eIF4B, and enhances the translation efficiency of spliced mRNAs via its interaction with SKAR, a component of exon-junction complexes (Moustafa-Kamal et al. 2020). 4EBP inhibits translation by binding and sequestering eIF4E to prevent assembly of the eIF4F complex, with phosphorylation by mTORC1 relieving this inhibition (Battaglioni et al. 2022). mTORC1 phosphorylates 4EBP1 at T37/46, T70, and S65. T37/46 and T70 are high quality substrates and are thought to mediate priming of 4EBP1 for S65 phosphorylation, which regulates EIF4E binding directly (Roux and Topisirovic 2018).

Lipid synthesis in response to energy-rich conditions is a highly conserved, evolutionary process. In mammalian cells, the elevation in circulating amino acids and insulin following food intake drives the synthesis of phospholipids and sterols, which growing cells require for new membrane formation and expansion. mTORC1 plays a central role in promoting *de novo* lipid biogenesis through the translational regulation of many lipogenic genes. One key family involved in lipid synthesis is the sterol responsive element binding proteins (SREBPs). SREBPs are basic helix-loop-helix leucine zipper transcription factors that regulate lipid homeostasis by controlling the expression of

metabolic genes involved in fatty acid and cholesterol biosynthesis (Caron et al. 2015). While SREBP1 is canonically activated by response to low sterol levels, mTORC1 signaling can also activate SREBP1 independently through an S6K1-dependent mechanism, as well as by phosphorylation of Lipin1, which inhibits SREBP1 in the absence of mTORC1 signaling (Peterson et al. 2011).

mTORC1 also promotes the synthesis of nucleotides necessary for DNA replication and ribosome biogenesis by increasing ATF-dependent expression of MTHFD2, a key component of the mitochondrial tetrahydrofolate cycle that provides one carbon units for purine synthesis. S6K1 also activates carbamoyl-phosphate synthetase (CAD), a critical component of the *de novo* pyrimidine synthesis pathway (Ben-Sahra et al. 2013, Ben-Sahra et al. 2016, Wu et al. 2022). Regarding glucose metabolism, mTORC1 promotes a shift from oxidative phosphorylation to glycolysis, which possibly facilitates the incorporation of nutrients into new biomass. Additionally, mTORC1 increases the translation of the transcription factor HIF1α, which drives the expression of several glycolytic enzymes like phosphofructokinase kinase (PFK). SREBP can also increase flux through the oxidative pentose phosphate pathway (PPP), which utilizes carbons from glucose to generate NADPH and other intermediary metabolites needed for proliferation and growth (Saxton and Sabatini 2017).

Suppression of protein catabolism, particularly autophagy, under nutrient rich conditions is another primary role of mTORC1 in facilitating cellular growth and proliferation. Formation of the autophagosome is initiated by the kinase ULK1, which, upon activation by the fundamental autophagy regulator AMP-activated protein kinase (AMPK), forms a complex with ATG13, FIP2000, and ATG101. mTORC1

phosphorylation of ULK1 prevents its activation by AMPK (Kim et al. 2011). In the fed state, mTORC1 suppresses the use of extracellular nutrients obtained via micropinocytosis (Palm et al. 2015, Palm and Thompson 2017). mTORC1 also regulates autophagy in part by phosphorylating and inhibiting the nuclear translocation of the transcription factor EB (TFEB), which drives the expression of genes for lysosomal biogenesis and the autophagy machinery (Martina et al. 2012). The ubiquitin-proteasome system (UPS), responsible for the majority of protein turnover in human cells, is another catabolic pathway that's regulated by mTORC1, although the precise mechanisms of this regulation remain to be elucidated. Through this pathway, proteins are selectively targeted for degradation by the 20S proteasome following covalent ubiquitin modification (Saxton and Sabatini 2017).

Fine-tune sensing of the environment is a fundamental requirement for the homeostatic maintenance of catabolic and anabolic processes. Hence, mTORC1 is subject to a plethora of regulatory environmental cues. mTORC1 activation is complex, and is thought to require a two-step mechanism, whereby amino acids first prime activation, followed by maximal induction by growth factors (Menon et al. 2014, Dibble and Cantley 2015, Saxton and Sabatini 2017). mTORC1 senses both glucose and amino acids, both of which must be in abundance for full activation. The mechanism by which glucose activates mTORC1 remains elusive, but is explained partly by the RAG GTPases, and AMPK (Peng et al. 2014). Growth factors activate mTORC1 via the PI3K-AKT-TSC axis, discussed in the preceding section. Amino acid dependent mTORC1 activation involves lysosomal and cytoplasmic signaling pathways (Hara et al. 1998, Dyachok et al. 2016).

Nutrient availability is sensed by mTORC1 through the small GTPases RAG-A, RAG-B, RAG-C, and RAG-D, which bind to Ragulator, a pentameric complex on the

surface of the lysosome. The RAGs form heterodimers – RAG-A or RAG-B with RAG-C or RAG-D – with the active configuration constituting GTP-bound RAG-A/RAG-B with GDP-bound RAG-C/RAG-D. This arrangement recruits mTORC1 to the lysosome where it can be activated by RHEB. GTP-bound RHEB allosterically activates mTORC1 by binding a tripartite surface of two HEAT repeats and the FAT domain in mTOR (Sancak et al. 2010, Bar-Peled et al. 2013). RAG-C/RAG-D is activated by the folliculin complex, composed of FLCN and the GAP activity inclusive factors FNIP1 or FNIP2, while RAG-A/RAG-B is activated upon suppression of its direct upstream inhibitor GAP toward RAGs (GATOR1), a three-protein complex. GATOR1 is inhibited by GATOR2, a complex of five proteins, which is negatively controlled by the amino acid sensors SESTRIN2 and CASTOR1.

In nutrient deplete conditions, SESTRIN2 and CASTOR1 sequester GATOR2, preventing its inhibition of GATOR1. In nutrient rich conditions, arginine binds CASTRO1, and leucine binds SESTRIN2, resulting in the release of GATOR2 and its subsequent inhibition of GATOR1 (Chantranupong et al. 2016, Wolfson et al. 2016). More recently, SAR1B was demonstrated to work in concert with SESTRIN2 in leucin sensing and GATOR2 regulation. While SESTRIN2 binds leucine with low affinity, SAR1B binds with high affinity, thus requiring a lower concentration for the release of GATOR2. KICKSTOR, a four-protein complex, anchors GATOR1 to the lysosome, mediating its inhibition of RAG-A/B and, by extension, mTORC1. SAMTOR, an S-adenosylmethionine (SAM) sensor, is yet another interacting partner of GATOR1, and indirectly senses methionine availability via SAM. High levels of methionine increases SAM levels, resulting in dissociation of SAMTOR from GATOR1, leading to GATOR1 inactivation.

Finally, α-ketoglutarate, produced by glutaminolysis, also regulates RAG activity by promoting RAG-B GTP loading and consequently promoting mTORC1 localization to the lysosome (Battaglioni et al. 2022).

AMPK senses the energy state of the cell and inhibits mTORC1 when energy is diminished. Low ATP levels increase the intracellular AMP:ATP and ADP:ATP ratios, provoking the allosteric activation of AMPK. AMPK subsequently restores ATP production by promoting glucose uptake and increasing β-oxidation, and it also activates ULK1 to promote autophagy. Thus, AMPK and mTORC1 are mutually antagonistic. Under energy stress, AMPK phosphorylates TSC2 at T1271 and S1387, resulting in TSC GAP-mediated suppression of RHEB and, in turn, mTORC1. AMPK also directly phosphorylates Raptor on S722 and S792 to inhibit mTORC1. Conversely, mTORC1 directly phosphorylates AMPK catalytic subunit α1 (S347) and α2 (S345, S377) that diminishes T172 phosphorylation in the AMPK activation loop, limiting its activity (Battaglioni et al. 2022). AMPK and mTOR also directly phosphorylate ULK1. Under glucose starvation, AMPK promotes autophagy by directly activating ULK1 through phosphorylation of S317 and S777. Under nutrient sufficiency, high mTOR activity prevents ULK1 activation by phosphorylating ULK1 at position S757, thereby disrupting the interaction between ULK1 and AMPK (Kim et al. 2011).

mTORC2 integrates signals from growth factors to regulate cell survival, metabolism, and cytoskeletal organization (**Figure 1.8**). Its most recognized substrates are the AGC protein kinases, which include AKT, SGK1, and PKC, and mTORC2 cooperates with PDK1 to fully activate these proteins. For example, AKT is phosphorylated by mTORC2 at S473 and PDK1 at T308 (Rodrik-Outmezguine et al. 2011, Manning and

Toker 2017). Among the most well-defined functions of AKT is insulin dependent glucose uptake, which heavily relies on mTORC2 (Hagiwara et al., 2012; Yuan et al., 2012). While all AKT isoforms have been implicated in glucose uptake, AKT2 is the dominant regulator of this process. AKT2 phosphorylation of AS160, a regulator of GLUT translocation, mobilizes GLUT4 containing vesicles to the membrane (Manning and Toker 2017). The events of AKT activation by mTORC2 are described in the preceding section.

The PKC family can be divided into three groups – the conventional PKCs (c-PKCs α, β, and γ), the novel PKCs (n-PKCs δ, ε, η, θ, and μ), and the atypical PKCs (a-PKCs ι and ζ). While PKCα was the first mTORC2 substrate to be identified, it's recently been shown to phosphorylate other members of the PKC family, all of which play a role in cytoskeletal reorganization and migration. mTORC2 phosphorylation of PKCα and SGK1 leads to their activation, with the former regulating actin polymerization, and the later involved in ion transport and cell survival (Brunet et al. 2001, Mikosz et al. 2001, Liu et al. 2010, Fu and Hall 2020).

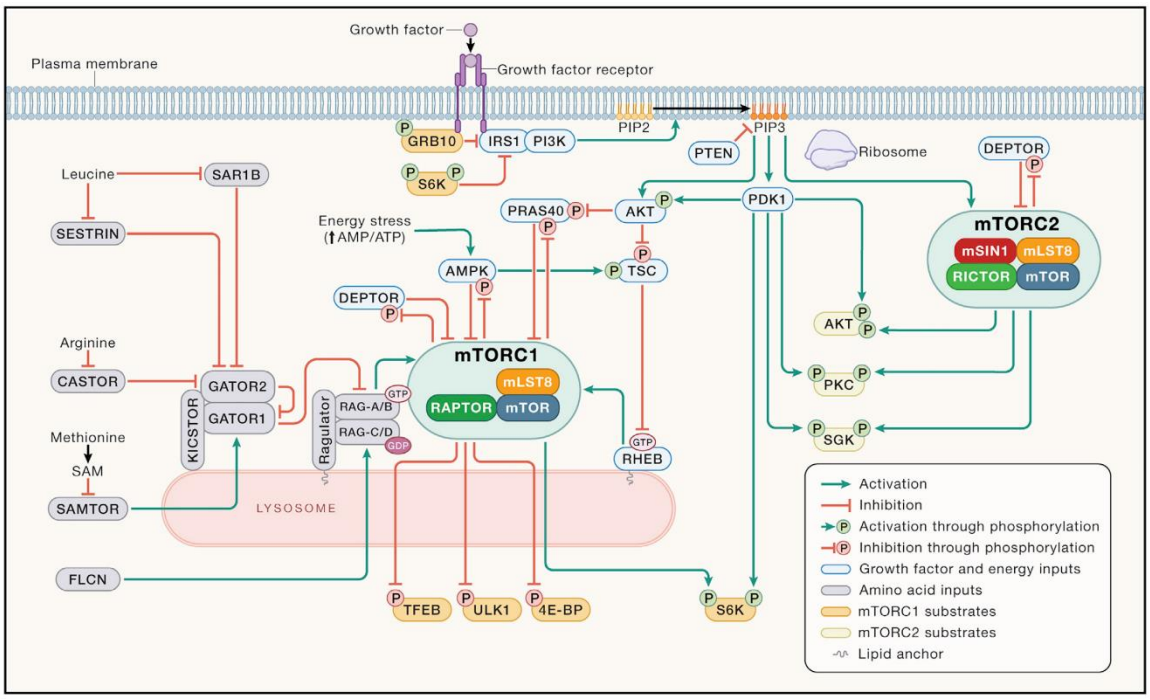

Figure 1.8 The mTORC1/2 Signaling Network.

From Battaglioni et al. *Cell*. (2022)

Role in Cancer

mTORC1 functions as a downstream effector for many frequently mutated oncogenic pathways, including the RAS/ERK and PI3K/AKT signaling cascades, resulting in mTORC1 hyperactivation in a large percentage of human cancers. Furthermore, the common tumor suppressor genes TP53 and LKB1, which are frequently inactivated or deleted in cancer, serve as negative regulators of mTORC1 upstream of TSC1 and TSC2, which are also tumor suppressors. Several components of the nutrient sensing input to mTORC1 have also been implicated in cancer progression. Among them are the three subunits of the GATOR1 complex, which are frequently mutated with low frequency in

glioblastoma, and RAG-C, which is mutated in about 18% of follicular lymphomas. mTORC2 signaling is also implicated in cancer, largely stemming from its role in activating AKT, which drives proliferative and survival processes. Mutations in mTOR itself are observed in about 3% of cancers (cBioPortal), consistent with a role for this kinase in promoting tumorigenesis (Saxton and Sabatini 2017).

Therapeutic Targeting

Dose-limiting toxicities have been a major barrier to PI3K, AKT, and mTOR inhibitors in the clinic, impeding the effective dose at which many of these agents achieve their most potent antitumor activity. The first mTOR inhibitors approved for use in cancer were a class of Rapamycin derivatives termed rapalogs (first generation mTOR inhibitors) which, like Rapamycin, bind to the FRB domain of mTOR to allosterically inhibit phosphorylation of S6K1, while weakly suppressing 4EBP phosphorylation, with negligible effects on mTORC2. The rapalog temsirolimus was approved for treatment of advanced renal cell carcinoma (RCC) in 2007, followed by everolimus in 2016 for the treatment of advanced endocrine gastrointestinal and lung cancers, and $ER^+/HER2^-$ breast tumors. Despite promising data in preclinical cancer models, rapalogs have only demonstrated modest antitumor activity in patients (Ali et al. 2022). This outcome can be explained, at least in part, by the allosteric nature of these agents, which block the phosphorylation of only a subset of mTORC1 substrates, and the modest suppression of 4EBP phosphorylation. While many mTORC1 regulated processes likely play a role in tumorigenesis, the translational program initiated by 4EBP phosphorylation is perhaps the most critical. Consistent with this, a variety of ERK- and AKT-driven cancer cell lines are

dependent on 4EBP phosphorylation, and the ratio of 4EBP to eIF4E expression correlates well with their sensitivity to mTOR inhibitors (Saxton and Sabatini 2017).

To address the primary limitation of rapalogs in substrate suppression, a subsequent class of mTOR inhibitors were developed. Termed pan-mTOR inhibitors (second generation), these agents target the catalytic site (orthosteric) and compete with ATP, precipitating powerful inhibition of mTORC1 and mTORC2 substrates. Despite a more impressive profile in preclinical models compared to rapalogs, the clinical activity of these inhibitors is marginal. The lack of achievable therapeutic efficacy can be attributed to several reasons. Inhibiting mTORC1 relieves its feedback suppression on a number of upstream targets, such as IRS1, provoking reactivation of AKT, which boosts the proliferative and survival networks AKT mediates. mTORC1 suppression can also induce autophagy, further promoting cancer cell survival under this therapeutic pressure. (Ali et al. 2022, Mao et al. 2022).

Hyperglycemia is a common on target side effect of AKT inhibition. Insulin stimulation activates AKT, promoting glucose uptake and storage as glycogen. When AKT is inhibited – either directly or through suppression of its activators such as PI3K or mTORC2 – insulin mediated glucose uptake and storage decreases, leading to an increase in blood sugar that can result in hyperglycemia if levels exceed a certain threshold (Li et al. 2018, Drullinsky and Hurvitz 2020). Furthermore, inhibiting AKT relieves feedback inhibition of RTK expression and activity, which can contribute to adaptive resistance of tumor cells to therapy (Chandarlapaty et al. 2011). mTOR mutations that increase the catalytic activity of the kinase dampen the efficacy of these inhibitors, and patients harboring these alterations will most likely have intrinsic resistance to these agents.

Notably, since mTOR is essential to the maintenance of normal cellular function, complete inhibition would be inimical to healthy cells, thus the therapeutic window is narrowed (Ali et al. 2022, Mao et al. 2022).

To address the issues of the second-generation, another class of mTOR inhibitors was developed by Shokat and colleagues. This third generation covalently links Rapamycin and the kinase inhibitor MLN0128, permitting concurrent suppression of allosteric and orthosteric sites. Termed "bi-steric" inhibitors, RapaLink-1, a model of this class, inhibits mTOR activity more potently than other mTOR kinase inhibitors, with modest selectivity for mTORC1 over mTORC2 (three- to four-fold) (Rodrik-Outmezguine et al. 2016, Fan et al. 2017, Kuroshima et al. 2020).

Seeking to further enhance the selectivity for mTORC1 over mTORC2 to avoid the drawbacks of AKT inhibition, while also enhancing suppression of 4EBP1 phosphorylation, a new series of mTORC1 bi-steric compounds were recently developed by Lee et. al. The Rapamycin-FKBP12 binary complex preferentially binds to the FRB domain in mTORC1, as the Rictor subunit of mTORC2 partially occludes this domain. Hence, the suppressive activity of RapaLink-1 towards mTORC2 is largely driven by its kinase inhibitor constituent. Modifications made to the Rapamycin core, covalent linker, and linker handle, as well as utilization of MLN0128 and a less potent kinas inhibitor analog, PP24, yielded several compounds that demonstrate more than 30-fold selectivity for mTORC1 over mTORC2, and effectively suppress 4EBP1 phosphorylation. Importantly, these mTORC1-selective inhibitors do not suppress mTORC2, and hence do not inhibit AKT S473 phosphorylation, relieve AKT-dependent feedback inhibition of RTKs *in vitro*, or induce hyperglycemia *in vivo* at doses that suppress mTORC1 signaling.

Given their enhanced specificity, these agents may also have a wider therapeutic index (Lee et al. 2021).

Crosstalk between the RAS/ERK and PI3K/AKT/mTOR Pathways

The RAS/ERK and PI3K/AKT/mTOR pathways exhibit considerable overlap and regulatory crosstalk. Many of the agonists involved in RAS/ERK activation also stimulate PI3K/AKT/mTOR signaling. However, each pathway exhibits a different degree of activation intensity and duration stemming from variability in the amount of agonist present, the expression and cell surface localization of cognate receptors, the expression of receptor family members and various docking proteins, and the extent of feedback loops. For example, phorbol 12-myristate 13-acetate (PMA) is generally a strong activator of the RAS/ERK pathway, while insulin and IGF1 are powerful mediators of PI3K/AKT/mTOR signaling. In the other pathway, these factors are weaker activators (Ray and Sturgill 1987, Hoshi et al. 1988, Boulton et al. 1990, Boulton et al. 1991, Mendoza et al. 2011).

The RAS/ERK and PI3K/AKT/mTOR pathways negatively regulate each other at several defined points. For example, activated ERK phosphorylates several sites on GAB1, inhibiting its ability to recruit PI3K to EGFR (Lehr et al. 2004). Strong IGF1R signaling can precipitate AKT phosphorylation of RAF inhibitory sites in the RAF N-terminus. In response to cAMP agonists, PKA, another AGC kinase family member, phosphorylates RAF at S259/S365. 14-3-3 dimers bind to this site and sequester the auto-inhibited RAF in the cytosol, leading to downregulation of ERK activity. These inhibitory phosphorylation

marks are removed by PP1 and/or PP2A during mitogen-stimulated RAF activation (Zimmermann and Moelling 1999, Guan et al. 2000).

The MEK/ERK and PI3K/AKT/mTOR pathways also positively regulate each other at several defined points. Strong and sustained ERK activation (e.g., by EGF, activating RAS alterations, etc.) can induce ERK- and RSK-mediated phosphorylation of TSC2 and Raptor. Although the sites on the TSC complex phosphorylated by ERK and RSK are different from those utilized by AKT, the function is nevertheless the same, thus promoting mTORC1 activation in a PI3K-independent fashion. ERK and PI3K signaling also converge on several downstream effectors involved in survival, proliferation, metabolism, and motility, including the FOXO and c-MYC transcription factors, BAD, and GSK3β (Mendoza et al. 2011). She et al. demonstrated that RAS/ERK and PI3K/AKT/mTOR signaling converge on 4E-BP1 to regulate cap-dependent translation, abrogating tumor addiction to one pathway (She et al. 2010). Several groups have also demonstrated that PI3K can function as an upstream activator of RAS and RAF (Duckworth and Cantley 1997, Wennström and Downward 1999, Yart et al. 2001, Moelling et al. 2002, Sasaki et al. 2007, Zahedi et al. 2011, Will et al. 2014).

The crosstalk and convergence between the RAS/ERK and PI3K/AKT/mTOR signaling axes underscores the gravity of this interplay in mediating tumor fitness, and the complexity of therapeutic targeting when inhibiting a node in one pathway can lead to the activation of one or more factors in a parallel network, compounded by the relief of feedback inhibition that can reactivate upstream elements within the pathway itself.

Regulated Cell Death Mechanisms

Regulated cell death (RCD) describes the set of genetically encoded mechanisms for the targeted elimination of superfluous, irreversibly damaged, and/or potentially harmful cells, a fundamental necessity of multicellular life forms for maintaining organismal homeostasis in both physiological and pathological settings. These mechanisms rely on dedicated molecular machinery, and therefore can be modulated (i.e., delayed or accelerated) by pharmacological or genetic interventions. Mammalian cells exposed to perturbations in their intracellular or extracellular microenvironment can activate one of many modes of RCD in a bid to recover or be eliminated (**Figure 1.9**). When detrimental insults are too intense or prolonged for adaptative responses to cope with the stress and restore cellular homeostasis, terminal effectors complete the death process (Galluzzi et al. 2018).

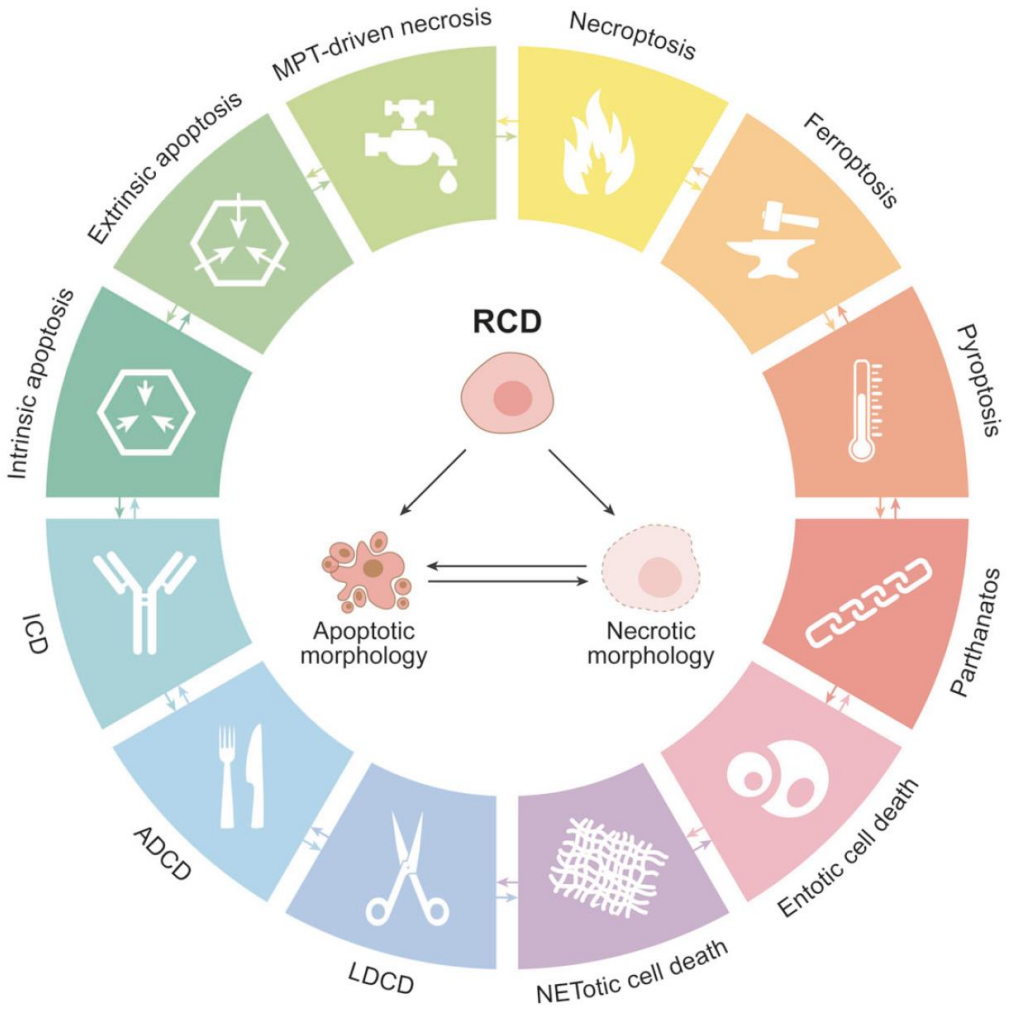

Figure 1.9 Major Mechanisms of Regulated Cell Death (RCD).

ADCD: autophagy-dependent cell death, ICD: immunogenic cell death,

LDCD: lysosome-dependent cell death, MPT: mitochondrial permeability transition.

From Galluzzi et al. *Cell Death Differ.* (2018)

The macroscopic morphological alterations accompanying cell death, along with the mechanisms whereby dead cells and their fragments are cleared, have historically been used to classify cell death into three different forms. The first is type I cell death or apoptosis, characterized by cytoplasmic shrinkage, chromatin condensation (pyknosis), nuclear fragmentation (karyorrhexis), and plasma membrane blebbing. Apoptosis culminates with the formation of intact small vesicles, termed apoptotic bodies, that are efficiently taken up by neighboring cells with phagocytic activity and degraded within lysosomes. The second is type II cell death or autophagy, manifesting with extensive cytoplasmic vacuolization and likewise terminating with phagocytic uptake and consequent lysosomal degradation. The third is type III cell death or necrosis, which does not display distinctive features of apoptosis or autophagy, with the disposal of cell corpses proceeding in the absence of obvious phagocytic or lysosomal involvement. Despite its multiple limitations and caveats, this morphological classification is still extensively employed by researchers (Galluzzi et al. 2018).

There is considerable overlap and interconnectivity in the underlying molecular mechanisms that initiate and propagate the various forms of RCD, as well as in the morphological features and immunomodulatory profile characterizing each mode. Morphological spectrums can range from fully necrotic to fully apoptotic, while immunomodulatory profiles can run the gamut from anti-inflammatory and tolerogenic to pro-inflammatory and immunogenic (Galluzzi et al. 2018). Two forms of RCD – apoptosis and ferroptosis – are relevant to this report, and their features are described in the following sections.

Apoptosis

Since its initial report in the early 1970s, apoptosis has been the longest and most widely studied form of RCD. Apoptosis is a tightly controlled process crucial for tissue homeostasis, and the ability to avert this RCD mechanism is a hallmark of cancer cells. In mammals, apoptosis is initiated by two pathways: the intrinsic pathway, activated by a variety of microenvironmental perturbations (e.g., growth factor withdrawal, DNA damage, endoplasmic reticulum (ER) stress, reactive oxygen species (ROS) overload, replication stress, microtubular alterations, and mitotic defects), and the extrinsic pathway, activated in response to the binding of death-inducing ligands to cell-surface death receptors in response to extrinsic perturbations. These pathways converge at the mitochondrial outer membrane (MOM), where the B-cell lymphoma-2 (BCL-2) family plays a pivotal role (Willis et al. 2003, Ashkenazi et al. 2017).

The BCL-2 family, inclusive of over 20 members with either pro-apoptotic or anti-apoptotic functions, regulates apoptosis by controlling the balance of these proteins in response to perturbations. Members of the BCL-2 family are classified according to the number of conserved BCL-2 homology (BH) domains they contain. Among the anti-apoptotic members are the multi-domain (BH1-4) proteins Bcl-2, Bcl-xL (BCL-2 extra-large), Bcl-w (BCL-2 like protein 2), Mcl-1 (myeloid leukemia 1), and A1 (BCL2A1). The pro-apoptotic, BH3-only members include BID (BH3-interacting domain death agonist), BIM (BCL-2-interacting mediator of cell death), and BAD (BCL-2-associated death promoter), among others. The pro-apoptotic effectors include BAX (BCL-2-associated X protein), BAK (BCL-2 antagonist killer), and BOK (BCL-2-related ovarian killer) (Willis et al. 2003, Ashkenazi et al. 2017).

Under conditions of cellular perturbation, an increase in the level of pro-apoptotic proteins results in suppression of anti-apoptotic factors, promoting activation, and subsequent oligeromization, of BAX and BAK. This results in mitochondrial outer membrane permeabilization (MOMP) and the release of cytochrome c. Cytochrome c subsequently binds to apoptosis activating factor 1 (APAF-1) and procaspase 9, generating an intracellular 'apoptosome' that activates caspase 9. Disrupted mitochondria also produce second mitochondria-derived activator of caspase (SMAC; also known as DIABLO), which releases caspase 3 from X-linked inhibitor of apoptosis (XIAP)-mediated suppression (**Figure 1.10**). BCL-2 anti-apoptotic members hinder this pathway by sequestering the pro-apoptotic BH3-only proteins via binding to their BH3 motifs. They also inhibit BAX and BAK (Willis et al. 2003, Ashkenazi et al. 2017).

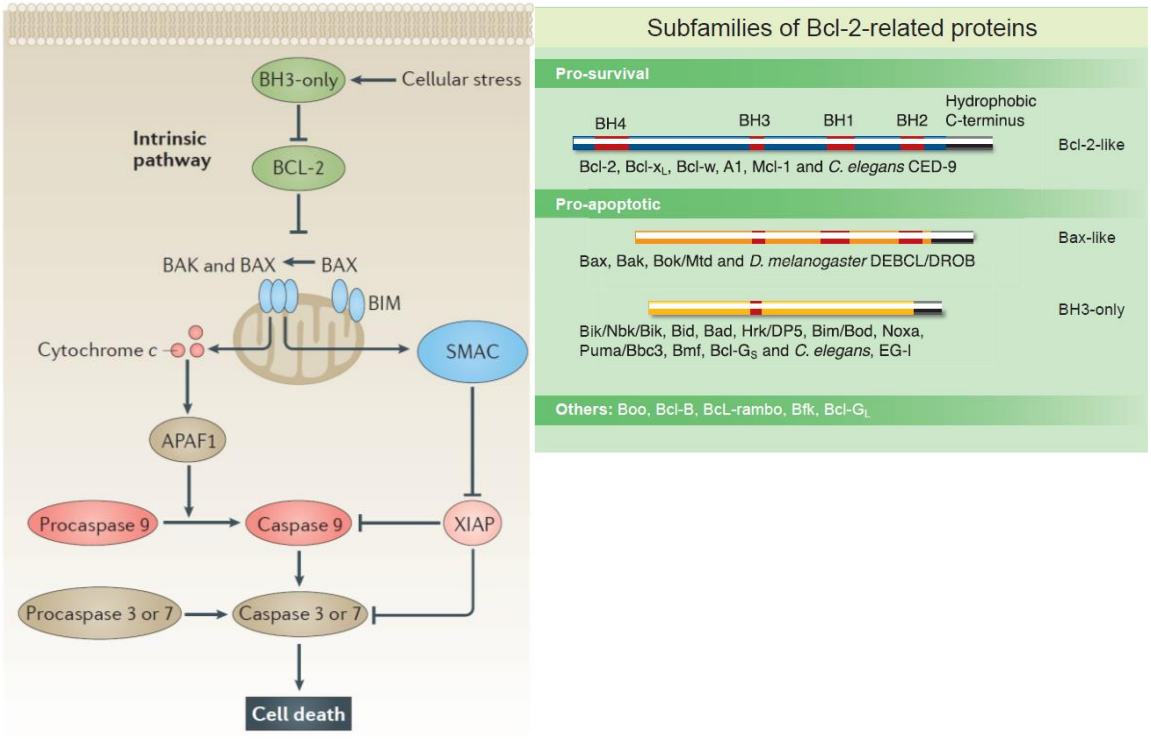

Figure 1.10 The Intrinsic Apoptosis Pathway and Regulatory BCL-2 Family Members. From Ashkenazi et al. *Nat Rev Drug Discov*. (2017) and Willis, et al. *J. Cell Sci*. (2003)

Extrinsic apoptosis is largely driven by two types of plasma membrane receptors: (1) death receptors, whose activation depends on the binding of the cognate ligand(s), and will be discussed herein, and (2) dependence receptors, whose activation occurs when levels of their specific ligand drop below a certain threshold. Death receptors are members of the tumor necrosis factor (TNF) superfamily, characterized by an intracellular death domain that's essential for transduction of the apoptotic signal. Among the death receptors are FAS (CD951/Apo-1), DR3, TNFR1, and two TNF-related apoptosis inducing ligand (TRAIL) receptors (TRAIL R1/DR4 and TRAIL R2/DR5). Death receptor ligands (death ligands) are members of the TNF family, and include FAS ligand, TNF-α, and Apo-2 ligand/TRAIL (Galluzzi et al. 2018).

Activation of death receptors results in the assembly of dynamic multiprotein complexes at the intracellular tail of the receptor, known as death-inducing signaling complexes (DISC) I and II, which operate as molecular scaffolds to predominantly regulate the activation and function of caspase 8 and, in more limited settings, caspase 10. The DISCs are constituted by an array of proteins, which can include TNF receptor associated factor 2 (TRAF2), TRAF5, c-IAP1, c-IAP2, and RIPK1, among many others. FAS and TRAIL receptors form homotrimers that are stabilized upon ligand binding. This induces a conformational change at the intracellular tails that enables the death-domain dependent association of the adapter protein FADD (Fas associated via death domain). FADD subsequently drives DISC assembly by promoting the death effector domain (DED)-dependent recruitment of caspase 8 or 10, and the apoptosis regulator FADD like apoptosis regulator (CFLAR; best known as c-FLIP). TNFR1 signaling involves association with

TADD (TNF receptor superfamily member 1A [TNFRSF1A] associated via death domain), which acts as an adaptor for DISC assembly (Schneider-Brachert et al. 2013).

The transition from the initiation to execution phase of extrinsic apoptosis can follow two routes. In type-I cells (e.g., thymocytes and mature lymphocytes), activation of initiator caspases is sufficient for robust triggering of the death machinery, yielding sufficient amounts of active effector caspases 3 and 7. In type-II cells (e.g., hepatocytes, pancreatic β cells, and a majority of cancer cells), initiator caspase induction is insufficient due to low cell surface death receptor expression, low caspase levels, and/or the presence of caspase inhibitory molecules, such as XIAP. Hence, these cells require a mitochondrial amplification loop to efficiently activate effector caspases. Caspase 8-mediated cleavage of BID generates truncated (tBID), which translocates to the outer mitochondrial membrane (OMM) and allosterically activates BAK, with subsequent steps following that of intrinsic apoptosis (**Figure 1.11**) (Schneider-Brachert et al. 2013).

Despite the connotations of its name, death receptor activation does not necessarily culminate in cell death, with some non-apoptotic pathways also regulated by these receptors. In particular, activation of TNFR1 can have diverse outcomes depending on multiple variables. Under physiologic conditions, TNFR1 signaling primarily exerts pro-inflammatory effects. This is potentially tumorigenic, and TNF has been demonstrated to promote tumor growth, proliferation, angiogenesis, invasiveness, and metastasis. Death receptor signaling can also lead to the activation of nuclear factor κB (NFκβ), which generally results in cell survival associated with a robust inflammatory response (Schneider-Brachert et al. 2013, Galluzzi et al. 2018).

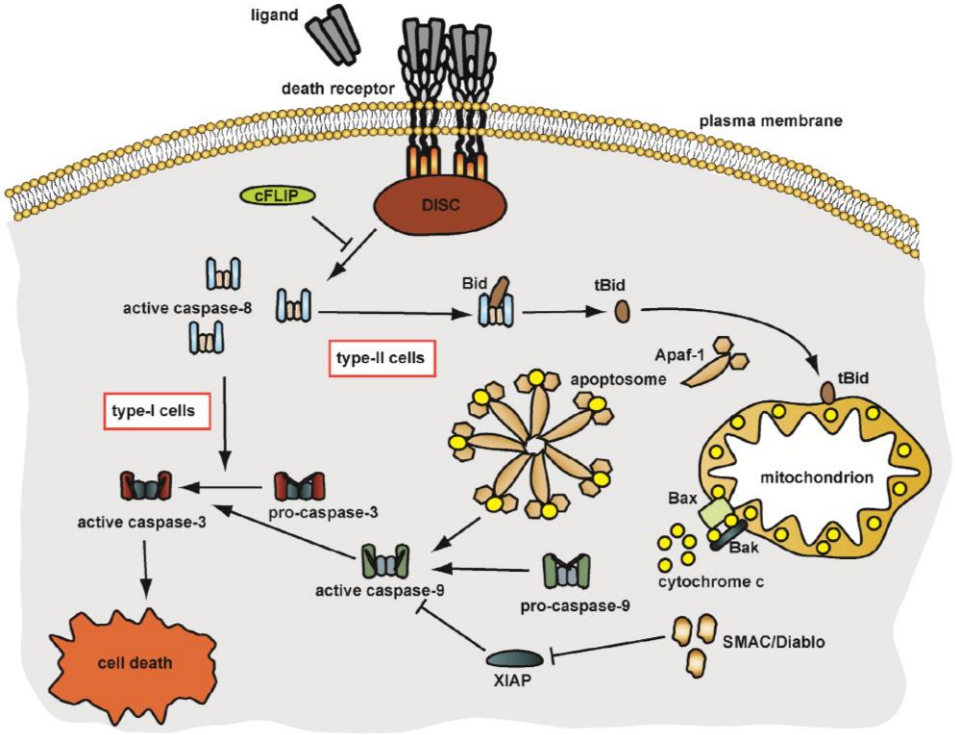

Figure 1.11 The Extrinsic Apoptosis Pathway.

From Schneider-Brachert et al. *Int J Mol Sci*. (2013)

Ferroptosis

Ferroptosis, coined by Stockwell and colleagues in 2012, is an iron-dependent form of RCD driven by excessive lipid peroxidation and subsequent plasma membrane rupture (Dixon et al. 2012). Although termed relatively recently, aspects of ferroptosis and ferroptosis-like cell death were reported much earlier. In the 1950s and 1960s, Harry Eagle and colleagues demonstrated that cysteine deprivation resulted in cell death, while endogenous cysteine synthesis yielded resistance to this death (Eagle 1955, Coltorti et al. 1956, Eagle et al. 1961). Tan and colleagues reported a type of oxidative-stress induced cell death in neuronal cells called ‘oxytosis’ (Tan et al. 2001). Before coining the term,

initial studies by Stockwell and colleagues demonstrated a type of cell death distinct from apoptosis and necroptosis when RAS mutant cells were treated with compounds discovered in synthetic lethal screens against RAS. This cell death could be rescued by iron chelators and lipophilic radical-trapping antioxidants (RTAs) (Dolma et al. 2003, Yagoda et al. 2007, Yang and Stockwell 2008). Collectively, ferroptosis is distinct from other forms of RCD, such as apoptosis, necroptosis, and autophagy, in both mechanism and morphology. While the effector molecules remain to be identified, iron accumulation, free radical production, fatty acid supply, and lipid peroxidation are critical for its induction, with the accumulation of lipid peroxides widely accepted as the lethal signal that triggers ferroptosis (Jiang et al. 2021).

The metabolic pathways involved in the metabolism of cystine and glutamate, glutathione (GSH), PUFAs, and iron modulate lipid peroxidation in cells to regulate ferroptosis (**Figure 1.12A**). As denoted by its name, ferroptotic cell death is defined by the requirement for iron. Extracellular iron is sequestered by the protein transferrin, internalized by the transferrin receptor (TfR), and released into the cytoplasm where it can participate in Fenton chemistry to generate hydroxyl radicals (Liu et al. 2020, Jiang et al. 2021). Lipid peroxidation follows the processes of initiation, propagation, and termination. In the initiation stage, lipid radicals are generated by ROS (**Figure 1.12B**), such as (HO•), that act as pro-oxidants to abstract a hydrogen molecule from the acyl chain of unsaturated fatty acid phospholipids (PLH), forming lipid radicals (PL•). Polyunsaturated fatty acid (PUFA) phospholipids (PUFA-PLs) are particularly susceptible to peroxidation by nature of their bis-allylic moieties, wherein a hydrogen atom is extracted between two carbon-carbon double bonds. In the “propagation” stage, (PL•) readily reacts with oxygen to

produce a lipid peroxyl radical (PLOO•), which slowly reacts with phospholipids (PLH) of neighboring chains to abstract a proton, forming a phospholipid hydroperoxide (PLOOH). In this reaction, (PL•) and (PLOOH) are newly formed, continuing the cycle, and eventually leading to the formation of numerous secondary products, including breakdown products of lipid peroxides (e.g., 4-hydroxynonenal [4-HNE] and malondialdehyde), along with oxidized and modified proteins. Hence, the damage is propagated throughout the membrane and, by extension, the cell, compromising cell and/or organelle membranes, and overall cellular function. Propagation continues until termination, wherein radicals are quenched by antioxidants, or by reacting with another radical. PUFAs and PUFA-PLs are also susceptible to oxidation by 12/15-lipoxygenase (LOX) enzymes, non-heme iron-dependent dioxygenases targeting PUFAs and PUFA-PLs in biological membranes (Gaschler and Stockwell 2017).

Glutathione peroxidase 4 (GPX4) and the transmembrane cystine/glutamate antiporter, commonly referred to as system x_c^- (xCT), were demonstrated to be key mechanistic regulators of ferroptosis by Stockwell and colleagues. Inhibition of GPX4 by RSL3, and system x_c^- by Erastin, agents discovered in their synthetic lethal screens against RAS mutant cells, precipitated this ferroptotic cell death (Dixon et al. 2012, Dixon et al. 2014). The selenoprotein GPX4 is the primary enzyme that catalyzes the reduction of highly reactive lipid radicals to their safe, non-reactive lipid alcohols. Mechanistically, this requires the catalytic selenocysteine residue of GPX4 and two electrons, most commonly provided by glutathione (GSH), the major endogenous cellular antioxidant, although other low molecular weight thiols and thiol proteins can serve this role. Oxidized GSH (GSSG)

is subsequently recycled via glutathione–disulfide reductase (GSR) using electrons donated by $NADPH/H^+$ (Jiang et al. 2021).

GSH is a tripeptide comprised of cysteine, glutamate, and glutamine. Cysteine is the rate-limiting substrate in GSH biosynthesis, an ATP-dependent process wherein cysteine is conjugated to glutamate and glycine. Cysteine can be taken up from the environment by a neutral amino acid transporter or synthesized from methionine via the transsulfuration pathway. Notably, cysteine can also be generated from cystine, its oxidized form. The antiporter system x_c^-, a heterodimer composed of the heavy chain xCT (encoded by SLC7A11) and the light chain 4F2 (encoded by SLC3A2), imports extracellular cystine while exporting intracellular glutamate with a 1:1 ratio. Cytosolic cystine is subsequently reduced to cysteine by glutathione (GSH) and/or thioredoxin reductase 1 (TXNRD1). Hence, by maintaining the intracellular pool of cysteine, system x_c^- plays a key role in preventing the onset of ferroptosis. When GSH levels fall below a certain threshold, GPX4 activity is severely diminished, lipid peroxides accumulate to toxic levels, and cells undergo ferroptotic death (Jiang et al. 2021).

Ferroptosis suppressor protein 1 (FSP1) was identified, or rather re-defined from apoptosis inducing factor mitochondria associated 2 (AIFM2), in 2019 by Conrad and colleagues. FSP1 rescues cells from pharmacologic and genetic (*GPX4* deletion) mechanisms that precipitate ferroptosis. Unlike GPX4, which reduces lipid peroxides to their corresponding lipid alcohols, FSP1 reduces ubiquinone, yielding ubiquinol (coenzyme Q), which can directly act as an RTA to scavenge lipid radicals in membranes, or regenerate oxidized α-Tocopherol radical to its non-radical form to mediate the same role. α-Tocopherol, a major component of vitamin E, serves as the most powerful, natural

chain-breaking antioxidant in lipid membranes (Burton and Ingold 1986, Doll et al. 2019). Additional ferroptosis-suppressive mechanisms include squalene mediated and di/tetrahydrobiopterin (BH2/BH4)-mediated inhibition of lipid peroxidation, likely by acting as endogenous RTAs. (Jiang et al., 2021).

The membrane remodeling enzymes acyl-CoA synthetase long-chain family member 4 (ACSL4) and lysophosphatidylcholine acyltransferase 3 (LPCAT3) have been recognized as important ferroptosis drivers. ACSL4 ligates PUFAs with coenzyme A, preferencing long-chain PUFAs such as arachidonic acid and adrenic acid. These products can subsequently be re-esterified into phospholipids by various LPCAT enzymes, increasing the cellular incorporation of long-chain PUFAs into lipids and, in turn, membranes. Genetic loss or pharmacological inhibition of ACSL4 leads to a dramatic shift from long-chain to short-chain PUFA and monounsaturated fatty acid (MUFA) incorporation into phospholipids, enabling ACSL4 deficient cells to proliferate in the absence of GPX4. MUFAs lack bis-allylic moieties, and hence are impervious to peroxidation. Incorporation of MUFAs into phospholipids can displace PUFAs, thereby inhibiting ferroptosis (D'Mello 2020, Liu et al. 2020, Jiang et al. 2021).

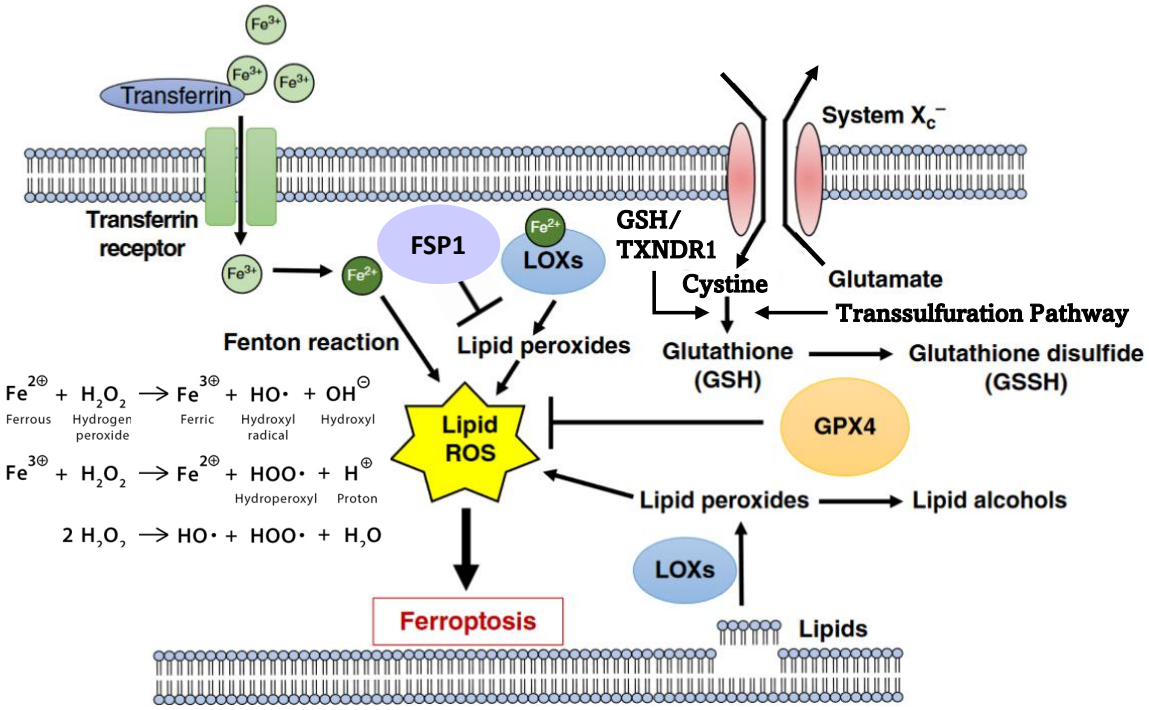

Figure 1.12 Overview of Ferroptosis.

Modified from Goodman's Medical Cell Biology, Fourth Edition, Chapter 11: Regulated Cell Death. (2020)

Thesis Outline

In the following study, we have investigated the therapeutic potential of combining KRAS G12C inhibitors with mTORC1 selective inhibitors for the treatment of KRAS G12C mutant cancers. The impetus for this study arose from clinical data revealing that current KRAS G12C inhibitors demonstrate an objective response rate approaching 40% in the most responsive patient cohort – NSCLC. Hence, rational combination strategies are required to improve efficacy. ERK and PI3K are key effectors of RAS. Although dual inhibition of these pathways has demonstrated synergistic effects in preclinical models, toxicity has hindered clinical efficacy.

With the recent advent of novel mTORC1 selective inhibitors, we hypothesized that combining these agents with KRAS G12C inhibitors would likewise yield synergistic effects, but with the added benefit of a safer toxicity profile due to restraint from suppressing AKT phosphorylation. In chapter 3, we interrogate this hypothesis by characterizing the effect these inhibitors have on the biological and functional properties of KRAS G12C mutant NSCLC and CRC models. We demonstrate that suppression of mTORC1 substrates correlates with sensitivity to KRAS G12C inhibition. mTORC1 selective inhibitors promoted KRAS G12C inhibitor mediated cell growth suppression, suppression of Cyclin D1 and pRB S807/811, and cell death induction. The combination also yielded dramatic tumor regression in NSCLC CDX and PDX models without inducing hyperglycemia.

In chapter 4, we explore the mechanisms underlying how the combination precipitates the observed cell death *in vitro* and tumor regression *in vivo*. We focus our studies largely on apoptosis and ferroptosis, given the regulatory roles RAS/ERK and

PI3K/AKT/mTOR signaling play in these modes of RCD. We demonstrate that mTORC1 inhibition enhances apoptosis induced by KRAS G12C suppression. The combination also demonstrates synergistic modulation of cell cycle regulators, intrinsic apoptosis factors, and extrinsic apoptosis factors. Furthermore, the combination suppresses key targets in the ferroptosis regulatory network such as xCT and SREBP1, leading to suppression of GSH and induction of ROS and lipid peroxidation. Curiously, liproxstatin-1, a potent inhibitor of ferroptosis, only yielded modest rescue of cell death induced by the combination, while α-tocopherol, a major component of vitamin E, led to an almost complete rescue of both cell death and growth suppression.

In chapter 5, we further investigate this α-tocopherol rescue. We demonstrate that α-tocopherol inhibits the activity of all mTOR bi-steric inhibitors assessed, rescuing/impeding p4EBP1 and pS6K suppression. These effects were not observed for several inhibitors of PI3K or AKT, nor for other inhibitors of mTOR. Furthermore, the remaining tocopherol analogues (β, δ, and γ), as well as the four tocotrienol analogues (α, β, δ, and γ) constituting vitamin E also provoke this interference, albeit with varying potency and durability. Although less durable, this α-Tocopherol interference is observed for RAS (ON) inhibitors, but not for KRAS G12C (OFF) inhibitors or evaluated inhibitors of MEK and ERK. While the mechanisms underlying this drug interference remain to be unequivocally elucidated, through several experiments we gain some insight into key features of this phenomenon.

In the final chapter, we discuss important details, clinical implications, and future directions as they relate to the current study.

Chapter 2: Materials and Methods

Mammalian Cell Culture and Reagents

NCI-H358, NCI-H2122, NCI-H2030, HCI-H1373, NCI-H1792, NCI-H23, HOP62, Calu-1, SW1573, SW837, SW1463, C106, MDA-MB-468, MCF7, T47D, LIM1215, and NCI-H508 were purchased from the American Type Culture Collection. HCC44 and SNU1411 were obtained from the Korean Cell Line Bank. LU-65 and LU-99A were obtained from the Japanese Cell Research Bank (Osaka, Japan). Endometrial cancer cell line MFE296 was purchased from Sigma-Aldrich. The PDX established endometrial cancer cell line X0007aS1 was generated from an in house PDX murine model. NCI-H358, NCI-H2122, NCI-H2030, HCI-H1373, NCI-H1792, NCI-H23, HOP62, HCC44, SW1573, LU-65, LU-99A, MDA-MB-468, MCF7, and T47D were cultured in RPMI; SW837, SW1463, and SNU1411 were cultured in DMEM/F-12; MFE296 and X0007aS1 were cultured in DMEM-F12; Calu-1 was cultured in McCoy's 5A; C106 was cultured in Iscove's modified medium.

All media were purchased from Corning, and supplemented with 4mM glutamine, 100 units/ml of penicillin and streptomycin, and 10% fetal bovine serum. All cells were maintained at 37°C in 5% CO_2. Cells were regularly screened for mycoplasma using a MycoAlert Mycoplasma Detection Kit (Lonza). AZD8055, AZD8186, BYL719, GDC0941, MK2206, MLN0128, Rapamycin, RapaLink-1, Trametinib, SCH772984, α-Tocopherol, β-Tocopherol, δ-Tocopherol, γ-Tocopherol, α-Tocotrienol, β-Tocotrienol,

δ-Tocotrienol, γ-Tocotrienol, α-Tocopherol Acetate, α-Tocotrienol Phosphate, Trolox, Vitamin A, Vitamin C, Vitamin D3, Vitamin K1, RSL3, Erastin, iFSP1, Liproxstatin-1, Z-VAD-FMK, N-acetylcysteine, and Deferoxamine mesylate were purchased from Selleck Chemicals (Houston, TX), MedChemExpress (South Brunswick Township, NJ), and/or Sigma-Aldrich (Burlington, MA). AMG510, MRTX849, MRTX1257, AZD8037, RM1, RM2, RM3, RM6, RM18, RM29, RM42, and RM44 were provided from Amgen, Mirati Therapeutics, AstraZeneca, and Revolution Medicines, respectively. Compounds were dissolved in DMSO to a final concentration of 10, 50, or 100 mmol/l and stored at –20°C.

Cell Titer Glo Determination of Cell Viability

Cell viability was determined using a CellTiter-Glo (CTG) Luminescent Cell Viability Assay Kit (Promega). Between 2000-5000 cells were plated in 96-well plates, and subsequently treated with the indicated compounds at their designated dose(s) for various times 24 hours post seeding. 50-100µl of prepared CTG reagent was added to each well. The contents of the wells were mixed on a plate shaker for 15-45 minutes, and then luminescence was measured on a SpectraMax M5 plate reader (Molecular Devices). The data was graphically displayed using GraphPad Prism 9. For GI_{50} curves, cells were treated for 72 hours, and day 0 values were subtracted from each group. The relative growth was normalized to the day 3 untreated samples. Sigmoidal growth inhibition curves were calculated using a four-parameter model in GraphPad Prism 9.

Trypan Blue Exclusion Determination of Cell Viability and Death

Cell death was measured using Trypan Blue Exclusion (Thermo Fisher Scientific). Cells were seeded at a density of $5.0e^5$-$8.0e^5$ in 6cm culture plates. The following day, cells were treated with the indicated compounds at their designated dose for 0 (day of treatment), 24, 48, and 72 hours. For measurement of cell viability, culture media from each sample was collected individually, and the plates washed once with 1ml PBS, which was also collected. Cells were detached with 1ml trypsin (incubated for 3-5 min at 37°C). Trypsinization was quenched with 2ml media, and the cell slurry was collected. Samples were centrifuged at 1200 RPM for 3 minutes, the supernatant aspirated off, and the cell pellet resuspended in 1-2ml media depending on the pellet's size. 10µl of sample was mixed 1:1 with 10µl of trypan blue, and 10µl of the mixture was loaded into separate ends of a hemacytometer slide. The slides were loaded into a Countess 3 FL hemacytometer for automatic cell counting (Invitrogen), with blue stained cells considered non-viable. Measures of total cell number, percent live cells, and percent dead cells were recorded in duplicate for each sample, and the average was taken. The data was displayed graphically using GraphPad Prism 9

Immunoblotting

Cells were lysed with RIPA buffer (Cell Signaling Technologies) supplemented with protease and phosphatase inhibitors (Pierce Chemical, Thermo Fisher Scientific). Lysates were briefly sonicated and cleared by centrifugation at 14,000 RPM for 10 minutes at 4°C. The supernatant was collected, and protein concentration was measured by BCA (Pierce).

Xenograft tumors were homogenized in SDS lysis buffer (50mM Tris-HCL pH 7.4, 10% Glycerol, 2% SDS) and boiled at 95°C for five minutes. Lysates were then briefly sonicated, boiled again for 5 minutes, and cleared by several rounds of centrifugation at 14,000rpm for 10 minutes at room temperature. The supernatant was collected, and protein concentration was determined by BCA (Pierce). The protein samples were mixed with an appropriate volume of 5 × SDS-PAGE sample buffer and incubated at 95°C for 5 minutes. Equal amounts of protein (20μg) were electrophoresed on a NuPAGE Bis-Tris protein gel (Invitrogen), and proteins transferred to nitrocellulose or PVDF membranes (Bio-Rad, Thermo Fisher Scientific). Membranes were blocked for 1 hour at room temperature with 5% milk in TBS-Tween, followed by incubation overnight with primary antibodies at 4°C. Membranes were incubated with secondary antibodies, and detected by chemiluminescence with ECL detection reagents (Thermo Fisher Scientific, Millipore). Antibodies used in this study are listed in Table 2.1. Signal was detected using iBright™ 1000 Imaging Systems (Thermo Fisher Scientific).

Annexin V-Propidium Iodide (PI) Assay

$5.0e^5$-$1e^6$ cells were seeded in 10cm culture plates and treated with DMSO, 1nM RM6, 100nM RM18, or their combination. After 72 hours, floating cells in media and adherent cells (detached by trypsinization) were collected in a single tube and stained with annexin V and propidium iodide using the FITC Annexin V Apoptosis Detection Kit I (BD Biosciences) according to the manufacturer's protocol. Data were obtained on a Cytek Aurora (Cytek) flow cytometer and analyzed with FlowJo software (version 11.2, BD Biosciences).

Apoptosis Arrays

$1.5e^6$-$3e^6$ cells were seeded in 10cm culture plates and treated with the indicated compounds at their designated dose for 24 or 72 hours. Sample lysates were assayed for cell death factors using apoptosis arrays from R&D Biosystems (Human Apoptosis Array Kit) and RayBiotech (Human Apoptosis Antibody Array C1, Human Apoptosis Signaling Pathway Array C1) according to the manufacturer's protocol.

Glutathione (GSH) Assay

Cells were seeded at a density of $5.0e^5$-$8.0e^5$ in 6cm culture plates. The following day, cells were treated with the indicated compounds at their designated dose for 48 or 72 hours. Cells were lysed in 5% Sulfosalicylic Acid provided by the Reduced Glutathione (GSH) Assay Kit (Sigma-Aldrich), supplemented with phosphatase and protease inhibitors (Pierce Chemical, Thermo Fisher Scientific). The assay was performed according to the manufacturer's protocol. Absorbance values reflecting chromophore reduction mediated by sample GSH was measured kinetically at 450nM for 60 minutes at room temperature, with 5-minute interval readings using a SpectraMax M5 plate reader (Molecular Devices). Relative GSH in each sample was calculated according to the manufacturer's protocol and plotted using GraphPad Prism 9.

Reactive Oxygen Species (ROS) Assay

Cells were seeded at a density of 2000-3000 cells/well in a 96-well clear plate. The following day, cells were treated with the indicated compounds at their designated dose for 24, 48, or 72 hours. ROS was measured using the ROS-Glo™ H2O2 Assay (Promega) according to the manufacturer's protocol. We chose this kit as H_20_2 has the longest half-life of all ROS in cultured cells, and various ROS are converted to H_2O_2 within cells. Luminescence values, reflective of the amount of H_20_2 in each sample, was measured using a SpectraMax M5 plate reader (Molecular Devices) and plotted using GraphPad Prism 9.

Lipid Peroxidation Assay

Cells were seeded at a density of $2.0e^5$ in 6-well culture plates. The following day, cells were treated with the indicated compounds at their designated dose for 48 or 72 hours. Lipid peroxidation was measured using the fluorescent reporter C-11 BODIPY from the Image-iT® Lipid Peroxidation Kit (Molecular Probes). Upon oxidation in live cells, fluorescence shifts from red to green of the phenylbutadiene segment of the fluorophore, providing a ratiometric indication of lipid peroxidation. Absorbance was measured at 581nm/565nm in the red channel, and 510nm/410nm in the green channel using a SpectraMax M5 plate reader (Molecular Devices) or by flow cytometry using Cytek Aurora (Cytek) and analyzed with FlowJo software (version 11.2, BD Biosciences). The data was plotted using GraphPad Prism 9.

Cell Imaging by Microscopy

Cells were seeded in 6cm ($5.0e^5$-$8.0e^5$) or 10cm ($1.5e^6$-$3.0e^6$) culture plates and treated with the indicated compounds at their designated dose(s) for various times. Cells were imaged by bright-field microscopy using an EVOS M500 microscope (Invitrogen). Detached, floating cells, small, rounded cells, and reduced cell number are indicators of diminshed cell viability.

Cell Death Imaging by Fluorescence Microscopy

Cells were seeded at a density of $2.5e^5$ in 6-well plates and treated with the indicated compounds at their designated dose for 48 or 72 hours. The cells were subsequently stained with Annexin V, DAPI, and Sytox Green, and imaged by fluorescence microscopy, with 10-fields of view captured for each treatment at each time point.

Xenograft Experiments

For CDX models, 6–8-week-old athymic female mice were injected subcutaneously at the flank region with 10 million cells together with matrigel (BD Biosciences). Indicated PDX models were expanded by the Memorial Sloan Kettering Cancer Center (MSKCC) Mouse Core. Once the mean tumor volume reached approximately 100-150mm^3, mice were randomized and treated with either vehicle, RM29 (80mg/kg, once a day, 5 times per week, oral gavage), RM6 (6mg/kg, once a week, intraperitoneal injection [i.p.]), or the combination of these drugs at the same monotherapy doses. Tumors were measured twice

a week using calipers and their volumes were calculated as length x width^2 x 0.5. Body weight was monitored twice a week. For the vitamin E study, mice were treated with vehicle, RM6 (3mg/kg, i.p.), vitamin E (100mg/kg or 400mg/kg, oral gavage), or the combination of these compounds at the same monotreatment doses. All animal experiments were performed according to the protocol approved by the MSKCC Animal Care and Use Committee.

Densitometry

Signal intensity of immunoblots were quantified using ImageJ (Fiji).

Statistical Analysis

Data from flow cytometry is presented as mean ± standard deviation (SD), and the tumor progression in animal studies as means ± standard error (SE), respectively. Student's t-test (two tailed) or one-way ANOVA, followed by post hoc pairwise analysis test, was performed using GraphPad Prism 9 (GraphPad Software, La Jolla, CA, USA, www.graphpad.com) as indicated in figure legends. P-value < 0.05 was considered significant. The stars in the graphs indicate significance, as detailed in the figure legends.

Table 2.1 Antibodies

RAS/ERK and PI3K/AKT/mTOR Signaling Factors		
Name	**Vendor**	**Catalogue #**
KRAS	LSBio	LS-C175665
Phospho-MEK1/2 (Ser217/221)	Cell Signaling Technologies	9154
Phospho-p44/42 MAPK (ERK1/2)	Cell Signaling Technologies	4370
p44/42 MAPK (ERK1/2)	Cell Signaling Technologies	4696
Phospho-AKT (Thr308)	Cell Signaling Technologies	2965 L
Phospho-AKT (Ser473)	Cell Signaling Technologies	4060
AKT	Cell Signaling Technologies	9272 S
Phospho-4E-BP1 (Ser65)	Cell Signaling Technologies	9451
Phospho-4E-BP1 (Thr37/46)	Cell Signaling Technologies	9459
Phospho-4E-BP1 (Thr70)	Cell Signaling Technologies	9455
4E-BP1	Cell Signaling Technologies	9452
Phospho-p70 S6 Kinase (Thr389)	Cell Signaling Technologies	9234
p70 S6 Kinase	Cell Signaling Technologies	9202L
Phospho-S6 Ribosomal Protein (Ser235/236)	Cell Signaling Technologies	4858L
Cell Cycle Regulators		
Name	**Vendor**	**Catalogue #**
CyclinD1	Cell Signaling Technologies	55506
Cyclin D2	Cell Signaling Technologies	3741S
Cyclin D3	Cell Signaling Technologies	2936S
Phospho-Rb (Ser807/811)	Cell Signaling Technologies	9308S
Survivin	Cell Signaling Technologies	2808S
Phospho-p27 Kip1 (Thr187)	Thermo Fisher	PA5-12651
p27 Kip1	Cell Signaling Technologies	2552S
Claspin	Cell Signaling Technologies	2800S

Intrinsic Apoptosis Factors		
Name	**Vendor**	**Catalogue #**
Bcl-2	Cell Signaling Technologies	4223S
Bcl-xL	Cell Signaling Technologies	2764S
Mcl-1	Cell Signaling Technologies	5453S
BID	Cell Signaling Technologies	2002S
BIM	Cell Signaling Technologies	2819S
BAX	Cell Signaling Technologies	2772S
BAK	Cell Signaling Technologies	3814S
Puma	Cell Signaling Technologies	4976S
Noxa	Cell Signaling Technologies	14766S
Phospho-Bad (Ser112)	Cell Signaling Technologies	9291S
Phospho-Bad (Ser136)	Cell Signaling Technologies	4366S
Caspase-9	Cell Signaling Technologies	9502S
Caspase-7	Cell Signaling Technologies	9492S
Caspase-3	Cell Signaling Technologies	9662S
Cleaved PARP (Asp214)	Cell Signaling Technologies	9541S
Extrinsic Apoptosis Factors		
Name	**Vendor**	**Catalogue #**
TNF-R1	Cell Signaling Technologies	3736S
Fas	Cell Signaling Technologies	4233S
TRAIL R1/DR4	Cell Signaling Technologies	42533S
TRAIL R2/DR5	Cell Signaling Technologies	8074S
Ferroptosis Regulators		
Name	**Vendor**	**Catalogue #**
Anti-SREBP-1	SantaCruz	sc-13551
Anti-SCD1	abcam	ab39969
GPX4	Cell Signaling Technologies	52455S

NRF2	Cell Signaling Technologies	12721S
KEAP1	Cell Signaling Technologies	8047S
xCT/SLC7A11	Cell Signaling Technologies	12691S
ATF-4	Cell Signaling Technologies	11815S
ETS-1	Cell Signaling Technologies	14069S
AIFM2/FSP1	Cell Signaling Technologies	24972S
NF-κB	Cell Signaling Technologies	8242S
SQSTM1/p62	Cell Signaling Technologies	5114S
FTH1	Cell Signaling Technologies	4393S
CD71	Cell Signaling Technologies	13113S
Loading Controls and Misc.		
Name	**Vendor**	**Catalogue #**
Vinculin	Cell Signaling Technologies	13901S
β-Actin (13E5)	Cell Signaling Technologies	
HO-1	Cell Signaling Technologies	5853S
HIF-1α	Cell Signaling Technologies	3716S
Phospho-Acetyl-CoA Carboxylase (Ser79)	Cell Signaling Technologies	3661L
FKBP1A/FKBP1	Cell Signaling Technologies	55104S

Chapter 3: Characterization and Combination Effects of KRAS G12C and mTORC1 Selective Inhibitors

Introduction

Activating KRAS alterations are predominantly observed in cancers of the pancreas, colon, and lung. Of the variant subtypes, G12C is the most common, accounting for 40% of all KRAS mutations, and demonstrating high prevalence in non-small cell lung cancer (NSCLC) (~11%) and colorectal cancer (CRC) (~3%) (Zuberi et al. 2020). Despite its discovery in the 1960s, for decades little progress was made in the treatment of KRAS mutant cancers, with RAS long believed to be 'undruggable' due to its smooth surface and picomolar affinity for GTP, making the design of both conventional allosteric and orthosteric inhibitors challenging. However, in 2013, the seminal report of an unrecognized pocket in the switch-II region of KRAS G12C by Shokat and colleagues led to a paradigm shift in RAS targeting, and the development of novel agents exploiting this region (Ostrem et al. 2013, Zuberi et al. 2020). In May 2021, the United States Food and Drug Administration (FDA) approved sotorasib (Lumakras™) for adult patients with NSCLC harboring a KRAS G12C mutation who have received at least one prior systemic therapy. Thus, sotorasib became the first FDA-approved therapy to directly target the KRAS oncoprotein in tumors (Kwan et al. 2022).

Initial clinical data on sotorasib (AMG510) demonstrated an objective response rate (ORR) of 32.2% (19/59 patients) in NSCLC, the most responsive patient cohort, with diminishing ORRs achieved for CRC (7.1%, 3/42 patients) and other KRAS G12C mutant tumor types (14.3%, 4/28 patients) (Hong et al. 2020). A subsequent trial focused on

NSCLC patients reported an ORR of 37.1% (46/126 patients) (Skoulidis et al. 2021). While this metric is a remarkable improvement over historical modalities for treating KRAS mutant lung cancer, the efficacy of these inhibitors is underwhelming compared to targeted therapies for NSCLC bearing other driver alterations, such as EGFR mutations and ALK translocations, wherein ORRs approach 60%-80% (Kwan et al. 2022). This data is not surprising though, as resistance to most targeted monotherapies, particularly against oncogenic proteins, is a frequent occurrence, often stemming from the outgrowth of pre-existing resistant clones, and/or the acquisition of one or more alterations that attenuate the inhibitor's efficacy, among other mechanisms that reduce the sensitivity of tumor cells to the therapeutic pressure (Jiao and Yang 2020).

Resistance to KRAS G12C inhibitors have presented as development of secondary KRAS mutations, amplification of the KRAS G12C allele, increased synthesis of other WT RAS isoforms (NRAS, HRAS), activating mutations in NRAS and BRAF, activation of RTKs through mutations and oncogenic fusions that drive signaling of WT RAS proteins, and epithelial to mesenchymal transition (EMT) (Jiao and Yang 2020). Furthermore, unlike BRAF driven melanoma and EGFR driven lung cancer that rely on continued expression of the oncogene to sustain their proliferation and survival, KRAS driven cancers exhibit differential dependencies on KRAS signaling stemming from co-occurring alterations, complex (epi)genetic abnormalities, and reliance on parallel signaling networks (Adachi et al. 2021). Hence, combination strategies are required to improve efficacy and overcome resistance mechanisms.

Targeting the PI3K/AKT/mTOR pathway in conjunction with KRAS inhibition is an attractive strategy for several reasons. First, PI3K is a well described effector of RAS,

and can serve to enhance proliferation and survival capacity of KRAS mutant cells (Simanshu et al. 2017). Second, there exists considerable interconnectivity between the RAS/ERK and PI3K/AKT/mTOR signaling networks, whereby constituents of each axis can positively and negatively regulate elements of the other pathway based on varying stimulatory, inhibitory, and environmental conditions. These networks also demonstrate convergent regulation of certain substrates, notably those involved in cell growth, proliferation, and survival (Mendoza et al. 2011). Finally, concurrent activation of the RAS/ERK and PI3K/AKT/mTOR pathways by separate alterations occurs in a significant fraction of human cancers (Millis et al. 2016). Prime examples include BRAF activating mutations with PTEN loss in melanoma (Tsao et al. 2004), BRAF and PI3K activating mutations in thyroid carcinoma (Z. Liu et al. 2008), variant EGFR expression with PTEN loss in glioblastoma (Mellinghoff et al. 2005), activating KRAS and PIK3CA mutations in CRC (Simi et al. 2008), and activating KRAS mutations with STK11 alterations/LKB1 loss in NSCLC (Cancer Genome Atlas Research Network 2014, Scheffler et al. 2019).

As predicted, dual targeting of RAS/ERK inhibitors with PI3K/AKT/mTOR pathway suppression has demonstrated remarkable efficacy in preclinical models of KRAS mutant cancers. For example, suppression of PI3K signaling abrogated adaptive resistance stemming from MAPK pathway inhibition in KRAS mutant cancers (Turke et al. 2012). Moreover, the combination of the KRAS G12C inhibitor ARS1620 with the pan PI3K inhibitor GDC0941 overcame resistance to ARS1620 monotherapy in both *in vitro* and *in vivo* models (Misale et al. 2019). Hallin et al. demonstrated enhanced efficacy with the combination of the KRAS G12C inhibitor MRTX849 with the pan-mTOR inhibitor Vistusertib (Hallin et al. 2020). While concurrent suppression of the RAS/ERK and

PI3K/AKT/mTOR networks is compelling in preclinical models, the clinical benefit of suppressing PI3K/AKT signaling has been limited due to toxicity, feedback reactivation of upstream signaling, and insufficient inhibition of the drug target (Hanker et al. 2019, Castel et al. 2021). Regarding toxicity, hyperglycemia is a common on target side effect of PI3K/AKT inhibition, resulting from AKT suppression that relieves feedback inhibition of IGF1R signaling (Bendell et al. 2012, André et al. 2019). To address these issues, we previously designed a series of mTORC1 selective inhibitors that yield potent and durable suppression of both mTOR substrates, S6K and 4EBP1, while avoiding suppression of AKT S473 phosphorylation. In breast cancer PDX models, these compounds suppressed tumor growth at doses that did not precipitate hyperglycemia (Lee et al. 2021). RMC-5552, an improved version of these mTORC1 selective inhibitors, and its preclinical *in vivo* compound RMC-6272, have likewise demonstrated remarkably potent, sustained suppression of S6K and 4EBP1, and suppression of tumor growth in preclinical *in vitro* and *in vivo* models (Burnett et al. 2023).

mTORC1 controls cell size and cap-dependent mRNA translation via phosphorylation of 4EBP1 and S6K. Phosphorylated 4EBP1 disassociates from eIF4E, allowing eIF4E to form a complex with eIF4A and eIF4G, generating the 5'-cap binding, translation competent, eIF4F complex that initiates protein synthesis of 5'-capped mRNAs (Saxton and Sabatini 2017). mTORC1 activation is regulated by both ERK and AKT through phosphorylation of the TSC1/2 complex. While the phosphorylation sites regulated by ERK and AKT differ, the result is the same – suppression of TSC1/2 complex GAP activity towards RHEB-GTPase, and subsequent activation of mTOR by RHEB (Manning et al. 2002, Potter et al. 2002, Ma et al. 2005, Ma et al. 2007). Furthermore, we

previously demonstrated that 4EBP1 is a convergent target of the RAS/ERK and PI3K/AKT/mTOR pathways, integrating their function at the level of translational regulation (She et al. 2010).

In light of previous work demonstrating synergistic effects of dual suppression of RAS/ERK and PI3K/AKT/mTOR signaling in KRAS mutant cancers, and the development of mTORC1 selective inhibitors that potently and durably suppresses mTORC1 targets without inhibiting AKT S473 phosphorylation, we rationalized that concurrent treatment of KRAS G12C mutant cancer models with a KRAS G12C inhibitor/mTORC1 inhibitor combination would yield similar synergistic effects demonstrated by combinations of KRAS G12C inhibitors with conventional PI3K, AKT, and mTOR inhibitors, but with the added benefit of a safer toxicity profile. In this chapter, we demonstrate that suppression of mTORC1 signaling is a meaningful marker of sensitivity to KRAS G12C GDP (OFF)/GTP (ON) inhibitors. Furthermore, we show that mTORC1 selective inhibitors enhance KRAS G12C inhibitor mediated suppression of Cyclin D1 and pRB S807/811, suppression of cell growth, induction of cell death, and tumor regression in a panel of NSCLC and CRC models.

Results

pS6K and p4EBP1 Suppression Correlate with Sensitivity to KRAS G12C Inhibitors

We first sought to determine the effect of three KRAS G12C-GDP (OFF) inhibitors (AZD8037, AMG510, MRTX849), and the KRAS G12C-GTP (ON) inhibitor RM18, on

the growth of KRAS G12C mutant NSCLC (n=12) and CRC (n=4) models. Cells were treated with escalating doses of AZD8037 (100nM-10μM), AMG510 (100nM-10μM), MRTX849 (0.1nM-1μM), or RM18 (0.1nM-1μM) for 72 hours, and their viability was assessed. AZD8037 and AMG510 showed comparable growth inhibition at a dose of 1μM in both NSCLC and CRC models (data not shown). We defined cell lines demonstrating less than 50% cell viability at this 1μM dose as 'sensitive', while those that demonstrated 75% or more cell viability at this dose were designated as 'resistant'. Cell lines with viability in between this range were categorized as 'intermediate.' A similar approach was used to define the sensitivity of the NSCLC panel to MRTX849 and RM18. Aside from H23, which demonstrated greater sensitivity to MRTX849 and RM18, the NSCLC models fell within the same sensitivity bracket across all four KRAS G12C inhibitors (**Figure 3.1A**). For our CRC models, C106 and SW1463 demonstrated sensitivity to AZD8037, while SNU1411 and SW837 were categorized as intermediate sensitive (**Figure 3.1B**).

To gain insight into the source(s) potentially governing this differential sensitivity, we evaluated signaling dynamics in the RAS/ERK and PI3K/AKT/mTOR pathways following treatment with AZD8037 over the course of 24 hours. We focused on our NSCLC panel, as the number of CRC models in our possession were inadequate to draw meaningfully broad conclusions from. We found that phosphorylation of mTORC1 substrates S6K (T389) and 4EBP1 (S65) was significantly suppressed in sensitive models compared to less sensitive cell lines (**Figure 3.1C**). To clarify this data, for each model we quantified the intensity of the pERK T20, pAKT S473, pS6K T389, and p4EBP1 S65 bands at the terminal 24-hour time point and compared each to the percent of cell viability at 72 hours. Interestingly, suppression of pS6K T389 and p4EBP5 S65 displayed high

correlation to growth inhibition, whereas pERK inhibition was not significantly correlated with this metric (**Figure 3.1D**). A similar correlation was also observed for the KRAS-GTP inhibitor RM18 (data not shown). Furthermore, PI3K pathway alterations themselves were not predictive of sensitivity to KRAS G12C inhibition (**Figure 3.1E**). These results suggest that the degree of suppression of PI3K/AKT/mTOR signaling, in particular mTORC1, in response to KRAS G12C inhibition can be predictive of drug sensitivity. In agreement with our finding, Corcoran et al. previously demonstrated that mTORC1 suppression predicted responsiveness to RAF and MEK inhibition in BRAF mutant melanoma (Corcoran et al. 2013). These findings were not observed in our CRC models, wherein the induction of c-PARP served as the only notable predictive marker of KRAS G12C inhibitor sensitivity in this smaller data set (data not shown).

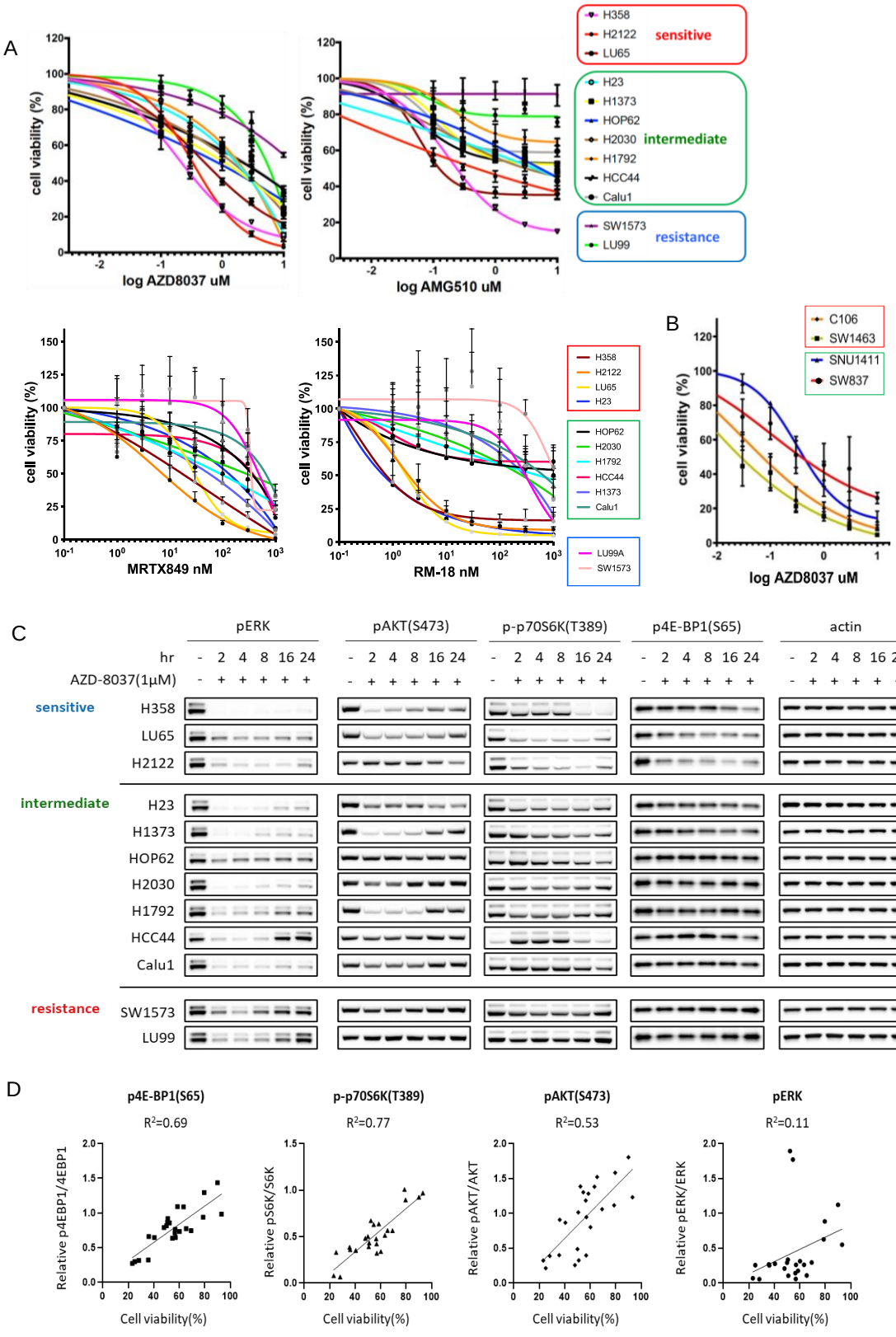
A
cell viability (%)
log AZD8037 uM
log AMG510 uM
H358
H2122
LU65
sensitive
H23
H1373
HOP62
H2030
H1792
HCC44
Calu1
intermediate
SW1573
LU99
resistance
MRTX849 nM
RM-18 nM
LU99A
SW1573
B
C106
SW1463
SNU1411
SW837
C
pERK
pAKT(S473)
p-p70S6K(T389)
p4E-BP1(S65)
actin
hr
AZD-8037(1μM)
D
p4E-BP1(S65)
R²=0.69
p-p70S6K(T389)
R²=0.77
pAKT(S473)
R²=0.53
pERK
R²=0.11
Relative p4EBP1/4EBP1
Relative pS6K/S6K
Relative pAKT/AKT
Relative pERK/ERK
Cell viability(%)

E

Cell Line	PI3K Pathway Alteration(s)	72 Hour AZD8037 GI_{50}
H358	None Detected	0.222
H2122	LKB1 Loss (STK11 Mutant), FGFR4 (p.P672T)	0.3331
LU65	None Detected	0.5449
H23	STK11 Loss (hom.), PDGFRA (p.P250H)	1.616
H1373	None Detected	1.034
HOP62	None Detected	0.792
H2030	LKB1 Loss (STK11 Mutant)	1.617
H1792	ERBB3 (p.V104_R106delVVR), MTOR (p.Q2072*), PDGFRA (p.Y962*)	1.368
HCC44	PIK3R5 C41R	1.951
Calu-1	None Detected	2.125
SW1573	PIK3CA K111G (het.)	15.28
LU99	None Detected	4.108

Figure 3.1 pS6K and p4EBP1 Suppression Correlate with Sensitivity to KRAS G12C Inhibitors.

(A) A panel of KRAS G12C mutant NSCLC cell lines were treated with escalating doses of KRAS G12C-GDP inhibitors (AZD8037, AMG510, MRTX849), or the KRAS G12C-GTP inhibitor RM18. Cell viability was determined 72 hours post treatment. Each concentration was assessed in eight technical replicates, and the averages and SDs are shown.

(B) KRAS G12C mutant CRC cell lines were treated with escalating doses of KRAS G12C-GDP inhibitor AZD8037. Cell viability was determined 72 hours post treatment. Each concentration was assessed in three biological replicates, with five technical replicates per assay. The averages and SDs are shown.

(C) KRAS G12C mutant NSCLC cell lines were treated with 1μM AZD8037 for the indicated time points, and lysates were probed with the indicated antibodies.

(D) Scatter plot analysis showing positive correlation between p4EBP1 (S65), p-p70S6K (T389), pAKT (S473), or pERK inhibition and correspondent 72-hour cell viability following treatment with 1μM AZD8037. The band intensities of p4EBP1 (S65), p-p70S6K (T389), pAKT (S473), and pERK against total protein expression at the terminal, 24-hour time point were quantified from C via densitometry and are presented as relative to untreated cells. The R^2 value of the linear regression analysis is shown.

(E) PI3K pathway alterations harbored by KRAS G12C mutant NSCLC models, and corresponding GI_{50} values after 72-hour treatment with 1μM AZD8037. PI3K pathway alterations were determined from the cBioPortal, COSMIC database, Expasy Cellosaurus, (Mahoney et al. 2009), and (Kaufman et al. 2014).

The KRAS G12C/mTORC1 Inhibitor Combination Demonstrates Enhanced Cytotoxic Effects Associated with Synergistic Suppression of Cyclin D1 and pRB

Encouraged by these findings, we next sought to evaluate the efficacy the combination of RM18 with mTORC1 selective inhibitors in our models. RM6 is an improved mTORC1 selective inhibitor showing approximately 10-fold greater potency of phosphorylated 4EBP1 suppression (phospho sites T37-46, S65, and T70) compared to RM3. At these doses whereby phosphorylated 4EBP1 and S6K are suppressed, AKT S473 phosphorylation is uninhibited. Rather, phosphorylation of AKT S473 is induced due to relief of upstream feedback inhibition stemming from mTORC1 suppression (data not shown) (Lee et al. 2021). Notably, these mTORC1 selective inhibitors achieve suppression of p4EBP1 at approximately 10-fold lower potency in the NSCLC models compared to the CRC models. This variation may stem from inherent lineage differences, whereby CRC cell lines receive greater upstream signaling inputs driving 4EBP1 phosphorylation. Indeed, CRC is largely characterized by increased EGFR signaling, which plays a pivotal role in its pathogenesis (Troiani et al. 2016). Analysis of basal RAS/ERK and PI3K/AKT/mTOR signaling across our models demonstrated generally higher levels of phosphorylated 4EBP1 (T37-46, S65, T70) in several of our CRC cell lines compared to our NSCLC models (data not shown). However, given the smaller CRC sample size, we're unable to draw any firm conclusions that resolve the differential response of these lineages to mTORC1 selective inhibitors.

The combination of RM18 with RM6 demonstrated profound growth suppression across our NSCLC models (**Figure 3.2A**). We also investigated growth dynamics in response to additional PI3K, AKT, and mTOR inhibitors, alone and in combination with

RM18. In our NSCLC models, the combination of RM18 with RM6 or RapaLink-1 achieved more than 50% growth inhibition after 72 hours in all cell lines, including those harboring PIK3CA mutations, compared to the combination with a PI3K inhibitor, AKT inhibitor, or Rapamycin (**Figure 3.2B**). In our CRC models, KRAS G12C inhibition with AZD8037 or MRTX1257 in combination with PI3K, AKT, or mTORC1 inhibition yielded similar growth suppression (**Figure 3.2C**). Notably, the mTORC1 inhibitor, RM3, was used at a suboptimal dose in these experiments, so this may account for the comparable growth inhibition. The improved growth suppression of the RM18/RM6 drug combination in our NSCLC models is associated with synergistic suppression of Cyclin D1 (**Figure 3.2D**), a transcriptional target of ERK (Weber et al. 1997), and translational target of mTORC1 (Averous et al. 2008), involved in the regulation of cell cycle progression (Qie and Diehl 2016). In our CRC models, the MRTX849/RM3 combination demonstrated synergistic suppression of Cyclin D1 in the intermediate sensitive lines, while the sensitive models exhibited strong suppression of Cyclin D1 compared to KRAS G12C inhibition alone (**Figure 3.2E**). Collectively, the combination of mTORC1 selective inhibitors with KRAS G12C-GDP or GTP inhibitors enhanced KRAS G12C inhibitor mediated suppression of cell growth, with this enhanced inhibition associated with reduction of Cyclin D1 and pRB S807/811 levels in our KRAS G12C mutant models.

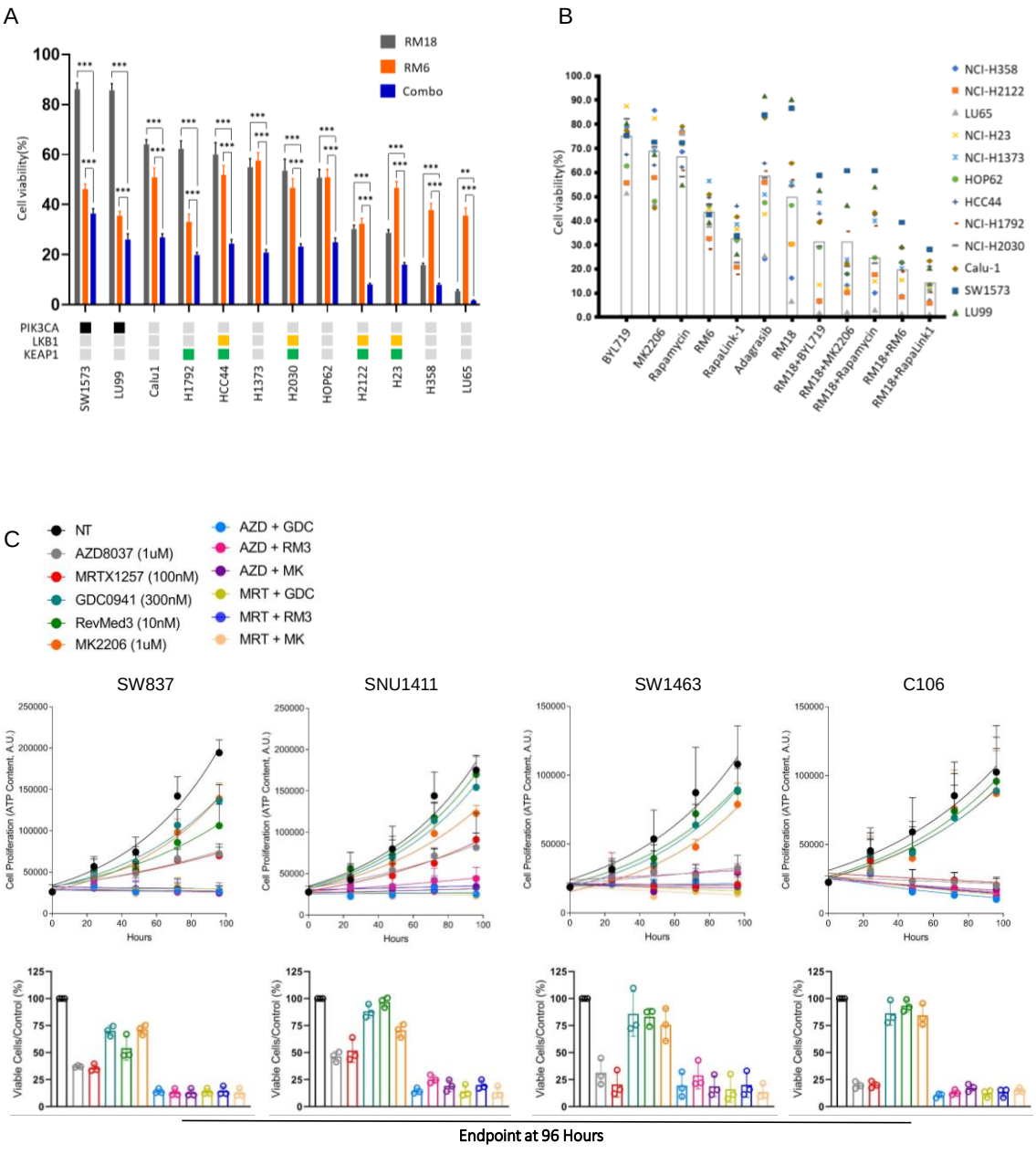
A
RM18
RM6
Combo
Cell viability(%)
PIK3CA
LKB1
KEAP1
SW1573
LU99
Calu1
H1792
HCC44
H1373
H2030
HOP62
H2122
H23
H358
LU65
B
Cell viability(%)
NCI-H358
NCI-H2122
LU65
NCI-H23
NCI-H1373
HOP62
HCC44
NCI-H1792
NCI-H2030
Calu-1
SW1573
LU99
BYL719
MK2206
Rapamycin
RM6
RapaLink-1
Adagrasib
RM18
RM18+BYL719
RM18+MK2206
RM18+Rapamycin
RM18+RM6
RM18+RapaLink1
C
NT
AZD8037 (1uM)
MRTX1257 (100nM)
GDC0941 (300nM)
RevMed3 (10nM)
MK2206 (1uM)
AZD + GDC
AZD + RM3
AZD + MK
MRT + GDC
MRT + RM3
MRT + MK
SW837
SNU1411
SW1463
C106
Cell Proliferation (ATP Content, A.U.)
Hours
Viable Cells/Control (%)
Endpoint at 96 Hours

D

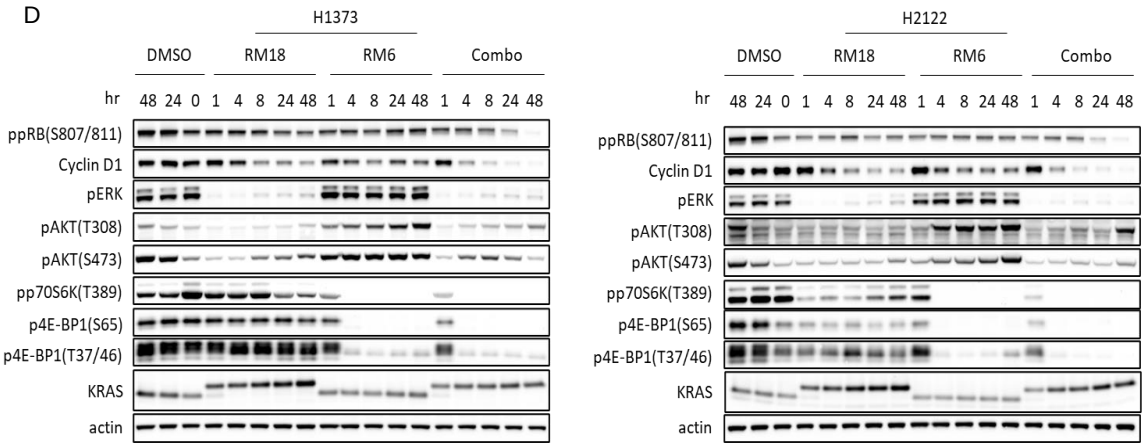
H1373
DMSO
RM18
RM6
Combo
hr
48 24 0 1 4 8 24 48 1 4 8 24 48 1 4 8 24 48
ppRB(S807/811)
Cyclin D1
pERK
pAKT(T308)
pAKT(S473)
pp70S6K(T389)
p4E-BP1(S65)
p4E-BP1(T37/46)
KRAS
actin
H2122
DMSO
RM18
RM6
Combo
hr
48 24 0 1 4 8 24 48 1 4 8 24 48 1 4 8 24 48
ppRB(S807/811)
Cyclin D1
pERK
pAKT(T308)
pAKT(S473)
pp70S6K(T389)
p4E-BP1(S65)
p4E-BP1(T37/46)
KRAS
actin

E

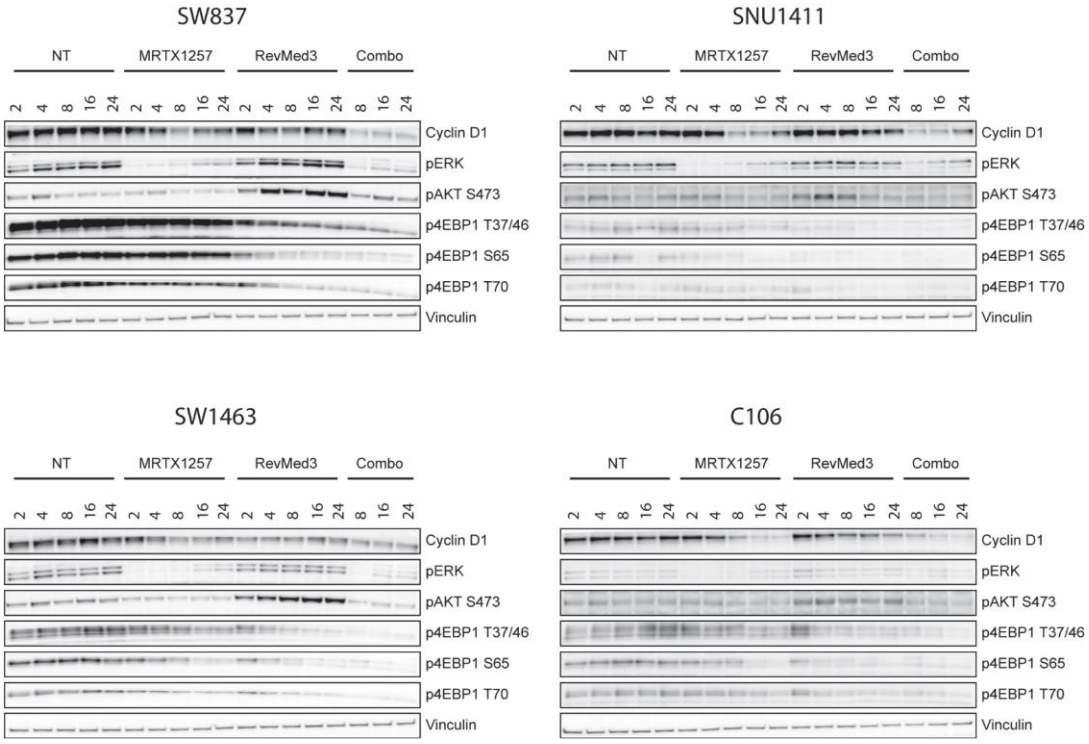
SW837
NT
MRTX1257
RevMed3
Combo
2 4 8 16 24 2 4 8 16 24 2 4 8 16 24 8 16 24
Cyclin D1
pERK
pAKT S473
p4EBP1 T37/46
p4EBP1 S65
p4EBP1 T70
Vinculin
SNU1411
NT
MRTX1257
RevMed3
Combo
2 4 8 16 24 2 4 8 16 24 2 4 8 16 24 8 16 24
Cyclin D1
pERK
pAKT S473
p4EBP1 T37/46
p4EBP1 S65
p4EBP1 T70
Vinculin
SW1463
NT
MRTX1257
RevMed3
Combo
2 4 8 16 24 2 4 8 16 24 2 4 8 16 24 8 16 24
Cyclin D1
pERK
pAKT S473
p4EBP1 T37/46
p4EBP1 S65
p4EBP1 T70
Vinculin
C106
NT
MRTX1257
RevMed3
Combo
2 4 8 16 24 2 4 8 16 24 2 4 8 16 24 8 16 24
Cyclin D1
pERK
pAKT S473
p4EBP1 T37/46
p4EBP1 S65
p4EBP1 T70
Vinculin

Figure 3.2 The KRAS G12C/mTORC1 Inhibitor Combination Demonstrates Enhanced Cytotoxic Effects Associated with Synergistic Suppression of Cyclin D1 and pRB

(A) KRAS G12C mutant NSCLC models were treated with 100nM RM18, 1nM RM6, or the combination for 72 hours and cell viability was assessed. The number of viable cells is presented as a percentage change from control. Each treatment group was assessed in eight technical replicates, and the averages and SDs are shown. The status of genetic co-alteration in PIK3CA, STK11, or KEAP1 are shown for each cell line. P values were calculated by Student's t-test. *$p < 0.05$, **$p < 0.01$, ***$p < 0.001$.

(B) KRAS G12C mutant NSCLC models were treated with 1μM BYL719, 1μM MK2206, 10nM Rapamycin, 1nM RM6, 10nM RapaLink-1, 100nM MRTX849 (Adagrasib), 100nM RM18, or the indicated combinations for 72 hours and cell viability was assessed. The number of viable cells is presented as a percentage change from control. Each treatment group was assessed in eight technical replicates, and the averages are shown.

(C) KRAS G12C mutant CRC models were treated with 1μM AZD8037, 100nM MRTX1257, 300nM GDC0941, 10nM RM3, 1μM MK2206, or the indicated combinations. Cell growth was assessed over 96 hours, with cell viability at the terminal time point as a percent of control depicted below each growth curve. Each treatment was assessed in three biological replicates, with five technical replicates per assay. The averages and SDs are shown.

(D) H1373 and H2122 were treated with 100nM RM18, 1nM RM6, or their combination for the indicated time points, and lysates were probed with the indicated antibodies.

(E) SW837, SNU1411, SW1463, and C106 were treated with 100nM MRTX1257, 10nM RM3, or their combination for the indicated time points, and lysates were probed with the indicated antibodies.

The KRAS G12C/mTORC1 Inhibitor Combination Induces Cell Death and Precipitates Tumor Regression without Causing Hyperglycemia

We also assessed the degree of cell death precipitated by the RM18/RM6 drug combination in two of our NSCLC models. In H2122, we observed that mTORC1 inhibition trended towards enhancement of cell death induced by the KRAS G12C-GTP inhibitor, while in H1373, KRAS-G12C inhibition alone was sufficient to induce a high percentage of cell death (**Figure 3.3A**). These findings led us to assess the combination of the KRAS-GTP/mTORC1 inhibitor combination *in vivo*. RM29 is a structural analogue of RM18 with improved oral bioavailability for *in vivo* use, demonstrating similar growth inhibition to RM18 in KRAS G12C mutant NSCLC models (data not shown). The combination of RM29 with RM6 achieved synergistic tumor shrinkage in an H2122 xenograft model (**Figure 3.3B**), and the combination was well tolerated, indicated by minor fluctuations in mouse body weight between treated and control subjects (data not shown). We also sought to test the effects of the mTORC1 selective inhibitor on glucose tolerance in this model. RM6, as well as the combination with RM29, had minimal effects on glucose levels in mice over four weeks of treatment (**Figure 3.3C**), similar to results observed for other mTORC1 selective inhibitors evaluated in breast cancer models (Lee et al. 2021).

We expanded this combination therapy to various KRAS G12C mutant lung cancer PDX models harboring genetic co-alterations in TP53, STK11/LKB1, and KEAP1, representative of the altered genetic landscape commonly observed in NSCLC patients (Pikor et al. 2013). Remarkably, the combination of RM29 with RM6 achieved dramatic tumor shrinkage for these KRAS G12C mutant NSCLC PDX models (**Figure 3.3D-G**). Fluctuations in body weight were minimal, demonstrating good tolerance (**Figure 3.3H**).

Moreover, the waterfall plot of LX349 and LX369 reveal that all tumors treated with the drug combination regressed by the end of treatment (**Figure 3.3I**).

The striking difference of the combination to induce prominent tumor regression *in vivo* versus cell death *in vitro* compared to KRAS G12C inhibition alone is notable. One likely explanation for this may be the involvement of the immune system in the *in vivo* setting promoting the efficacy of the KRAS G12C/mTORC1 inhibitor combination. KRAS mutations can promote an immunosuppressive environment, with KRAS G12C inhibitors provoking positive immune responses (Coelho et al. 2017, Mugarza et al. 2022). mTOR plays an essential regulatory role in the differentiation and function of both innate and adaptive immune cells, hence, suppressing mTORC1 would appear to be counterintuitive due to the immunosuppressive properties of mTOR inhibitors. However, recent studies have highlighted the complex role mTOR plays in immune cell biology. These studies have revealed that mTOR inhibitors can promote or repress the immune response in a context-dependent manner, and pre-clinical studies have demonstrated that these agents have the potential to increase the antitumor efficacy of immunotherapies (El Hage and Dormond 2021). While speculative, it's conceivable that the KRAS G12C/mTORC1 inhibitor combination synergizes to promote a positive immune response within the tumor microenvironment.

Collectively, these data suggest that the KRAS G12C-GTP/mTORC1 selective inhibitor combination is a feasible therapeutic strategy for the treatment of KRAS G12C mutant NSCLC, and that this treatment modality can potentially eliminate the issue of hyperglycemia, which has limited the tolerance and efficacy of conventional PI3K, AKT, and mTOR inhibitors in the clinic to date.

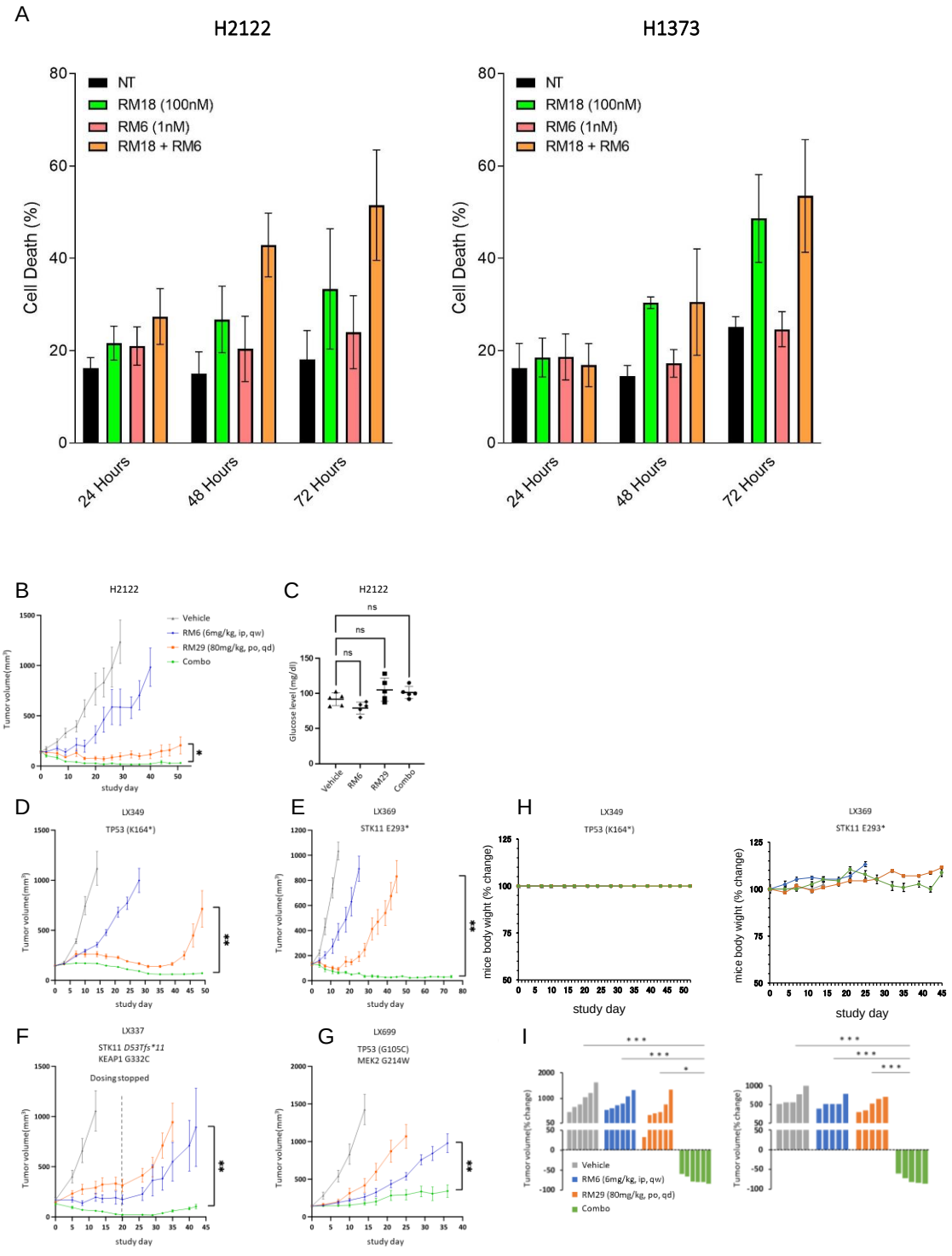
A
H2122
H1373
NT
RM18 (100nM)
RM6 (1nM)
RM18 + RM6
Cell Death (%)
24 Hours
48 Hours
72 Hours
B
H2122
Vehicle
RM6 (6mg/kg, ip, qw)
RM29 (80mg/kg, po, qd)
Combo
Tumor volume(mm³)
study day
C
H2122
ns
Glucose level (mg/dl)
Vehicle
RM6
RM29
Combo
D
LX349
TP53 (K164*)
E
LX369
STK11 E293*
H
LX349
TP53 (K164*)
LX369
STK11 E293*
mice body wight (% change)
study day
F
LX337
STK11 D537fs*11
KEAP1 G332C
Dosing stopped
G
LX699
TP53 (G105C)
MEK2 G214W
I
Tumor volume(% change)
Vehicle
RM6 (6mg/kg, ip, qw)
RM29 (80mg/kg, po, qd)
Combo

Figure 3.3 The KRAS G12C/mTORC1 Inhibitor Combination Induces Cell Death and Precipitates Tumor Regression without Causing Hyperglycemia.

(A) H2122 and H1373 were treated with 100nM RM18, 1nM RM6, or their combination for the indicated times, and cell death was determined by trypan blue exclusion viability assay. Each treatment was assessed in three biological replicates, and the averages and SDs are shown.

(B) H2122 xenografts were treated with vehicle (control), RM6 (6 mg/kg), RM29 (80 mg/kg), or their combination at the same monotherapy dose (n = 5 in each cohort). RM6 was administered once weekly by intraperitoneal injection, and RM29 was administered once daily by oral gavage. Tumor volumes were plotted over time from the start of treatment (mean ± SEM). P values were calculated by Student's t-test. *p < 0.05, **p < 0.01, ***p < 0.001.

(C) Tail snip blood samples in mice were collected at day 29 of treatment, followed by glucose assessment with a glucometer. The data shown represent the means ± SD of five samples. P values were calculated by one-way ANOVA with post-hoc Tukey's test. *p < 0.05, **p < 0.01, *** < 0.001.

(D) - (G) Four KRAS G12C mutant NSCLC PDX tumors were implanted into NSG mice. PDXs were treated with vehicle (control), RM6 (6 mg/kg), RM29 (80 mg/kg), or their combination at the same monotherapy doses (n = 5 in each cohort for LX349 and LX699, n = 6 in each cohort for LX369 and LX337). RM6 was administered once weekly by intraperitoneal injection, and RM29 was administered once daily by oral gavage. Tumor volumes were plotted over time from the start of treatment (mean ± SEM). P values were calculated by Student's t-test. *p < 0.05, **p < 0.01, ***p < 0.001.

(H) Average body weights of LX349 and LX699 PDX mice treated with vehicle (control), RM6 (6 mg/kg), RM29 (80 mg/kg), or their combination at the same monotherapy dose are shown relative to starting body weight. Error bars represent (mean ± SEM).

(I) Waterfall plot showing the percentage change in tumor volume (relative to initial volume) for individual LX349 (K) and LX369 (L) tumors at the end in each treatment group. P values were calculated by one-way ANOVA with post-hoc Tukey's test used. *p < 0.05, **p < 0.01, *** < 0.001.

Chapter 4: Mechanism(s) Precipitating Cell Death and Tumor Regression Induced by the KRAS G12C/mTORC1 Inhibitor Combination

Introduction

Regulated cell death (RCD) encompasses the set of genetically encoded mechanisms for the targeted elimination of superfluous, irreversibly damaged, and/or potentially harmful cells. RCD is involved in two diametrically opposed scenarios. On one hand, RCD can occur in the absence of exogenous environmental perturbations, operating as a built-in effector of physiological programs for development or tissue turnover (Conradt 2009, Fuchs and Steller 2011). These completely physiological forms of RCD are generally referred to as programmed cell death (PCD). On the other hand, RCD can originate from perturbations of the intracellular or extracellular microenvironment. When these insults are too intense or prolonged for adaptative responses to cope with the stress and restore cellular homeostasis, terminal cell death is carried out. Currently, over ten forms of RCD have been described. While there exists considerable overlap in the underlying mechanisms regulating these various modes of RCD, variability remains in the stimuli that drive their initiation and the effectors that mediate their terminal completion. The reliance of these death mechanisms on dedicated molecularly machinery implies that they can be modulated (i.e., accelerated or delayed) by pharmacologic or genetic interventions (Galluzzi et al. 2018).

Apoptosis, also known as type I PCD, is a crucial process for maintaining tissue homeostasis. It's characterized morphologically by cell shrinkage, membrane blebbing, chromatin condensation, and nuclear fragmentation. In mammals, apoptosis is initiated by

two pathways: extrinsic and intrinsic. Extrinsic apoptosis is initiated by perturbations of the extracellular microenvironment detected by plasma membrane death receptors, propagated by caspase 8, and precipitated by executioner caspases, mainly caspases 3 and 7. Intrinsic apoptosis is initiated by cellular stress stimuli such as growth factor deprivation, DNA damage, oxidative stress, and excessive oncogene activation. It's demarcated by MOMP, and precipitated by executioner caspases, chiefly caspases 3 and 7. The molecular web of apoptosis is broadly regulated by the following three proteins: the BCL-2 family, gatekeepers of death involved in the intrinsic pathway, the TNF death receptor family, involved in the extrinsic pathway, and the tumor suppressor p53, guardian of the genome (Bansal 2022).

The BCL-2 family plays a pivotal role in the regulation of intrinsic apoptosis by controlling the balance of pro- and anti-apoptotic proteins in response to internal perturbations. When an appropriate level of BH3-only proteins is stimulated by cellular stress, they suppress pro-survival factors, promoting the oligeromization of BAX and BAK. This results in MOMP, and the release of cytochrome c, which activates APAF1. APAF1 in turn interacts with procaspase 9 to generate caspase 9, which subsequently activates effector caspases 3 and 7 to further propagate the signal towards cell death. SMAC and HtRA2/Omi inhibit inhibitor of apoptosis proteins (IAPs) and X-linked IAP (XIAP), respectively, which are endogenous suppressors of caspase function. BCL-2 pro-survival proteins hinder this pathway by sequestering BH3-only proteins via binding to their BH3 motifs. They also inhibit BAX and BAK. While Bcl-2 only inhibits BAX, the higher protein stability of Bcl-xL enables it to inhibit both BAX and BAK. Mcl-1 has a short half-life, providing interim, rapidly inducible enhancement of cell viability. It also

serves as a cell cycle regulator, inhibiting cell cycle progression through S phase when DNA is damaged, and ensuring cell survival until repair is completed (Ashkenazi et al. 2017, Bansal 2022).

The RAS/ERK and PI3K/AKT/mTOR pathways play a definitive role in regulating apoptosis by the post-translational phosphorylation of apoptotic regulatory molecules, including Bad, Bim, Mcl-1, and caspase 9 (Green and Llambi 2015). AKT phosphorylates Bad at S136 (mouse)/S99 (human), attenuating apoptosis by raising the threshold at which mitochondria release cytochrome c (Datta et al. 1997, del Peso et al. 1997, Datta et al. 2002), while S6K phosphorylates Bad at the same phospho site, leading to its inactivation (Harada et al. 2001). ERK also phosphorylates Bad at S112 (mouse)/S75 (human), likewise leading to suppression of its activity (Zha et al. 1996, Fang et al. 1999). A major mechanism regulating Bim-dependent apoptosis is control of its expression. Transcripts derived from *Bim* are alternatively spliced to create several Bim variants (Bouillet et al. 2001). BimEL is encoded by sequences derived from exons 2–6, while alternative splicing can delete sequences derived from exon 3, generating BimL, or exons 3 and 4, yielding BimS. These alternatively spliced exons encode the major sites of Bim phosphorylation. ERK and its substrate RSK phosphorylate BimEL at S55, S65, and S73 (sites encoded by exon 3), promoting its proteasome-mediated degradation (Ley et al. 2003, Hübner et al. 2008, Dehan et al. 2009). FOXO3a positively regulates the transcription of Bim (Dijkers et al. 2000, Gilley et al. 2003) and Puma (Jeffers et al. 2003, Villunger et al. 2003, You et al. 2006, Ekoff et al. 2007). Activated AKT suppresses FOXO3a and, by extension, levels of these pro-apoptotic factors. mTORC1 has been demonstrated to regulate the translation of pro-survival factor Mcl-1 (Mills et al. 2008, Anderson et al. 2016). Myc, a target of ERK,

positively regulates the transcription and protein stabilization of the proapoptotic factor Noxa (Fernández et al. 2005, Qin et al. 2005, Nikiforov et al. 2007, Allan 2009). ERK also phosphorylates caspase-9 at T125 in the region between its prodomain and large subunit, inhibiting its activation (Allan et al., 2009).

Death receptors are part of the TNF/nerve growth factor-receptor superfamily. They're characterized by an intracellular death domain that's essential for transduction of the apoptotic signal. This subfamily includes TNFR1, FAS, DR3, TRAIL RI/DR4, and TRAIL R2/DR5. Death receptors are activated by their cognate ligands (death ligands), which are members of the TNF family (TNFα, FAS ligand, and Apo-2 ligand/TRAIL). In the case of FAS, ligand binding leads to receptor trimerization, while TNF receptors can undergo clustering by ligand binding, particularly in the case of soluble trimeric ligands. This results in sequential recruitment of adaptor proteins FADD/TRADD, and pro-caspase 8, forming a death inducing signaling complex (DISC). Induction of apoptosis subsequently takes place by one of two routes: (1) in type I cells, activation of caspases 8 and 10 is sufficient for the rapid cleavage of effector caspases 3 and 7, which execute apoptosis. (2) In type II cells, whereby activation of caspase 8/10 is inadequate (e.g., due to low expression of death receptors, presence of IAP factors, etc.), BID is cleaved by caspase 8, generating truncated BID (tBID) which translocates to the mitochondria and recruits the intrinsic pathway towards cell death (Schneider-Brachert et al. 2013, Bansal 2022). RAS/ERK signaling potentiates activation of death receptors by increasing the expression of death ligands such as TNFα (Jo et al. 2005) and FasL (Ulisse et al. 2000), as well as death receptors such as FAS (Tanaka et al. 2002, Cagnol et al. 2006, Tewari et al. 2008), TRAIL R1/DR4, and TRAIL R2/DR5 (Nesterov et al. 2004, Drosopoulos et al.

2005, Shenoy et al. 2009, Yao et al. 2016). ERK activity also promotes the induction of FADD (Cagnol et al. 2006, Tewari et al. 2008).

The tumor suppressor p53 functions as a transcriptional regulator influencing cell cycle arrest through regulation of p21Waf1/Cip1, DNA repair, and apoptosis in response to DNA damage through activation of BAX, Noxa, and FAS, as well as p53-inducible genes. p53 is negatively regulated by MDM2, an E3 ligase that promotes nuclear and proteasomal degradation of the p53 protein through a ubiquitin-dependent pathway. In unstressed cells, p53 is highly unstable with a short half-life of ~30 minutes owing to rapid degradation mediated by MDM2. Cellular stresses lead to stabilization of p53 by blocking its degradation (Mantovani et al. 2019, Bansal 2022). The RAS/ERK and PI3K/AKT/mTOR pathways also play a role in regulating this crucial factor and its mediators. Activated AKT increases the cytoplasmic availability of p53's negative regulator MDM2, while activated mTORC1 regulates the translation of p53 and its stabilization following nucleolar localization and inactivation of MDM2 (Astle et al. 2012, Abraham and O'Neill 2014). RAS signaling selectively inactivates p53-mediated induction of p21Cip1 expression by inhibiting acetylation of specific lysine residues in the p53 DNA binding domain (Drosten et al. 2014). ERK can also mediate p53 upregulation via phosphorylation of S15 (Persons et al. 2000, She et al. 2000, Shih et al. 2002, Woessmann et al. 2002, Brown and Benchimol 2006, Lin et al. 2008, J. Liu et al. 2008), which stabilizes p53 protein and promotes its accumulation by inhibiting its association with MDM2. Moreover, sustained ERK activation inhibits MDM2 phosphorylation at S166, a phospho site associated with its ubiquitin ligase activity toward p53.

Ferroptosis was coined by the Stockwell lab in 2012, although this form of RCD, and elements like it, were discovered much earlier by the same and preceding investigators. Ferroptosis is an iron-dependent form of RCD distinct from other modes of RCD like apoptosis, necroptosis, and pyroptosis, in both mechanism and morphology (Dixon et al. 2012). While the effector molecules of ferroptosis remain to be identified (does not involve the activity of caspases (apoptosis), MLKL (necroptosis), or gasdermin D6 (pyroptosis)), iron accumulation, free radical production, fatty acid supply, and lipid peroxidation are critical for its induction, with the accumulation of lipid peroxides widely accepted as the lethal signal that triggers ferroptotic death. Polyunsaturated fatty acid (PUFA) phospholipids (PUFA-PLs) are particularly susceptible to lipid peroxidation by both enzymatic and non-enzymatic mechanisms owing to their bis-allylic moieties. The resultant PUFA-PLs can disrupt the integrity of plasma and organelle membranes and, by extension, cellular function (Liu et al. 2020, Jiang et al. 2021).

Recent reports have indicated that ferroptosis serves as a natural barrier for tumor development, mediating the repressive function of several tumor suppressors, including p53, BAP1, and KEAP1 (Stockwell et al. 2020). Hence, cancer cells must implement strategies to counteract ferroptotic mechanisms for tumor promotion and maintenance. Several reports have demonstrated that cancer cells cope with ROS, a key mediator of ferroptosis, through varied approaches that induce NRF2 expression (DeNicola et al. 2011, Taguchi et al. 2012, Liang et al. 2019, Lim et al. 2019). NRF2 is a master regulator of the antioxidant response, coordinating a series of genes involved in detoxification through binding of their antioxidant response elements (ARE) (Loboda et al. 2016). mTORC1 has been demonstrated to play several roles in regulating ferroptosis. Most notably is its

upregulation of the transcriptional activity of SREBPs, which promote *de novo* synthesis of fatty acids and cholesterol. SREBP1 also transcriptionally regulates SCD1, which mediates the ferroptosis-suppressing activity of SREBP1 by producing monounsaturated fatty acids (MUFAs) (Bertolio et al. 2019, Tesfay et al. 2019, Yi et al. 2020). In contrast to PUFAs, MUFAs do not contain bis-allylic moieties, and hence are impervious to peroxidation. Incorporation of MUFAs into PLs can displace PUFAs, thereby inhibiting ferroptosis (Magtanong et al. 2019). mTORC1 also mediates the synthesis of the selenoprotein GPX4, a pivotal inhibitor of ferroptosis that reduces membrane lipid hydroperoxides to non-toxic/non-reactive lipid alcohols using GSH as a substrate (Torrence et al. 2021).

Having established that the KRAS G12C/mTORC1 inhibitor combination induces cell death *in vitro*, and tumor regression *in vivo*, we next turned our attention to uncovering the mechanism(s) of cell death responsible for mediating these effects. We focused our initial efforts on apoptosis and ferroptosis, given the definitive roles RAS/ERK and PI3K/AKT/mTOR signaling play in regulating these modes of RCD. In this chapter we demonstrate that the KRAS G12C/mTORC1 inhibitor combination induces caspase-dependent apoptosis, and modulates proteins involved in cell cycle regulation, intrinsic apoptosis, and extrinsic apoptosis. We further show that the drug combination suppresses protective key factors of the ferroptosis regulatory network, resulting in suppression of GSH, as well as induction of ROS and lipid peroxidation. Despite this, liproxstatin-1, a well-known ferroptosis inhibitor, fails to appreciably rescue cell death induced by the drug combination. We subsequently reveal that our NSCLC models are broadly resistant to ferroptosis inducers. However, α-Tocopherol, a primary constituent of vitamin E often

employed in ferroptosis studies, almost completely rescues cell death mediated by the drug combination.

Results

The KRAS G12C/mTORC1 Inhibitor Combination Induces Apoptosis

To determine if apoptosis played a role in cell death induced by the RM18/RM6 drug combination, we evaluated apoptosis using the annexin V-propidium iodide (PI) assay following treatment with RM18, RM6, or their combination after 72 hours in H1373, H2122, and HOP62. While RM6 induced a minimal fraction of apoptosis alone, it significantly enhanced the fraction of apoptotic cells induced by RM18 (**Figure 4.1A**). We also evaluated the expression of cell death markers cleaved caspase 3 (c-Caspase 3) and cleaved PARP (c-PARP) in our panel of NSCLC models 48 hours post treatment. In half of our models, RM18 alone was sufficient to induce robust expression of these markers at this time point, with RM6 potentiating RM18 mediated induction of c-Caspase 3 and/or c-PARP in the remaining six cell lines, of which H1373, H2122, and HOP62 were amongst (**Figure 4.1B**). To ascertain the extent to which apoptosis contributed to overall cell death, we employed the pan-caspase inhibitor Z-VAD-FMK (Z-VAD). Z-VAD suppressed the induction of c-PARP and/or c-Caspase 3 precipitated by RM18 alone, and in combination with RM6, at a minimal dose of 50μM in H2122 and H1373 at 48 and 72 hours (**Figure 4.1C**). It should be noted that at this and higher doses, pERK and p4EBP1 were slightly suppressed by Z-VAD in the treatment setting. Z-VAD partially mitigated total cell death induced by the drug combination at 48 and 72 hours in H2122, and only at 48 hours in

H1373 (**Figure 4.1D**), suggesting that the combination indeed mediates a degree of apoptotic cell death, but that other mechanisms of RCD might also play a contributing role.

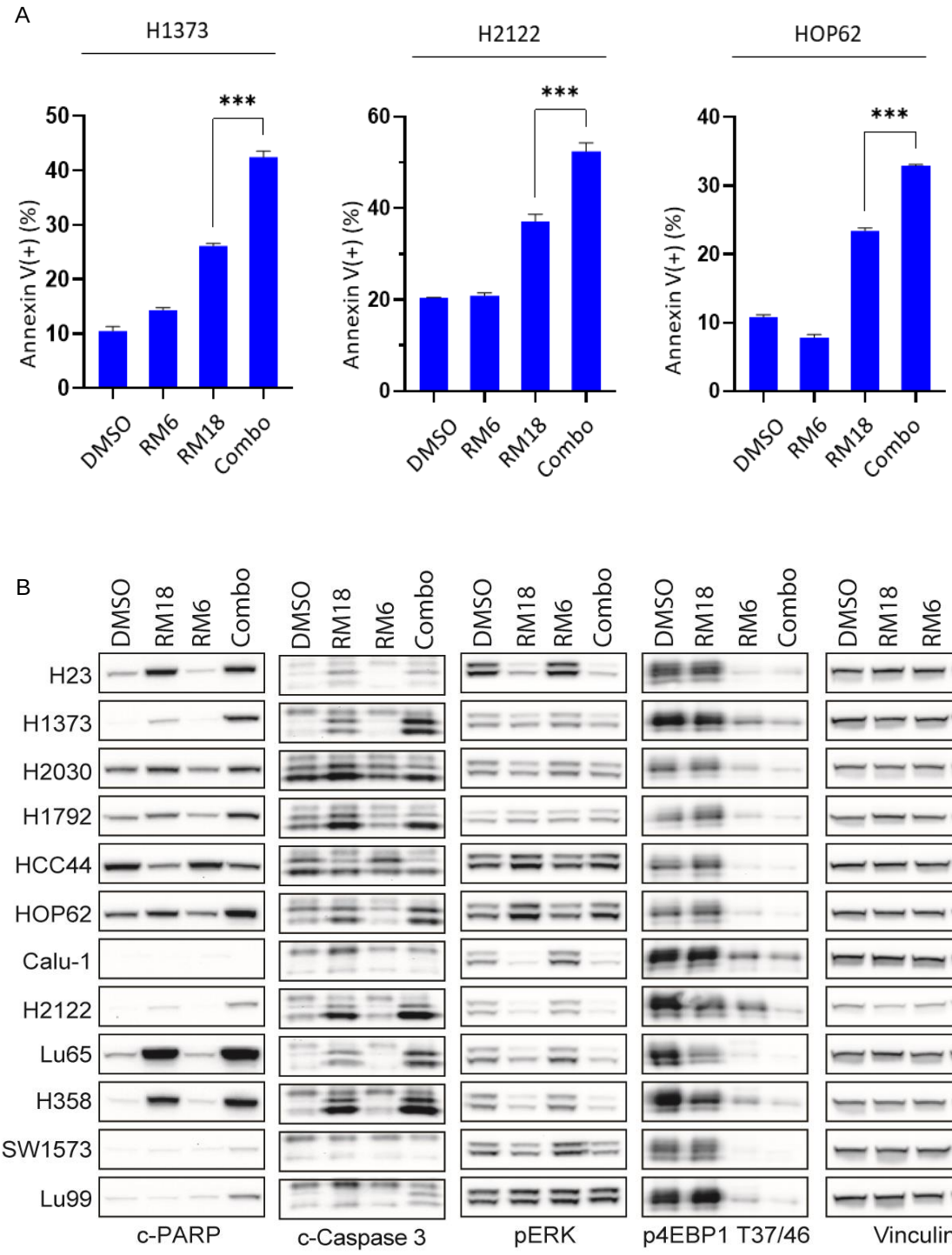
A
H1373
H2122
HOP62
***
Annexin V(+) (%)
DMSO
RM6
RM18
Combo
B
DMSO
RM18
RM6
Combo
H23
H1373
H2030
H1792
HCC44
HOP62
Calu-1
H2122
Lu65
H358
SW1573
Lu99
c-PARP
c-Caspase 3
pERK
p4EBP1 T37/46
Vinculin

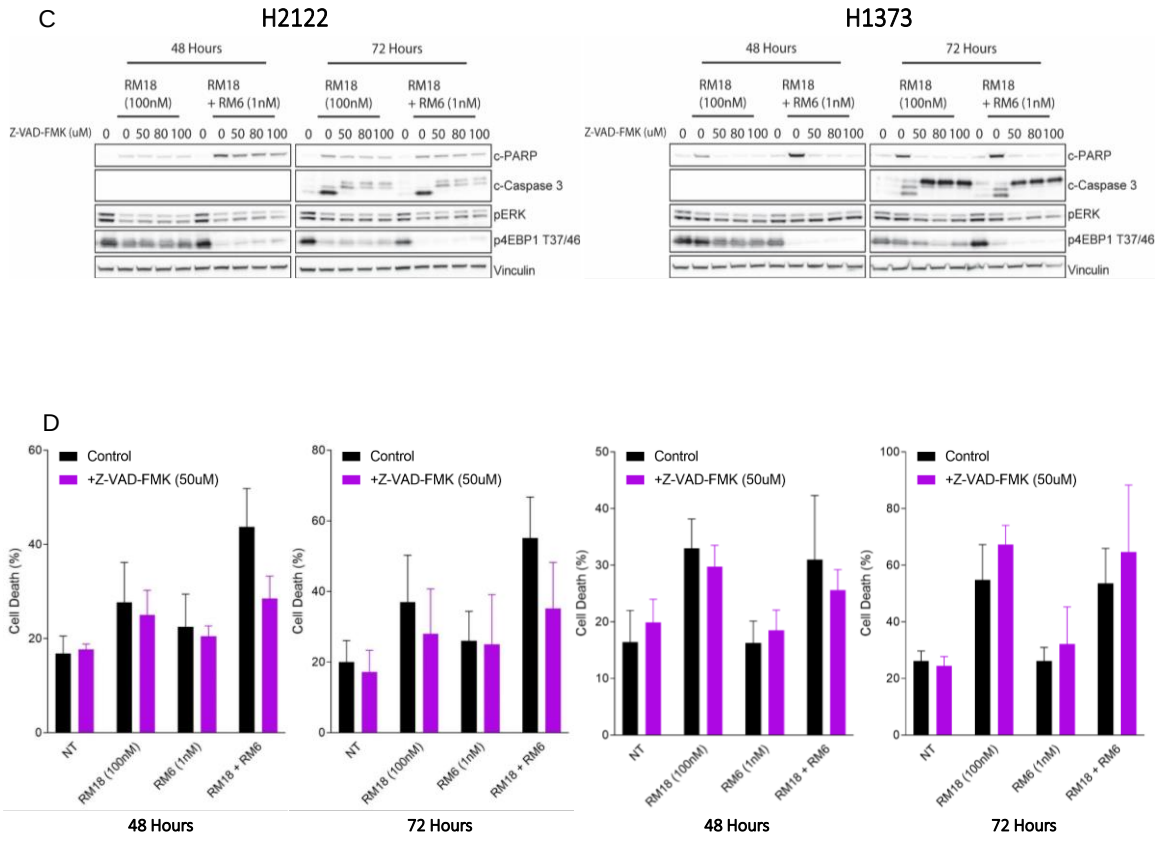

Figure 4.1 The KRAS G12C/mTORC1 Inhibitor Combination Induces Apoptosis.

(A) H1373, H2122, and HOP62 were treated with 100nM RM18, 1nM RM6, or their combination for 72 hours, and analyzed by flow cytometry to quantify Annexin V positive cells. P values were calculated by one-way ANOVA with post-hoc Tukey's test. *$p < 0.05$, **$p < 0.01$, *** < 0.001.

(B) KRAS G12C mutant NSCLC models were treated with 100nM RM18, 1nM RM6, or their combination for 48 hours, and lysates were probed with the indicated antibodies.

(C) H2122 and H1373 were treated with the combination of RM18 (100nM) and RM6 (1nM) with or without the pan caspase inhibitor Z-VAD-FMK, evaluated at 50μM, 80μM, and 100μM doses. Lysates were prepared 48 and 72 hours post treatment and probed with the indicated antibodies.

(D) H2122 and H1373 were treated with the combination of RM18 (100nM) and RM6 (1nM) with or without Z-VAD-FMK, and cell death was assessed 48 and 72 hours post treatment by trypan blue exclusion viability assay. Each treatment was assessed in three biological replicates, and the averages and SDs are shown.

The KRAS G12C/mTORC1 Inhibitor Combination Modulates Various Cell Cycle Regulators, Extrinsic Apoptosis Factors, and Intrinsic Apoptosis Factors

To gain a better understanding of the molecular mechanism(s) by which mTORC1 inhibition enhanced KRAS G12C inhibitor mediated cell death, we employed apoptosis arrays for a broad, unbiased assessment of cell death regulators differentially modulated between single agents and the combination. We utilized three proteome profilers – two human apoptosis arrays (R&D Systems, RayBiotech) and a human apoptosis signaling pathway array (RayBiotech) – to capture a wider range of total and phosphorylated proteins involved in apoptotic cell death. H1373 (NSCLC) and SW837 (CRC), two cell lines demonstrating intermediate sensitivity to KRAS G12C inhibition alone, were used as representatives. For each assay, cells were treated with MRTX849 or RM6 for 24 and/or 72 hours before assessment. Across these assays, a number of factors demonstrated differential modulation (reduction or induction) in the drug combination setting compared to KRAS G12C inhibition alone. Changes in expression were determined qualitatively, and factors were binned into seven categories – no appreciable change, slightly reduced, reduced, greatly reduced, slightly induced, induced, or greatly induced (**Figure 4.2A-K**). Among the factors that were reduced or greatly reduced in the combination compared to single agent KRAS G12C inhibition were FAS, TRAIL R1/DR4, TRAIL R2/DR5, HIF1α, claspin, survivin, livin, and p27/Kip1, while targets induced or greatly induced included c-Caspase 3 and catalase.

A

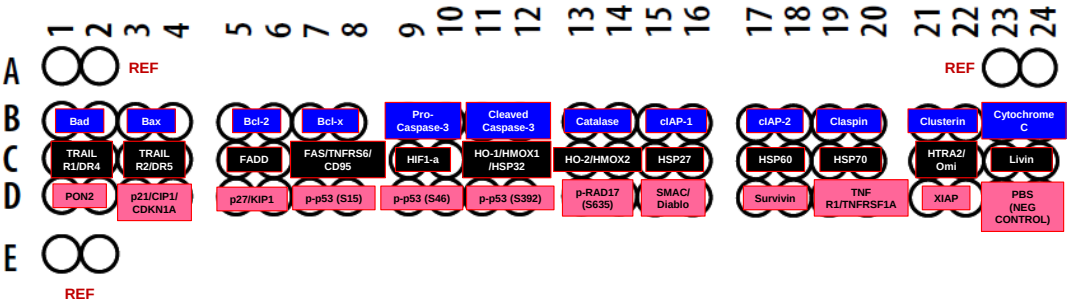

B

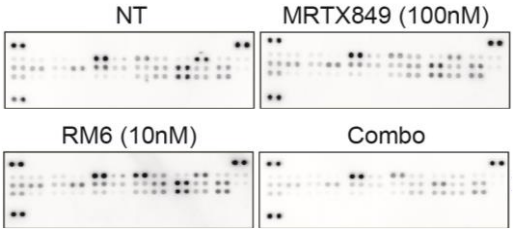

Row	Target	MRTX849	RM6	Combo	Combo	Combo
-	-	Compared to Control	Compared to Control	Compared to Control	Compared to MRT	Compared to RM6
B1,2	Bad					
B3,4	Bax					
B5,6	Bcl-2					
B7,8	Bcl-x					
B9,10	Pro-Caspase-3					
B11,12	Cleaved Caspase-3					
B13,14	Catalase					
B15,16	cIAP-1					
B17,18	cIAP-2					
B19,20	Claspin					
B21,22	Clusterin					
B23,24	Cytochrome c					
C1,2	TRAIL R1/DR4					
C3,4	TRAIL R2/DR5					
C5,6	FADD					
C7,8	Fas/TNFRSF6/CD95					
C9,10	HIF-1a					
C11,12	HO-1/HMOX1/HSP32					
C13,14	HO-2/HMOX2					
C15,16	HSP27					
C17,18	HSP60					
C19,20	HSP70					
C21,22	HTRA2/Omi					
C23,24	Livin					
D1,2	PON2					
D3,4	p21/CIP1/CDKN1A					
D5,6	p27/Kip1					
D7,8	Phospho-p53 (S15)					
D9,10	Phospho-p53 (S46)					
D11,12	Phospho-p53 (S392)					
D13,14	Phospho-RAD17 (S635)					
D15,16	SMAC/Diablo					
D17,18	Survivin					
D19,20	TNF R1/TNFRSF1A					
D21,22	XAIP					
D23,24	PBS (NEG. CONTROL)					

Qualitative Scale
No appreciable change
Slightly induced
Induced
Greatly induced
Slightly reduced
Reduced
Greatly reduced

C

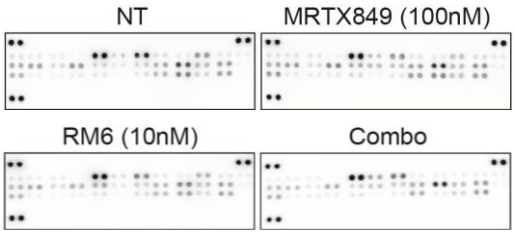

Row	Target	MRTX849 (100nM)	RM6 (10nM)	Combo	Combo	Combo
-	-	Compared to Control	Compared to Control	Compared to Control	Compared to MRT	Compared to RM6
B1,2	Bad					
B3,4	Bax					
B5,6	Bcl-2					
B7,8	Bcl-x					
B9,10	Pro-Caspase-3					
B11,12	Cleaved Caspase-3					
B13,14	Catalase					
B15,16	cIAP-1					
B17,18	cIAP-2					
B19,20	Claspin					
B21,22	Clusterin					
B23,24	Cytochrome c					
C1,2	TRAIL R1/DR4					
C3,4	TRAIL R2/DR5					
C5,6	FADD					
C7,8	Fas/TNFRSF6/CD95					
C9,10	HIF-1a					
C11,12	HO-1/HMOX1/HSP32					
C13,14	HO-2/HMOX2					
C15,16	HSP27					
C17,18	HSP60					
C19,20	HSP70					
C21,22	HTRA2/Omi					
C23,24	Livin					
D1,2	PON2					
D3,4	p21/CIP1/CDKN1A					
D5,6	p27/Kip1					
D7,8	Phospho-p53 (S15)					
D9,10	Phospho-p53 (S46)					
D11,12	Phospho-p53 (S392)					
D13,14	Phospho-RAD17 (S635)					
D15,16	SMAC/Diablo					
D17,18	Survivin					
D19,20	TNF R1/TNFRSF1A					
D21,22	XAIP					
D23,24	PBS (NEG. CONTROL)					

Qualitative Scale
No appreciable change
Slightly induced
Induced
Greatly induced
Slightly reduced
Reduced
Greatly reduced

D

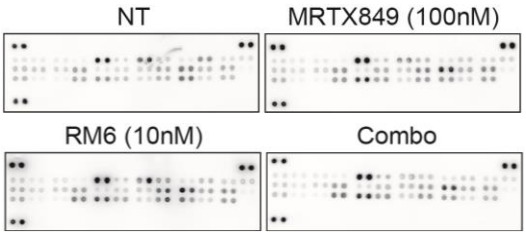

Row	Target	MRTX849 (100nM)	RM6 (10nM)	Combo	Combo	Combo
-	-	Compared to Control	Compared to Control	Compared to Control	Compared to MRT	Compared to RM6
B1,2	Bad					
B3,4	Bax					
B5,6	Bcl-2					
B7,8	Bcl-x					
B9,10	Pro-Caspase-3					
B11,12	Cleaved Caspase-3					
B13,14	Catalase					
B15,16	cIAP-1					
B17,18	cIAP-2					
B19,20	Claspin					
B21,22	Clusterin					
B23,24	Cytochrome c					
C1,2	TRAIL R1/DR4					
C3,4	TRAIL R2/DR5					
C5,6	FADD					
C7,8	Fas/TNFRSF6/CD95					
C9,10	HIF-1a					
C11,12	HO-1/HMOX1/HSP32					
C13,14	HO-2/HMOX2					
C15,16	HSP27					
C17,18	HSP60					
C19,20	HSP70					
C21,22	HTRA2/Omi					
C23,24	Livin					
D1,2	PON2					
D3,4	p21/CIP1/CDKN1A					
D5,6	p27/Kip1					
D7,8	Phospho-p53 (S15)					
D9,10	Phospho-p53 (S46)					
D11,12	Phospho-p53 (S392)					
D13,14	Phospho-RAD17 (S635)					
D15,16	SMAC/Diablo					
D17,18	Survivin					
D19,20	TNF R1/TNFRSF1A					
D21,22	XAIP					
D23,24	PBS (NEG. CONTROL)					

Qualitative Scale
No appreciable change
Slightly induced
Induced
Greatly induced
Slightly reduced
Reduced
Greatly reduced

E

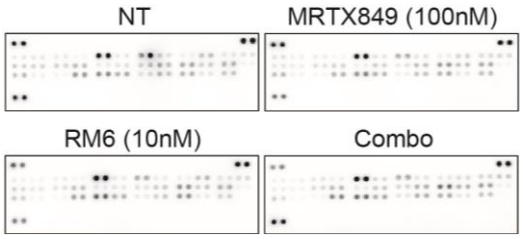

Row	Target	MRTX849 (100nM)	RM6 (10nM)	Combo	Combo	Combo
-	-	Compared to Control	Compared to Control	Compared to Control	Compared to MRT	Compared to RM6
B1,2	Bad					
B3,4	Bax					
B5,6	Bcl-2					
B7,8	Bcl-x					
B9,10	Pro-Caspase-3					
B11,12	Cleaved Caspase-3					
B13,14	Catalase					
B15,16	cIAP-1					
B17,18	cIAP-2					
B19,20	Claspin					
B21,22	Clusterin					
B23,24	Cytochrome c					
C1,2	TRAIL R1/DR4					
C3,4	TRAIL R2/DR5					
C5,6	FADD					
C7,8	Fas/TNFRSF6/CD95					
C9,10	HIF-1a					
C11,12	HO-1/HMOX1/HSP32					
C13,14	HO-2/HMOX2					
C15,16	HSP27					
C17,18	HSP60					
C19,20	HSP70					
C21,22	HTRA2/Omi					
C23,24	Livin					
D1,2	PON2					
D3,4	p21/CIP1/CDKN1A					
D5,6	p27/Kip1					
D7,8	Phospho-p53 (S15)					
D9,10	Phospho-p53 (S46)					
D11,12	Phospho-p53 (S392)					
D13,14	Phospho-RAD17 (S635)					
D15,16	SMAC/Diablo					
D17,18	Survivin					
D19,20	TNF R1/TNFRSF1A					
D21,22	XAIP					
D23,24	PBS (NEG. CONTROL)					

Qualitative Scale
No appreciable change
Slightly induced
Induced
Greatly induced
Slightly reduced
Reduced
Greatly reduced

F

Each antibody is spotted in duplicate vertically	A	B	C	D	E	F	G	H	I	J	K	L	M	N
1	POS	POS	NEG	NEG	BLANK	BLANK	bad	bax	bcl-2	bcl-w	BID	BIM	Caspase-3	Caspase-8
2														
3	CD40 (TNFRSF5)	CD40 Ligand (TNFSF5)	cIAP-2	CytoC	DR6 (TNFRSF21)	Fas (Apo-1)	Fas Ligand (TNFSF6)	BLANK	HSP27	HSP60	HSP70	HTRA2	IGF-1	IGF-2
4														
5	IGFBP-1	IGFBP-2	IGFBP-3	IGFBP-4	IGFBP-5	IGFBP-6	IGF-1 R	livin	p21	p27	p53	SMAC	Survivin	TNF RI (TNFRSF1A)
6														
7	TNF RII (TNFRSF1B)	TNF alpha	TNF beta	TRAIL R1 (TNFRSF10A)	TRAIL R2 (TNFRSF10B)	TRAIL R3 (TNFRSF10C)	TRAIL R4 (TNFRSF10D)	XIAP	BLANK	BLANK	NEG	NEG	NEG	POS
8														

G

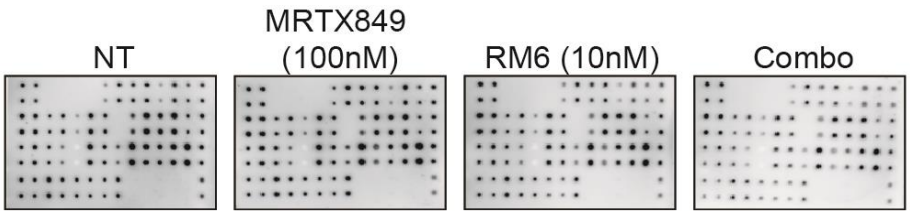

Row	Target	MRTX849 (100nM)	RM6 (10nM)	Combo	Combo	Combo
-	-	Compared to Control	Compared to Control	Compared to Control	Compared to MRT	Compared to RM6
A1,2	Positive Control					
A3,4	CD40 (TNFRSF5)					
A5,6	IGFBP-1					
A7,8	TNF RII (TNFRSF1B)					
B1,2	Positive Control					
B3,4	CD40 Ligand (TNFSF5)					
B5,6	IGFBP-2					
B7,8	TNF-alpha					
C1,2	Negative Control					
C3,4	cIAP-2					
C5,6	IGFBP-3					
C7,8	TNF-beta					
D1,2	Negative Control					
D3,4	Cytochrome c					
D5,6	IGFBP-4					
D7,8	TRAIL R1 (TNFRSF10A)					
E1,2	Blank					
E3,4	DR6 (TNFRSF21)					
E5,6	IGFBP-5					
E7,8	TRAIL R2 (TNFRSF10B)					
F1,2	Blank					
F3,4	Fas (Apo-1)					
F5,6	IGFBP-6					
F7,8	TRAIL R3 (TNFRSF10c)					
G1,2	Bad					
G3,4	Fas Ligand (TNFSF6)					
G5,6	IGF-1R					
G7,8	TRAIL R4 (TNFRSF10D)					
H1,2	Bax					
H3,4	Blank					
H5,6	Livin					
H7,8	XIAP					
I1,2	Bcl-2					
I3,4	HSP27					
I5,6	p21					
I7,8	Blank					
J1,2	Bcl-w					
J3,4	HSP60					
J5,6	p27					
J7,8	Blank					
K1,2	BID					
K3,4	HSP70					
K5,6	p53					
K7,8	Negative Control					
L1,2	BIM					
L3,4	HTRA2					
L5,6	SMAC					
L7,8	Negative Control					
M1,2	Caspase-3					
M3,4	IGF-1R					
M5,6	Survivin					
M7,8	Negative Control					
N1,2	Caspase-8					
N3,4	IGF-2					
N5,6	TNF R1 (TNFRSF1A)					
N7,8	Positive Control					

Qualitative Scale
No appreciable change
Slightly induced
Induced
Greatly induced
Slightly reduced
Reduced
Greatly reduced

H

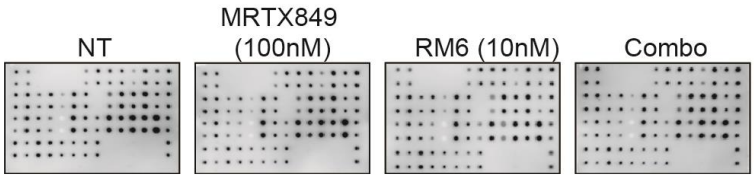

Row	Target	MRTX849 (100nM)	RM6 (10nM)	Combo	Combo	Combo
-	-	Compared to Control	Compared to Control	Compared to Control	Compared to MRT	Compared to RM6
A1,2	Positive Control					
A3,4	CD40 (TNFRSF5)					
A5,6	IGFBP-1					
A7,8	TNF RII (TNFRSF1B)					
B1,2	Positive Control					
B3,4	CD40 Ligand (TNFSF5)					
B5,6	IGFBP-2					
B7,8	TNF-alpha					
C1,2	Negative Control					
C3,4	cIAP-2					
C5,6	IGFBP-3					
C7,8	TNF-beta					
D1,2	Negative Control					
D3,4	Cytochrome c					
D5,6	IGFBP-4					
D7,8	TRAIL R1 (TNFRSF10A)					
E1,2	Blank					
E3,4	DR6 (TNFRSF21)					
E5,6	IGFBP-5					
E7,8	TRAIL R2 (TNFRSF10B)					
F1,2	Blank					
F3,4	Fas (Apo-1)					
F5,6	IGFBP-6					
F7,8	TRAIL R3 (TNFRSF10c)					
G1,2	Bad					
G3,4	Fas Ligand (TNFSF6)					
G5,6	IGF-1R					
G7,8	TRAIL R4 (TNFRSF10D)					
H1,2	Bax					
H3,4	Blank					
H5,6	Livin					
H7,8	XIAP					
I1,2	Bcl-2					
I3,4	HSP27					
I5,6	p21					
I7,8	Blank					
J1,2	Bcl-w					
J3,4	HSP60					
J5,6	p27					
J7,8	Blank					
K1,2	BID					
K3,4	HSP70					
K5,6	p53					
K7,8	Negative Control					
L1,2	BIM					
L3,4	HTRA2					
L5,6	SMAC					
L7,8	Negative Control					
M1,2	Caspase-3					
M3,4	IGF-1R					
M5,6	Survivin					
M7,8	Negative Control					
N1,2	Caspase-8					
N3,4	IGF-2					
N5,6	TNF R1 (TNFRSF1A)					
N7,8	Positive Control					

Qualitative Scale
No appreciable change
Slightly induced
Induced
Greatly induced
Slightly reduced
Reduced
Greatly reduced

I

Each antibody is spotted in duplicate vertically		A	B	C	D	E	F	G	H
	1	POS	POS	NEG	Akt (P-Ser473)	ATM (P-Ser1981)	BAD (P-Ser112)	Caspase-3 (Cleaved Asp175)	Caspase-7 (Cleaved Asp198)
	2								
	3	CHK1 (P-Ser296)	CHK2 (P-Thr68)	eIF-2a (P-Ser51)	ERK1 (P-T202/Y204) ERK2 (P-Y185/Y187)	HSP27 (P-Ser82)	IKBa (P-Ser32)	JNK (P-Thr183/Tyr185)	NFKBP65 (P-Ser536)
	4								
	5	PARP1 (Cleaved Asp214/Gly215)	p27 (P-Thr198)	P38 (P-Thr180/Tyr182)	P53 (P-Ser15)	SMAD2 (P-Ser245/250/255)	TAK1 (P-Ser412)	NEG	POS
	6								

J

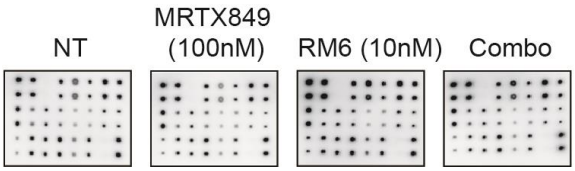

Row	Target	MRTX849 (100nM)	RM6 (10nM)	Combo	Combo	Combo
-	-	Compared to Control	Compared to Control	Compared to Control	Compared to MRT	Compared to RM6
A1,2	Positive Control					
A3,4	CHK1 (pS296)					
A5,6	PARP1 (Cleaved Asp214/Gly215)					
B1,2	Positive Control					
B3,4	CHK2 (pT68)					
B5,6	p27 (pT198)					
C1,2	Negative Control					
C3,4	eIF-2a (pS51)					
C5,6	P38 (pT180/Y182)					
D1,2	AKT (pS473)					
D3,4	ERK1 (pT202/Y204); ERK2 (pY185/y187)					
D5,6	P53 (pS15)					
E1,2	ATM (pS1981)					
E3,4	HSP27 (pS82)					
E5,6	SMAD2 (pS245/250/255)					
F1,2	BAD (pS112)					
F3,4	IKBa (pS32)					
F5,6	TAK1 (pS412)					
G1,2	Caspase 3 (Cleaved Asp175)					
G3,4	JNK (pT183/Y185)					
G5,6	Negative Control					
H1,2	Caspase 7 (Cleaved Asp198)					
H3,4	NFKBP65 (pS536)					
H5,6	Positive Control					

Qualitative Scale
No appreciable change
Slightly induced
Induced
Greatly induced
Slightly reduced
Reduced
Greatly reduced

K

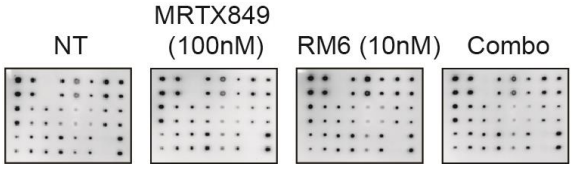

Row	Target	MRTX849 (100nM)	RM6 (10nM)	Combo	Combo	Combo
-	-	Compared to Control	Compared to Control	Compared to Control	Compared to MRT	Compared to RM6
A1,2	Positive Control					
A3,4	CHK1 (pS296)					
A5,6	PARP1 (Cleaved Asp214/Gly215)					
B1,2	Positive Control					
B3,4	CHK2 (pT68)					
B5,6	p27 (pT198)					
C1,2	Negative Control					
C3,4	eIF-2a (pS51)					
C5,6	P38 (pT180/Y182)					
D1,2	AKT (pS473)					
D3,4	ERK1 (pT202/Y204); ERK2 (pY185/y187)					
D5,6	P53 (pS15)					
E1,2	ATM (pS1981)					
E3,4	HSP27 (pS82)					
E5,6	SMAD2 (pS245/250/255)					
F1,2	BAD (pS112)					
F3,4	IKBa (pS32)					
F5,6	TAK1 (pS412)					
G1,2	Caspase 3 (Cleaved Asp175)					
G3,4	JNK (pT183/Y185)					
G5,6	Negative Control					
H1,2	Caspase 7 (Cleaved Asp198)					
H3,4	NFKBP65 (pS536)					
H5,6	Positive Control					

Qualitative Scale
No appreciable change
Slightly induced
Induced
Greatly induced
Slightly reduced
Reduced
Greatly reduced

Figure 4.2 The KRAS G12C/mTORC1 Inhibitor Combination Modulates Various Cell Cycle and Apoptosis Regulators (Apoptosis Array Data)

(A) R&D Biosystems Human Apoptosis Array Map

(B) - (E) H1373 and SW837 were treated with 100nM MRTX849, 10nM RM6, or their combination for 24 and 72 hours, and cell lysates assessed by the R&D Biosystems human apoptosis array according to the manufacturer's protocol. Treatment groups were qualitatively compared to control for changes in levels of each factor. The drug combination was additionally compared to single agent treatments. Qualitative assortment is tabulated below each array map. (B) H1373, 24-hours post treatment. (C) H1373, 72-hours post treatment. (D) SW837, 24-hours post treatment. (E) SW837, 72-hours post treatment.

(F) RayBiotech Human Apoptosis Antibody Array C1 Map

(G), (H) H1373 (G) and SW837 (H) were treated with 100nM MRTX849, 10nM RM6, or their combination for 24 hours, and cell lysates assessed by the RayBiotech human apoptosis antibody array C1 according to the manufacturer's protocol. Treatment groups were qualitatively compared to control for changes in levels of each factor. The drug combination was additionally compared to single agent treatments. Qualitative assortment is tabulated below each array map.

(I) RayBiotech Human Apoptosis Signaling Pathway Array C1 Map

(J) , (K) H1373 (J) and SW837 (K) were treated with 100nM MRTX849, 10nM RM6, or their combination for 24 hours, and cell lysates assessed by the RayBiotech human apoptosis signaling pathway array C1 according to the manufacturer's protocol. Treatment groups were qualitatively compared to control for changes in levels of each factor. The drug combination was additionally compared to single agent treatments. Qualitative assortment is tabulated below each array map.

Validation of select and additional targets in several of our NSCLC and CRC models demonstrated synergistic reduction of Cyclin D1, survivin, and pRB (S807/811) (**Figure 4.3A-C**). Previously, we and others have demonstrated that inhibition of RAS/ERK and PI3K/AKT/mTOR signaling cooperate to suppress translation through inhibition of survivin (an inhibitor of apoptosis), D-cyclins, and other regulators of growth and survival (She et al. 2010, Ye et al. 2014). Of note, phosphorylation of RB at S807/811 is required for its association with BAX, resulting in suppressed apoptosis due to BAX sequestration (Antonucci et al. 2014), suggesting that inhibition of these phospho sites by the combination contributes to apoptosis.

p27/Kip1, an inhibitor of cell cycle progression (Sherr and Roberts 1999, Razavipour et al. 2020), was generally induced by KRAS G12C and mTORC1 inhibition. (**Figure 4.3D**). ERK activity contributes to downregulation of p27 in late G1/S phase through Skp2, an E3 ligase regulating p27 levels via the ubiquitin-mediated pathway (Villanueva et al. 2007). mTORC1 likewise reduces p27 levels through Skp2 (Shapira et al., 2006). Given that ERK and mTORC1 suppress p27 levels, and their suppression leads to induction of this factor, one would expect dual inhibition of RAS/ERK and mTORC1 to synergize, further inducing p27 levels. Instead, the combination demonstrated a dampening of p27 protein expression at later time points in most of the evaluated models. This discrepancy might be explained by the reduced cell number, and hence cell-cell contacts, in the combination setting. Cell-cell contact is a primary regulator of p27, increasing its levels as a measure to suppress proliferation when space is no longer available to support cell division (Polyak et al. 1994). While loss of contact inhibition is a hallmark of cancer (Hanahan and Weinberg 2011), in the context of treatment, the reduction in cell number in

the drug combination compared to single agents may account for the attenuation of p27 levels. Collectively, these results suggest that the combination yields improved suppression of cell growth, and induction of cell death, through modulation of factors involved in proliferation and survival.

We also evaluated factors involved in the extrinsic apoptosis pathway detected in our array data. In several of our models, TNFR1 was notably reduced at later time points in the drug combination compared to single agents, while FAS did not demonstrate any striking differences between treatment groups (**Figure 4.3E-F**). Levels of TRAIL R1/DR4 and TRAIL R2/DR5 were increasingly diminished in the drug combination by later time points (**Figure 4.3G-H**). RAS/ERK signaling potentiates the level of certain death receptors and their cognate death ligands, such as FAS and both TRAIL receptors (Cagnol and Chambard 2010), suggesting that inhibition of RAS/ERK signaling could be a contributing factor in the reduced levels. However, diminished levels might also arise from receptor mediated endocytosis, and subsequent lysosome mediated degradation and/or recycling, which typically occurs upon ligand binding. Depending on the receptor, endocytosis can either propagate the apoptotic signal downstream of ligand binding, or attenuate apoptotic signaling through these channels (Schneider-Brachert et al. 2013). In the case of TNFR1, pro-apoptotic signaling emanates from intracellular vesicles, and requires receptor internalization. Additionally, this internalization terminates TNFR mediated NFkβ pro-inflammatory, pro-survival signaling, favoring DISC assembly and subsequent caspase activation (Schneider-Brachert et al. 2004, Schneider-Brachert et al. 2006, Liao et al. 2008).

Regarding FAS, although DISC formation is initiated at the plasma membrane, assembly of additional components, and subsequent activation of caspase 8, occurs predominantly in FAS-containing intracellular compartments. Hence, induction of apoptosis by FAS is critically dependent on its internalization (Parlato et al. 2000, Algeciras-Schimnich et al. 2002, Lee et al. 2006, Feig et al. 2007). TRAIL R1/DR4 and TRAIL R2/DR5 require death domain-dependent recruitment of FADD and caspase 8. In contrast to TNFR1 and FAS, these TRAIL receptors exhibit robust DISC formation at the plasma membrane, thereby readily triggering pro-apoptotic signaling. Internalization of TRAIL R1/DR4 and TRAIL R2/DR5 is a critical determinant of signaling outcome, and it's also cell-type dependent. In type-I cells, activation at the plasma membrane is sufficient for apoptotic signaling, with internalization ultimately dampening these effects, while in type-II cells, receptor internalization is critical for apoptotic signaling (Austin et al. 2006, Kohlhaas et al. 2007). Cancer cells are predominantly characterized as type-II. Hence, in our models, the lower levels of these receptors in the drug combination could reflect internalization towards apoptotic signaling. However, more refined experiments are required to determine the degree of expression and/or internalization contributing to the reduced level of these death receptors, and the nature of what these effects mean in the context of apoptotic signaling.

We also evaluated levels of claspin, a checkpoint mediator of the cell cycle that arrests cells in response to inhibition of DNA replication or DNA damage (Tsimaratou et al. 2007, Azenha et al. 2019), and HIF1α, a master regulator of cellular and systemic homeostatic response to hypoxia that activates transcription of genes involved in energy metabolism, angiogenesis, apoptosis, and other processes towards facilitating metabolic

adaptation to hypoxia (Lee et al., 2019). In the assessed models, claspin was synergistically suppressed by the drug combination (**Figure 4.3I**), suggesting that DNA repair was perturbed by dual inhibition of KRAS G12C and mTORC1. Notably, claspin overexpression is associated with chemotherapy resistance and poor prognosis in some cancers, such as prostate and renal clear cell carcinoma (RCC), serving to protect cancer cells from replication stress in a checkpoint dependent manner (Haas et al. 2018, Bianco et al. 2019, Kobayashi et al. 2020, Babasaki et al. 2021). HIF1α was difficult to detect in the evaluated NSCLC cell lines, but in the CRC models where detection was feasible, HIF1α expression did not exhibit any striking differences between single agents and the combination (data not shown).

Assessment of the intrinsic apoptosis BCL-2 family was less striking, and more variable, among the evaluated models. Bcl-2 was lowly expressed and difficult to detect in all of our models (data not shown). Bcl-xL was synergistically suppressed in H1373 and H2122, most prominently at later time points (**Figure 4.3J**). In most of the assessed cell lines, Mcl-1 demonstrated improved suppression in the mTORC1 single agent setting, owing to the induction of Mcl-1 by the KRAS G12C-GDP inhibitor that persisted in the combination (**Figure 4.3K**). Where assessed, Noxa, Puma, BAX, BID, and phosphorylated BAD (S136/99, S112/75) did not demonstrate any striking differences between single agents and the combination (data not shown). Expectedly, KRAS G12C inhibition resulted in BIM induction to varying degrees across our models (**Figure 4.3L**). This induction prevailed in the combination, albeit partially attenuated in some cases by the mTORC1 inhibitor.

We also evaluated levels of heme oxygenase 1 (HMOX-1/HO-1), a factor that was greatly induced by KRAS G12C inhibition in our apoptosis array data. Notably, this induction of HO-1 was attenuated to varying degrees by the addition of the mTORC1 inhibitor (**Figure 4.3M**). HO-1 (HSP32) is one of the most sensitive and reliable indicators of cellular oxidative stress. Normally HO-1 is difficult to detect in cells other than macrophages, but it's strongly induced by several chemical and physical stressors, including heat shock, heme and hemin, cytokines, LPS, growth factors, oxidative stress, hydrogen peroxide, hypoxia, CO, and iron starvation. HO-1 activity decreases the levels of heme, the most potent catalyst for lipid peroxidation and oxygen radical formation, and provides protection to cells via multiple avenues, including the induction of ferritin to store redox-active iron, the antioxidant actions of biliverdin and bilirubin, and the anti-inflammatory and anti-apoptotic effects of CO.

The HO-1 gene, containing an ARE, is regulated in a cell type-specific and inducer-specific fashion by AP-1, AP-2, HSF-1, HIF-1, Egr-1, NFkβ, CREB, and NRF2 (Loboda et al. 2016, Ryter 2021). HO-1 has been demonstrated to confer resistance to apoptosis induced by a variety of biological (e.g., serum deprivation) and pharmacological (e.g., TNFα, cycloheximide) stimuli in several types of normal and neoplastic cells (Petrache et al. 2000, Inguaggiato et al. 2001, Chen et al. 2004, Liu et al. 2004, Lang et al. 2005, Busserolles et al. 2006, Banerjee et al. 2011, Hu et al. 2013, Vanella et al. 2013, Zhu et al. 2015, Fan et al. 2019). Therefore, it's possible that HO-1 serves to attenuate some degree of apoptosis induced by KRAS G12C inhibition, while mTORC1 suppression may potentially mitigate, at least in part, this protection through dampening HO-1 levels.

Regulatory signaling factors pERK, p4EBP1 T37/46, pS6K T389, pAKT S473, and the loading control Vinculin are shown in **Figure 4.3N-R**.

While collectively these data suggest that the KRAS G12C/mTORC1 inhibitor combination mediates cell growth suppression and apoptosis through modulating a multiplicity of factors involved in regulating these processes, additional experiments are required to definitively resolve the contribution, necessity, and sufficiency each one plays in provoking these effects.

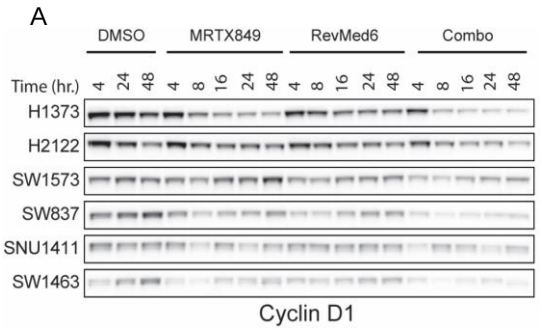
A
DMSO
MRTX849
RevMed6
Combo
Time (hr.)
H1373
H2122
SW1573
SW837
SNU1411
SW1463
Cyclin D1

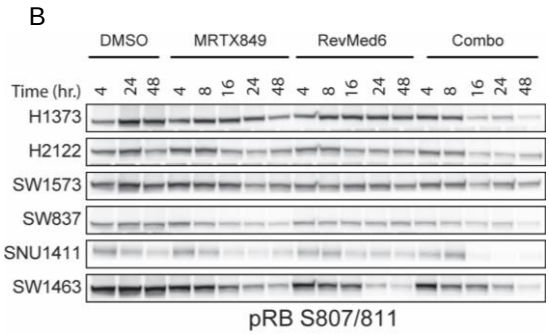
B
DMSO
MRTX849
RevMed6
Combo
Time (hr.)
H1373
H2122
SW1573
SW837
SNU1411
SW1463
pRB S807/811

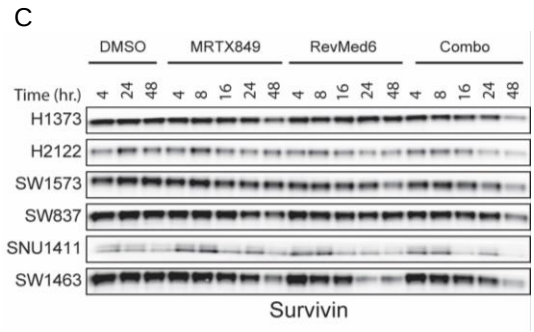
C
DMSO
MRTX849
RevMed6
Combo
Time (hr.)
H1373
H2122
SW1573
SW837
SNU1411
SW1463
Survivin

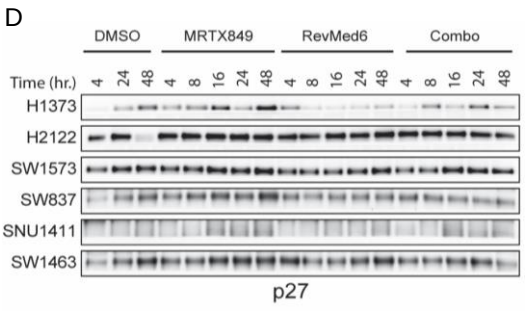
D
DMSO
MRTX849
RevMed6
Combo
Time (hr.)
H1373
H2122
SW1573
SW837
SNU1411
SW1463
p27

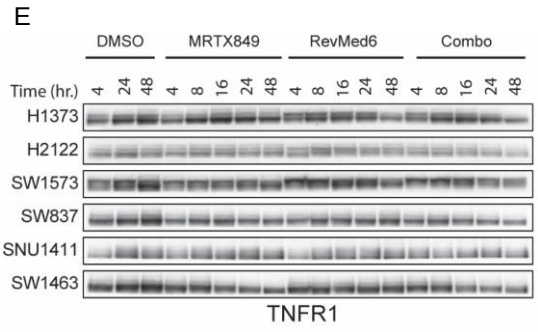
E
DMSO
MRTX849
RevMed6
Combo
Time (hr.)
H1373
H2122
SW1573
SW837
SNU1411
SW1463
TNFR1

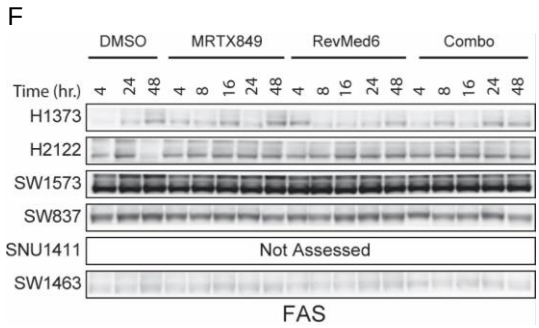
F
DMSO
MRTX849
RevMed6
Combo
Time (hr.)
H1373
H2122
SW1573
SW837
SNU1411
Not Assessed
SW1463
FAS

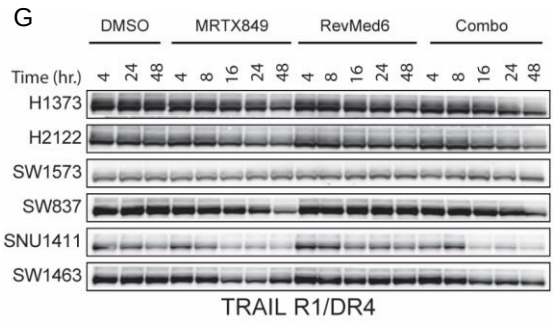
G
DMSO
MRTX849
RevMed6
Combo
Time (hr.)
H1373
H2122
SW1573
SW837
SNU1411
SW1463
TRAIL R1/DR4

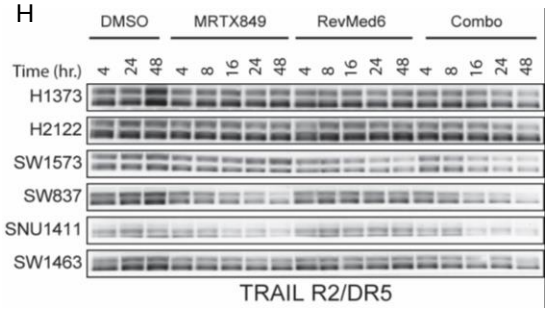
H
DMSO
MRTX849
RevMed6
Combo
Time (hr.)
H1373
H2122
SW1573
SW837
SNU1411
SW1463
TRAIL R2/DR5

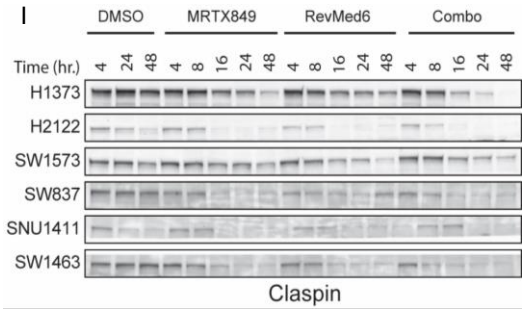
I
DMSO
MRTX849
RevMed6
Combo
Time (hr.)
4 24 48 4 8 16 24 48 4 8 16 24 48 4 8 16 24 48
H1373
H2122
SW1573
SW837
SNU1411
SW1463
Claspin

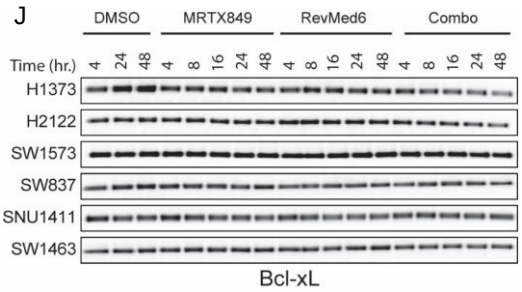
J
DMSO
MRTX849
RevMed6
Combo
Time (hr.)
4 24 48 4 8 16 24 48 4 8 16 24 48 4 8 16 24 48
H1373
H2122
SW1573
SW837
SNU1411
SW1463
Bcl-xL

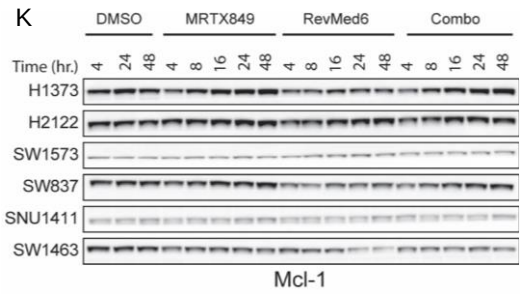
K
DMSO
MRTX849
RevMed6
Combo
Time (hr.)
4 24 48 4 8 16 24 48 4 8 16 24 48 4 8 16 24 48
H1373
H2122
SW1573
SW837
SNU1411
SW1463
Mcl-1

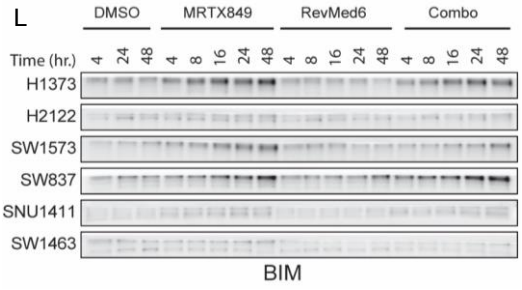
L
DMSO
MRTX849
RevMed6
Combo
Time (hr.)
4 24 48 4 8 16 24 48 4 8 16 24 48 4 8 16 24 48
H1373
H2122
SW1573
SW837
SNU1411
SW1463
BIM

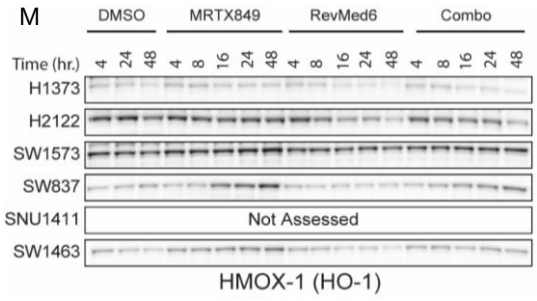
M
DMSO
MRTX849
RevMed6
Combo
Time (hr.)
4 24 48 4 8 16 24 48 4 8 16 24 48 4 8 16 24 48
H1373
H2122
SW1573
SW837
SNU1411
Not Assessed
SW1463
HMOX-1 (HO-1)

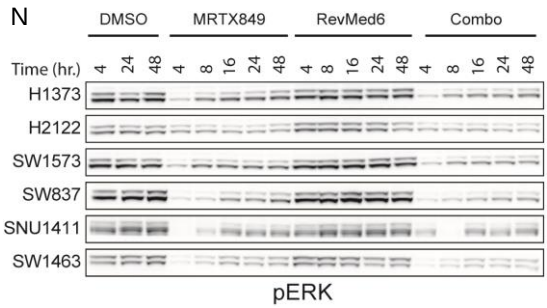
N
DMSO
MRTX849
RevMed6
Combo
Time (hr.)
4 24 48 4 8 16 24 48 4 8 16 24 48 4 8 16 24 48
H1373
H2122
SW1573
SW837
SNU1411
SW1463
pERK

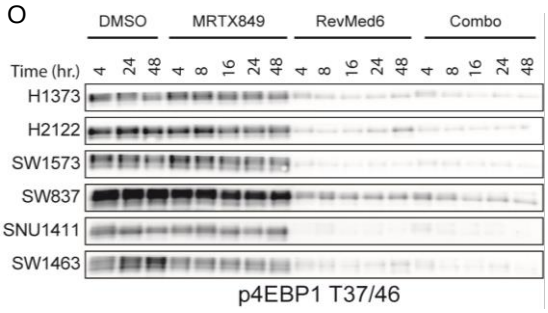
O
DMSO
MRTX849
RevMed6
Combo
Time (hr.)
4 24 48 4 8 16 24 48 4 8 16 24 48 4 8 16 24 48
H1373
H2122
SW1573
SW837
SNU1411
SW1463
p4EBP1 T37/46

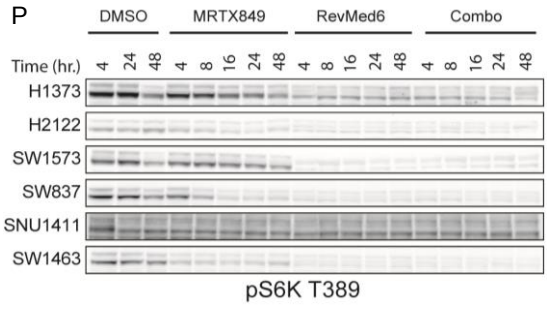
P
DMSO
MRTX849
RevMed6
Combo
Time (hr.)
4 24 48 4 8 16 24 48 4 8 16 24 48 4 8 16 24 48
H1373
H2122
SW1573
SW837
SNU1411
SW1463
pS6K T389

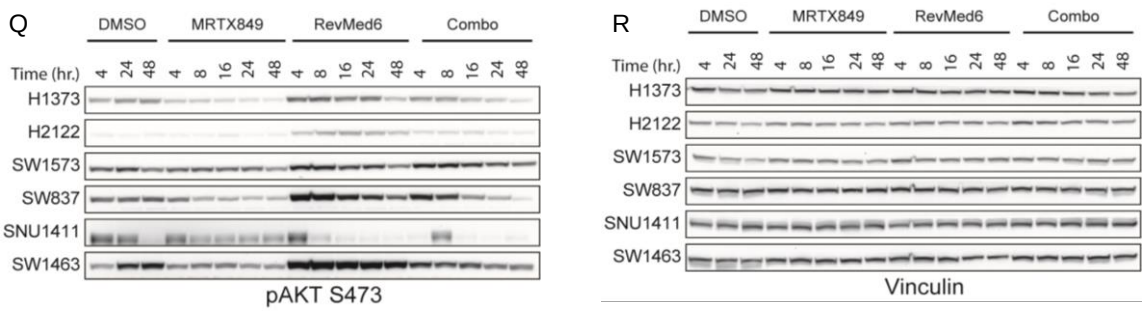

Figure 4.3 The KRAS G12C/mTORC1 Inhibitor Combination Modulates Various Cell Cycle Regulators, Extrinsic Apoptosis Factors, and Intrinsic Apoptosis Factors.

(A) - (R) Representative NSCLC models H1373, H2122, and SW1573, and CRC models SW837, SNU1411, and SW1463 were treated with MRTX849 (100nM), RM6 (1nM for NSCLC, 10nM for CRC), or their combination for the indicated time points, and lysates were probed with the indicated antibodies.

The KRAS G12C/mTORC1 Inhibitor Combination Suppresses Protective Ferroptosis Regulators and GSH Levels, while also Inducing ROS and Lipid Peroxidation

Our interest in pursuing ferroptosis as a potential mechanism of cell death mediated by the KRAS G12C/mTORC1 inhibitor combination was piqued by three events. The first was the publication by Yi et al. demonstrating that activating PI3K mutations or PTEN loss confer resistance to ferroptosis inducers through constitutive mTORC1 activation. This increase in mTORC1 signaling induces SREBP1 activation which, in turn, activates its downstream target SCD1. SCD1 subsequently promotes synthesis of MUFAs, which inhibit ferroptosis (Yi et al. 2020). The second was our HO-1 data. While HO-1 has demonstrated roles in conferring resistance to apoptosis, it's also been shown to mediate ferroptotic cell death in response to pharmacologic agents in several contexts (Ferris et al. 1999, Kwon et al. 2015, Chang et al. 2018). The third was the publication by Hu et al. demonstrating that oncogenic KRAS alterations greatly increase cysteine and glutathione biosynthesis, essential regulators of ferroptosis, in lung adenocarcinoma. Furthermore, genetic depletion or pharmacologic inhibition of xCT (SLC7A11, system x_c^-) resulted in selective killing across a panel of KRAS mutant cancer cells *in vitro* and tumor growth inhibition *in vivo* (Hu et al. 2020). Previously, Lim et al. had demonstrated that RAS/ERK signaling promotes the transcription of xCT mediated by its transcription factor ETS1 (Lim et al. 2019). Zhang et al. later established that mTORC1 couples cysteine/cystine availability with GPX4 protein synthesis (Zhang et al. 2021), while Torrence et al. reported that mTORC1 stimulates cellular cystine uptake and glutathione synthesis through ATF4, another transcription factor of xCT (Torrence et al. 2021).

With a potent, mTORC1 selective inhibitor in hand that readily lends itself to the possibility of promoting ferroptosis by nature of its target, in addition to the KRAS G12C inhibitor, which likewise might contribute to ferroptosis through suppression of xCT, compounded by its induction of potentially ferroptosis-promoting HO-1, we were motivated to evaluate ferroptosis as a promising mechanism by which the KRAS G12C/mTORC1 inhibitor combination could induce cell death.

We evaluated the expression of key ferroptosis regulators such as SREBP1 and xCT, and interrogated levels of GSH, ROS, and lipid peroxidation in response to single agent and combination treatment with our KRAS G12C and mTORC1 inhibitors. We began by assessing levels of SREBP1 and SCD1 in response to mTORC1 inhibition mediated by RM6. As expected, these factors were suppressed by RM6 in a time dependent manner in H23 and H1373 (**Figure 4.4A**). While suppression was durable in H23, rebound was observed in H1373 at 24 and 48 hours. This was not caused by a reduction in activity of the inhibitor, as p4EBP1 remained suppressed throughout the experiment's duration. We next evaluated levels of xCT in response to KRAS G12C inhibition mediated by RM18. In H23 and H1373, RM18 suppressed xCT expression at 24 and 48 hours (**Figure 4.4B**). The combination also suppressed mRNA levels of ETS1, ATF4, and xCT in H1373 24 hours post treatment (data not shown). Levels of xCT, SREBP1, and SCD1 were also assessed 48 hours post treatment with RM18, RM6, or their combination in H1373 and H23. Aside from improved suppression of xCT by the combination in H1373, KRAS G12C inhibition contributed the most to suppression of xCT, while mTORC1 inhibition was largely responsible for the suppression of SREBP1 and SCD1 (**Figure 4.4C**).

We subsequently evaluated levels of GSH, the major cellular antioxidant predominantly regulated by xCT. H1373, H2030, and H23 were treated with RM18, RM6, or their combination for 48 hours. While the combination demonstrated the lowest levels of GSH in H1373 and H2030, synergy mediated by single agents was only observed in H1373, congruous with our signaling data whereby the drug combination demonstrated greater suppression of xCT at this time point compared to single agents. In H2030, reduced GSH levels in the combination aligned closely with RM6 (discrepant between signaling data not shown), and in H23 levels of GSH were similar to those obtained for RM18 (concordant with signaling data) (**Figure 4.4D**).

We next evaluated levels of ROS in representative NSCLC models H1373, H2122, and H2030. Cells were treated with RM18, RM6, or their combination, and ROS assessed 48 and 72 hours post treatment. In H1373 and H2030, RM6 greatly contributed to the levels of ROS induced by the drug combination, while in H2122, single agents synergized to demonstratably induce ROS in the combination (**Figure 4.4E**). H2122 exhibited the highest levels of ROS compared to H1373 and H2303. Differences in mutation status of *KEAP1*, a negative regulator of NRF2, or *STK11*, leading to LKB1 loss, a negative regulator of mTORC1, could not definitively account for this difference, as H2030 likewise harbors these alterations. However, the nature of the KEAP1 mutation, and its functional implications, are undetermined, so we cannot ascribe significance of the mutation status to the induction of ROS levels.

Finally, we assessed the degree of lipid peroxidation in response to single agents and the combination (**Figure 4.4F**). In these assays, lipid peroxidation was measured by a plate reader using a 24-well plate, with samples assayed in triplicate. These multi-well

plates can be subject to signal interference caused by stray light emitted from surrounding wells. To clarify the contribution of KRAS G12C inhibition and mTORC1 inhibition to levels of lipid peroxidation induced by the combination, we also implemented imaging and flow cytometry for the readout in H23 and H1373. Cumene hydroperoxide, a strong oxidizing agent, was included as a positive control. While the overall levels of lipid peroxidation were consistent between both readouts, single agents demonstrated clearer synergy when assessed qualitatively and by flow cytometry (**Figure 4.4G, H**).

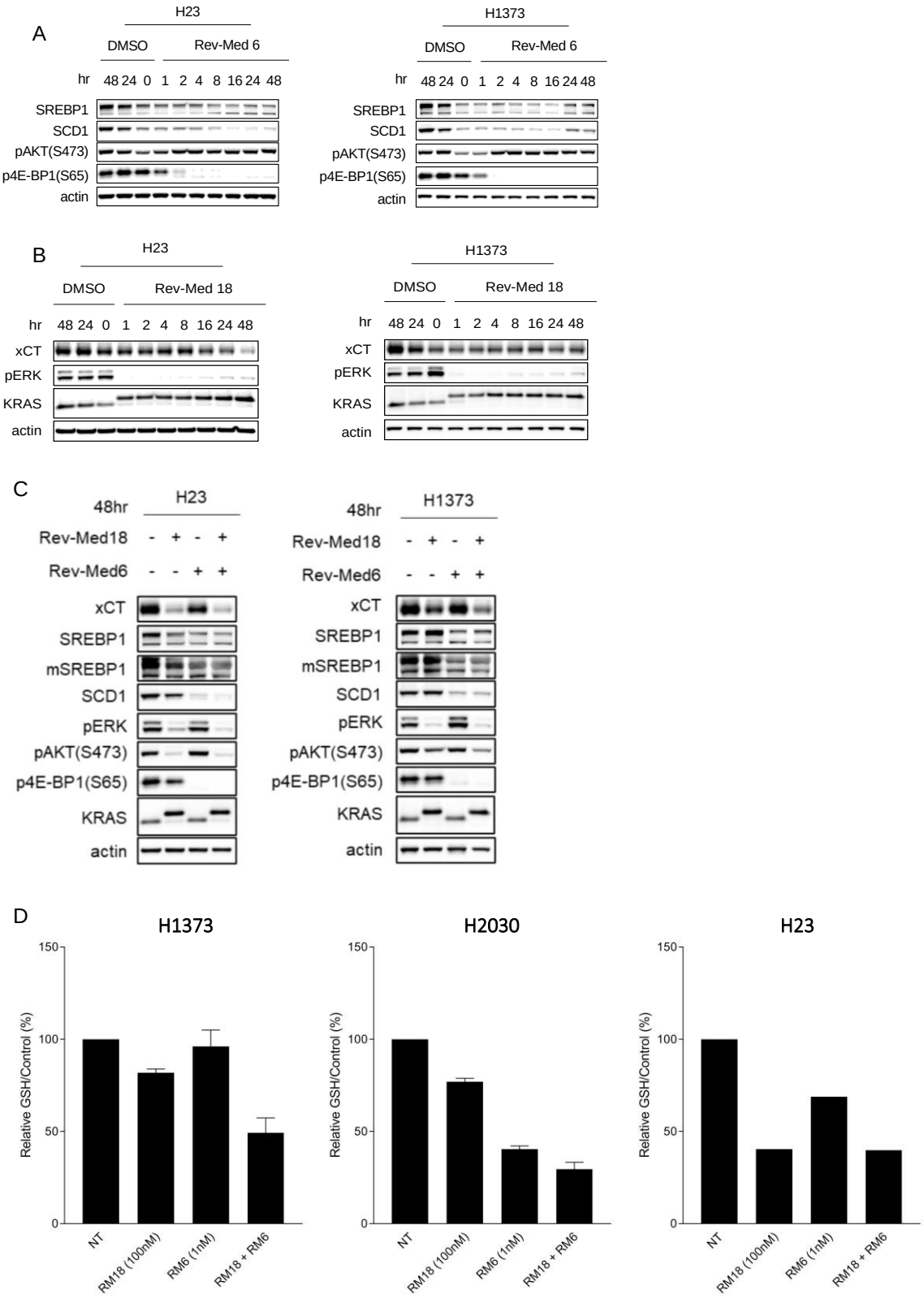
A
H23
DMSO
Rev-Med 6
hr 48 24 0 1 2 4 8 16 24 48
SREBP1
SCD1
pAKT(S473)
p4E-BP1(S65)
actin
H1373
DMSO
Rev-Med 6
hr 48 24 0 1 2 4 8 16 24 48
SREBP1
SCD1
pAKT(S473)
p4E-BP1(S65)
actin
B
H23
DMSO
Rev-Med 18
hr 48 24 0 1 2 4 8 16 24 48
xCT
pERK
KRAS
actin
H1373
DMSO
Rev-Med 18
hr 48 24 0 1 2 4 8 16 24 48
xCT
pERK
KRAS
actin
C
48hr
H23
Rev-Med18 - + - +
Rev-Med6 - - + +
xCT
SREBP1
mSREBP1
SCD1
pERK
pAKT(S473)
p4E-BP1(S65)
KRAS
actin
48hr
H1373
Rev-Med18 - + - +
Rev-Med6 - - + +
xCT
SREBP1
mSREBP1
SCD1
pERK
pAKT(S473)
p4E-BP1(S65)
KRAS
actin
D
H1373
H2030
H23
Relative GSH/Control (%)
150
100
50
0
NT
RM18 (100nM)
RM6 (1nM)
RM18 + RM6

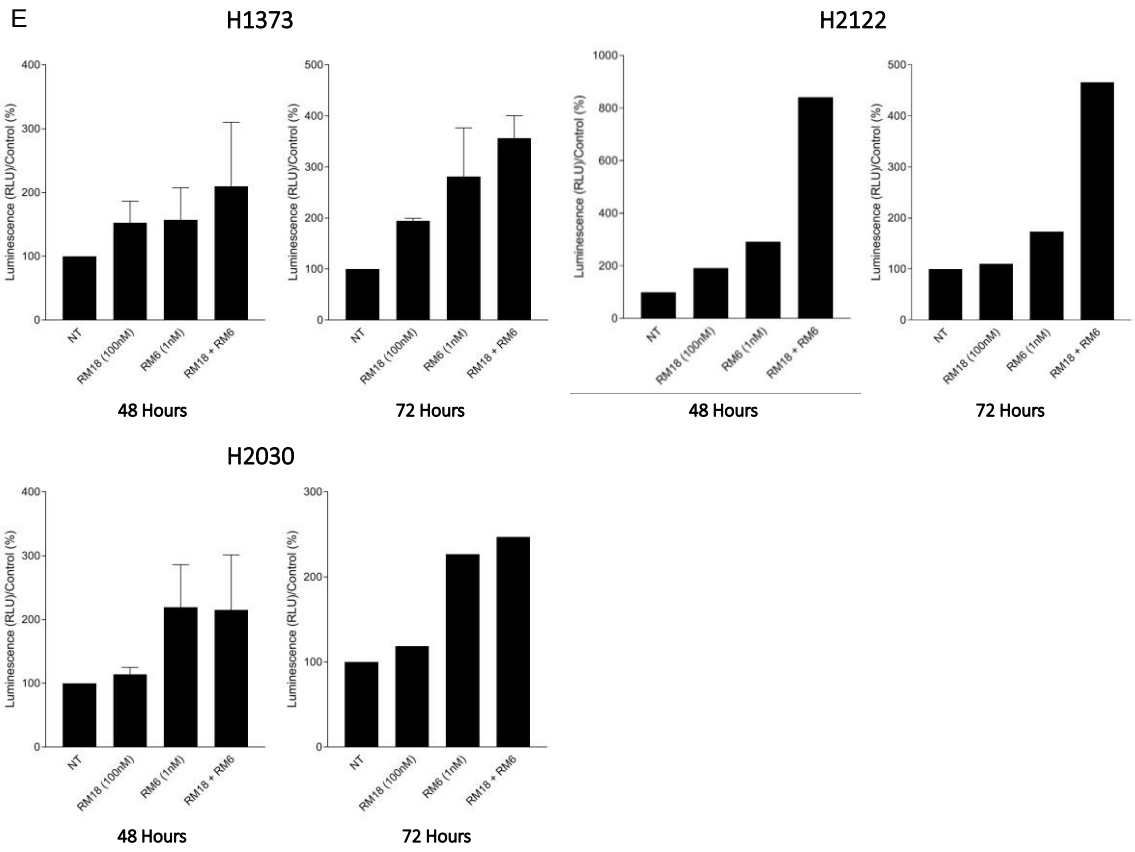
E
H1373
H2122
Luminescence (RLU)/Control (%)
NT
RM18 (100nM)
RM6 (1nM)
RM18 + RM6
48 Hours
72 Hours
48 Hours
72 Hours
H2030
48 Hours
72 Hours

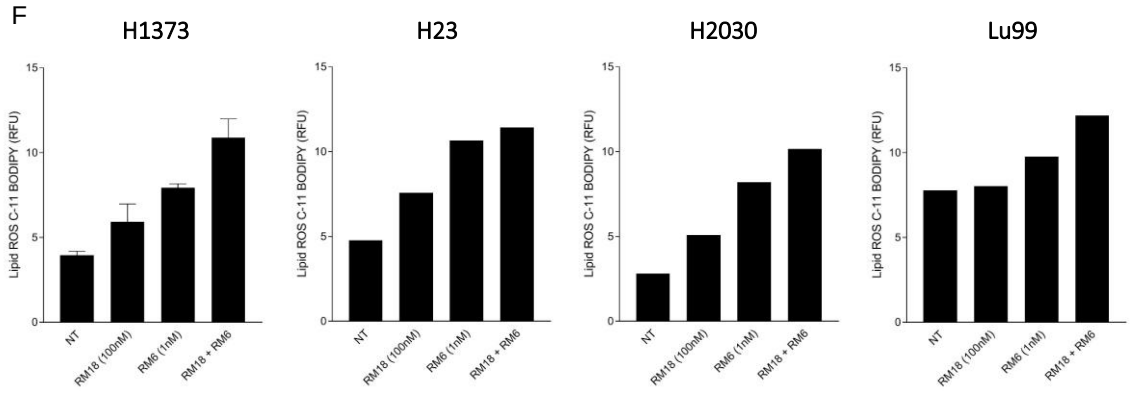
F
H1373
H23
H2030
Lu99
Lipid ROS C-11 BODIPY (RFU)
NT
RM18 (100nM)
RM6 (1nM)
RM18 + RM6

G

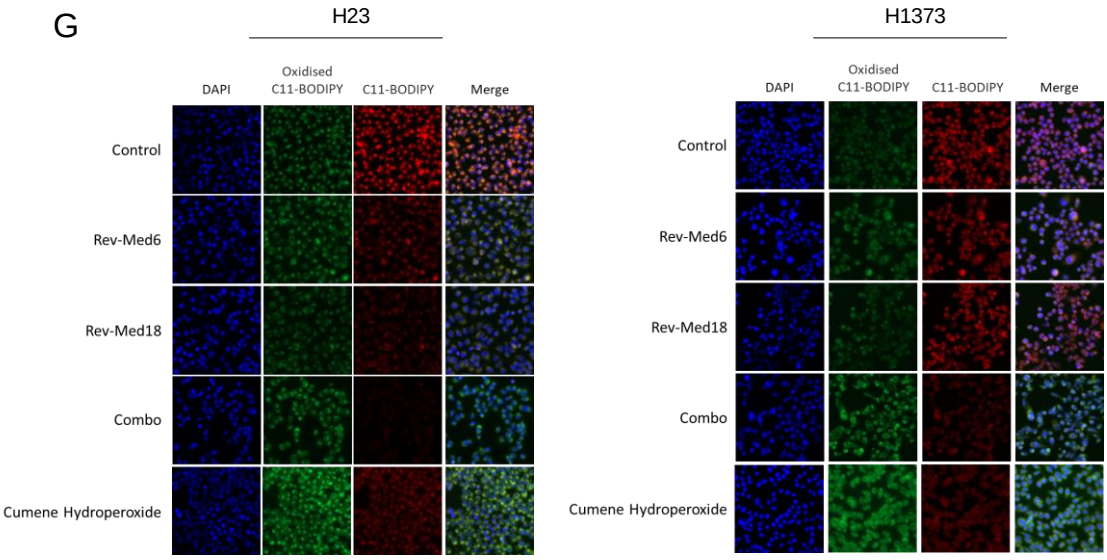
H23
H1373
DAPI
Oxidised C11-BODIPY
C11-BODIPY
Merge
Control
Rev-Med6
Rev-Med18
Combo
Cumene Hydroperoxide

H

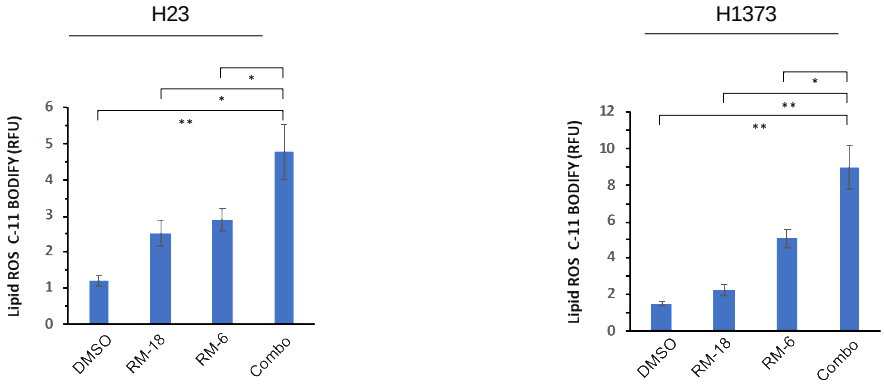
H23
H1373
Lipid ROS C-11 BODIFY (RFU)
DMSO
RM-18
RM-6
Combo

Figure 4.4 The KRAS G12C/mTORC1 Inhibitor Combination Suppresses Protective Ferroptosis Regulators and GSH, while also Inducing ROS and Lipid Peroxidation.

(A) H23 and H1373 were treated with 1nM RM6 for the indicated time points, and lysates probed with the indicated antibodies.

(B) H23 and H1373 were treated with 100nM RM18 for the indicated time points, and lysates probed with the indicated antibodies.

(C) H23 and H1373 were treated with 100nM RM18, 1nM RM6, or their combination for 48 hours, and lysates probed with the indicated antibodies.

(D) H1373, H2030, and H23 were treated with 100nM RM18, 1nM RM6, or their combination for 48 hours, and levels of GSH were evaluated. Each treatment group was assessed in 3 technical replicates. H1373 and H2030 were assessed in an additional 2 biological replicates, and the averages and SDs are shown. Data is presented as percentage of relative GSH normalized to control.

(E) H1373, H2122, and H2030 were treated with 100nM RM18, 1nM RM6, or their combination for 48 and 72 hours, and levels of ROS were evaluated. Each treatment group was assessed in 3-5 technical replicates. H1373 and H2030 were assessed in an additional 2-3 biological replicates, and the averages and SDs are shown. Data is presented as percentage of ROS luminescence normalized to control.

(F) H1373, H23, H2030, and Lu99 were treated with 100nM RM18, 1nM RM6, or their combination for 48 hours, and lipid peroxidation of the fluorescent reporter C-11 BODIPY was evaluated. Each treatment group was assessed in 3 technical replicates. H1373 was assessed in an additional biological replicate, and the averages and SDs are shown. Data is presented as relative lipid ROS C-11 BODIPY.

(G), (H) H23 and H1373 were treated with 100nM RM18, 1nM RM6, or their combination for 48 hours, and lipid peroxidation of the fluorescent reporter C-11 BODIPY was evaluated qualitatively by imaging (G), and quantitatively by flow cytometry (H). Upon oxidation, fluorescence shifts from the red to green channel, providing a ratiometric indication of lipid peroxidation. Cumene hydroperoxide, a strong oxidizing agent, was used as a positive control. Data is presented as relative lipid ROS C-11 BODIPY. Each treatment group was assessed in 3 technical replicates, and the averages and SDs are shown. P values were calculated by Student's t-test. *$p < 0.05$, **$p < 0.01$, ***$p < 0.001$.

Liproxstatin-1, a Potent Ferroptosis Inhibitor, Variably Rescues Cell Death Induced by the KRAS G12C/mTORC1 Inhibitor Combination

The cumulative results of **Figure 4.4** led us to believe that ferroptosis could be a mechanism of death mediated by the drug combination in our models. Currently, there is no specific biomarker to detect ferroptosis. Instead, ferroptosis is usually confirmed by assessing whether cell death can be rescued by specific ferroptosis inhibitors (e.g., ferrostatin-1, liproxstatin-1) and by measuring lipid peroxidation in cells (Liu et al. 2020). Having satisfied the latter requirement, we next sough to determine if a potent ferroptosis inhibitor, liproxstatin-1 (Friedmann Angeli et al. 2014), could rescue cell death mediated by the drug combination. H2122 and H1373 were treated with RM18, RM6, or their combination with or without 1.67μM of liproxstatin-1 (Lip-1), and cell death was evaluated at 48 and 72 hours. Lip-1 demonstrated only modest rescue of cell death induced by the combination in H2122 and H1373 at 72 hours (**Figure 4.5A**). In parallel, we also assessed Lip-1 with Z-VAD across treatment groups, rationalizing that, if apoptosis and ferroptosis were playing a role in mediating cell death induction by the combination, then utilizing suppressors of both might conceivably rescue more cell death, while also enabling us to discern the degree of cell death attributed by each mechanism. However, we did not observe synergy of death rescue (**Figure 4.5B**).

The underwhelming results of the cell death rescue experiment led us to question if Lip-1 was effectively abating the primary indicator of ferroptosis, lipid peroxidation, in our models. To address this, we treated H1373, H2122, and H23 with the RM18/RM6 drug combination with or without Lip-1 and assessed lipid peroxidation 48 hours post treatment. We also treated cells with 1μM of the ferroptosis inducer RSL3 as a positive control. RSL3

inhibits the activity of GPX4, and it's readily blocked by Lip-1 (Friedmann Angeli et al. 2014, Yi et al. 2020, Fan et al. 2021). In H1373 and H23, lipid peroxidation induced by the combination was modestly suppressed by Lip-1, while lipid peroxidation induced by RSL3 was more robustly suppressed (**Figure 4.5C**). RSL3 only modestly induced lipid peroxidation in H2122, with very slight rescue by Lip-1, while lipid peroxidation induced by the drug combination was not suppressed to any degree by Lip-1.

The relatively modest rescue of lipid peroxidation in 2/3 models next led us to question if a higher dose of Lip-1 would promote greater suppression of lipid peroxidation induced by the combination and, in turn, enhance rescue of cell death. To this end, H1373 was treated with the RM18/RM6 drug combination with or without escalating doses of Lip-1, and lipid peroxidation assessed. Surprisingly, these higher doses did not promote greater rescue of lipid peroxidation induced by the combination, with several doses instead compounding this metric (**Figure 4.5D**). Nevertheless, we proceeded with assessing the 4μM dose of Lip-1 in a subsequent cell death rescue experiment, as it demonstrated the greatest rescue, relatively speaking, among the evaluated doses. H1373 was treated with RM18, RM6, or the combination with or without 4μM Lip-1, and cell death assessed at 48 and 72 hours. This higher dose of Lip-1 did not rescue cell death amongst any of the treatment groups (**Figure 4.5E**).

Collectively, these results suggest that ferroptosis may not be a mechanism of cell death mediated by the combination. However, it is difficult to say with certainty if this is the case, as liproxstatin-1 was simply unable to effectively rescue the primary indicator of ferroptosis – lipid peroxidation – in our models. Since iron also plays a crucial role in regulating ferroptosis, and is upstream of lipid peroxidation, we asked whether suppressing

reactive iron would serve as a better suppressor of ferroptosis in the context of our drug combination. To address this, H2122 and H1373 were treated with RM18, RM6, or their combination with or without Deferoxamine mesylate (DFO), an iron chelating agent utilized in ferroptosis studies as a means to inhibit the process (Yao et al. 2019). In both our models, DFO failed to rescue cell death mediated by the combination at 48 and 72 hours. Rather, the dose of DFO used appeared to be toxic, substantially increasing cell death in the control and various treatment settings (**Figure 4.5F**). These collective results led us to question the intrinsic sensitivity of our models to the mechanism of ferroptosis itself.

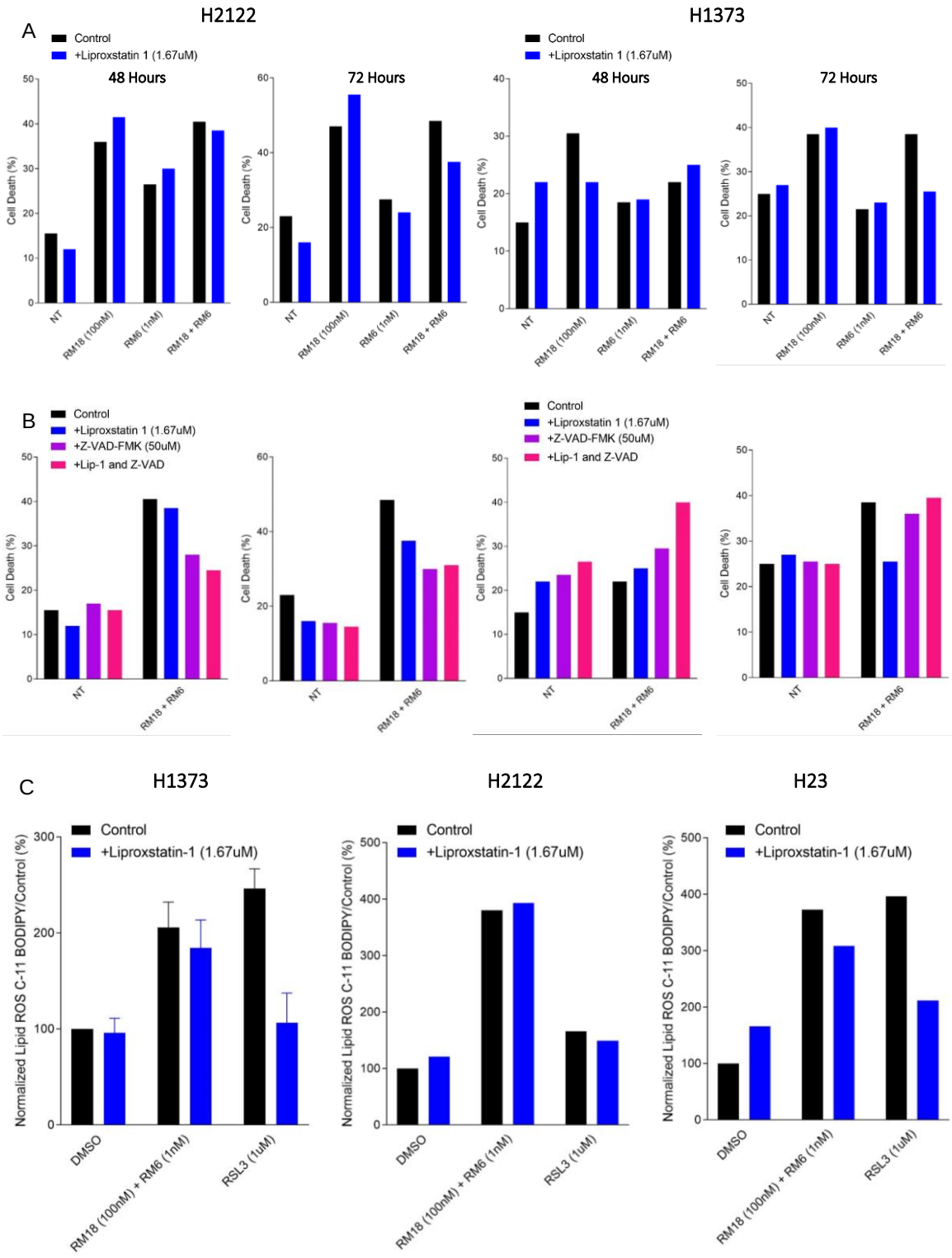
A
H2122
H1373
Control
+Liproxstatin 1 (1.67uM)
48 Hours
72 Hours
Cell Death (%)
NT
RM18 (100nM)
RM6 (1nM)
RM18 + RM6
B
+Z-VAD-FMK (50uM)
+Lip-1 and Z-VAD
C
H23
+Liproxstatin-1 (1.67uM)
Normalized Lipid ROS C-11 BODIPY/Control (%)
DMSO
RM18 (100nM) + RM6 (1nM)
RSL3 (1uM)

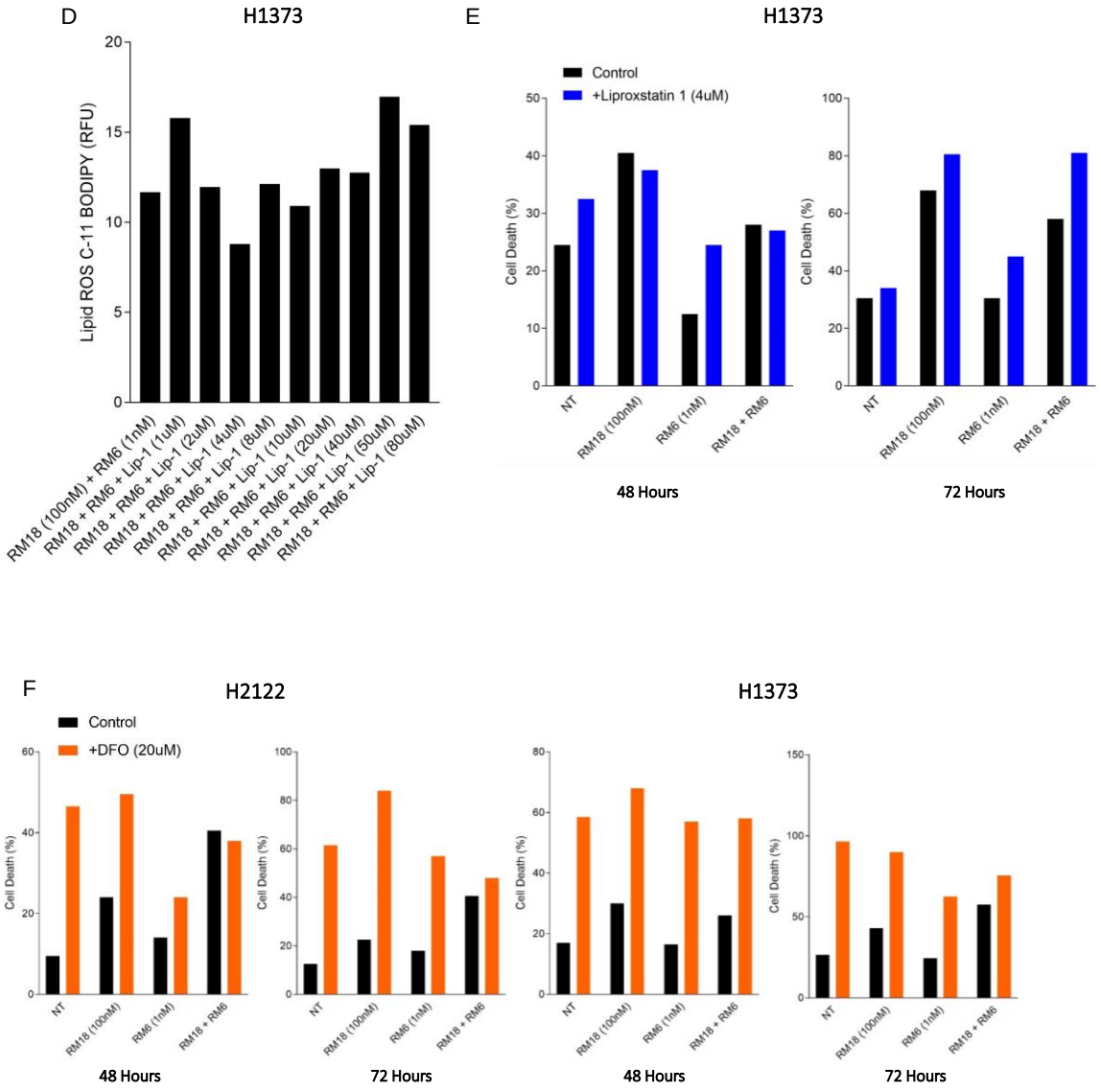
D
H1373
Lipid ROS C-11 BODIPY (RFU)
RM18 (100nM) + RM6 (1nM)
RM18 + RM6 + Lip-1 (1uM)
RM18 + RM6 + Lip-1 (2uM)
RM18 + RM6 + Lip-1 (4uM)
RM18 + RM6 + Lip-1 (8uM)
RM18 + RM6 + Lip-1 (10uM)
RM18 + RM6 + Lip-1 (20uM)
RM18 + RM6 + Lip-1 (40uM)
RM18 + RM6 + Lip-1 (50uM)
RM18 + RM6 + Lip-1 (80uM)
E
H1373
Control
+Liproxstatin 1 (4uM)
Cell Death (%)
NT
RM18 (100nM)
RM6 (1nM)
RM18 + RM6
48 Hours
72 Hours
F
H2122
H1373
Control
+DFO (20uM)
Cell Death (%)
NT
RM18 (100nM)
RM6 (1nM)
RM18 + RM6
48 Hours
72 Hours
48 Hours
72 Hours

Figure 4.5 Liproxstatin-1, a Potent Ferroptosis Inhibitor, Variably Rescues Cell Death Induced by the KRAS G12C/mTORC1 Inhibitor Combination.

(A) H2122 and H1373 were treated with 100nM RM18, 1nM RM6, or their combination with or without 1.67μM Lip-1, and cell death was assessed 48 and 72 hours post treatment by trypan blue exclusion viability assay.

(B) Same as in (A) for the control and combination groups, but with the addition of 50μM Z-VAD-FMK.

(C) H1373, H2122, and H23 were treated with 100nM RM18, 1nM RM6, or their combination with or without 1.67μM Lip-1 for 48 hours, and lipid peroxidation of the fluorescent reporter C-11 BODIPY was evaluated. RSL3, a ferroptosis inducer targeting GPX4, was added as a positive control. Each treatment group was assessed in 3 technical replicates. H1373 was assessed in an additional 2 biological replicates, and the averages and SDs are shown. Data is presented as a percentage of relative lipid ROS C-11 BODIPY normalized to control.

(D) H1373 was treated with the combination of 100nM RM18 and 1nM RM6, with or without escalating doses of Lip-1 for 48 hours, and lipid peroxidation of the fluorescent reporter C-11 BODIPY was evaluated. Each treatment group was assessed in 3 technical replicates. Data is presented as relative lipid ROS C-11 BODIPY.

(E) H1373 was treated with 100nM RM18, 1nM RM6, or their combination with or without 4μM Lip-1, and cell death was assessed 48 and 72 hours post treatment by trypan blue exclusion viability assay.

(F) H2122 and H1373 were treated with 100nM RM18, 1nM RM6, or their combination with or without 20μM DFO, an iron chelator, and cell death was assessed 48 and 72 hours post treatment by trypan blue exclusion viability assay.

The Majority of KRAS G12C Mutant NSCLC Models are Inherently Resistant to the Ferroptosis Inducers RSL3, Erastin, and iFSP1

KRAS G12C Mutant NSCLC Models are Broadly Resistant to the GPX4 Inhibitor RSL3

To understand the inherent degree of sensitivity of our models to ferroptosis, we evaluated the ferroptosis inducers RSL3, Erastin, and inhibitor of FSP1 (iFSP1) across the majority of our NSCLC models. We first began by assessing RSL3. We treated 10 cell lines with escalating doses of RSL3, from 10nM-3μM, and visually assessed the cells over the course of 24 and 48 hours. Bright-field microscopy images were captured for each treatment, and the cells were qualitatively evaluated for measures of cell viability, denoted by the degree of cell number reduction, and detached, floating cells in comparison to the control. H1373, H23, and H358 were the only cell lines that demonstrated measurable sensitivity to RSL3, with H23 exhibiting the greatest sensitivity among the three (**Figure 4.6A**). Overexpression of WT KRAS in H358 did not serve to modulate its sensitivity to RSL3 (data not shown). As expected, Lip-1 rescued RSL3 mediated cell death in H1373 and H23 (**Figure 4.6B**)

We subsequently evaluated levels of xCT and GPX4 in response to RSL3 to hopefully gain a better understanding of the molecular basis accounting for these differential sensitivities. RSL3 binds to GPX4 and inactivates it, thereby promoting ferroptosis (Yang and Stockwell 2008, Yang et al. 2014). Indeed, a band shift is readily observed for GPX4 in the presence of RSL3 at relevant doses that provoked cell death in H1373 (**Figure 4.6C**). Due to the massive death induced by RSL3 in H23 and H358, we

were unable to evaluate cells treated with appropriate concentrations of RSL3 that promoted this death. However, we can still observe this band shift in H358 at lower doses (**Figure 4.6D, E**). The GPX4 band shift mediated by RSL3 was also observed in models lacking sensitivity to RSL3 (**Figure 4.6F-I**), suggesting that RSL3 was indeed entering these cells and reaching its target, but still failed to cause associated cell death. Notably, levels of xCT and GPX4 were induced by RSL3 in some cell lines, likely reflective of homeostatic feedback control to increase cystine for GSH and/or GPX4 synthesis to counteract its suppression. As expected, c-PARP, a measure of apoptosis, was not significantly induced by RSL3 across our models.

To determine if resistant cell lines would be more responsive to a higher dose of RSL3, H2030, H2122, and Lu99 were treated with 10μM and 20μM of RSL3 for 24 and 48 hours. Cells were assessed visually by bright-field microscopy imaging, and protein expression of xCT, GPX4, and c-PARP was assayed by western blot. At these higher doses, RSL3 induced robust cell death, but was concomitant with substantial induction of c-PARP, suggesting off-target toxicity rather than pure ferroptosis (**Figure 4.6J-L**).

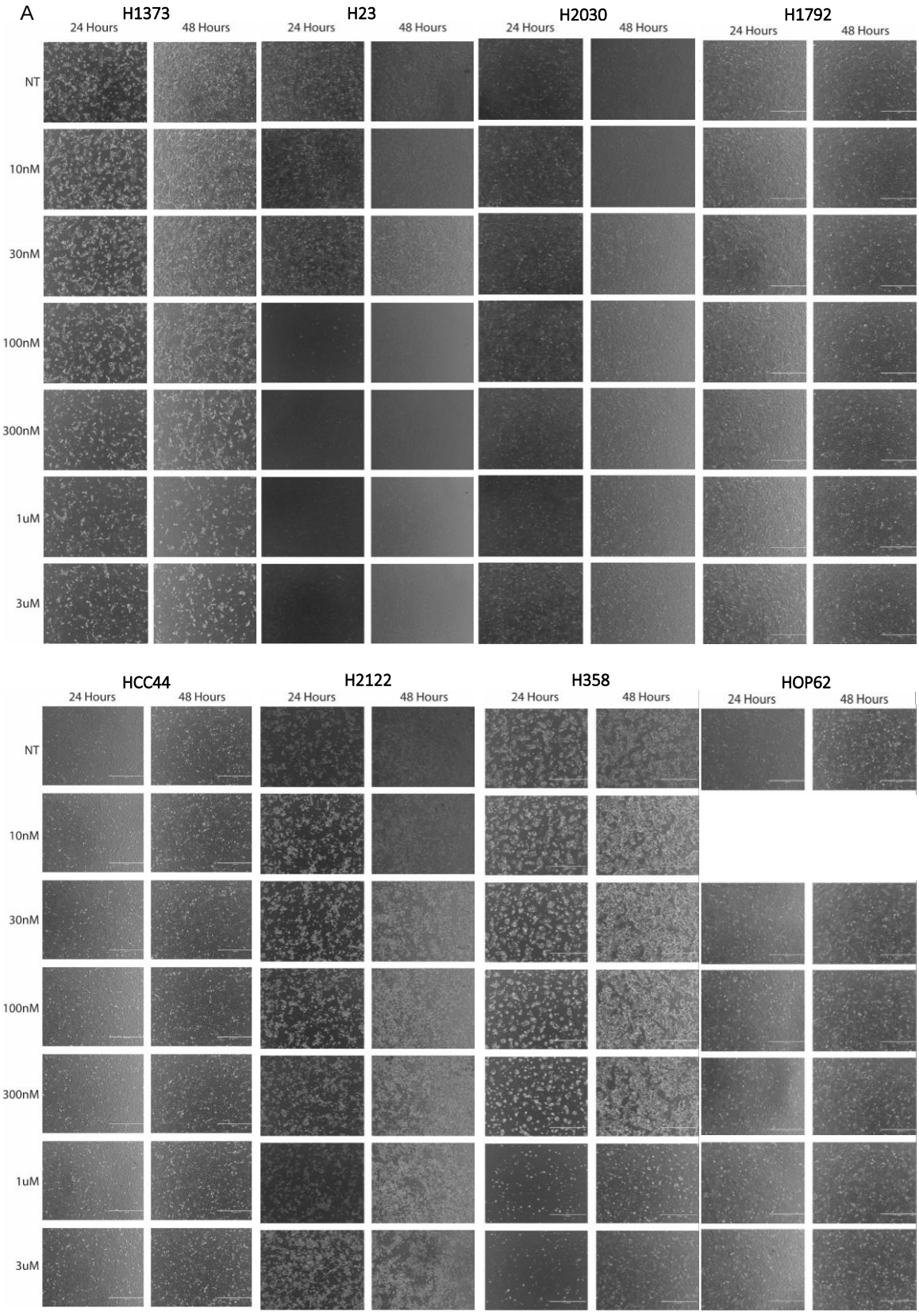
A
H1373
H23
H2030
H1792
24 Hours
48 Hours
NT
10nM
30nM
100nM
300nM
1uM
3uM
HCC44
H2122
H358
HOP62

A (cont.)

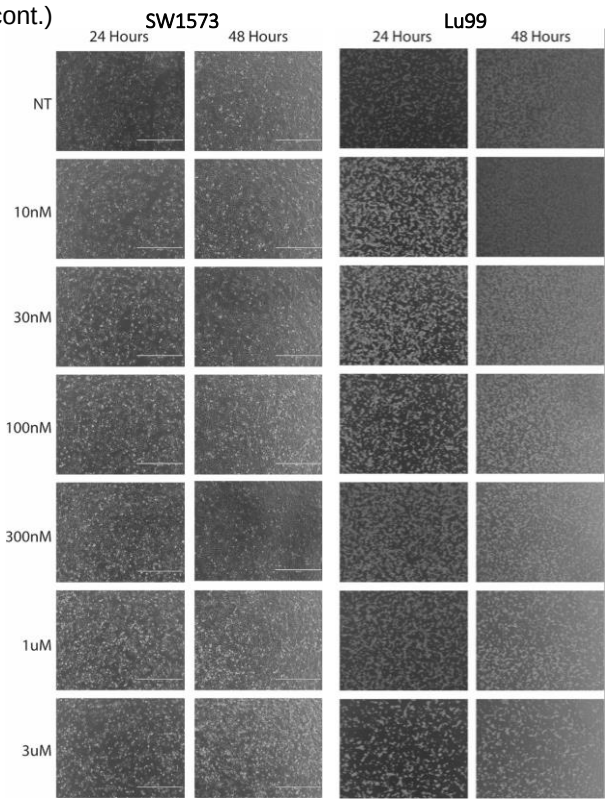
SW1573
Lu99
24 Hours
48 Hours
24 Hours
48 Hours
NT
10nM
30nM
100nM
300nM
1uM
3uM

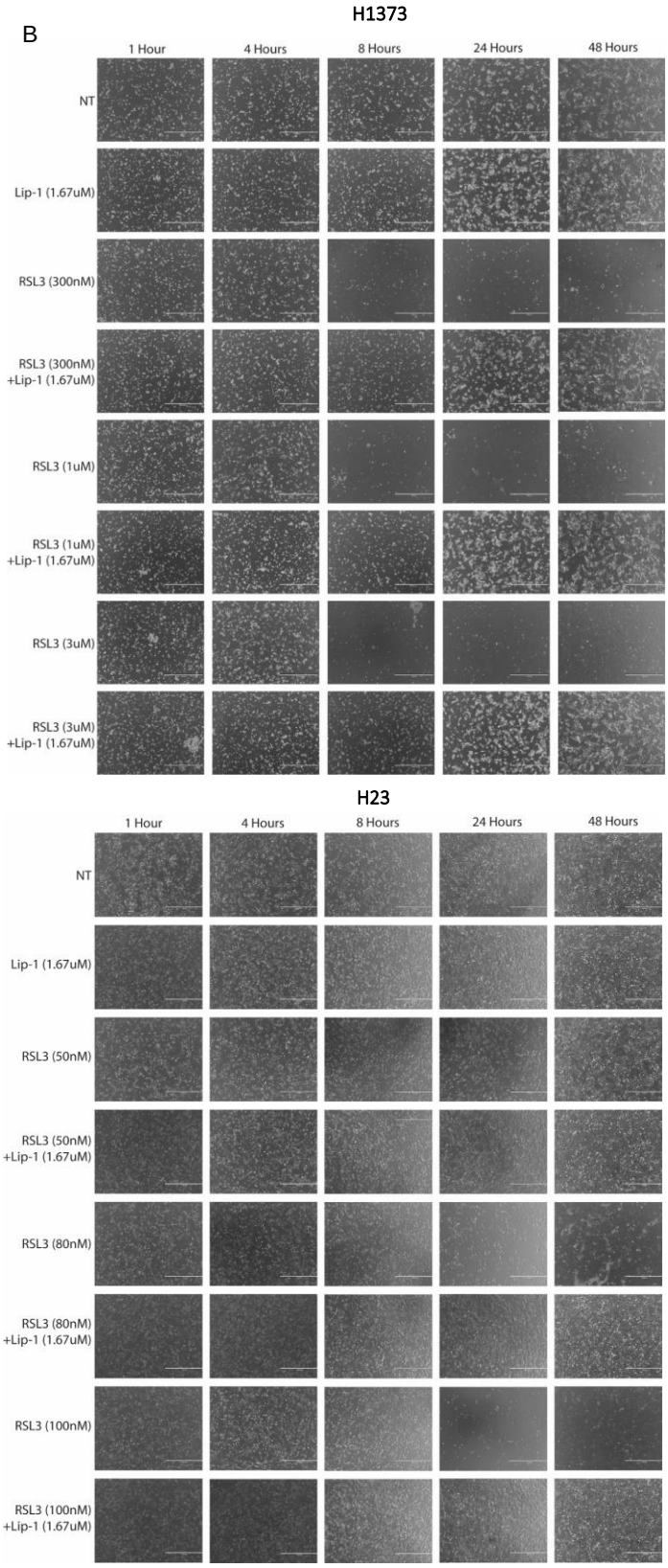
B
H1373
1 Hour
4 Hours
8 Hours
24 Hours
48 Hours
NT
Lip-1 (1.67uM)
RSL3 (300nM)
RSL3 (300nM) +Lip-1 (1.67uM)
RSL3 (1uM)
RSL3 (1uM) +Lip-1 (1.67uM)
RSL3 (3uM)
RSL3 (3uM) +Lip-1 (1.67uM)
H23
1 Hour
4 Hours
8 Hours
24 Hours
48 Hours
NT
Lip-1 (1.67uM)
RSL3 (50nM)
RSL3 (50nM) +Lip-1 (1.67uM)
RSL3 (80nM)
RSL3 (80nM) +Lip-1 (1.67uM)
RSL3 (100nM)
RSL3 (100nM) +Lip-1 (1.67uM)

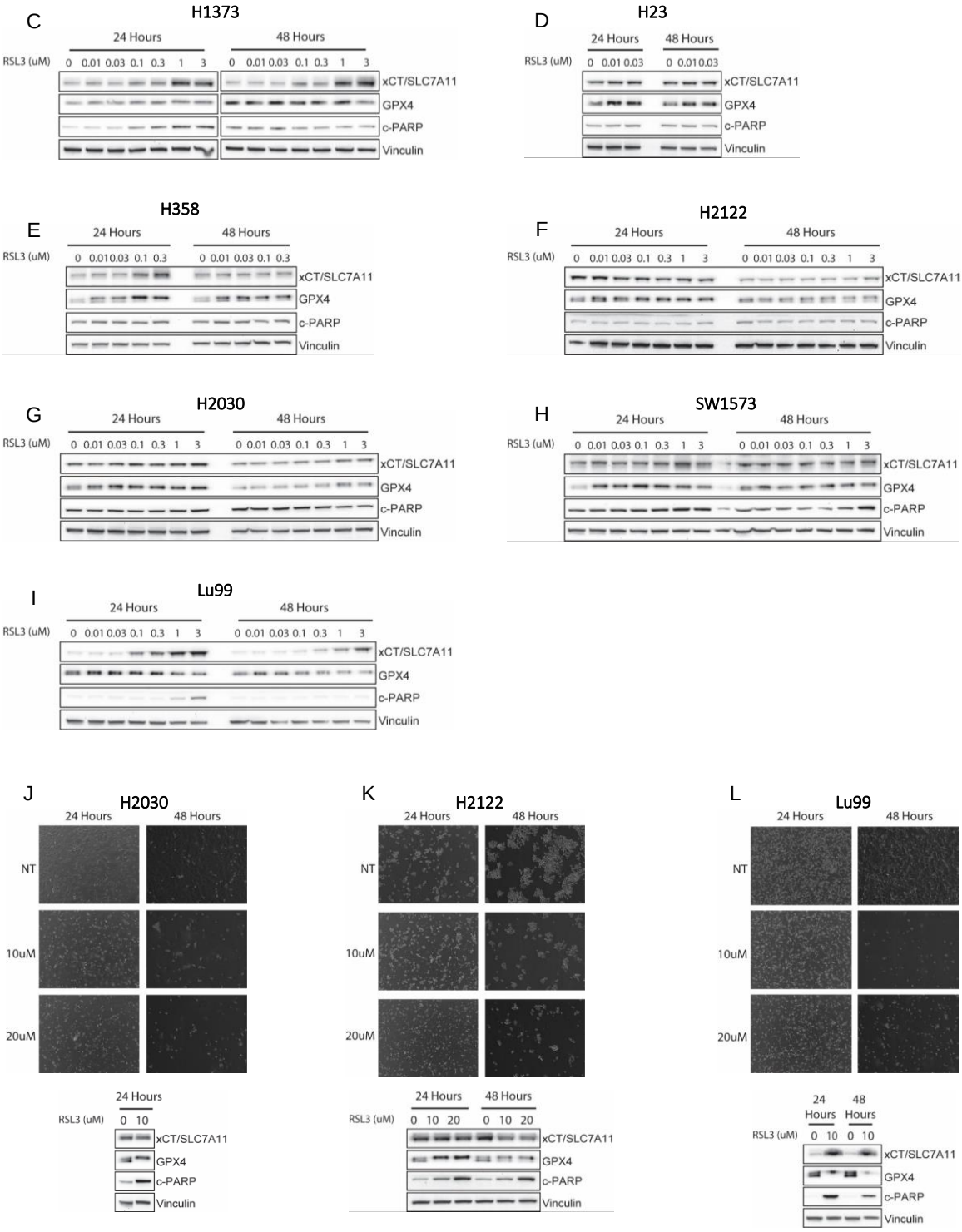
C
H1373
24 Hours
48 Hours
RSL3 (uM)
0 0.01 0.03 0.1 0.3 1 3
0 0.01 0.03 0.1 0.3 1 3
xCT/SLC7A11
GPX4
c-PARP
Vinculin
D
H23
24 Hours
48 Hours
RSL3 (uM)
0 0.01 0.03
0 0.01 0.03
xCT/SLC7A11
GPX4
c-PARP
Vinculin
E
H358
24 Hours
48 Hours
RSL3 (uM)
0 0.01 0.03 0.1 0.3
0 0.01 0.03 0.1 0.3
xCT/SLC7A11
GPX4
c-PARP
Vinculin
F
H2122
24 Hours
48 Hours
RSL3 (uM)
0 0.01 0.03 0.1 0.3 1 3
0 0.01 0.03 0.1 0.3 1 3
xCT/SLC7A11
GPX4
c-PARP
Vinculin
G
H2030
24 Hours
48 Hours
RSL3 (uM)
0 0.01 0.03 0.1 0.3 1 3
0 0.01 0.03 0.1 0.3 1 3
xCT/SLC7A11
GPX4
c-PARP
Vinculin
H
SW1573
24 Hours
48 Hours
RSL3 (uM)
0 0.01 0.03 0.1 0.3 1 3
0 0.01 0.03 0.1 0.3 1 3
xCT/SLC7A11
GPX4
c-PARP
Vinculin
I
Lu99
24 Hours
48 Hours
RSL3 (uM)
0 0.01 0.03 0.1 0.3 1 3
0 0.01 0.03 0.1 0.3 1 3
xCT/SLC7A11
GPX4
c-PARP
Vinculin
J
H2030
24 Hours
48 Hours
NT
10uM
20uM
24 Hours
RSL3 (uM)
0 10
xCT/SLC7A11
GPX4
c-PARP
Vinculin
K
H2122
24 Hours
48 Hours
NT
10uM
20uM
24 Hours
48 Hours
RSL3 (uM)
0 10 20
0 10 20
xCT/SLC7A11
GPX4
c-PARP
Vinculin
L
Lu99
24 Hours
48 Hours
NT
10uM
20uM
24 Hours
48 Hours
RSL3 (uM)
0 10
0 10
xCT/SLC7A11
GPX4
c-PARP
Vinculin

Figure 4.6 KRAS G12C Mutant NSCLC Models are Broadly Resistant to the GPX4 Inhibitor RSL3.

(A) KRAS G12 mutant NSCLC models were treated with escalating doses of RSL3, from 10nM-1μM. Cell dynamics were qualitatively assessed 24 and 48 hours post treatment by image capture bright-field microscopy.

(B) H1373 and H23 were treated with escalating doses of RSL3 with or without 1.67μM Lip-1. Cell dynamics were qualitatively assessed over the course of 48 hours by image capture bright-field microscopy.

(C) - (I) KRAS G12C mutant NSCLC cell lines were treated with escalating doses of RSL3 for 24 and 48 hours, and lysates probed with the indicated antibodies.

(K) - (L) H2030, H2122, and Lu99 were treated with 10μM and 20μM doses of RSL3. Cell dynamics were qualitatively assessed 24 and 48 hours post treatment by image capture bright-field microscopy. Lysates were also probed at the indicated time points with the indicated antibodies.

KRAS G12C Mutant NSCLC Models are Resistant to the xCT Inhibitor Erastin

We subsequently evaluated Erastin, an xCT inhibitor, in our models (Dolma et al. 2003). We treated 7 of our NSCLC cell lines with escalating doses of Erastin, from 500nM-10μM, and visually assessed the cells over the course of 24 and 48 hours. As before, bright-field microscopy images were captured for each treatment to qualitatively assess cell viability. At these doses, none of the models exhibited sensitivity to Erastin, including the cell lines with demonstrated sensitivity to RSL3 (**Figure 4.7A**). To determine if Erastin was functionally suppressing its target, H1373 and H2030 were treated with RM18, RM6, or their combination with or without 10μM Erastin, and GSH levels were assessed. In both control and drug treated cells, Erastin substantially suppressed GSH to near undetectable levels (**Figure 4.7B**). Mechanistically, Erastin suppressed GPX4 protein levels dose dependently at 24 and/or 48 hours in all assessed models, demonstrating that Erastin entered these cells and functioned as intended (**Figure 4.7C-I**).

To determine if a higher dose of Erastin would provoke cell death, H23, H2030, H2122, and Lu99 were treated with 20μM and 50μM doses of Erastin for 24 and 48 hours. Cells were assessed visually by bright-field microscopy imaging, and protein expression of xCT, GPX4, and c-PARP was assayed by western blot. At these higher doses, Erastin prompted considerable cell death in these models barring Lu99, which remained largely viable (**Figure 4.7J-M**). However, as with higher doses of RSL3, the increased cell death may stem from off-target toxicity, as evidenced by substantial induction of c-PARP at varying time points in H23, H2030, and H2122. To determine if mTORC1 inhibition could sensitize our models to Erastin, we treated Lu99, which harbors a PIK3CA mutation, and H1373, which harbors no known PI3K/AKT/mTOR pathway alteration, with RM6,

Erastin, or their combination. Cells were assessed visually by bright-field imaging at defined points over the course 48 hours. Cells were also collected at 1, 4, 8, 24, and 48 hours post treatment for signaling assessment by western blot. Erastin did not further enhance the growth suppressive effects of RM6 in either cell line, and no meaningful synergy was observed on the effect of RM6 towards the evaluated ferroptosis regulatory targets or factors within the PI3K/AKT/mTOR signaling axis (**Figure 4.7N, O**).

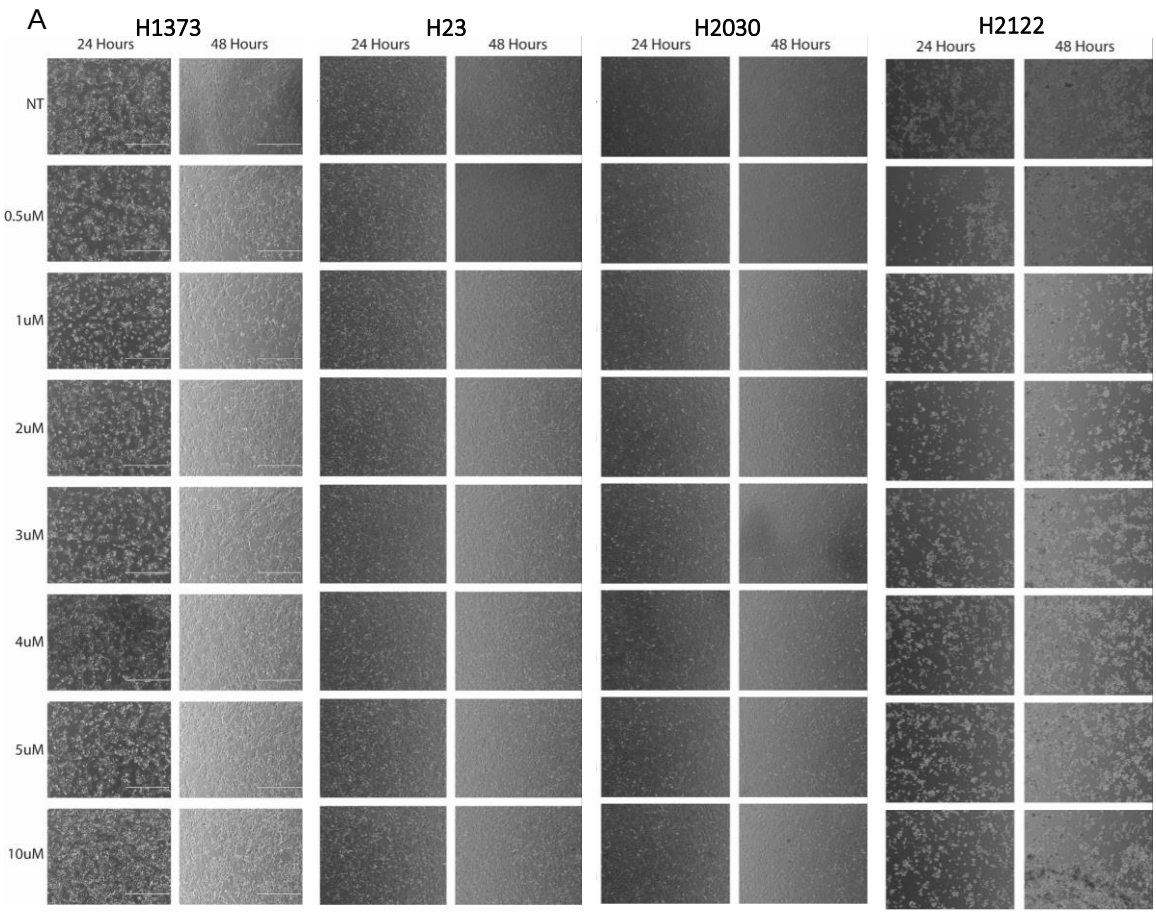
A
H1373
H23
H2030
H2122
24 Hours
48 Hours
NT
0.5uM
1uM
2uM
3uM
4uM
5uM
10uM

A (cont.)

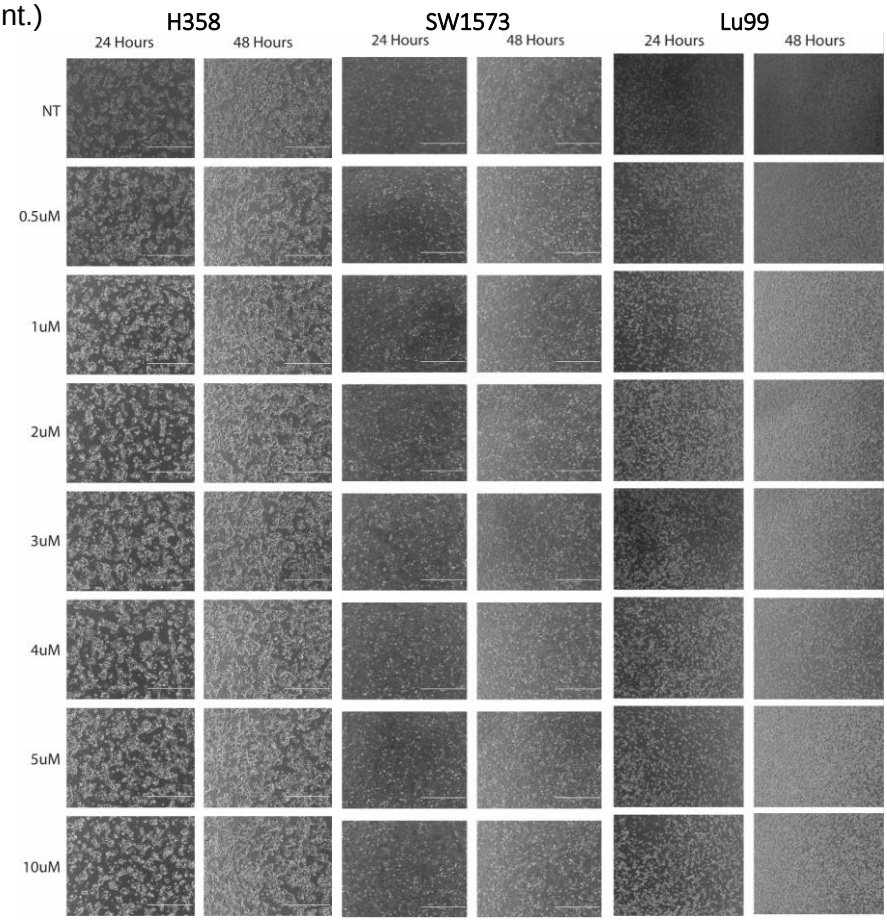
H358
SW1573
Lu99
24 Hours
48 Hours
24 Hours
48 Hours
24 Hours
48 Hours
NT
0.5uM
1uM
2uM
3uM
4uM
5uM
10uM

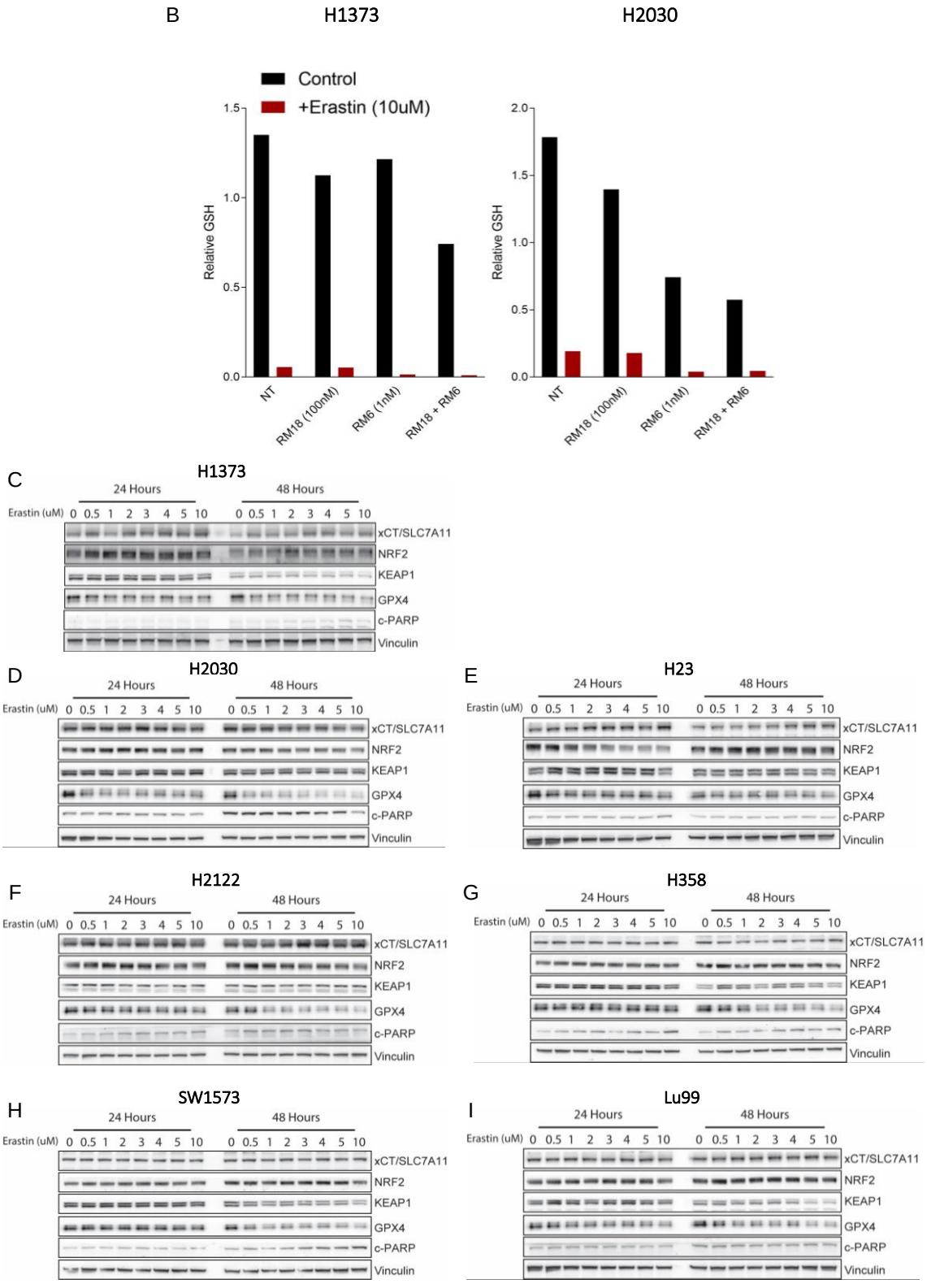
B
H1373
H2030
Control
+Erastin (10uM)
Relative GSH
1.5
1.0
0.5
0.0
2.0
1.5
1.0
0.5
0.0
NT
RM18 (100nM)
RM6 (1nM)
RM18 + RM6
C
H1373
24 Hours
48 Hours
Erastin (uM) 0 0.5 1 2 3 4 5 10 0 0.5 1 2 3 4 5 10
xCT/SLC7A11
NRF2
KEAP1
GPX4
c-PARP
Vinculin
D
H2030
E
H23
F
H2122
G
H358
H
SW1573
I
Lu99

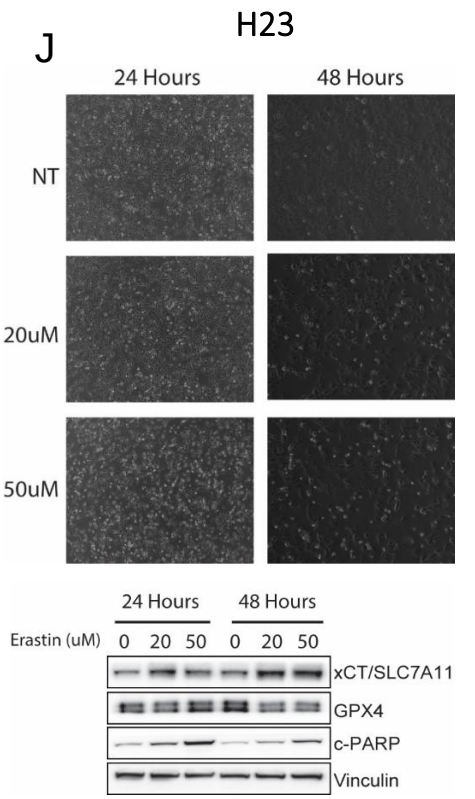
J
H23
24 Hours
48 Hours
NT
20uM
50uM
24 Hours
48 Hours
Erastin (uM)
0 20 50 0 20 50
xCT/SLC7A11
GPX4
c-PARP
Vinculin

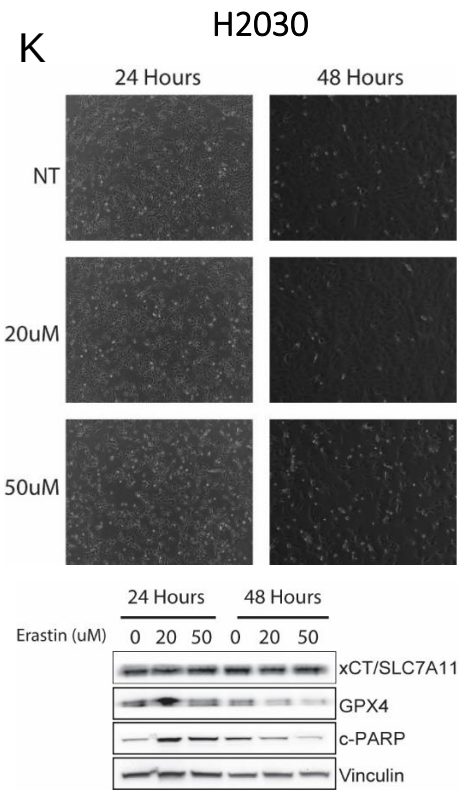
K
H2030
24 Hours
48 Hours
NT
20uM
50uM
24 Hours
48 Hours
Erastin (uM)
0 20 50 0 20 50
xCT/SLC7A11
GPX4
c-PARP
Vinculin

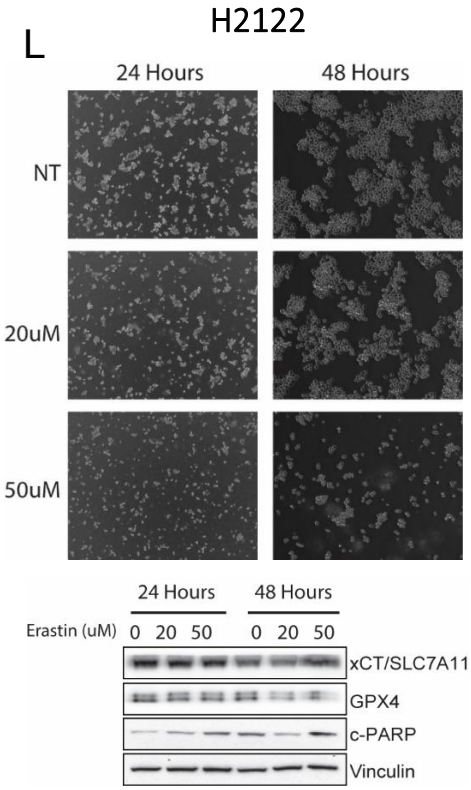
L
H2122
24 Hours
48 Hours
NT
20uM
50uM
24 Hours
48 Hours
Erastin (uM)
0 20 50 0 20 50
xCT/SLC7A11
GPX4
c-PARP
Vinculin

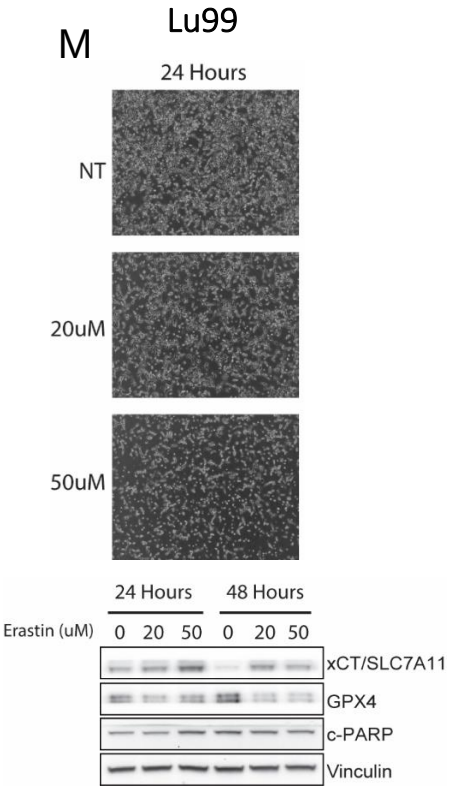
M
Lu99
24 Hours
NT
20uM
50uM
24 Hours
48 Hours
Erastin (uM)
0 20 50 0 20 50
xCT/SLC7A11
GPX4
c-PARP
Vinculin

H1373

N

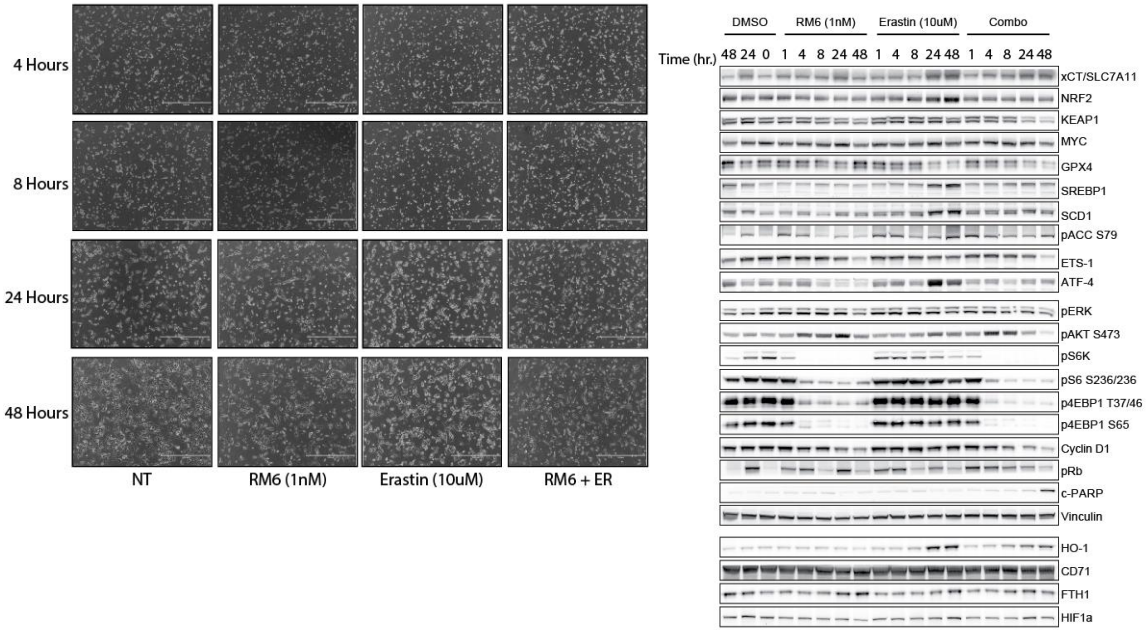

Lu99

O

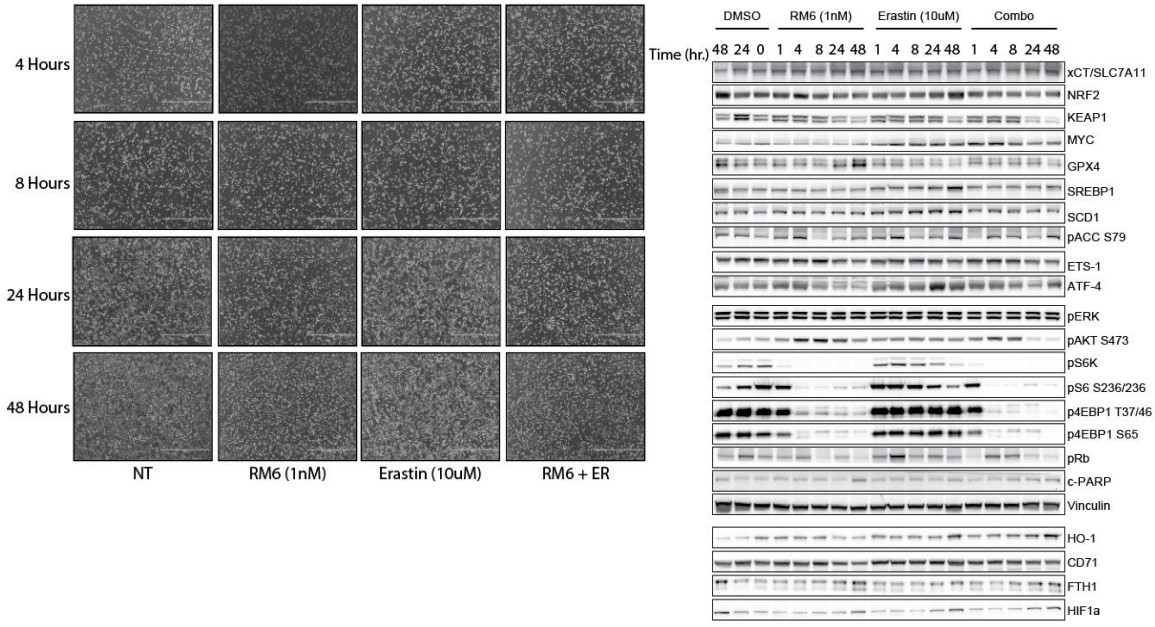

Figure 4.7 KRAS G12C Mutant NSCLC Models are Resistant to the xCT Inhibitor Erastin.

(A) KRAS G12C mutant NSCLC models were treated with escalating doses of Erastin, from 500nM-10μM. Cell dynamics were qualitatively assessed 24 and 48 hours post treatment by image capture bright-field microscopy.

(B) H1373 and H2030 were treated with 100nM RM18, 1nM RM6, or their combination with or without 10μM Erastin for 48 hours, and GSH levels were assessed.

(C) - (I) KRAS G12C mutant NSCLC cell lines were treated with escalating doses of Erastin for 24 and 48 hours, and lysates probed with the indicated antibodies.

(J) - (M) H23, H2030, H2122, and Lu99 were treated with 20μM and 50μM doses of Erastin. Cell dynamics were qualitatively assessed 24 and 48 hours post treatment by image capture bright-field microscopy. Lysates were probed at the indicated time points with the indicated antibodies.

(N), (O) H1373 and Lu99 were treated with 1nM RM6, 10μM Erastin, or their combination. Cell dynamics were qualitatively assessed over the course of 48 hours by image capture bright-field microscopy. Lysates were probed at the indicated times with the indicated antibodies.

KRAS G12C Mutant NSCLC Models are Resistant to FSP1 Inhibition

Although the data thus far strongly indicated that, by and large, our NSCLC models were inherently resistant to ferroptosis as a cell death mechanism, at least in the context of ferroptosis inducers, to complete these studies we evaluated FSP1, another key regulator of ferroptosis. Unlike GPX4, which reduces hydroperoxide groups in polyunsaturated fatty acid residues to their corresponding alcohols, FSP1 reduces ubiquinone, yielding ubiquinol, which, in turn, can directly or indirectly (through recycling α-tocopherol) scavenge lipid radicals in membranes, thereby halting lipid peroxidation and associated ferroptosis (Bersuker et al. 2019, Doll et al. 2019). We reasoned that: (1) our models may be more dependent on FSP1 to mitigate ferroptosis as opposed to GPX4, (2) in the setting of GPX4 suppression, FSP1 might mitigate ferroptosis, and (3) that inhibiting both FSP1 and GPX4 may be required to induce ferroptosis in our models.

To determine if FSP1 played a major role in mitigating ferroptosis in our models, we treated H23, H1373, and SW1573 with escalating doses of an FSP1 inhibitor, iFSP1, from 10nM-10μM, for 24 and 48 hours. Bright-field microscopy images were captured for each treatment to qualitatively assess cell dynamics. At these doses, none of the models exhibited sensitivity to FSP1 (**Figure 4.8A**). We also evaluated signaling after treatment at the corresponding time points. FSP1 protein levels were induced by iFSP1 at 48 hours in H23 and SW1573 at doses of 1, 3, and 10μM, while FSP1 levels were modestly suppressed at these same doses in H1373 (**Figure 4.8B-D**). Basal assessment of GPX4 and FSP1 levels in several of our models revealed that some cell lines expressed high levels of GPX4 and low levels of FSP1, while others expressed higher levels of FSP1 and lower levels of GPX4 (**Figure 4.8E**). To determine if dual suppression of FSP1 and GPX4 would synergize to

induce ferroptosis in our models, H23, H1373, H2122, and SW1573 were treated with RSL3, iFSP1, or their combination. As before, bright-field microscopy images were captured for each treatment to qualitatively assess cell dynamics. The exquisite sensitivity of H23 to RSL3 alone, even at a lower dose, precluded an observation of synergy in this cell line (**Figure 4.8F**). Similarly, iFSP1 did not appear to add to the cell death induction mediated by RSL3 in H1373 (**Figure 4.8G**). No appreciable synergy was observed for H2122 or SW1573 at the doses used (**Figure 4.8H, I**).

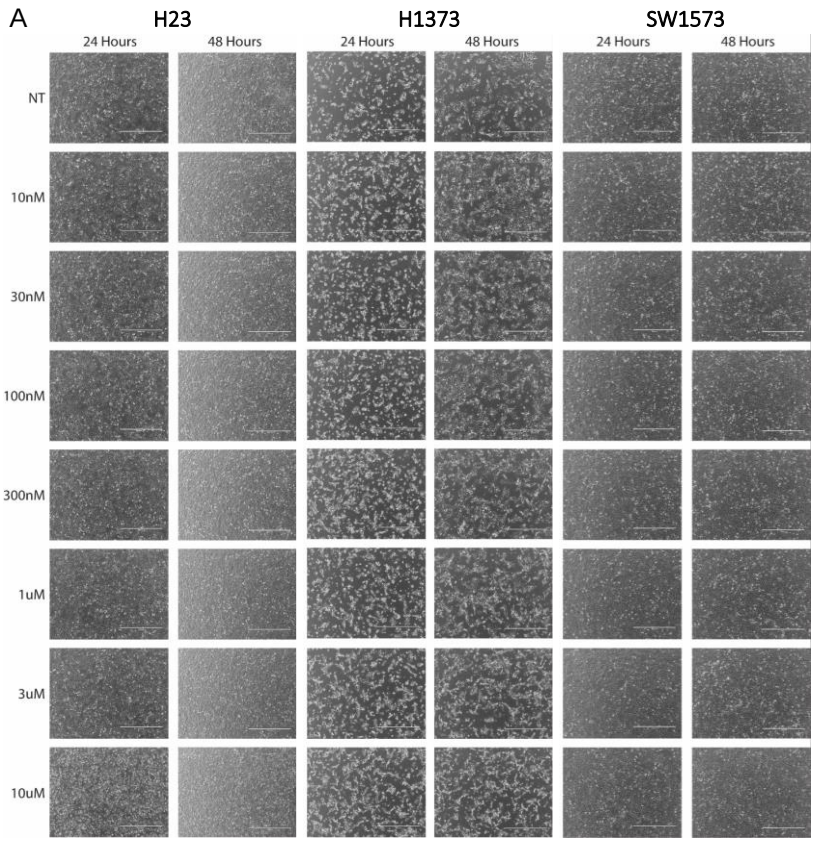
A
H23
H1373
SW1573
24 Hours
48 Hours
NT
10nM
30nM
100nM
300nM
1uM
3uM
10uM


B
H23
24 Hours
48 Hours
iFSP1 (uM)
0 .01 .03 .1 .3 1 3 10
FSP1
GPX4
xCT
NRF2
NFkB
Vinculin

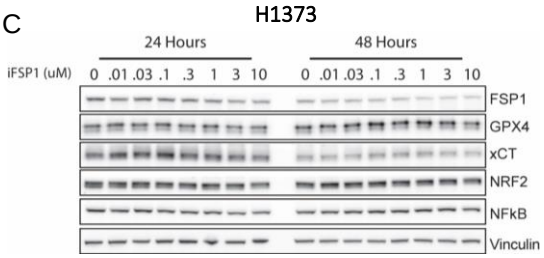
C
H1373
24 Hours
48 Hours
iFSP1 (uM)
0 .01 .03 .1 .3 1 3 10
FSP1
GPX4
xCT
NRF2
NFkB
Vinculin

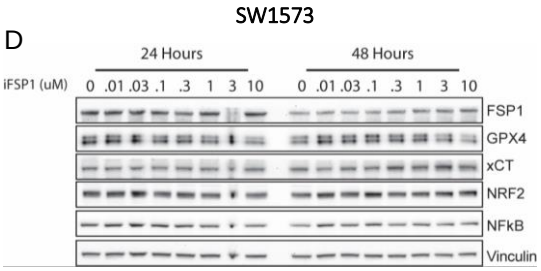
D
SW1573
24 Hours
48 Hours
iFSP1 (uM)
0 .01 .03 .1 .3 1 3 10
FSP1
GPX4
xCT
NRF2
NFkB
Vinculin

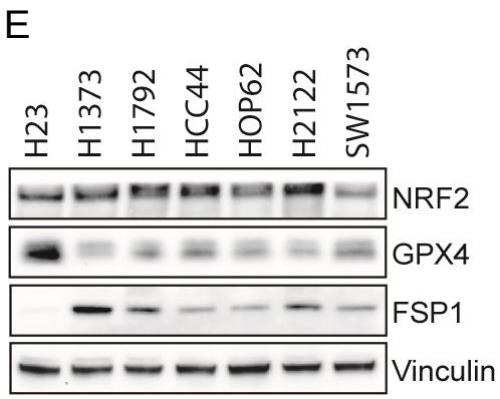
E
H23
H1373
H1792
HCC44
HOP62
H2122
SW1573
NRF2
GPX4
FSP1
Vinculin

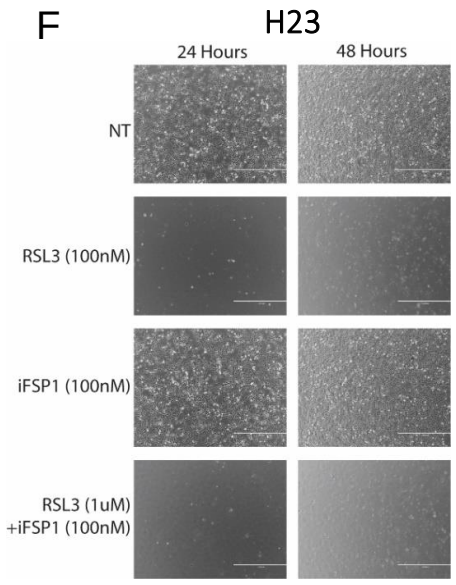
F
H23
24 Hours
48 Hours
NT
RSL3 (100nM)
iFSP1 (100nM)
RSL3 (1uM)
+iFSP1 (100nM)

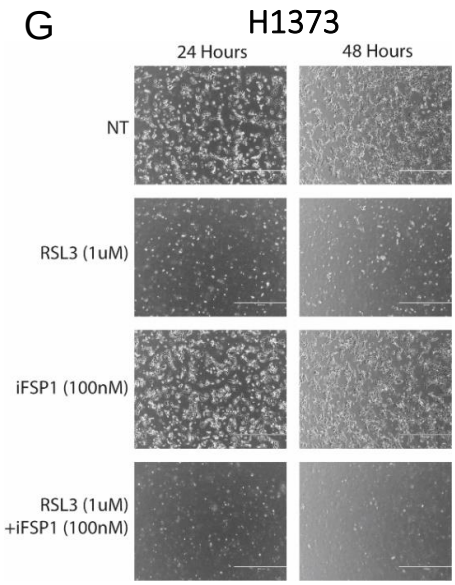
G
H1373
24 Hours
48 Hours
NT
RSL3 (1uM)
iFSP1 (100nM)
RSL3 (1uM)
+iFSP1 (100nM)

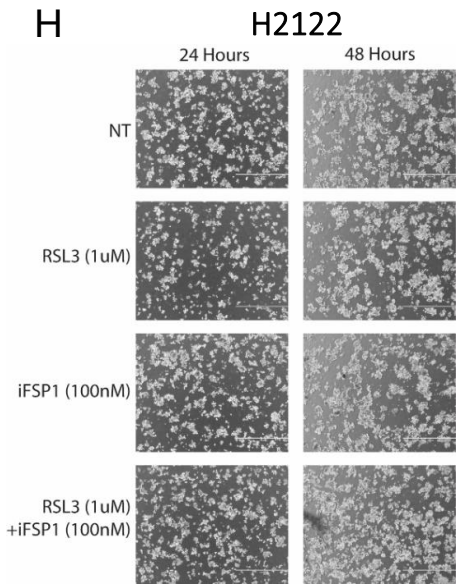
H
H2122
24 Hours
48 Hours
NT
RSL3 (1uM)
iFSP1 (100nM)
RSL3 (1uM)
+iFSP1 (100nM)

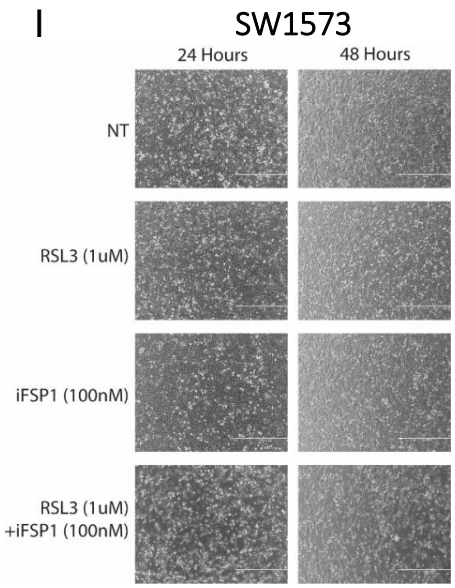
I
SW1573
24 Hours
48 Hours
NT
RSL3 (1uM)
iFSP1 (100nM)
RSL3 (1uM)
+iFSP1 (100nM)

Figure 4.8 KRAS G12C Mutant NSCLC Models are Resistant to FSP1 Inhibition.

(A) H23, H1373, and SW1573 were treated with escalating doses of iFSP1, from 10nM-10μM. Cell dynamics were qualitatively assessed 24 and 48 hours post treatment by image capture bright-field microscopy.

(B) - (D) H23, H1373, and SW1573 were treated with escalating doses of iFSP1 for 24 and 48 hours, and lysates probed with the indicated antibodies.

(E) Basal assessment of GPX4, FSP1, and NRF2 expression at 24 hours in KRAS G12C mutant NSCLC models.

(F) - (I) H23, H1373, H2122, and SW573 were treated with RSL3, iFSP1, or their combination. Cell dynamics were qualitatively assessed over the course of 48 hours by image capture bright-field microscopy. Lysates were probed at the indicated times with the indicated antibodies.

α-Tocopherol Rescues Cell Death Induced by the KRAS G12C/mTORC1 Inhibitor Combination, and Suppressed Cell Growth Precipitated by All Treatment Groups

Despite the overwhelming evidence suggesting that ferroptosis was most likely not a mechanism of death induced by the KRAS G12C/mTORC1 inhibitor combination, we wanted to determine if vitamin E, specifically its major component, α-Tocopherol, which serves as the most powerful, natural chain-breaking antioxidant in lipid membranes (Burton and Ingold 1986), could attenuate lipid peroxidation induced by the drug combination and, in turn, rescue cell death. H2122 and H1373 were treated with the RM18/RM6 drug combination with or without α-Tocopherol (α-Toc), and levels of ROS, lipid peroxidation, and cell death were evaluated. In both models α-Toc demonstrated substantial rescue of ROS (**Figure 4.9A**), and relatively modest rescue of lipid peroxidation (**Figure 4.9B**). Despite this, α-Toc almost completely rescued cell death induced by the combination in H2122, with a lower rescue observed in H1373 (**Figure 4.9C**). Furthermore, α-Toc considerably rescued cell growth suppression mediated by RM18, RM6, and their combination, even in H1373 where cell death rescue was less striking, without notably impacting the control (**Figure 4.9D**). Similar results were also obtained for H23 (data not shown). Since α-Toc robustly rescued cell death induced by the combination in H2122, we did not expect pan caspase inhibition to add further gains to α-Toc mediated death rescue, and this was indeed the case for H2122, as well as for H1373, where α-Toc rescue of cell death was not as complete (data not shown).

To more definitively determine the type of cell death rescued by α-Toc, we treated H2122 with the KRAS G12C/mTORC1 inhibitor combination with or without α-Toc for 48 and 72 hours, stained the cells with Annexin V, DAPI, and Sytox Green, a nuclear and

chromosome counterstain impermeant to live cells that's commonly used to assess non-apoptotic (e.g., ferroptotic, necrotic) cell death, and performed fluorescence microscopy imaging. We also included Z-VAD for comparison. The combination exhibited considerable Annexin V staining, and notable Sytox Green staining, at 48 and 72 hours (**Figure 4.9E**). Z-VAD substantially reduced Annexin V and Sytox Green staining at 48 hours in the drug combination, but these effects were significantly dampened, towards Annexin V in particular, by 72 hours. In contrast, α-Toc considerably reduced both Annexin V and Sytox Green staining in the combination at both time points. If we observe the overlay in the combination setting, we see that Annexin V positive cells and Sytox Green positive cells considerably overlap, indicating that the same population of cells were stained by both markers. These results highlight the improved ability of α-Toc to durably rescue cell death induced by the drug combination, regardless of if the death mechanism is apoptotic, a dominant contributor, or a mechanism that's more minor/infrequent, such as necroptosis.

Collectively, these data strongly suggest that apoptosis is the primary mechanism of cell death induced by the KRAS G12C/mTORC1 inhibitor combination in our NSCLC models. Furthermore, the majority of our cell lines demonstrate substantial resistance to ferroptosis inducers, regardless of the node(s) targeted (GPX4, xCT, FSP1). Despite ferroptosis not being an apparent contributor to the cell death induced by the drug combination, the antioxidant α-Toc significantly rescued this death. Compelled to better understand these results, and the molecular underpinnings contributing to this effect, we dived into investigating this phenomenon, presented in the next chapter.

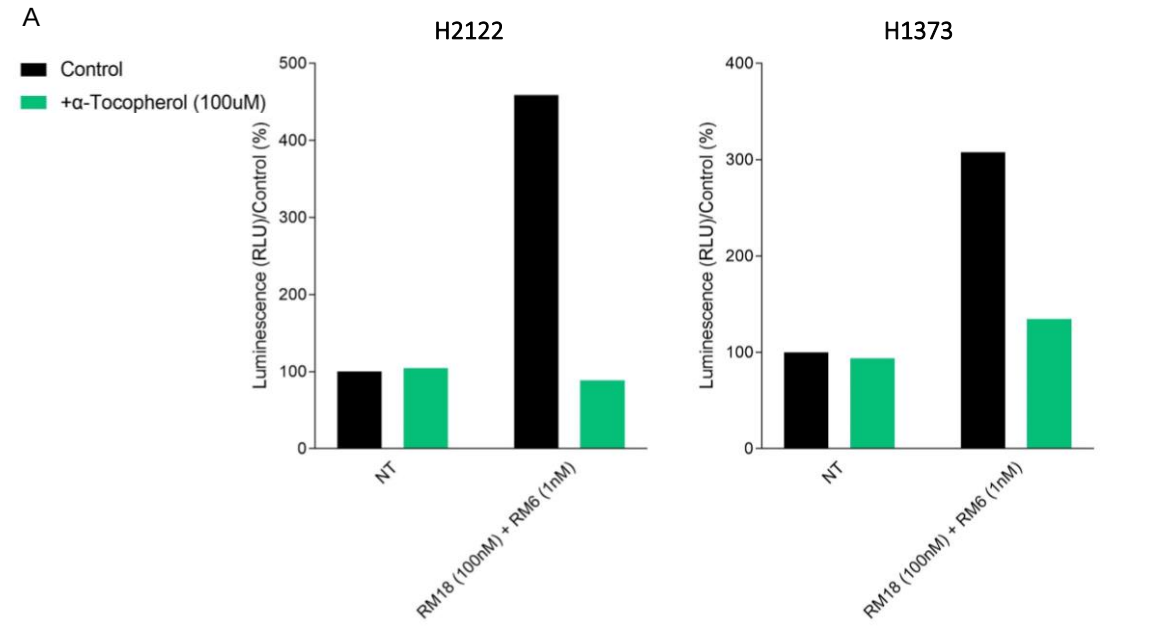
A
H2122
H1373
Control
+α-Tocopherol (100uM)
Luminescence (RLU)/Control (%)
500
400
300
200
100
0
NT
RM18 (100nM) + RM6 (1nM)

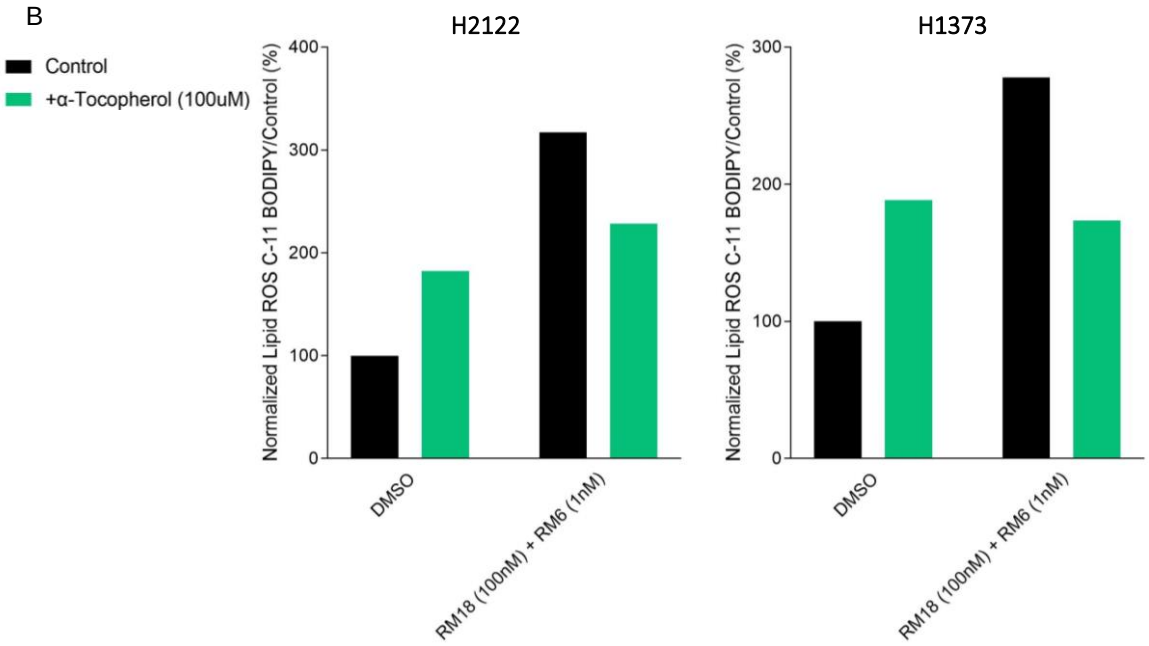
B
H2122
H1373
Control
+α-Tocopherol (100uM)
Normalized Lipid ROS C-11 BODIPY/Control (%)
400
300
200
100
0
DMSO
RM18 (100nM) + RM6 (1nM)

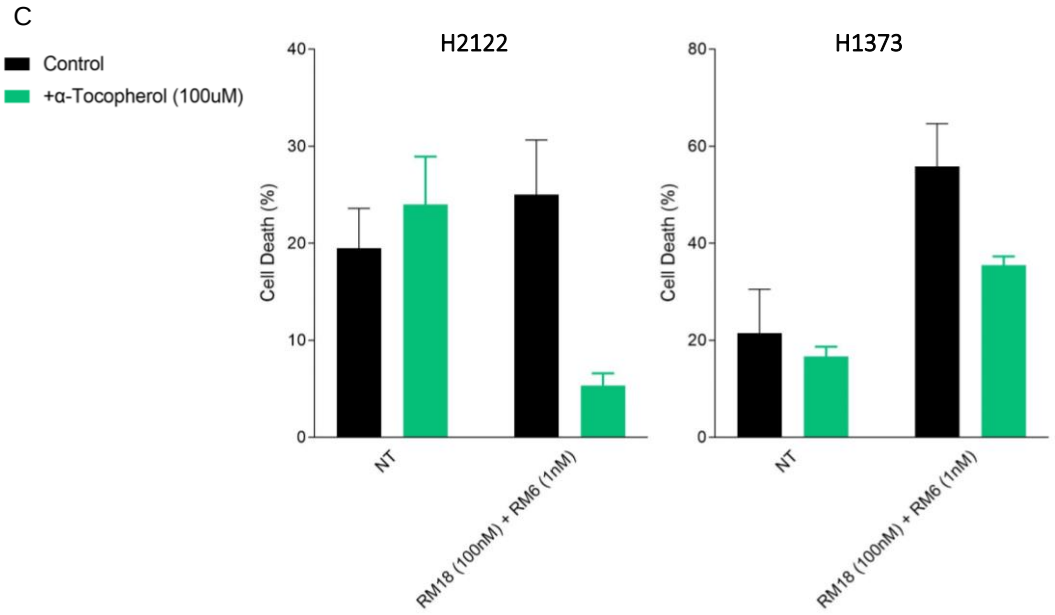
C
Control
+α-Tocopherol (100uM)
H2122
H1373
Cell Death (%)
NT
RM18 (100nM) + RM6 (1nM)

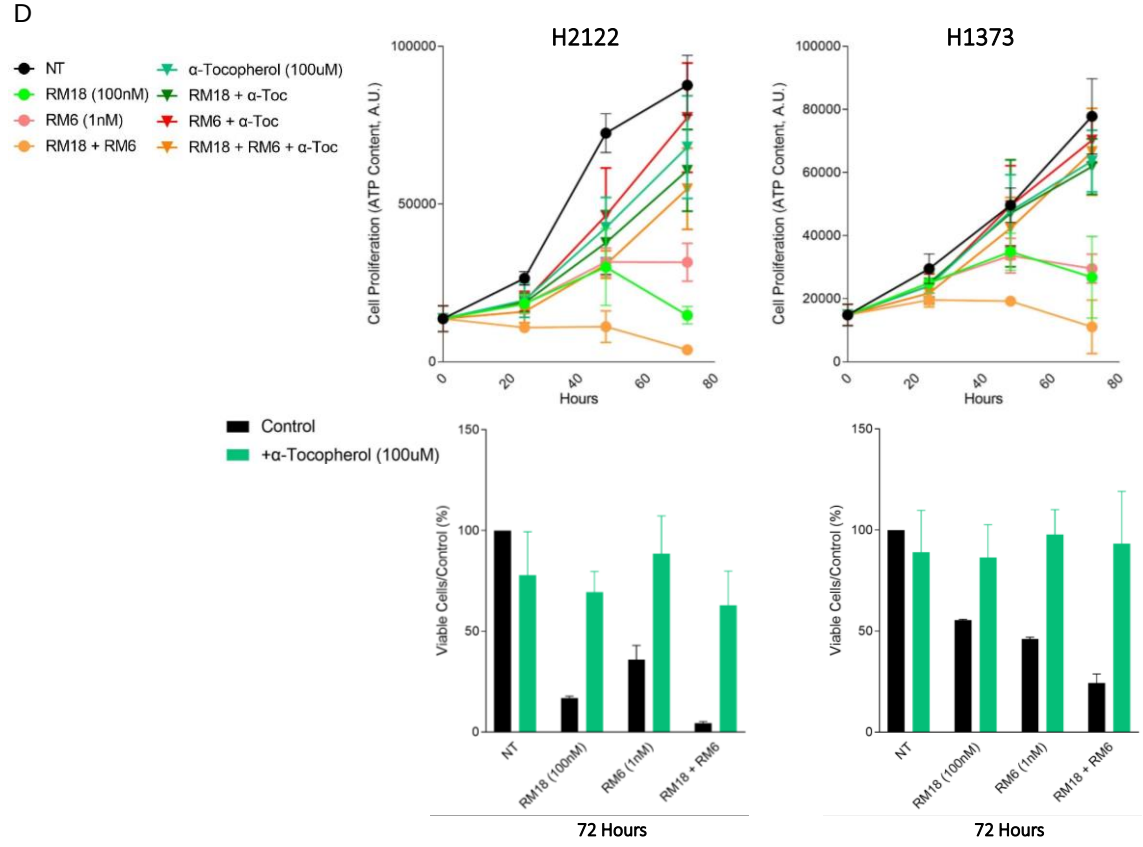
D
NT
RM18 (100nM)
RM6 (1nM)
RM18 + RM6
α-Tocopherol (100uM)
RM18 + α-Toc
RM6 + α-Toc
RM18 + RM6 + α-Toc
H2122
H1373
Cell Proliferation (ATP Content, A.U.)
Hours
Control
+α-Tocopherol (100uM)
Viable Cells/Control (%)
NT
RM18 (100nM)
RM6 (1nM)
RM18 + RM6
72 Hours

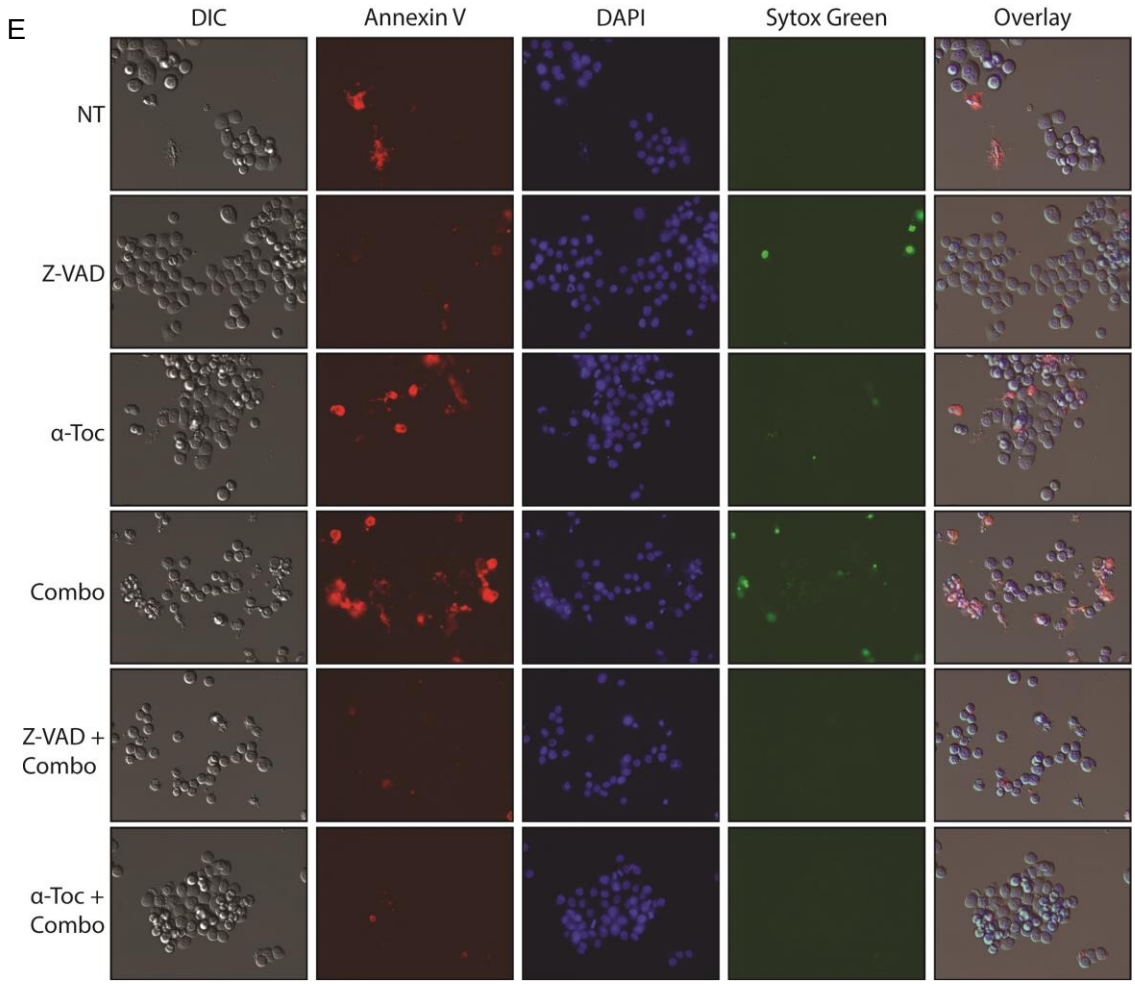
E
DIC
Annexin V
DAPI
Sytox Green
Overlay
NT
Z-VAD
α-Toc
Combo
Z-VAD + Combo
α-Toc + Combo

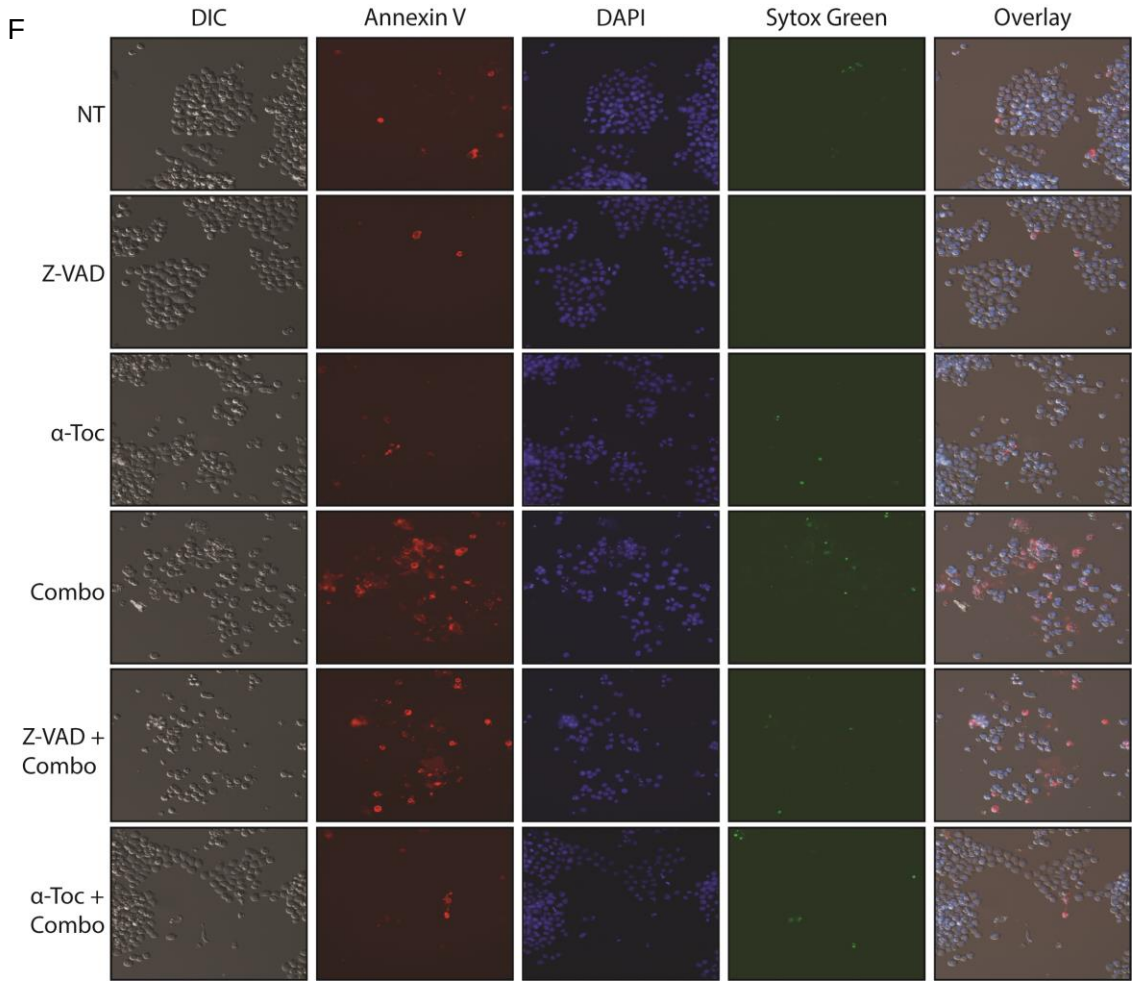
F
DIC
Annexin V
DAPI
Sytox Green
Overlay
NT
Z-VAD
α-Toc
Combo
Z-VAD +
Combo
α-Toc +
Combo

Figure 4.9 α-Tocopherol Rescues Cell Death Induced by the KRAS G12C/mTORC1 Inhibitor Combination, and Suppressed Cell Growth Precipitated by all Treatment Groups.

(A) H2122 and H1373 were treated with the combination of 100nM RM18 and 1nM RM6 for 48 hours, and levels of ROS were evaluated. Each treatment group was assessed in 3-5 technical replicates. Data is presented as percentage of ROS luminescence normalized to control.

(B) H2122 and H1373 were treated with the combination of 100nM RM18 and 1nM RM6 for 48 hours, and lipid peroxidation of the fluorescent reporter C-11 BODIPY was evaluated. Each treatment group was assessed in 3 technical replicates. Data is presented as a percentage of relative lipid ROS C-11 BODIPY normalized to control.

(C) H2122 and H1373 were treated with the combination of 100nM RM18 and 1nM RM6 for 72 hours, and cell death was evaluated. Each treatment group was assessed in 3 biological replicates, and the averages and SDs are shown.

(D) H2122 and H1373 were treated with the 100nM RM18, 1nM RM6, or their combination with or without 100μM α-Toc, and cell viability was assessed over the course of 72 hours. Each treatment group was assessed in 2 biological replicates, with 5 technical replicates per assay, and the averages and SDs are shown. Below each growth curve is the corresponding cell viability presented as a percent normalized to control at the terminal time point.

(E) , (F) H2122 was treated with the combination of 100nM RM18 and 1nM RM6 with or without 100μM α-Toc for 48 (E) and 72 (F) hours. The cells were subsequently stained with Annexin V, DAPI, and Sytox Green, a nuclear and chromosome counterstain impermeant to live cells. We also included 50μM Z-VAD for comparison. For each treatment at each timepoint, ten fields of view were captured, and representative images are shown. The staining is merged in the overlay.

Chapter 5: Vitamin E – A Drug Interference is Discovered against RAS GTP Inhibitors and mTOR Bi-Steric Inhibitors

Introduction

Vitamin E is an essential, lipid-soluble molecule that plays a central role in maintaining redox homeostasis by scavenging ROS and reactive nitrogen species (RNS), with consequent reduction in the formation and accumulation of damaged molecules such as membrane lipids, proteins, and nucleic acids. The vitamin E family consists of eight natural analogues – α-, β-, γ-, and δ-tocopherol, and α-, β-, γ-, and δ-tocotrienol – that exhibit varying degrees of biological activity (**Figure 5A**). Natural vitamin E is a composite of three functional and structural entities: (1) the hydrophobic side chain that anchors vitamin E in the plasma membrane (phytyl side chain for tocopherols, unsaturated isoprenoid side chain for tocotrienols), (2) the methylated chromane ring, and (3) the redox-active hydroxyl, which can become phosphorylated. Natural vitamin E metabolites can have a shorter hydrophobic and/or hydroxylated side chain, an oxidized chromane group, and a modified hydroxyl group (**Figure 5B**). Vitamin E analogues demonstrate differential efficiency of cellular uptake, transport, intracellular distribution, and conversion to different metabolites. α-Toc is selectively recognized and enriched by the liver α-tocopherol transfer protein (αTTP), and therefore in plasma and most tissues reaches much higher (~50x) concentrations than the remaining analogues, which are more readily metabolized and excreted (Zingg 2015).

Numerous foods provide vitamin E, with nuts, seeds, vegetable oils, green leafy vegetables, and fortified cereals among the best sources of α-Toc. Most vitamin E in the

American diet is in the form of γ-tocopherol from soybean, canola, corn, and other vegetable oils and food products (National Institutes of Health 2021). Oral ingestion of vitamin E results in the formation of micelles with bile acids, cholesterol, phospholipid, and triacylglycerol to facilitate transport to the intestinal lumen. Subsequent uptake of vitamin E across the intestinal epithelium is mediated by various transport proteins, including MTTP, NPC1L1, ABCA1, ABCG1, SR-BI, and CD36, after which it's secreted within chylomicrons, consisting of cholesterol, phospholipids, and triacylglycerols into the bloodstream.

Lipoprotein lipase (LPL) releases vitamin E from chylomicrons to peripheral tissues, where cellular uptake is facilitated once more by transport proteins, including SR-BI, CD36, LDLR, afamin, and albumin. In cells, vitamin E is transported by αTTP and tocopherol associated proteins 1/2/3 (TAP1/2/3), secreted by ABCA1 and ABCG1, and assembled with a certain vitamin E analogue selectivity into LDLs and HDLs. The liver takes up vitamin E from chylomicron remnants and LDLs/HDLs via SR-BI, CD36, and LDLR. In the liver α-Toc, recognized by αTTP, is incorporated into VLDLs, leading to an ~50-fold enrichment of this analogue in plasma (**Figure 5C**). The remaining vitamin E analogues, and excess α-Toc, are metabolized by cytochromes P450 (CYP)3A/(CYP)4F2 and secreted in urine and bile involving MDR2 (Zingg 2015, Jiang 2022).

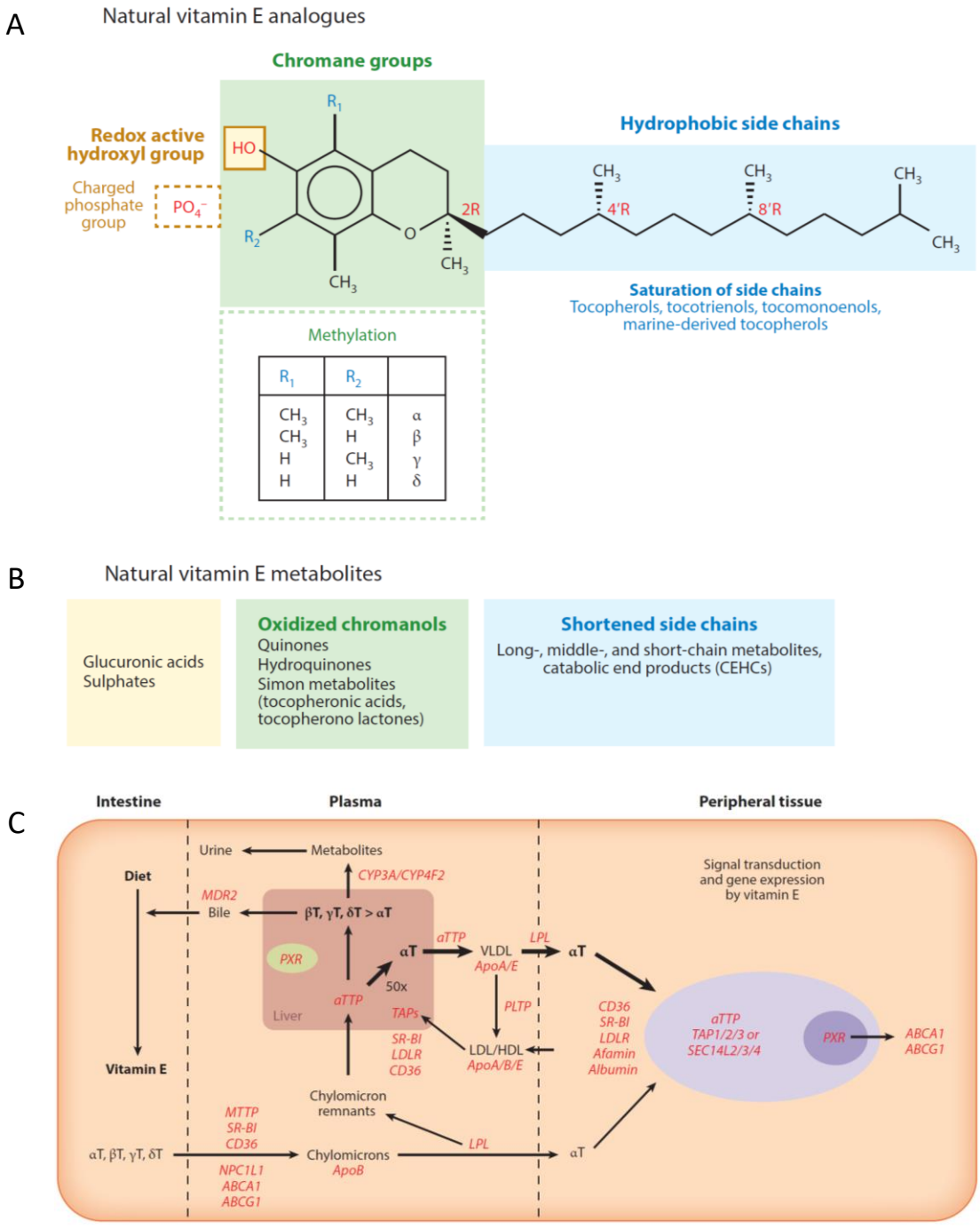

Figure 5 Structure, Metabolism, and Intracellular Transport of Vitamin E.

(A) Chemical structure of natural vitamin E analogues. **(B)** Metabolites of natural vitamin E. **(C)** Uptake, distribution, metabolism, and secretion of vitamin E (explained in text)

From Zingg. *Annu Rev Nutr*. (2015)

In addition to its role as an antioxidant, vitamin E also serves as a modulator of signal transduction and gene expression. Demonstrated primarily by *in vitro* studies, and with cell-specific and stimulus-specific effects, α-Toc has been shown to modulate various protein and lipid kinases, protein and lipid phosphatases, and lipid metabolic enzymes. For example, α-Toc inhibits the activity of PKC, an enzyme involved in cell proliferation and differentiation of smooth muscle cells, platelets, and monocytes. Vitamin E also increases the expression of two enzymes that suppress arachidonic acid metabolism, thereby increasing the release of prostacyclin from the endothelium which, in turn, dilates blood vessels and inhibits platelet aggregation (Zingg 2015, Miyazawa et al. 2019).

Since its discovery in 1922, a compendium of research has sought to determine if vitamin E promotes health and prevents diseases and disorders such as cancer, heart disease, eye disorders, and cognitive decline, with some studies claiming positive benefits, and others reporting no benefit or even deleterious effects (Peh et al. 2016, National Institutes of Health 2021). Regarding cancer, although epidemiological observations support the preventative effects of vitamin E on multiple types of cancer (Byers and Perry 1992), preclinical and clinical trials have demonstrated inconsistent outcomes. For example, in the preclinical setting, vitamin E and its analogous have been reported to inhibit the growth of cultured melanoma cells (Prasad and Prasad, 1982), protect against nitrosamine-induced esophageal tumor incidence in immunocompromised mice (Odeleye et al. 1992), reduce spontaneous, chemically induced, and cancer cell implant mediated lung tumorigenesis in mice (Yano et al. 1994, Yano et al. 1997, Kishimoto et al. 1998, Yano et al. 2000, Quin et al. 2005, Li et al. 2011, Rajasinghe et al. 2018), inhibit metastatic

murine breast cancer tumor growth (Cameron et al. 2003, Hahn et al. 2006, Bachawal et al. 2010, Idriss et al. 2020), induce apoptosis in human gastric cancer, lung cancer, and glioblastoma cells (Sun et al. 2008, Lim et al. 2014, Zhang et al. 2018), and suppress growth of murine tumors induced by TC-1 cells (Kang et al. 2014). Conversely, vitamin E and its derivatives have been reported to increase the incidence of chemically induced colonic (Cook and McNamara 1980, Toth and Patil 1983), hepatic (Glauert et al. 1990, Kolaja and Klaunig 1997), and skin tumors in mice (Mitchel and McCann 1993, Mitchel and McCann 2003), as well as accelerate lung cancer progression (Sayin et al. 2014) and metastasis of melanoma (Le Gal et al. 2015).

More recently, Yuan et al. reported that vitamin E increases the antitumor efficacy of immune-checkpoint therapy by reinvigorating dendritic cells (DC). Mechanistically, vitamin E directly binds to and inhibits the protein tyrosine phosphatase SHP1, a DC-intrinsic checkpoint that regulates multiple Toll-like receptors (TLR) and cytokine signaling responses, suppressing their signaling output (Yuan et al. 2022). In stark contrast, Sun et al. revealed that α-Toc increases cancer cell viability *in vitro* and promotes tumor growth in a Lewis lung carcinoma (LLC) PDX model. Mechanistically, α-Toc activates PD-L1-mediated tumor-intrinsic signaling and immune suppression via JAK/STAT3-dependent transcriptional and ERK-dependent post-transcriptional mechanisms, resulting in tumor-intrinsic immune escape (Sun et al. 2022).

In the clinical setting, a large-scale human intervention trial set out to evaluate if long-term supplementation with vitamin E decreases the risk of cancer, cancer death, and major cardiovascular events. The Heart Outcomes Prevention Evaluation [HOPE] trial was conducted between December 21, 1993, and April 15, 1999, and subsequently extended

from April 16, 1999, to May 26, 2003. Among all patients, there were no significant differences in primary outcomes (Lonn et al. 2005). In the Alpha-Tocopherol, Beta-Carotene Cancer Prevention (ATBC) Study, higher serum concentrations of α-Toc were associated with lower pancreatic cancer incidence in a cohort of male smokers (Stolzenberg-Solomon et al. 2009). Conversely, in another large-scale human intervention study with α-Toc – the Selenium and Vitamin E Cancer Prevention Trial (SELECT) conducted in North America – α-Toc demonstrated a 17% increase in prostate cancer incidence compared to the placebo (Lippman et al. 2009).

Collectively, the data remains conflicting regarding the effects of vitamin E on cancer and cancer therapy. A primary barrier to characterizing the roles of vitamin E in health and disease is the lack of validated biomarkers for intake and status that can help relate these measures to conclusive predictors of clinical outcomes (National Institutes of Health 2021). However, the broad mechanisms by which vitamin E might provide protection largely revolve around its antioxidant and immunomodulatory properties.

In this chapter, we demonstrate that α-Toc selectively impedes the activity of mTOR bi-steric inhibitors and KRAS GTP (ON) inhibitors independent of its antioxidant function. In the case of the mTORC1 selective inhibitor RM6, interference mediated by α-Toc is potent, durable, and dynamic. Moreover, the entire vitamin E family exhibits this interference pattern, albeit to varying degrees, notably between the tocopherols and tocotrienols.

Results

α-Tocopherol Rescues Cell Death Induced by the RM18/RM6 Drug Combination by Impeding the Activity of RM6 and, to a Lesser Extent, RM18

Given α-Toc's fundamental role in mitigating ROS, which can contribute to cell death mechanisms such as apoptosis (Redza-Dutordoir and Averill-Bates 2016), we first asked whether α-Toc mediated its rescue effects through a more robust suppression of ROS induced by the RM18/RM6 drug combination. To address this, we ascertained if another antioxidant, N-Acetylcysteine (NAC), could promote substantial suppression of ROS induced by the drug combination and, in turn, significant rescue of cell death. H2122 and H1373 were treated with the RM18/RM6 drug combination with or without escalating doses of NAC, and levels of ROS and cell death were evaluated. NAC considerably suppressed ROS in a dose dependent manner in both cell lines (**Figure 5.1A**) but failed to rescue cell death (**Figure 5.1B-D**). These data suggest that the rescue effects of α-Toc were likely not mediated by its antioxidant properties.

We next asked whether α-Toc modulated RAS/ERK and/or PI3K/AKT/mTOR signaling in the treatment setting. H2122 was treated with RM18, RM6, or their combination with or without α-Toc, and signaling was assessed after 24, 48, and 72 hours. Surprisingly, α-Toc lead to a complete and durable rescue of mTORC1 targets suppressed by RM6 (**Figure 5.1E**). RM6 induction of pAKT S473 was likewise considerably diminished. Partial rescue of suppressed pERK mediated by RM18 was also observed, but rescue was not seen at 72 hours. In the combination, α-Toc demonstrated significant rescue

of p4EBP1 suppression, while also strongly diminishing the induction of cell death markers.

Intrigued by these results, we sought to gain a broader understanding of α-Toc's effect on these inhibitors. We began by ascertaining the timing and durability by which α-Toc mediated its effects. H2122, H1373, and H23 were treated with RM18, RM6, or their combination with or without α-Toc, and signaling kinetics were assessed over time from 1-48 hours. α-Toc was able to considerably and durably block the suppression of p4EBP1 mediated by RM6 in both the single agent and combination settings (**Figure 5.1F**). Appreciable rescue of pERK was also observed in H2122 and H1373, but not H23. Furthermore, c-PARP induction was diminished, most notably in the combination setting, and inhibitor effects on Cyclin D1 were likewise reduced.

We next asked if α-Toc could interfere with these inhibitors after they had significant time to suppress their targets. To answer this, we treated H2122, H1373, and H23 with RM18, RM6, or their combination for 24 hours before the addition of α-Toc for an additional 1-48 hours. By 24 hours, p4EBP1 remained notably suppressed by RM6 and the combination in H1373 and H23, with a comparably dampened suppression in H2122. Between 1-4 hours of α-Toc addition, p4EBP1 started to become de-inhibited in the RM6 and drug combination settings (**Figure 5.1G**). pERK remained significantly suppressed by RM18 24 hours after treatment in H2122 and H23, with notable suppression compared to the control in H1373. This suppression was rescued by α-Toc to varying degrees, and at varying time points, across these cell lines. Suppression of c-PARP induction by α-Toc was observed at later timepoints, particularly in the combination, where complete rescue was coincident with return of p4EBP1 to control levels. Cyclin D1 suppression was also

diminished at varying time points depending on the model, particularly in the drug combination.

To round out our assessment of α-Toc's interference towards these agents, we subsequently ascertained if the inhibitors could suppress their targets after α-Toc pre-treatment. H2122, H1373, and H23 were treated with α-Toc for 24 hours before the addition of RM18, RM6, or their combination for an additional 1-48 hours. In both the RM6 and drug combination settings, α-Toc pre-treatment robustly prevented suppression of p4EBP1, with levels remaining at or near control levels (**Figure 5.1H**). This was also largely the case for c-PARP induction mediated by the combination, which was considerably blocked by α-Toc in H2122, H1373, and H23, only diminishing in H1373 at the terminal time point. Cyclin D1 likewise demonstrated diminished suppression, notably in the RM6 and drug combination settings in H2122 and H23. pERK suppression mediated by RM18 was largely unaffected by α-Toc pre-treatment. It should be noted that in all three experiments, α-Toc did not demonstrate any appreciable modulation of the assessed targets in the non-treatment setting, with protein levels generally reflecting those observed for the control.

Collectively, these data suggest that α-Toc can interfere with the activity of RM6 and, to a lesser extent, RM18 in a blocking capacity when α-Toc is added concurrently with treatment or is pre-treated before inhibitor addition (i.e., inhibitors are delayed [RM18, concurrent] or entirely prevented [RM6, concurrent and pre-treatment] from maximally suppressing their targets), and in a rescue capacity when α-Toc is given post inhibitor treatment (i.e., targets suppressed by the inhibitors can become de-inhibited/rebound in the presence of α-Toc).

A

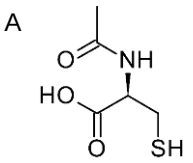

N-Acetylcysteine (NAC)

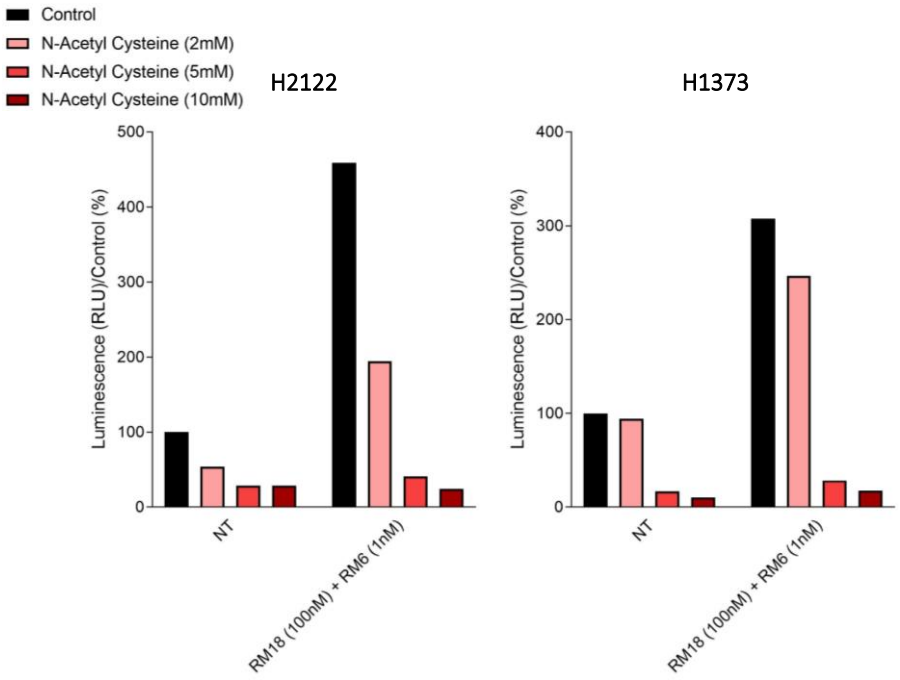

B

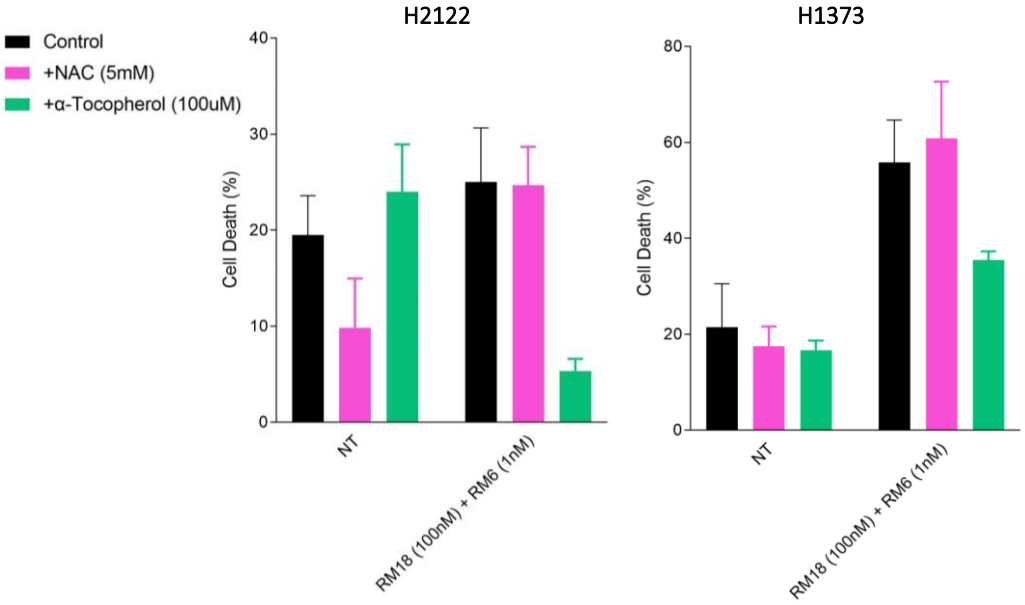

C

H2122

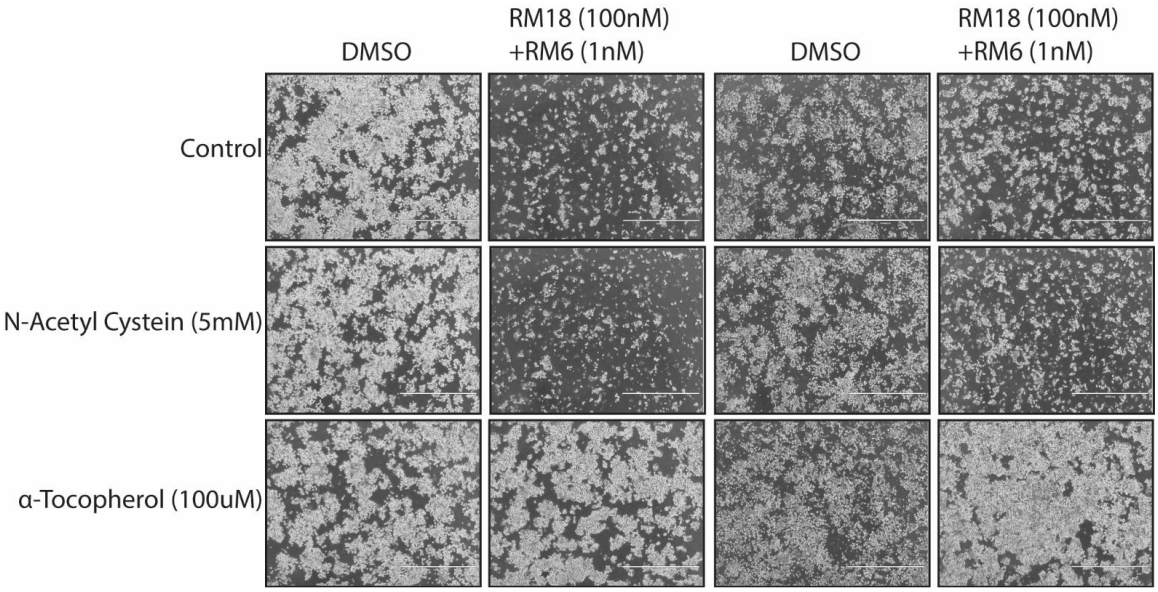

D

H1373

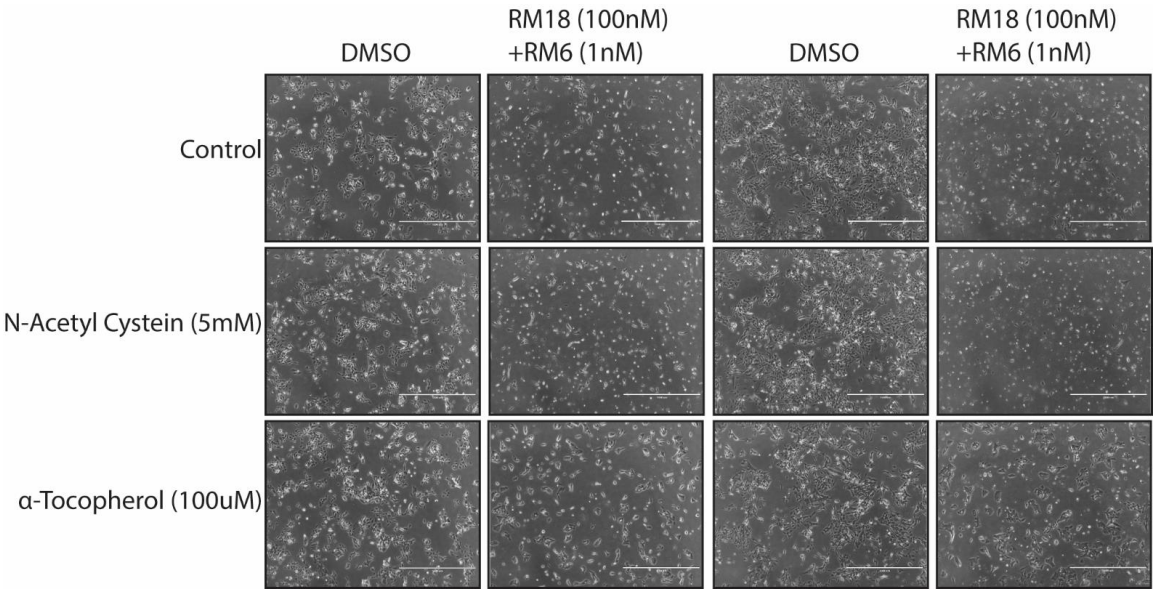

E

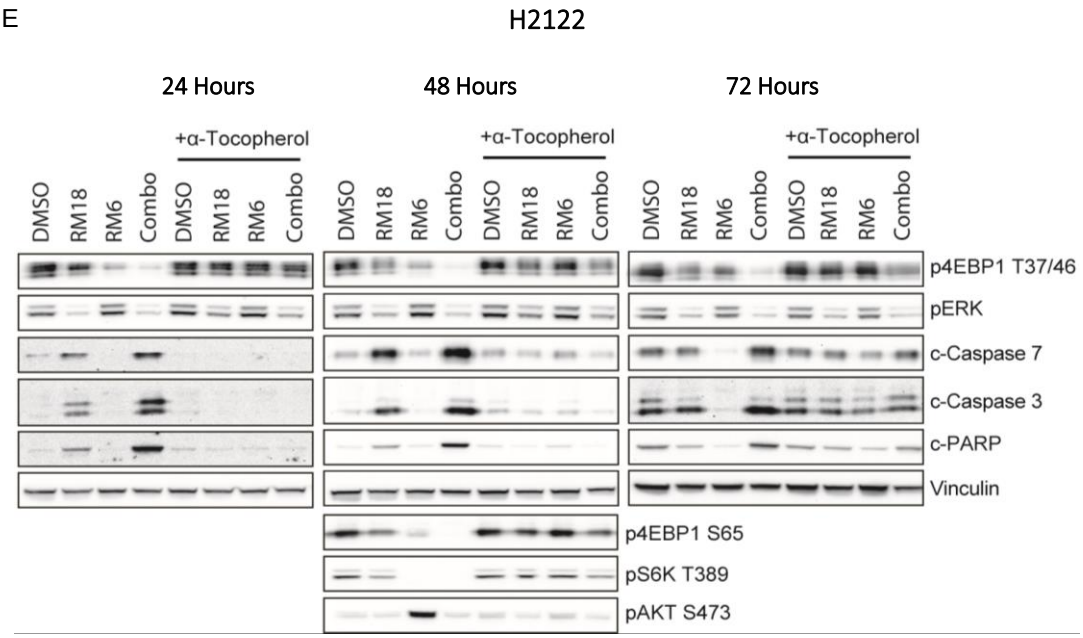
H2122
24 Hours
48 Hours
72 Hours
+α-Tocopherol
DMSO
RM18
RM6
Combo
p4EBP1 T37/46
pERK
c-Caspase 7
c-Caspase 3
c-PARP
Vinculin
p4EBP1 S65
pS6K T389
pAKT S473

F

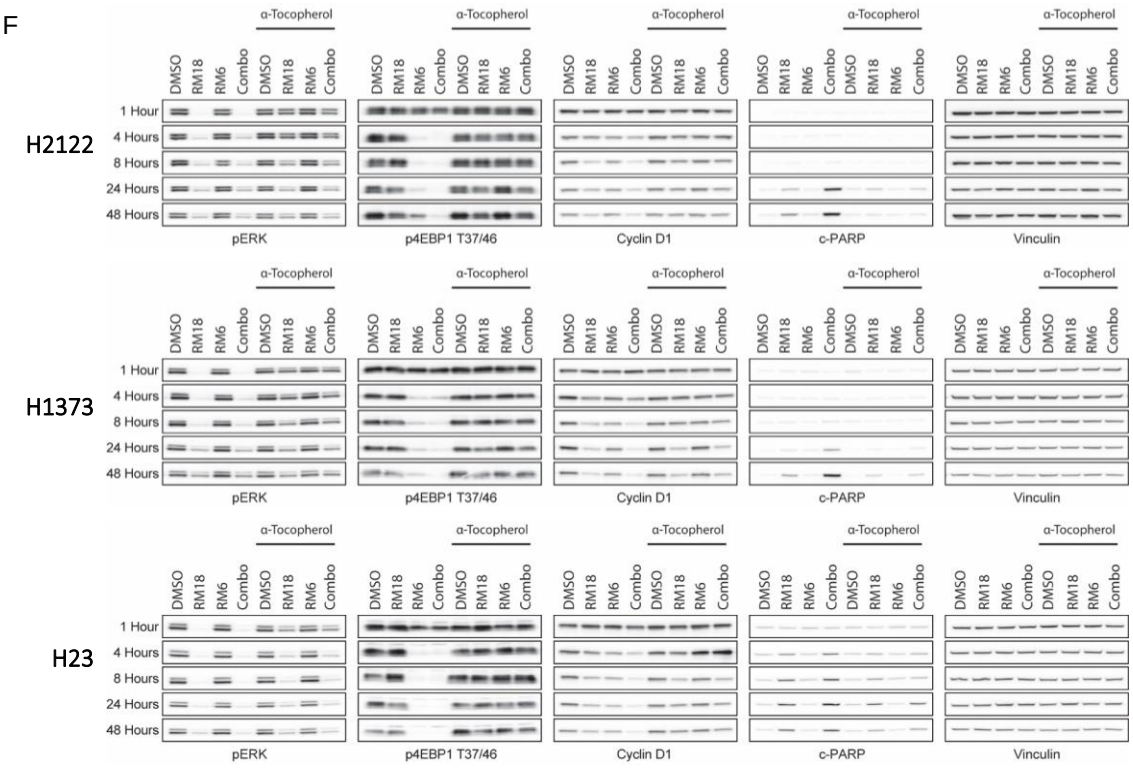
H2122
H1373
H23
α-Tocopherol
DMSO
RM18
RM6
Combo
1 Hour
4 Hours
8 Hours
24 Hours
48 Hours
pERK
p4EBP1 T37/46
Cyclin D1
c-PARP
Vinculin

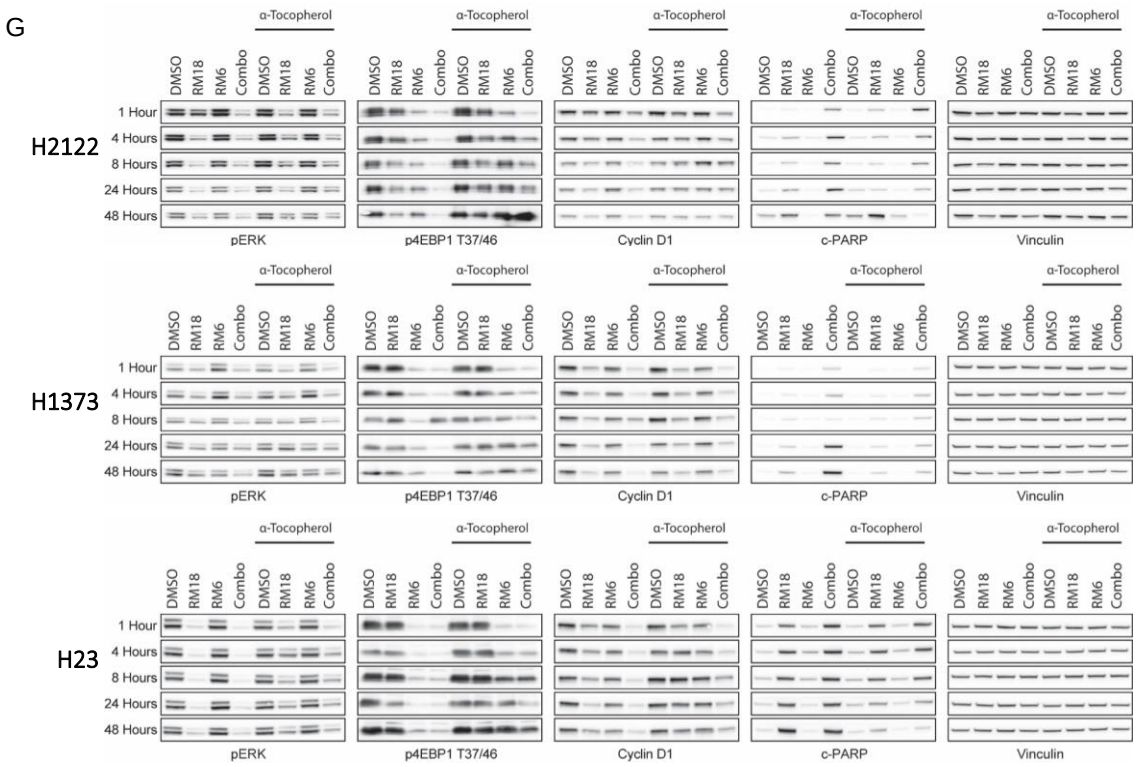
G
H2122
H1373
H23
α-Tocopherol
DMSO
RM18
RM6
Combo
1 Hour
4 Hours
8 Hours
24 Hours
48 Hours
pERK
p4EBP1 T37/46
Cyclin D1
c-PARP
Vinculin

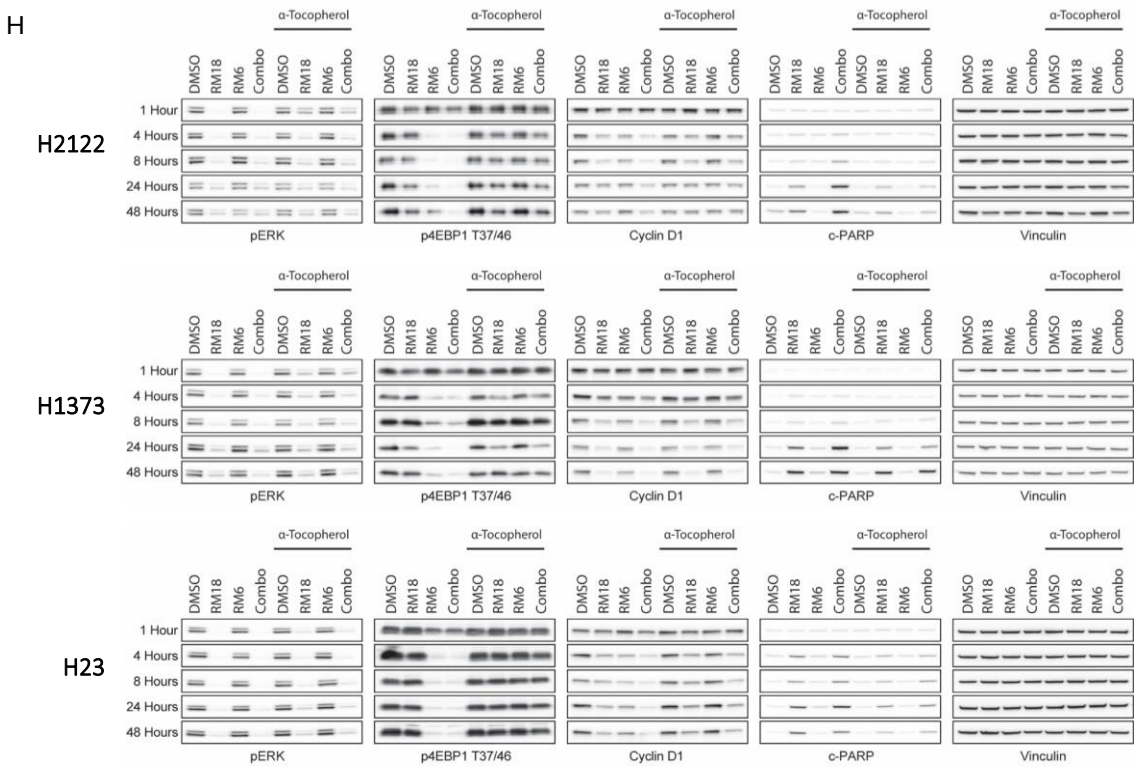
H
H2122
H1373
H23
α-Tocopherol
DMSO
RM18
RM6
Combo
1 Hour
4 Hours
8 Hours
24 Hours
48 Hours
pERK
p4EBP1 T37/46
Cyclin D1
c-PARP
Vinculin

Figure 5.1 α-Tocopherol Rescues Cell Death Induced by the RM18/RM6 Drug Combination by Impeding the Activity of RM6 and, to a Lesser Extent, RM18.

(A) H2122 and H1373 were treated with 100nM RM18, 1nM RM6, or their combination with or without escalating doses of NAC for 48 hours, and levels of ROS were evaluated. Each treatment group was assessed in 3-5 technical replicates. Data is presented as percentage of ROS luminescence normalized to control. Structure of NAC is shown on the right.

(B) H2122 and H1373 were treated with 100nM RM18, 1nM RM6, or their combination with or without 5mM NAC or 100μM α-Toc, and cell death was assessed 72 hours post treatment by trypan blue exclusion viability assay. Each treatment was assessed in three biological replicates, and the averages and SDs are shown.

(C), (D) Same as (B), but cell dynamics for H2122 (C) and H1373 (D) were qualitatively assessed 48 and 72 hours post treatment by image capture bright-field microscopy.

(E) H2122 was treated with 100nM RM18, 1nM RM6, or their combination with or without 100μM α-Toc, and lysates were assessed at the indicated time points with the indicated antibodies.

(F) H2122, H1373, and H23 were treated with 100nM RM18, 1nM RM6, or their combination with or without 100μM α-Toc, and lysates were assessed at the indicated time points with the indicated antibodies.

(G) H2122, H1373, and H23 were treated with 100nM RM18, 1nM RM6, or their combination for 24 hours, followed by the addition of 100μM α-Toc or an equivalent volume of DMSO, for an additional 1-48 hours. Lysates were assessed at the indicated time points with the indicated antibodies.

(H) H2122, H1373, and H23 were treated with 100μM α-Toc or an equivalent volume of DMSO for 24 hours, followed by the addition of 100nM RM18, 1nM RM6, or their combination for an additional 1-48 hours. Lysates were assessed at the indicated time points with the indicated antibodies.

α-Tocopherol Impedes the Activity of RAS GTP Inhibitors, but not KRAS G12C-GDP Inhibitors or General Inhibitors of the RAS/ERK Pathway

While notable, the effects α-Toc had on the activity of RM18 were less striking and durable compared to its effects on RM6. Nevertheless, we sought to gain more insight into the extent of this drug interference. We asked whether α-Toc could also interfere with other KRAS G12C inhibitors. To address this, we treated H2122 with RM18, MRTX849, AMG510, or AZD8037 with or without α-Toc, and assessed signaling 1, 8, and 24 hours post treatment. α-Toc only demonstrated rescue of pERK suppressed by RM18 (**Figure 5.2A**). Of note, α-Toc interfered with the degree of RM18 binding to KRAS, which is visually detected by the KRAS band shift.

Unlike MRTX849, AMG510, and AZD8037, the KRAS G12C-GDC (OFF) inhibitors, RM18, a KRAS G12C-GTP (ON) inhibitor, exhibits a different mechanism of action. Rather than simply binding to the switch-II region of KRAS in its GDP bound state and trapping it through covalent cysteine modification (Lito et al. 2016), RM18 first binds to an abundant cellular chaperon protein, cyclophilin A, creating a binary complex that engages KRAS G12C in a final tri-complex. RM18 also covalently modifies the G12C cysteine residue, trapping KRAS in its GTP bound state while preventing its ability to interact with effectors. The high molecular weight of this tri-complex due to the presence of cyclophilin A, compounded with its covalent modification, enables qualitative detection of drug binding by the degree of the KRAS band shift (Revolution Medicines 2023).

Given that α-Toc is known to exhibit immunomodulatory properties, we questioned if α-Toc would likewise interfere with other KRAS (ON) inhibitors that engaged cyclophilin A. To answer this, we utilized RM42, a pan RAS inhibitor, and RM44, a KRAS

G12D inhibitor. We've shown that RM44 lacks specificity, and hence can mediate suppressive effects in KRAS G12C mutant models. H2122 was treated with RM18, RM42, or RM44 with or without α-Toc, and signaling kinetics were assessed over time from 0.5-24 hours. α-Toc significantly blocked pERK suppression mediated by RM18 and RM44, while sparing RM42 (**Figure 5.2B**). This interference significantly wore off by 24 hours. α-Toc hampered the degree of drug binding to KRAS for both RM18 and, to a lesser extent, RM44, at early time points. By 6-8 hours, α-Toc no longer appreciably impacted drug binding. In line with its drug interference activity, α-Toc also rescued/blocked pMEK suppression mediated by RM18 and RM42, with effects diminishing at later time points (**Figure 5.2C**). RM42 did not appreciably suppress pMEK, with levels similar to that of the control. Interestingly though, α-Toc suppressed pMEK levels in the context of RM42 treatment. This may account for why pERK remained suppressed, rather than rescued, in the α-Toc/RM42 combination. These results demonstrate that α-Toc does have an effect on RM42, but it presents differently to the effects observed for RM18 and RM44.

We next asked if α-Toc could interfere with inhibitors targeting other nodes of the RAS/ERK pathway. H2122 was treated with escalating doses of the MEK inhibitor trametinib or the ERK inhibitor SCH277894 with or without α-Toc, and signaling was assessed 1 and 24 hours post treatment. α-Toc did not rescue/block p4EBP1 suppression mediated by either inhibitor (**Figure 5.2D, E**). We also evaluated varying doses of RM18 and MRTX849 for comparison (**Figure 5.2F, G**). No effect was observed for MRTX849 at the lowest dose assessed. While additional experiments are required to fully resolve the mechanism by which α-Toc interferes with KRAS GTP inhibitors, these data highlight a role for its interference at the level of drug engagement with its target, potentially through

cyclophilin A. Furthermore, these data suggest that α-Toc's interference is not broadly applicable to RAS/ERK pathway inhibition.

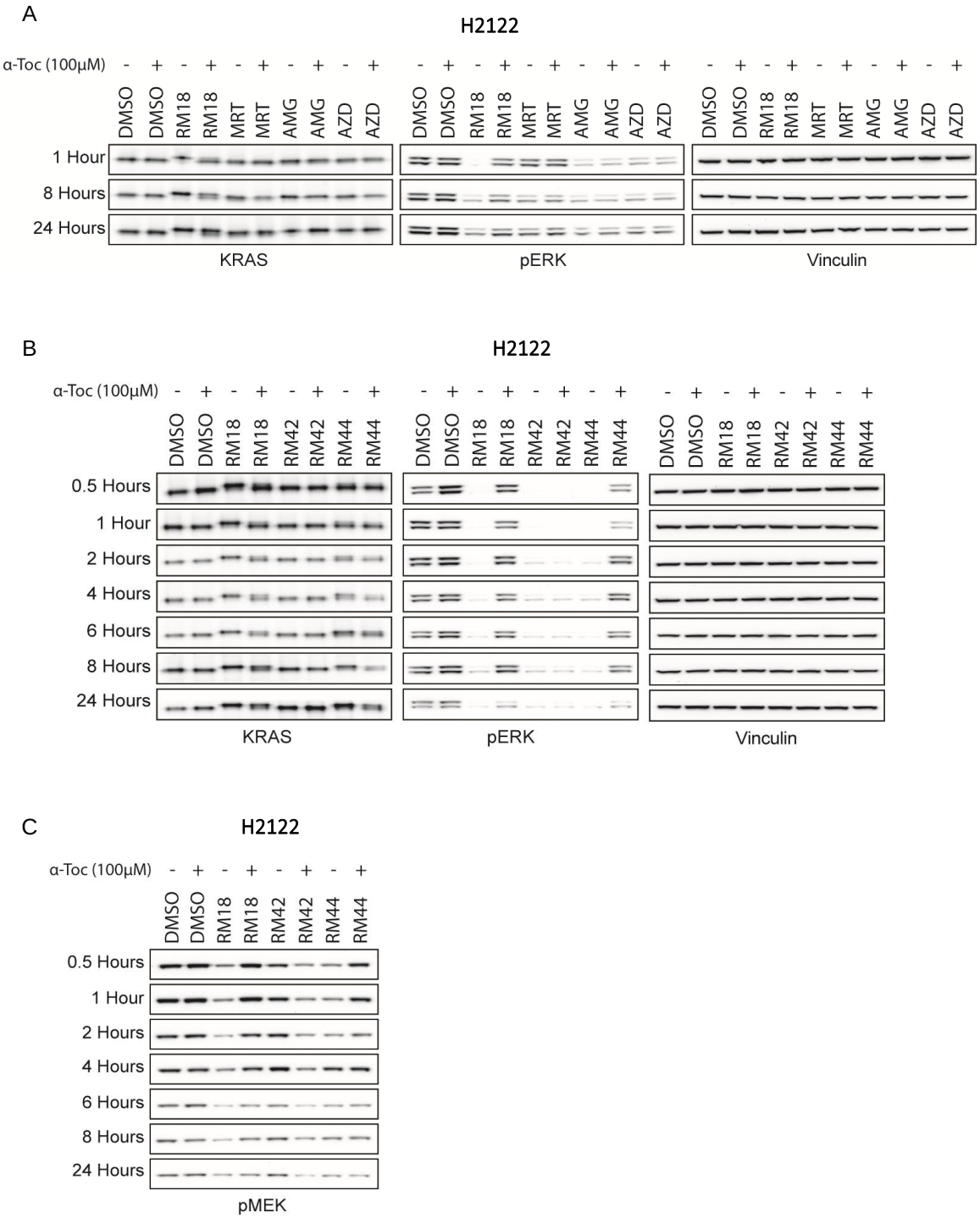

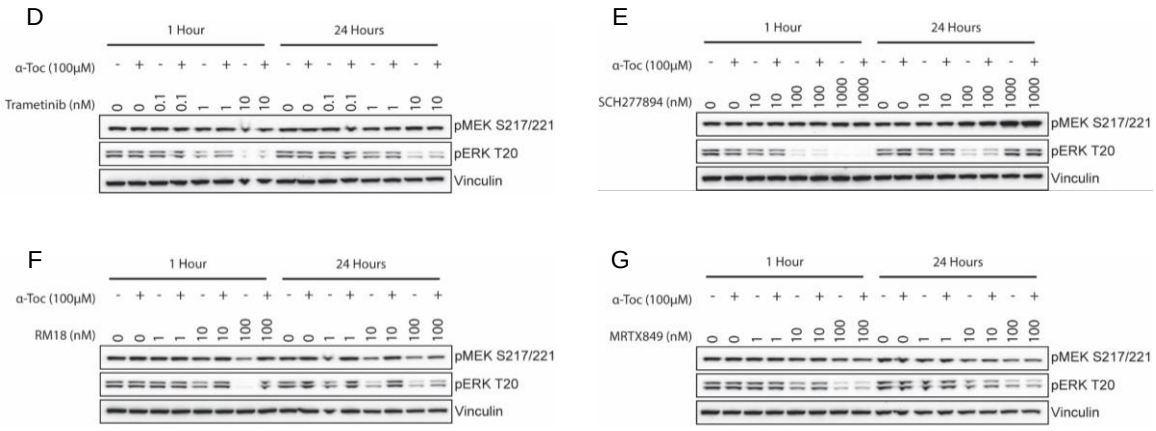

Figure 5.2 α-Tocopherol Impedes the Activity of RAS GTP Inhibitors, but not KRAS G12C-GDP Inhibitors or General Inhibitors of the RAS/ERK Pathway.

(A) H2122 was treated with 100nM RM18, 100nM MRTX849, 1μM AMG510, and 1μM AZD8037 with or without 100μM α-Toc. Lysates were assessed at the indicated time points and probed with the indicated antibodies.

(B) H2122 was treated with 100nM RM18, 100nM RM42, and 100nM RM44 with or without 100μM α-Toc. Lysates were assessed at the indicated time points and probed with the indicated antibodies.

(C) Same as in (B), with effects on pMEK shown.

(D) - (G) H2122 was treated with escalating doses of Trametinib (D), the ERK inhibitor SCH277894 (E), RM18 (F), or MRTX849 (G) with or without 100μM α-Toc. Lysates were assessed at the indicated time points and probed with the indicated antibodies.

α-Tocopherol Impedes the Activity of Rapalink and mTORC1 Selective Inhibitors, but not General Inhibitors of the PI3K/AKT/mTOR Pathway

Following off our assessment of other RAS/ERK pathway inhibitors, we asked if α-Toc could interfere with alternative inhibitors of the PI3K/AKT/mTOR pathway. To address this, H2122, H1373, and H23 were treated with the PI3Kα/δ inhibitor GDC0941, the AKT inhibitor MK2206, or RM6 with or without α-Toc, and signaling was assessed 1-24 hours post treatment. α-Toc demonstrated no interference towards the activity of GDC0941 or MK2206, with pAKT T308, pAKT S473, and pS6K T389 remaining well inhibited in the presence of α-Toc (**Figure 5.3A**). Given the initial high dose used for MK2206, we inquired if an effect of α-Toc would be seen at a lower dose that suppressed relevant targets. We also profiled another two PI3K inhibitors, BYL719, a PI3Kα inhibitor, and AZD8186, a PI3Kβ/δ inhibitor. MDA-MB-468 was treated with escalating doses of AZD8186, BYL719, GDC0941, or MK2206 with or without α-Toc, and signaling was assessed 4 and 24 hours post treatment. We used this breast cancer model since it demonstrates more robust PI3K/AKT/mTOR signaling, and a greater reliance on the pathway to maintain its proliferation and survival. α-Toc did not interfere with the suppressive activity of any of these inhibitors at any of the assessed doses (**Figure 5.3B-E**).

We next questioned if this drug interference was more specific to mTOR inhibitors. To address this, we treated H2122 with Rapamycin or the mTOR kinase inhibitor MLN0128 with or without α-Toc and assessed signaling 1-24 hours post treatment. α-Toc did not interfere with the suppressive activity of these inhibitors towards the assessed targets, with pAKT S473, pS6K T389, and/or p4EBP1 T37/46 remaining inhibited in the

presence of α-Toc (**Figure 5.3F**). Coincident with these results, α-Toc did not demonstrate any rescue of growth suppression mediated by MLN0128 (**Figure 5.3G**). At the dose used, Rapamycin did not appreciably suppress cell growth. Similar results were also obtained for H23 and H1373 (data not shown). Another mTOR kinase inhibitor, AZD8055, assessed at varying doses, was also unaffected by α-Toc (data not shown).

Rapamycin and MLN0128 are core components of RapaLink-1, connected by an inert chemical linker. RapaLink-1 is termed a 'bi-steric' inhibitor for its concurrent engagement of the allosteric (Rapamycin-FRB) and orthosteric (MLN0128) sites of mTORC1/2. The series of mTORC1 selective inhibitors are also 'bi-steric,' with preferential engagement of mTORC1 over mTORC2 (**Figure 5.3H**) (Lee et al. 2021). Given that α-Toc significantly interfered with RM6, we next asked if this drug interference could be broadly applied to other members of this bi-steric class. To address this, we treated H2122 with RapaLink-1 (RL), RM1, RM2, RM3, or RM6 with or without α-Toc and assessed signaling 1-48 hours post treatment. α-Toc demonstrated considerably rescue/block of p4EBP1 suppression mediated by all inhibitors, as well as pS6K suppression, although with comparably dampened and less durable effects for all but RM3 and RM6 (**Figure 5.3F**). This isn't surprising though, as the S6K T389 phospho site is a weaker substrate for mTORC1 due to steric hindrance, and hence is more readily not phosphorylated when mTOR is evenly weakly inhibited, in contrast to the stronger 4EBP1 T37/46 phospho site substrate, which requires more robust mTOR inhibition to suppress its phosphorylation (Kang et al. 2013). pAKT S473 induction by RM1, RM2, RM3, and RM6 was also diminished to varying degrees by α-Toc. α-Toc also rescued cell growth suppression mediated by these inhibitors to varying degrees (**Figure 5.3G**).

Curious about the status of these bi-steric inhibitors, and the mechanism by which α-Toc impeded their activity, we next asked if α-Toc would interfere with Rapamycin and MLN0128 in a combined setting. In other words, if the core components of these bi-steric inhibitors, which are unaffected on their own, are put together sans linker, would α-Toc cause interference. To address this question, H2122 was treated with the combination of Rapamycin and MLN0128 with or without α-Toc, and signaling was assessed from 1-24 hours. α-Toc did not lead to any rescue/block of suppressed pAKT S473, pS6K T389, or p4EBP1 T37/46 and S65 mediated by the drug combination (**Figure 5.3H**). Taken together, our data thus far demonstrates that α-Toc significantly impacts the activity of bi-steric mTOR inhibitors. Furthermore, these effects are not broadly applicable to PI3K/AKT/mTOR signaling, nor to general inhibition of the pathway.

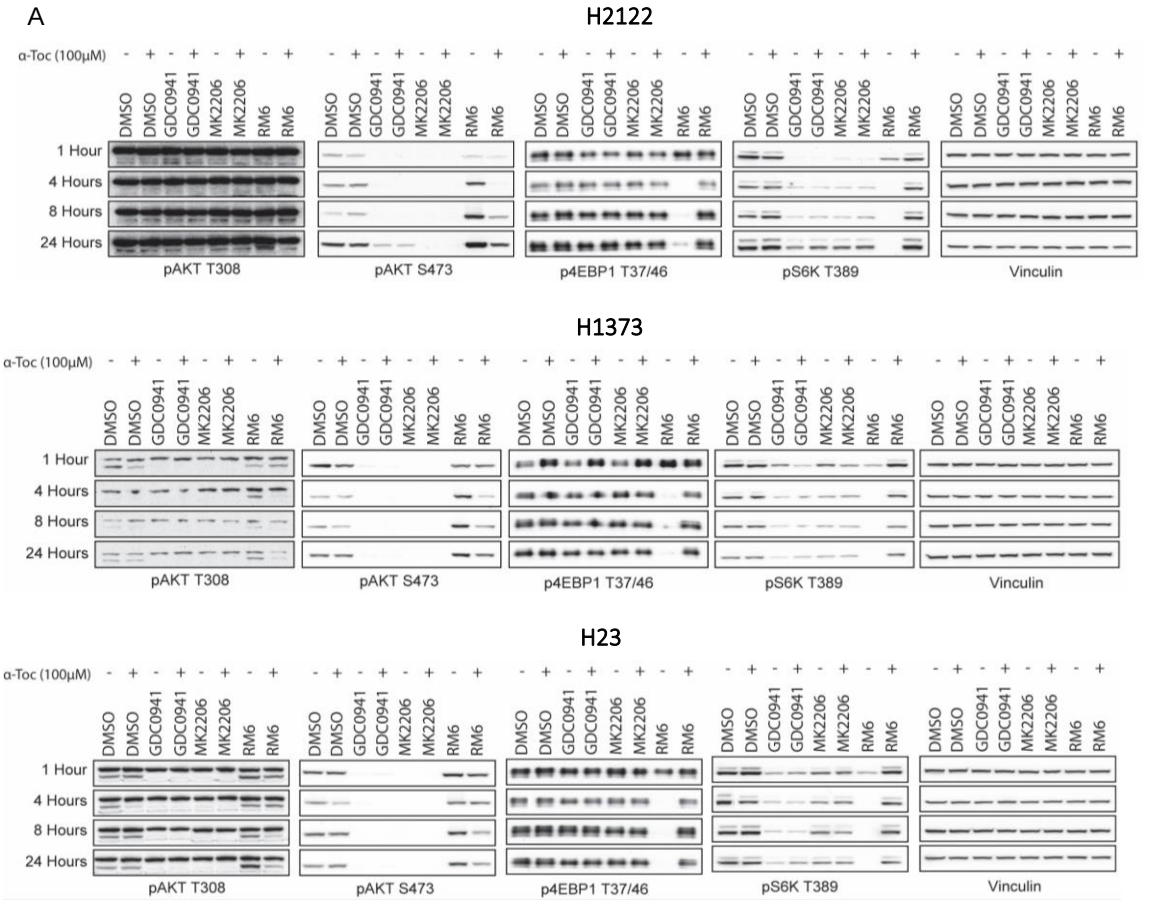
A
H2122
α-Toc (100μM)
DMSO
GDC0941
MK2206
RM6
1 Hour
4 Hours
8 Hours
24 Hours
pAKT T308
pAKT S473
p4EBP1 T37/46
pS6K T389
Vinculin
H1373
H23
MDA-MB-468
B
4 Hours
24 Hours
AZD8186 (nM)
0
2.5
25
250
pAKT S473
pS6K T389
p4EBP1 T37/46
p4EBP1 S65
Vinculin
C
BYL719 (nM)
10
100
1000
D
GDC0941 (nM)
3
30
300
E
MK2206 (nM)

F

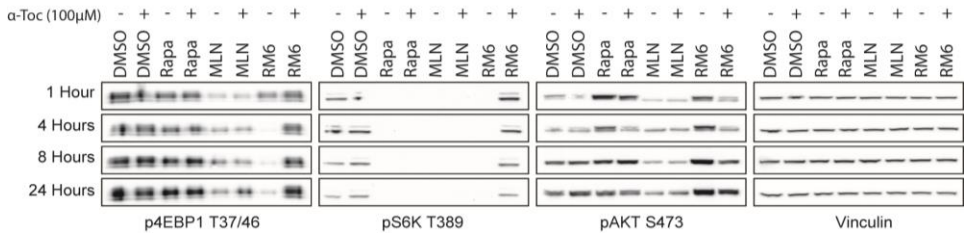
H2122
α-Toc (100μM)
DMSO
Rapa
MLN
RM6
1 Hour
4 Hours
8 Hours
24 Hours
p4EBP1 T37/46
pS6K T389
pAKT S473
Vinculin

G

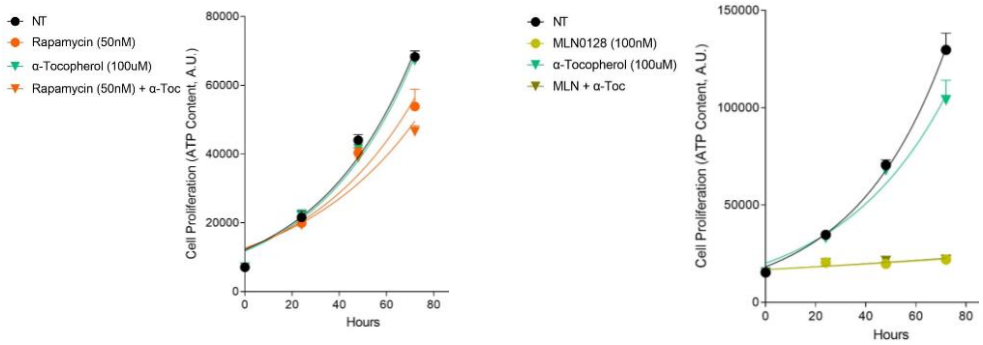
NT
Rapamycin (50nM)
α-Tocopherol (100uM)
Rapamycin (50nM) + α-Toc
Cell Proliferation (ATP Content, A.U.)
Hours
NT
MLN0128 (100nM)
α-Tocopherol (100uM)
MLN + α-Toc
Cell Proliferation (ATP Content, A.U.)
Hours

H

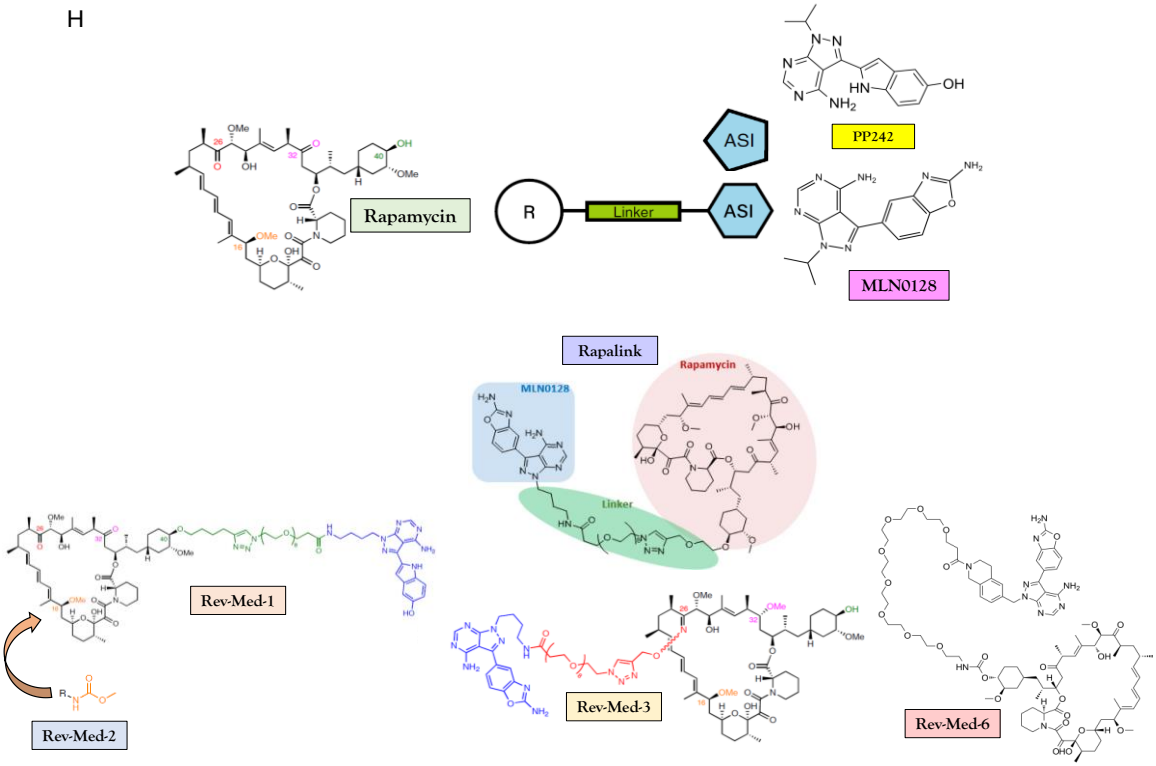
Rapamycin
R
Linker
ASI
ASI
PP242
MLN0128
Rapalink
MLN0128
Rapamycin
Linker
Rev-Med-1
Rev-Med-2
Rev-Med-3
Rev-Med-6

I H2122

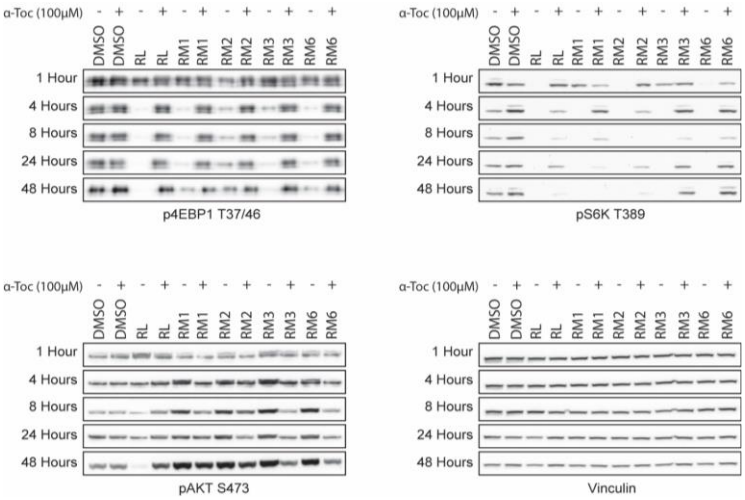

J H2122

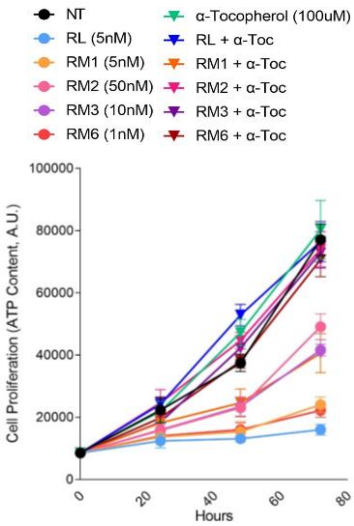

K H2122

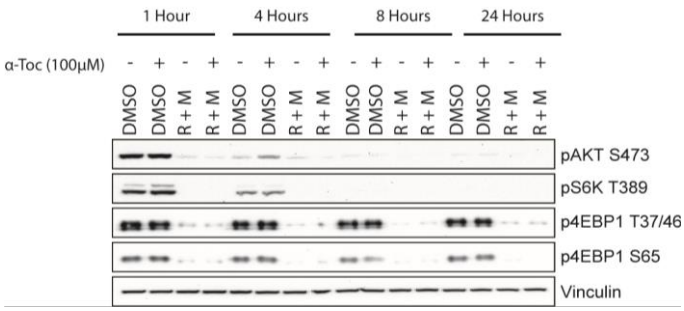

Figure 5.3 α-Tocopherol Impedes the Activity of Rapalink and mTORC1 Selective Inhibitors, but not General Inhibitors of the PI3K/AKT/mTOR Pathway.

(A) H2122, H1373, and H23 were treated with 300nM GDC0941, 1μM MK2206, or 1nM RM6 with or without 100μM α-Toc. Lysates were assessed at the indicated time points and probed with the indicated antibodies.

(B) - (E) MDA-MB-468 was treated with escalating doses of AZD8186 (B), BYL719 (C), GDC0941 (D), or MK2206 (E) with or without 100μM α-Toc. Lysates were assessed at the indicated time points and probed with the indicated antibodies.

(F) H2122 was treated with 10nM Rapamycin, 10nM MLN0128, or 1nM RM6 with or without 100μM α-Toc. Lysates were assessed at the indicated time points and probed with the indicated antibodies.

(G) H2122 was treated with 50nM Rapamycin or 100nM MLN0128 with or without 100μM α-Toc, and cell growth was assessed over the course of 72 hours. Each treatment was assessed in five technical replicates, and the averages and SDs are shown.

(H) The key components of mTOR bi-steric inhibitors, with structures of Rapamycin, the mTOR kinase inhibitors PP242 and MLN0128, and RevMed-1, 2, 3, and 6 shown. Modified from Lee et al., *Nat Chem Biol.* (2021).

(I) H2122 was treated with 5nM RapaLink-1, 5nM RM1, 50nM RM2, 10nM RM3, or 1nM RM6 with or without 100μM α-Toc. Lysates were assessed at the indicated time points and probed with the indicated antibodies.

(J) H2122 was treated as in (I), with cell growth assessed over the course of 72 hours. Each treatment was assessed in five technical replicates, and the averages and SDs are shown.

(K) H2122 was treated with the combination of 10nM MLN0128 with 10nM Rapamycin with or without 100μM α-Toc. Lysates were assessed at the indicated time points and probed with the indicated antibodies.

α-Tocopherol Impedes RM6 Activity in a Dose Dependent Manner and Across Tumor Types

In these initial studies, the high dose of α-Toc we used was selected based on several ferroptosis studies that used this 100μM dose to suppress ROS and inhibit ferroptosis. We therefore questioned if this drug interference would occur at a lower dose of α-Toc. To ascertain this, H2122 was treated with RM6 and escalating doses of α-Toc, from 100nM-100μM, and signaling was assessed 4 and 24 hours post treatment. While a 1μM dose of α-Toc demonstrated appreciable rescue/block of p4EBP1 at 4 hours, these effects were largely diminished by 24 hours (**Figure 5.4A**). 10μM of α-Toc demonstrated considerable and durable rescue/block of mTORC1 substrates, with comparable effects to the 100μM dose. In H2122, this lower dose of α-Toc also showed considerable rescue of cell death induced by the RM18/RM6 drug combination at 72 hours, comparable to the 100μM dose (**Figure 5.4B**), as well as cell growth suppression mediated by RM6 and the RM18/RM6 drug combination (**Figure 5.4C**). Growth suppression mediated by RM18 was not rescued by this lower dose of α-Toc, further accentuating the greater degree of drug interference mediated by α-Toc towards RM6 in comparison to RM18.

We expanded these findings to other NSCLC models, wherein 10μM of α-Toc demonstrated considerable rescue of mTORC1 targets suppressed by RM6 in Calu-1, H358, and Lu99 (**Figure 5.4D**). Thus far, our evaluation of this α-Toc/RM6 drug interference phenomenon was exclusively explored in NSCLC models. To determine if lineage played a role in mediating this interference, we broadened our studies to breast cancer, CRC, and endometrial cancer models. α-Toc demonstrated rescue/block of

mTORC1 targets suppressed by RM6 in the breast cancer cell lines MDA-MB-468 (**Figure 5.4E**), MCF7 (**Figure 5.4F**), and T47D (**Figure 5.4G**), the CRC cell line SW837 (**Figure 5.4H**), the endometrial cancer cell line MFE296 (**Figure 5.4I**), and the endometrial PDX established cell line X0007aS1 (**Figure 5.4J**). α-Toc also rescued suppressed growth mediated by RM6 in the CRC cell lines LIM1215 and NCIH508, whike no rescue of Cetuximab mediated growth suppression was observed (**Figure 5.4K, L**). Thus, this α-Toc drug interference is not lineage specific, and it's expected to occur in any cell line susceptible to mTORC1 inhibition by RM6.

A H2122

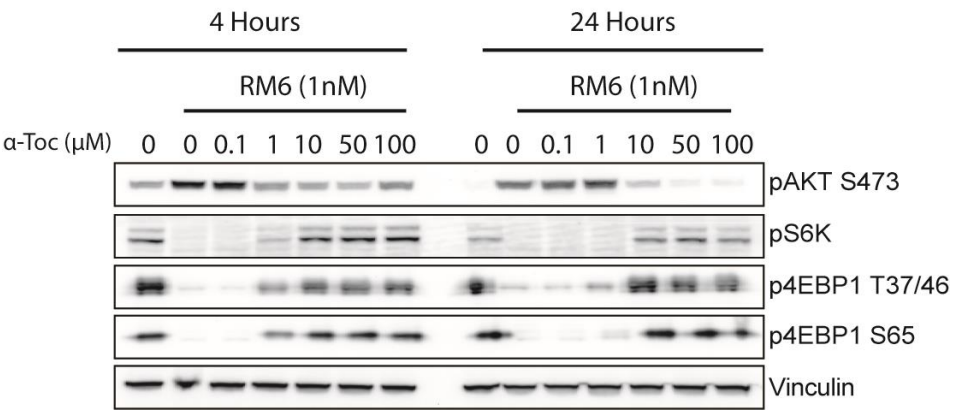

B H2122

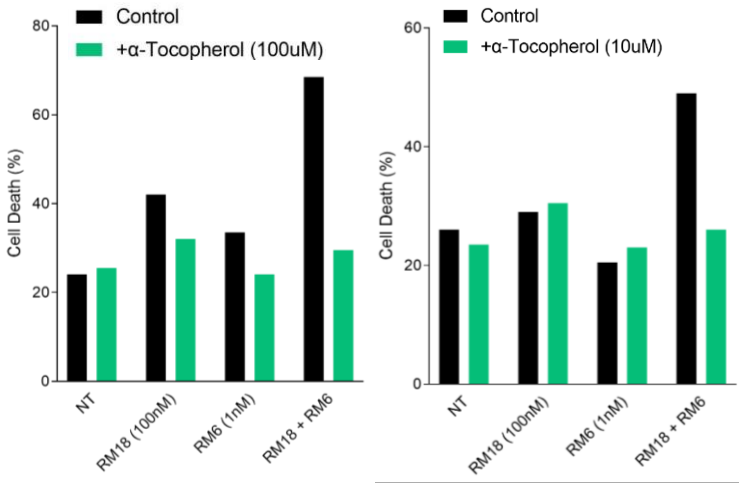

C H2122

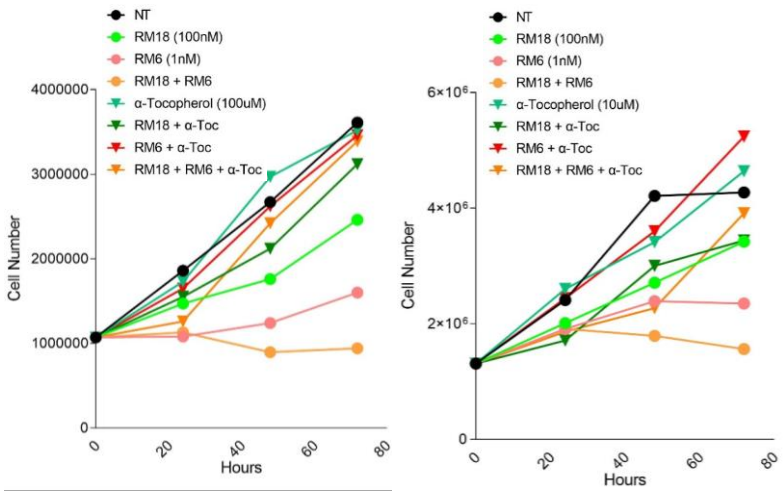

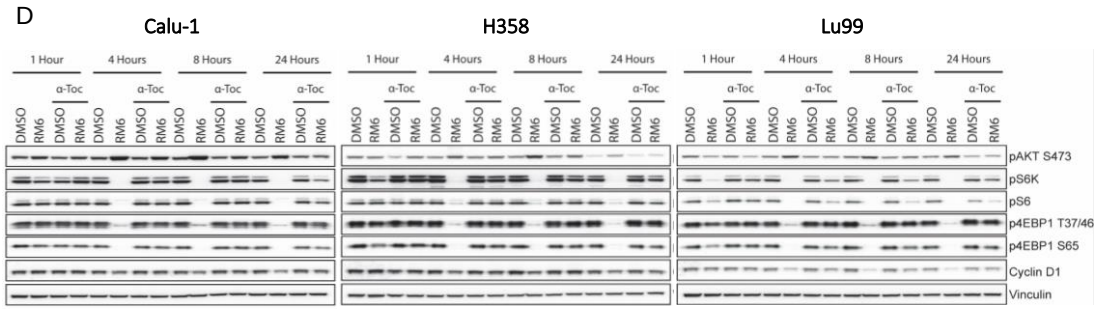
D
Calu-1
H358
Lu99
1 Hour
4 Hours
8 Hours
24 Hours
α-Toc
DMSO
RM6
pAKT S473
pS6K
pS6
p4EBP1 T37/46
p4EBP1 S65
Cyclin D1
Vinculin

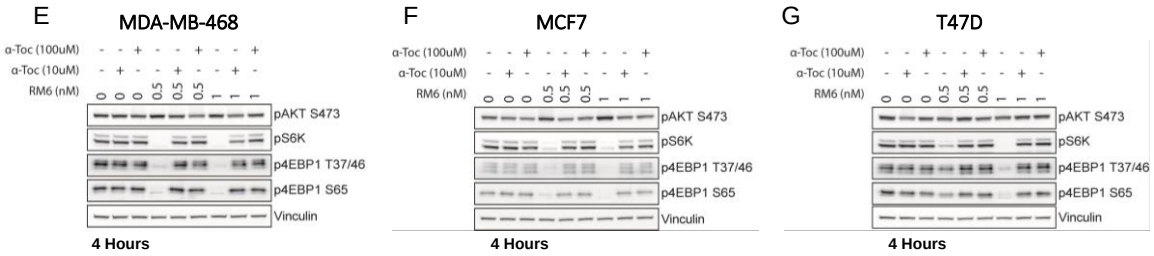
E
MDA-MB-468
F
MCF7
G
T47D
α-Toc (100uM)
α-Toc (10uM)
RM6 (nM)
pAKT S473
pS6K
p4EBP1 T37/46
p4EBP1 S65
Vinculin
4 Hours

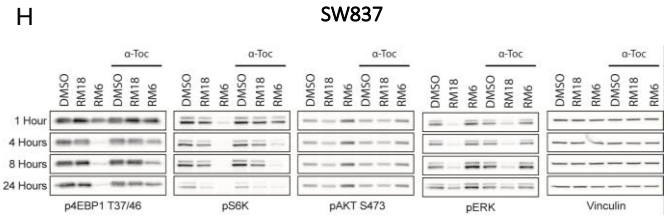
H
SW837
α-Toc
DMSO
RM18
RM6
1 Hour
4 Hours
8 Hours
24 Hours
p4EBP1 T37/46
pS6K
pAKT S473
pERK
Vinculin

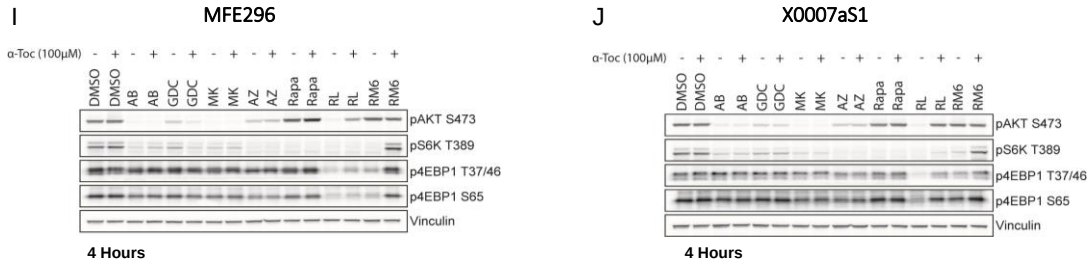
I
MFE296
J
X0007aS1
α-Toc (100μM)
DMSO
AB
GDC
MK
AZ
Rapa
RL
RM6
pAKT S473
pS6K T389
p4EBP1 T37/46
p4EBP1 S65
Vinculin
4 Hours

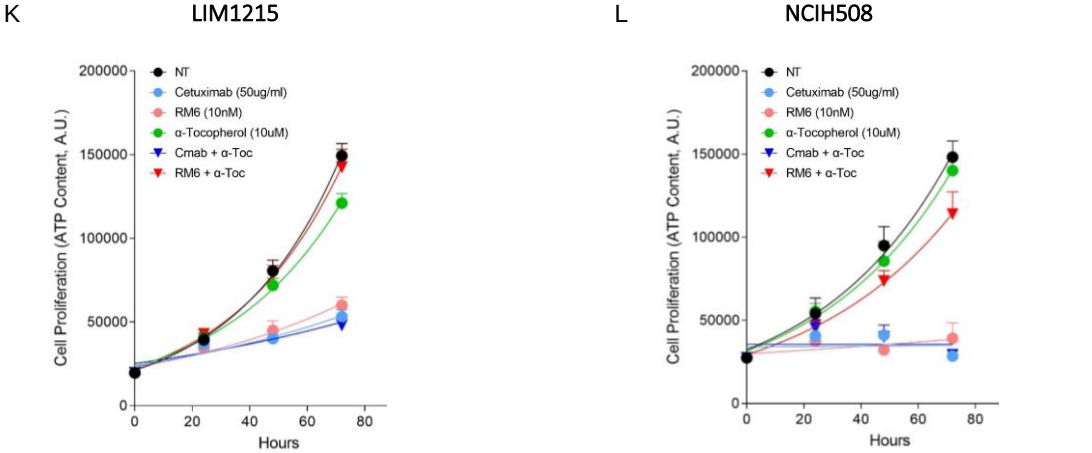
K
LIM1215
L
NCIH508
NT
Cetuximab (50ug/ml)
RM6 (10nM)
α-Tocopherol (10uM)
Cmab + α-Toc
RM6 + α-Toc
Cell Proliferation (ATP Content, A.U.)
Hours

Figure 5.4 α-Tocopherol Impedes RM6 Activity in a Dose Dependent Manner and Across Tumor Types.

(A) H2122 was treated with 1nM RM6 with or without escalating doses of α-Toc. Lysates were assessed at the indicated time points and probed with the indicated antibodies.

(B) H2122 was treated with 100nM RM18, 1nM RM6, or their combination with or without 10μM α-Toc, and cell death was assessed 72 hours post treatment (right) by trypan blue exclusion assay. Cell death measures are compared to those obtained for a 100μM dose of α-Toc (left).

(C) Same as in (B), but cell growth was assessed over the course of 72 hours (right) using trypan blue exclusion viability assay. Cell growth measures are compared to those for a 100μM dose of α-Toc (left).

(D) Calu-1, H358, and Lu99 were treated with 100nM RM18, 1nM RM6, or their combination with or without 10μM α-Toc. Lysates were assessed at the indicated time points and probed with the indicated antibodies.

(E) - (G) Breast cancer cell lines MDA-MB-468, MCF7, and T47D were treated with 0.5nM or 1nM of RM6 with or without 10μM or 100μM α-Toc for 4 hours. Lysates were probed with the indicated antibodies.

(H) CRC cell line SW837 was treated with 100nM RM18 or 10nM RM6 with or without 10μM α-Toc. Lysates were assessed at the indicated time points and probed with the indicated antibodies.

(I) , (J) Endometrial cancer cell line MFE296, and the cell line established PDX X0007aS1, were treated with the combination of 250nM AZD8186 and 1μM BYL719 (AB), 300nM GDC0941, 1μM MK2206, 50nM Rapamycin, 10nM RapaLink-1, or 0.5nM RM6 with or without 100μM α-Toc for 4 hours. Lysates were probed with the indicated antibodies.

(K), (L) CRC cell lines LIM1215 and NCIH508 were treated with 50μg/ml Cetuximab or 10nM RM6 with or without 10μM α-Toc, and cell growth assessed over the course of 72 hours. Each treatment was assessed in five technical replicates, and the averages and SDs are shown.

α-Tocopherol does not Impede RM6 Upon Washout, and it does not Interfere with the Physiological Function of mTORC1

We next asked if α-Toc would interfere with RM6 activity if removed from culture media before RM6 addition. In other words, is α-Toc retained in cells after washout to a degree that will permit its drug interference. To address this, H2122, H1373, and H23 were treated with α-Toc for 24 hours before washout and RM6 addition for 1, 4, and 24 hours. In all cases, RM6 was able to suppress mTORC1 targets robustly and durably with α-Toc removed from culture media (**Figure 5.5A**). To determine if α-Toc interfered with mTOR itself, we evaluated mTOR's ability to physiologically activate S6K in the context of α-Toc. H2122, H1373, and H23 were starved of amino acids for 60 minutes with or without α-Toc, followed by re-stimulation with amino acids for 15 minutes with or without α-Toc. α-Toc did not demonstrate any modulation of the ability of mTORC1 to phosphorylate S6K T389 after amino acid starvation and re-stimulation (**Figure 5.5B**). A 24-hour pre-treatment period with α-Toc before amino acid starvation and re-stimulation likewise did not lead to modulation of mTORC1 activity (MDA-MB-468). Collectively, these results demonstrate that α-Toc interferes with RM6 in a drug specific manner.

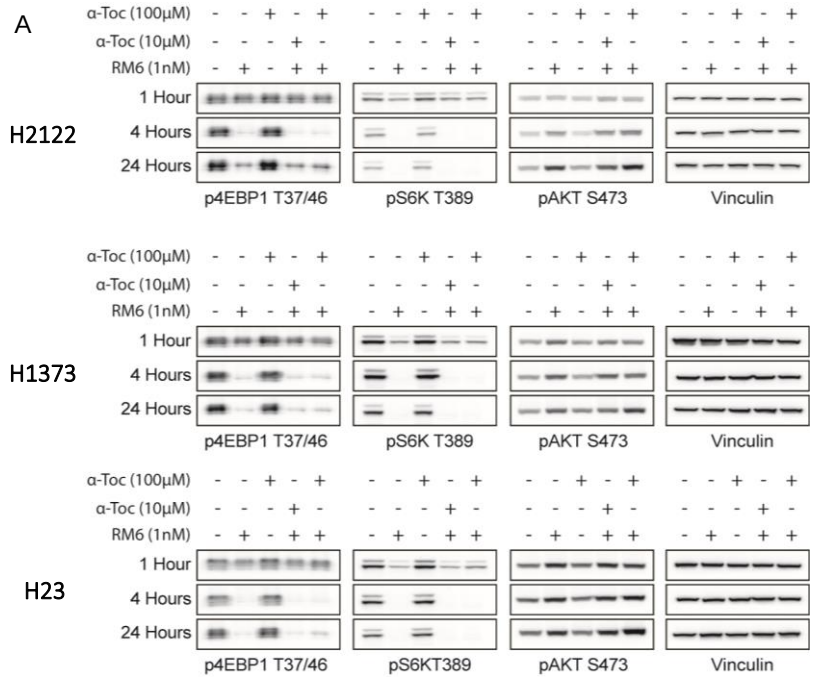
A
α-Toc (100μM)
α-Toc (10μM)
RM6 (1nM)
1 Hour
4 Hours
24 Hours
H2122
H1373
H23
p4EBP1 T37/46
pS6K T389
pS6KT389
pAKT S473
Vinculin

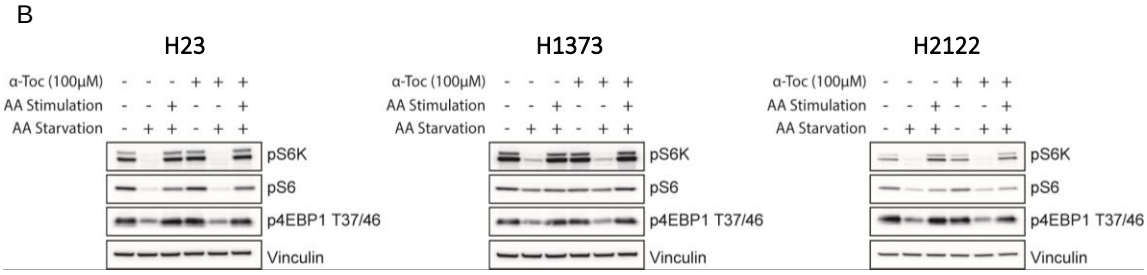
B
H23
H1373
H2122
α-Toc (100μM)
AA Stimulation
AA Starvation
pS6K
pS6
p4EBP1 T37/46
Vinculin

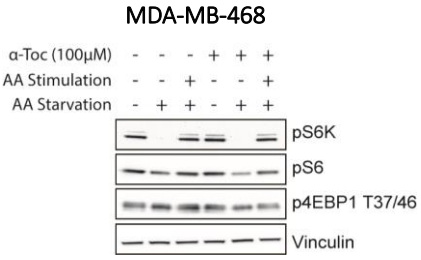
MDA-MB-468
α-Toc (100μM)
AA Stimulation
AA Starvation
pS6K
pS6
p4EBP1 T37/46
Vinculin

Figure 5.5 α-Tocopherol does not Impede RM6 Upon Washout, and it does not Interfere with the Physiological Function of mTORC1.

(A) H2122, H1373, and H23 were treated with 10μM or 100μM α-Toc, or an equivalent volume of DMSO in the control setting, for 24 hours. Media was removed, cells washed with PBS (3X), and media replenished before the addition of 1nM RM6 for the indicated time points. Lysates were probed with the indicated antibodies.

(B) H23, H1373, H2122, and MDA-MB-468 were incubated in serum and amino acid free media for 60 minutes with or without 100μM α-Toc. Controls were incubated in normal media minus serum. After this period, media was removed, cells washed with PBS (3X), and serum free, amino acid replete media added back to cells with or without 100μM α-Toc. For both control and experimental groups, one plate was replenished with serum free, amino acid free media as the internal control. Lysates were probed with the indicated antibodies. MDA-MB-468 underwent an additional 24-hour pre-incubation period with 100μM α-Toc before the experiment began.

The Vitamin E Family Collectively Interferes with the Activity of RM6

Other Vitamins do not Impede the Activity of RM6

The drug interference of α-Toc towards RM6 was quite striking. We next sought to ascertain the specificity of this interference in the context of other vitamins, as well as other analogues and derivatives of vitamin E. We began by assessing the fat-soluble vitamins A, D, and K, and the water-soluble vitamin C (**Figure 5.6A**). H2122 was treated with RM6 with or without these vitamins or α-Toc, and signaling was assessed 4, 8, and 24 hours post treatment, using100μM doses for all vitamins. This dose of vitamin A proved too toxic for cells, leading to substantial cell detachment and loss. Vitamin A was therefore excluded from downstream analysis. Vitamin K demonstrated appreciable rescue/block of p4EBP1 suppression at 4 hours, but this was significantly diminished by later time points compared to α-Toc (**Figure 5.6B**). Furthermore, no coincident rescue of cell growth suppression mediated by RM6 was observed for vitamin K (**Figure 5.6C**), suggesting that the initial p4EBP1 rescue/block was not specific to an interference towards RM6 itself, but likely stemmed from general effects caused by the high dose used. Vitamins C and D demonstrated no target or cell growth rescue. It should be noted that significant cell detachment and loss of viability was induced by vitamin D at 24 hours, and this is reflected by the cell growth data, suggesting this high dose was toxic to cells.

A

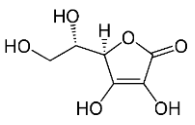

Vitamin C

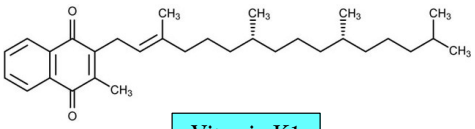

Vitamin K1

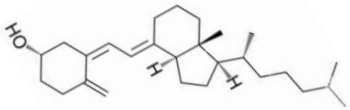

Vitamin D3

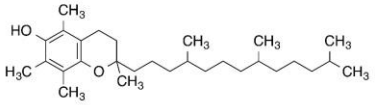

α-Tocopherol

B

H2122

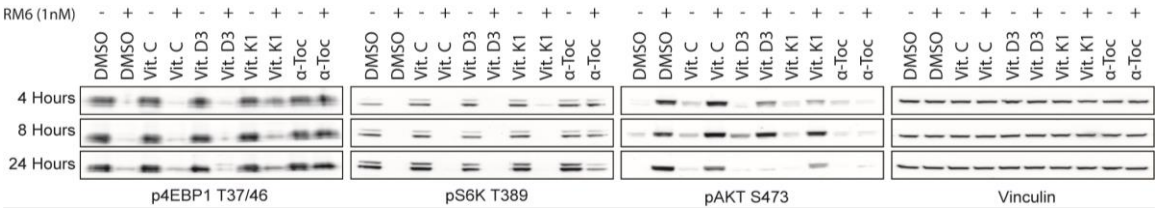

C

H2122

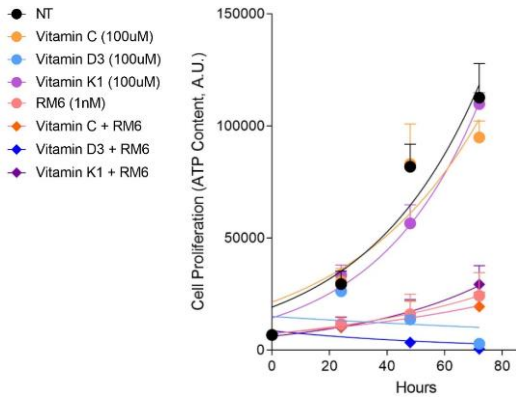

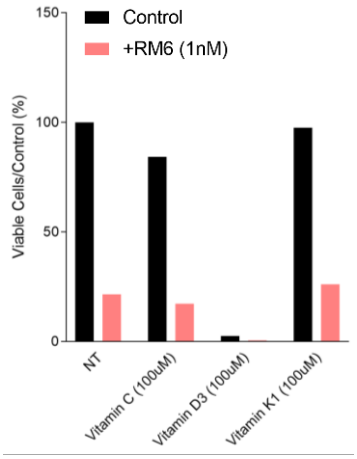

Figure 5.6 Other Vitamins do not Impede the Activity of RM6.

(A) Structures of water-soluble vitamin C, and fat-soluble vitamins K1 and D3, in comparison to α-Tocopherol.

(B) H2122 was treated with 1nM RM6 with or without 100μM vitamin C, vitamin D3, vitamin K1, or α-Toc. Lysates were assessed at the indicated time points and probed with the indicated antibodies.

(C) H2122 was treated with 1nM RM6 with or without 100μM vitamin C, vitamin D3, vitamin K1, or α-Toc, and cell growth assessed over the course of 72 hours. Each treatment was assessed in five technical replicates, and the averages and SDs are shown. To the right is cell viability at the terminal, 72-hour time point, presented as a percentage normalized to control.

Vitamin E Tocopherols and Tocotrienols Impede the Activity of RM6 to Varying Degrees, while α-Tocopherol Derivatives do not Diminish RM6 Activity

We next ascertained if other analogues of vitamin E could impede RM6 activity. H2122 was treated with RM6 with or without β-tocopherol (β-Toc), δ-Tocopherol (δ-Toc), γ-Tocopherol (γ-Toc), α-Tocotrienol (α-TT), β-Tocotrienol (β-TT), δ-Tocotrienol (δ-TT), or γ-Tocotrienol (γ-TT), and signaling was assessed 4, 8, and 24 hours post treatment. The remaining tocopherols (**Figure 5.7A**) rescued mTORC1 targets (**Figure 5.7B**) and cell growth (**Figure 5.7C**) suppressed by RM6 to a comparable extent as α-Toc. However, the tocotrienols (**Figure 5.7D**) unexpectedly exhibited variable rescue of mTORC1 targets (**Figure 5.7E**) and cell growth suppressed by RM6 (**Figure 5.7F**). While α-TT rescued/blocked p4EBP1 and growth suppression mediated by RM6 to a near comparable extent as α-Toc (barring pS6K T389 rescue/block), β-TT and γ-TT exhibited diminishing effects at later time points, no longer rescuing/blocking p4EBP1 suppression by 24 hours, and likewise failing to appreciably rescue RM6 mediated growth suppression, with the γ-TT/RM6 combination demonstrating reduced cell growth compared to RM6 alone. δ-TT fared worse, only rescuing/blocking p4EBP1 suppression at the initial 4-hour time point, and to a lesser extent than the other tocotrienols, while also further suppressing cell growth when combined with RM6. δ-TT and γ-TT also reduced cell proliferation in the control setting.

The diminishing activity of these tocotrienols may arise from their unique structural differences related to both the number of methyl groups on the chromanol ring and the unsaturated nature of their side chain, with reduced methyl groups trending with reduced potency and durability of the drug interference across these vitamin E tocotrienol

analogues. Moreover, different mechanisms of uptake and intracellular transport may also be at play, with each cell type likely having a different selectivity for the tocotrienols (Szewczyk et al. 2021). For example, in human derived fibroblasts (HDF), it was found that sirtuin 1 (SIRT 1) regulates the uptake and bioavailability of tocotrienol analogues (Jaafar et al. 2018). NSCLC cells may likewise demonstrate preferential uptake and transport, as well as degradation, of the various tocotrienol analogues.

Furthermore, the deleterious effects of δ-TT and γ-TT can likely be accounted for by their increased anti-tumor activity, demonstrated to be more robust than tocopherols and their α/β-TT counterparts in various preclinical models (Liu and Jiang 2020, Ranasinghe et al. 2022). For example, δ-TT has been reported to inhibit NSCLC cell invasion by suppressing NF-κB, uPA activator, and MMP-9 (Rajasinghe et al. 2018). γ-TT has been demonstrated to induce apoptosis, necrosis, and autophagy in pancreatic cancer cells by suppressing NF-κB, EGFR, and Id family proteins (Id1 and Id3), while also inducing JNK-signaling and increasing the intracellular levels of dihydroceramide and dihydrosphingosine. γ-TT also attenuated expression of mesenchymal markers and restored E-cadherin and γ-catenin expression, promoting cell invasion (Yap et al. 2008, Jiang et al. 2012). Furthermore, in mammary tumor cells γ-TT significantly inhibited cell proliferation over a 96-hour period and considerably reduced Cyclin D1, CDK2, CDK4, CDK6, and pRB S780 and S807/811 levels between 4 and 24 hours after EGF stimulation, while also significantly increasing CDK inhibitor p27, collectively reducing cell cycle progression from the G1/S phase (Samant et al. 2010).

In line with these data, at a higher dose of 100μM, δ-TT lead to significant cell death in H2122 as a single agent by 24 hours. α-TT and β-TT also provoked significant

loss of cell viability as single agents at 100μM doses (assessed at day 6). Unexpectedly, the higher dose of γ-TT demonstrated a similar level of cell viability to control and α-Toc treated cells (assessed at day 6) (data not shown). This may stem from the degradation or loss of γ-TT by/before this time point, allowing the cells to have recovered and achieved a normal proliferation rate by the time of measurement. However, further studies are required to interrogate this speculation.

Taken together, these data demonstrate that the RM6 drug interference is distinct to vitamin E as a collective family, although significant differences exist in the degree and durability of the interference mediated by the tocotrienols, particularly β-TT, δ-TT, and γ-TT. Whether the diminished drug interference of the tocotrienols towards RM6 is related to their inter- and intra- structural differences, variability in uptake, transport, or loss, preferential modulation of elements that mediate anti-tumor activity, or a combination of these factors remains to be determined.

For completion, we also evaluated three α-Toc derivatives: α-Tocopherol acetate (α-Toc Ac.), α-Tocopherol phosphate (α-Toc Ph.), and its water soluble derivative Trolox (**Figure 5.7G**). H2122 was treated with RM6 with or without these α-Toc derivatives, and signaling was assessed 4, 8, and 24 hours post treatment. Neither of these derivatives rescued mTORC1 targets (**Figure 5.6H**) or cell growth suppressed by RM6 (**Figure 5.6I**). Even at higher doses of 100μM, rescue of mTORC1 targets or cell growth was not observed for any derivative (data not shown). These results have two major implications: (1) the unmodified chromanol ring of vitamin E may be essential to mediate this effect, with the acetate and phosphate functional groups prohibiting this activity, either by precluding the redox reactive hydroxyl, or changing the overall structure such that it's no longer able to

mediate its interference activity, and (2) the fat solubility of vitamin E may be essential for this drug interference.

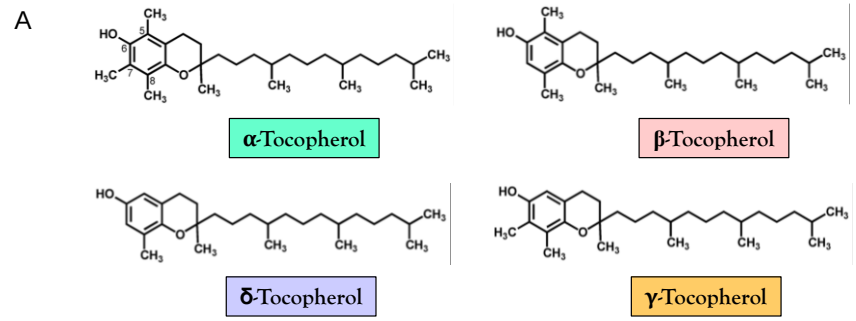

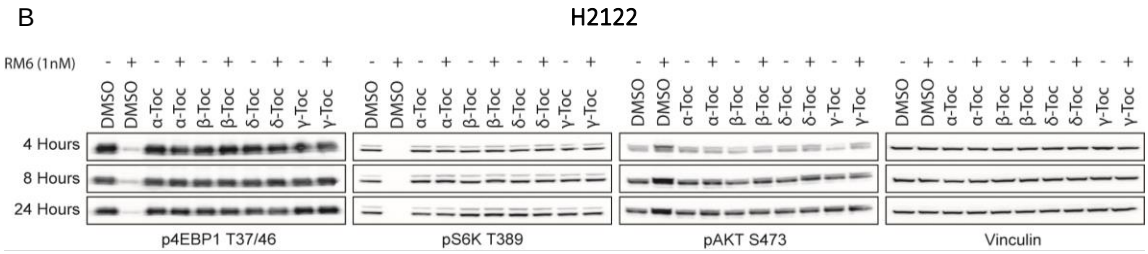

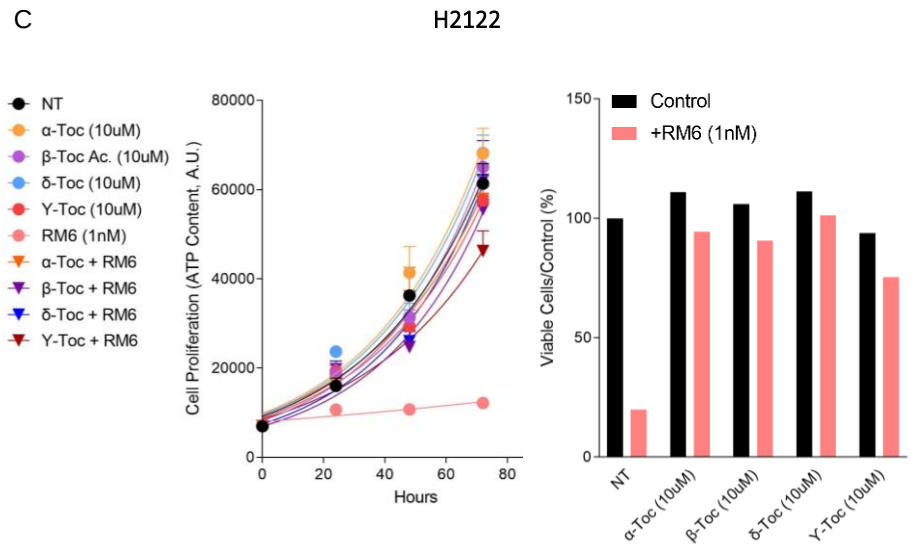

D

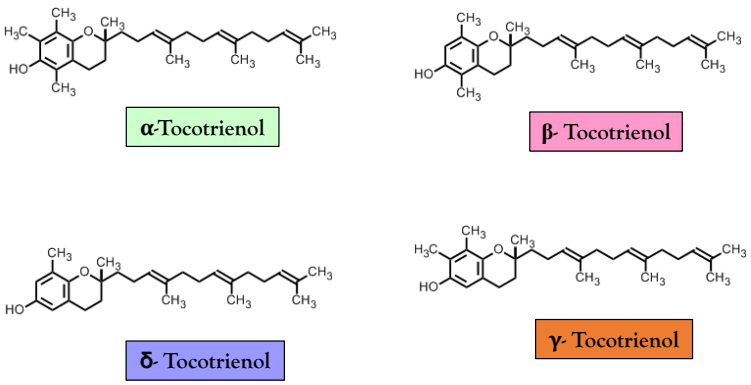
α-Tocotrienol
β- Tocotrienol
δ- Tocotrienol
γ- Tocotrienol

E

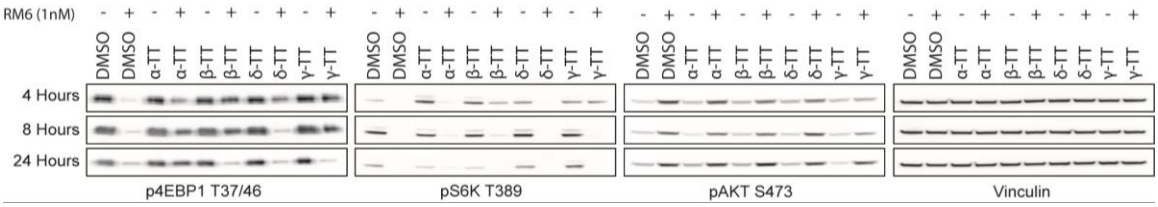
H2122
RM6 (1nM)
DMSO
α-TT
β-TT
δ-TT
γ-TT
4 Hours
8 Hours
24 Hours
p4EBP1 T37/46
pS6K T389
pAKT S473
Vinculin

F

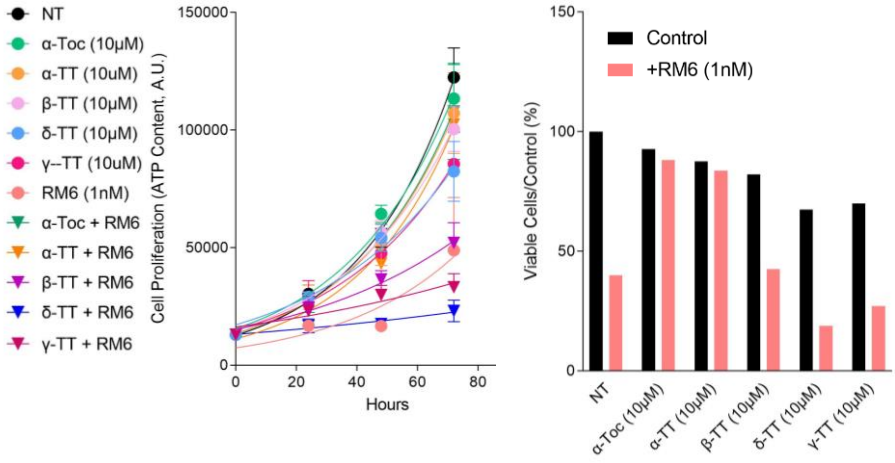
H2122
NT
α-Toc (10μM)
α-TT (10uM)
β-TT (10μM)
δ-TT (10μM)
γ--TT (10uM)
RM6 (1nM)
α-Toc + RM6
α-TT + RM6
β-TT + RM6
δ-TT + RM6
γ-TT + RM6
Cell Proliferation (ATP Content, A.U.)
Hours
Control
+RM6 (1nM)
Viable Cells/Control (%)

G

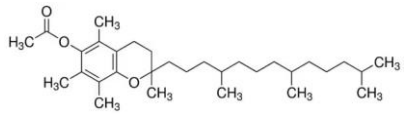

α-Tocopherol Acetate

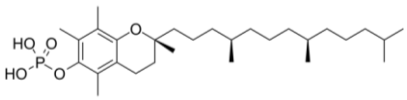

α-Tocopherol Phosphate

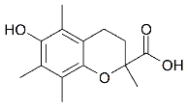

Trolox

H

H2122

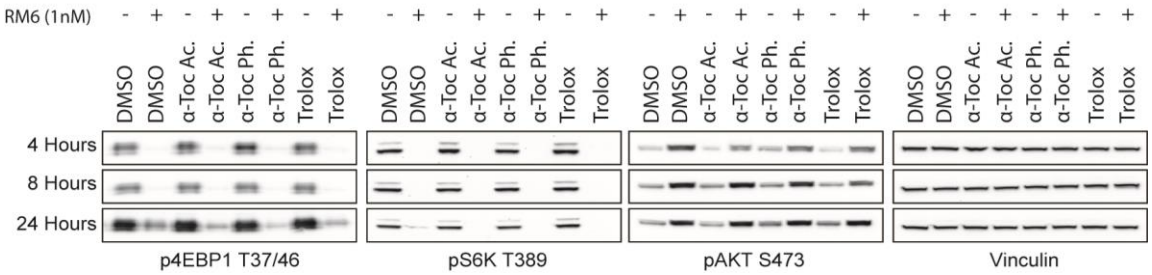

I

H2122

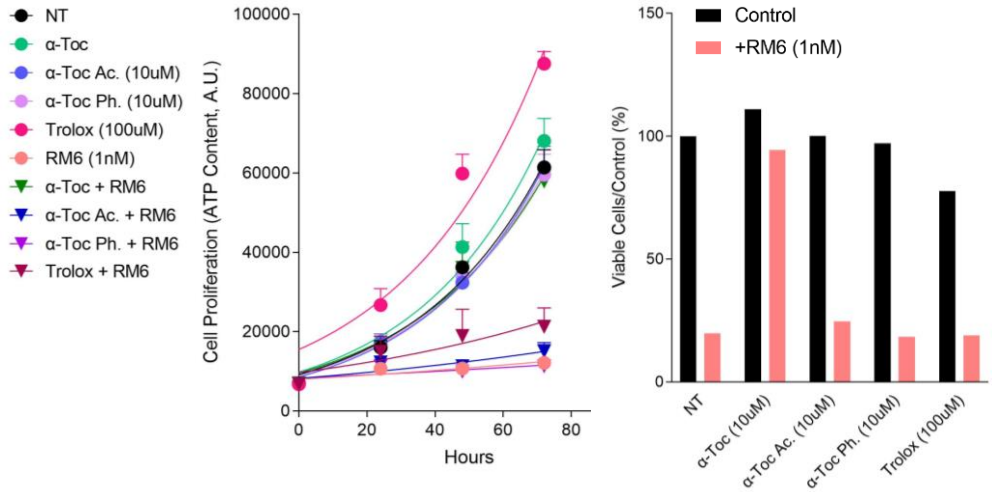

Figure 5.7 Vitamin E Tocopherols and Tocotrienols Impede the Activity of RM6 to Varying Degrees, while α-Tocopherol Derivatives do not Diminish RM6 Activity.

(A) Structures of the four tocopherols (Toc).

(B) H2122 was treated with 1nM RM6 with or without 10μM α-Toc, 10μM β-Toc, 10μM δ-Toc, or 10μM γ-Toc. Lysates were assessed at the indicated time points and probed with the indicated antibodies.

(C) H2122 was treated with 1nM RM6 with or without 10μM α-Toc, 10μM β-Toc, 10μM δ-Toc, or 10μM γ-Toc, and cell growth assessed over the course of 72 hours. Each treatment was assessed in five technical replicates, and the averages and SDs are shown. To the right is cell viability at the terminal, 72-hour time point, presented as a percentage normalized to control.

(D) Structure of the four tocotrienols (TT).

(E) H2122 was treated with 1nM RM6 with or without 10μM α-TT, 10μM β-TT, 10μM δ-TT, or 10μM γ-TT. Lysates were assessed at the indicated time points and probed with the indicated antibodies.

(F) H2122 was treated with 1nM RM6 with or without 10μM α-TT, 10μM β-TT, 10μM δ-TT, or 10μM γ-TT, and cell growth assessed over the course of 72 hours. Each treatment was assessed in five technical replicates, and the averages and SDs are shown. To the right is cell viability at the terminal, 72-hour time point, presented as a percentage normalized to control.

(G) Structure of α-Tocopherol Acetate (α-Toc Ac.), α-Tocopherol Phosphate (α-Toc Ph.), and Trolox.

(H) H2122 was treated with 1nM RM6 with or without 10μM α-Toc Ac., 10μM α-Toc Ph., or 10μM Trolox. Lysates were assessed at the indicated time points and probed with the indicated antibodies.

(I) H2122 was treated with 1nM RM6 with or without 10μM α-Toc Ac., 10μM α-Toc Ph., or 10μM Trolox, and cell growth assessed over the course of 72 hours. Each treatment was assessed in five technical replicates, and the averages and SDs are shown. To the right is cell viability at the terminal, 72-hour time point, presented as a percentage normalized to control.

Stoichiometry, Kinetics, Dynamics, and Preclinical Assessment of the α-Tocopherol/RM6 Drug Interference

Stoichiometry of the α-Tocopherol/RM6 Drug Interference

Our α-Toc dose response data demonstrated that there is an obvious stoichiometry to this drug interference, whereby higher doses of α-Toc can 'outcompete,' so to speak, a given dose of RM6, preventing its activity. Conversely, higher doses of RM6 can outcompete a given dose of α-Toc and effectively suppress its targets. We sought to characterize this stoichiometry in more detail. We first evaluated the degree to which doses between 1-10μM of α-Toc rescued/blocked the target and growth suppression mediated by 1nM of RM6. MDA-MB-468 was treated with 1μM, 3 μM, 5 μM, and 10μM of α-Toc with or without 1nM of RM6, and signaling was assessed over the course of 48 hours. The 1μM dose of α-Toc appreciably rescued/blocked RM6 mediated suppression of p4EBP1, with diminishing effects by 24 hours, while the 3μM, 5μM, and 10μM doses demonstrated a more considerable and durable rescue of both p4EBP1 and pS6K suppression (**Figure 5.8A**). These results were reflected in the growth response data, whereby all doses barring 1μM rescued the growth suppression mediated by RM6 (**Figure 5.8B**).

We performed the converse experiment in H2122, treating cells with escalating doses of RM6, from 10nM to 10μM, with or without 100μM α-Toc and assessing signaling 4 hours post treatment. α-Toc only demonstrated rescue of mTORC1 targets suppressed by 10nM of RM6 (**Figure 5.8C**). At higher doses, an induction of pAKT S473 was observed only in the context of RM6 treatment. This induction was potentiated by a 200μM dose of α-Toc in the 1μM RM6 condition. The induction of pAKT S473 was not coincident with

increased levels of mTORC1 targets. The 100μM α-Toc dose rescued cell growth suppression mediated by all but the 10μM RM6 dose, but with diminishing effects with increasing RM6 dose (**Figure 5.8D**). The α-Toc rescue of growth suppression mediated by the 100nM and 1μM dose of RM6 may stem from activated AKT driving cell growth and survival signaling independent of mTORC1. We asked if an even higher dose of α-Toc could rescue mTORC1 targets suppressed by the 100nM dose of RM6. To address this, H23, H1373, H2122, and MDA-MB-468 were treated with 10μM, 100μM, and 1000μM of α-Toc with or without 100nM of RM6. At the $10e^4$-fold higher dose above RM6, α-Toc demonstrated considerable rescue/block of p4EBP1 suppression (**Figure 5.8E**). Moreover, the 10μM α-Toc dose did not induce pAKT S473 in the context of RM6, while the 100μM and 1000μM doses did. In H2122, the 1000μM dose did not have this effect. Collectively, these data highlight the stoichiometry of this drug interference. Regarding the induction of pAKT S473 mediated by α-Toc in the RM6 treatment setting, it remains to be determined what mechanism(s) drives this induction, and what AKT targets are subsequently influenced by its activation in this manner.

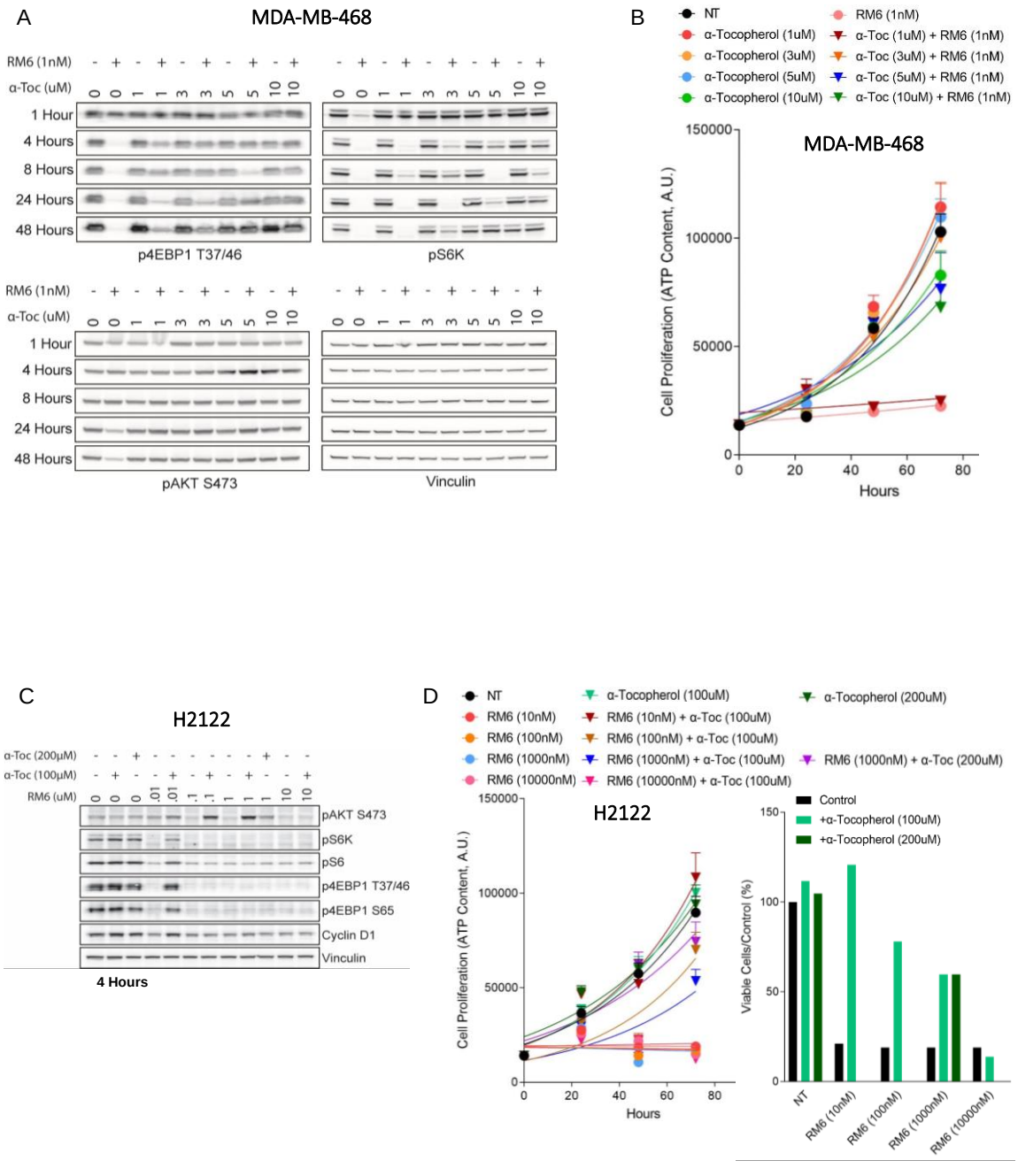
A
MDA-MB-468
RM6 (1nM)
α-Toc (uM)
1 Hour
4 Hours
8 Hours
24 Hours
48 Hours
p4EBP1 T37/46
pS6K
pAKT S473
Vinculin
B
NT
α-Tocopherol (1uM)
α-Tocopherol (3uM)
α-Tocopherol (5uM)
α-Tocopherol (10uM)
RM6 (1nM)
α-Toc (1uM) + RM6 (1nM)
α-Toc (3uM) + RM6 (1nM)
α-Toc (5uM) + RM6 (1nM)
α-Toc (10uM) + RM6 (1nM)
MDA-MB-468
Cell Proliferation (ATP Content, A.U.)
Hours
C
H2122
α-Toc (200μM)
α-Toc (100μM)
RM6 (uM)
pAKT S473
pS6K
pS6
p4EBP1 T37/46
p4EBP1 S65
Cyclin D1
Vinculin
4 Hours
D
NT
RM6 (10nM)
RM6 (100nM)
RM6 (1000nM)
RM6 (10000nM)
α-Tocopherol (100uM)
RM6 (10nM) + α-Toc (100uM)
RM6 (100nM) + α-Toc (100uM)
RM6 (1000nM) + α-Toc (100uM)
RM6 (10000nM) + α-Toc (100uM)
α-Tocopherol (200uM)
RM6 (1000nM) + α-Toc (200uM)
H2122
Cell Proliferation (ATP Content, A.U.)
Hours
Control
+α-Tocopherol (100uM)
+α-Tocopherol (200uM)
Viable Cells/Control (%)
NT
RM6 (10nM)
RM6 (100nM)
RM6 (1000nM)
RM6 (10000nM)

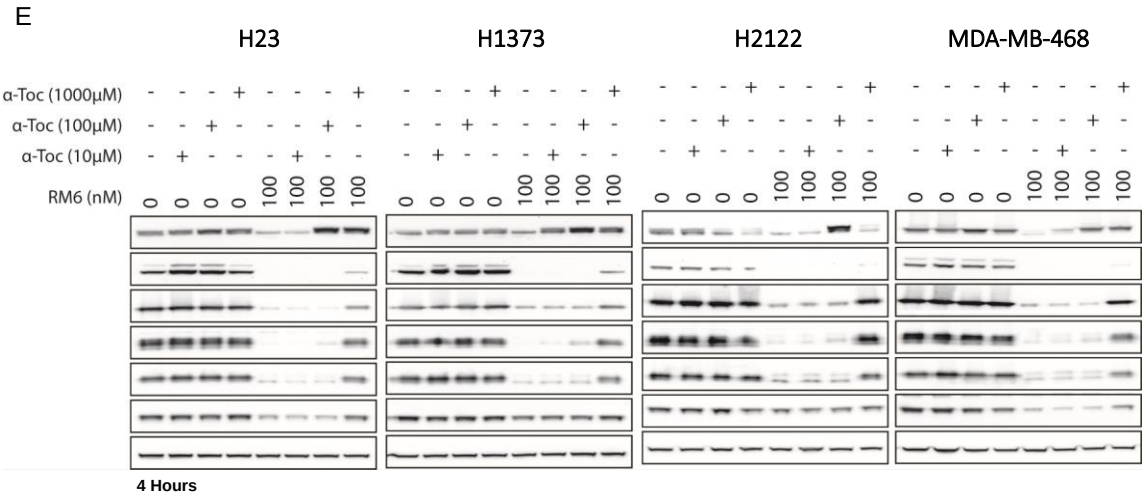

Figure 5.8 Stoichiometry of the α-Tocopherol/RM6 Drug Interference.

(A) MDA-MB-468 was treated with 1nM RM6 with or without 1μM, 3μM, 5μM, or 10μM α-Toc. Lysates were assessed at the indicated time points and probed with the indicated antibodies.

(B) MDA-MB-468 was treated with 1nM RM6 with or without 1μM, 3μM, 5μM, or 10μM α-Toc, and cell growth assessed over the course of 72 hours. Each treatment was assessed in five technical replicates, and the averages and SDs are shown.

(C) H2122 was treated with 10nM, 100nM, 1μM, or 10μM RM6 with or without 100μM or 200μM α-Toc for 4 hours. Lysates were probed with the indicated antibodies.

(D) H2122 was treated with 10nM, 100nM, 1μM, or 10μM RM6 with or without 100μM or 200μM α-Toc, and cell growth assessed over the course of 72 hours. Each treatment was assessed in five technical replicates, and the averages and SDs are shown. To the right is cell viability at the terminal, 72-hour time point, presented as a percentage normalized to control.

(E) H23, H1373, H2122, and MDA-MB-468 were treated with 100nM RM6 with or without 10μM, 100μM, or 1000μM α-Toc for 4 hours. Lysates were probed with the indicated antibodies.

Kinetics and Dynamics of the α-Tocopherol/RM6 Drug Interference

We next turned our attention to the broader kinetics and dynamics of this drug interference. We first sought to ascertain the length of time α-Toc mediated this interference towards RM6. Like RapaLink-1, RM6 is considered to be a 'sticky' molecule, and its suppressive effects last for an extensive period of time. In our *in vivo* experiments, RM6 was dosed once weekly, so we decided to evaluate this drug interference for this length of time. MDA-MB-468 was treated with RM6 with or without α-Toc, and signaling was assessed from 5 minutes to 168 hours. RM6 suppressed mTORC1 targets for the duration of the experiment, while α-Toc rescued/blocked RM6 activity for equally as long (**Figure 5.9A**).

We next asked if α-Toc could rescue suppression of mTORC1 targets mediated by RM6 after a longer period of RM6 treatment. To address this, we first determined the timing of substrate de-inhibition after 4 hours of RM6 treatment, the time at which suppression of p4EBP1 is maximal, followed by washout in MDA-MB-468. RM6 demonstrated protracted inhibition of p4EBP1 and pS6K after washout (**Figure 5.9B**). By 72 hours, p4EBP1 rebound was modest under continued RM6 presence, while cells in which RM6 was washed out demonstrated appreciably more p4EBP1 at this time point. We subsequently treated MDA-MB-468 with RM6 for 44 hours before washout and addition of α-Toc for an additional 0.5-48 hours. α-Toc caused de-inhibition of p4EBP1 around 4 hours, with considerable return of both p4EBP1 and pS6K by 24 hours (**Figure 5.9C**). These data demonstrate that α-Toc can mediate drug interference once RM6 has entered the cell and engaged its target.

We next questioned if RM6 could suppress its targets in the presence of α-Toc if re-added to cells, both in an α-Toc/RM6 continued treatment setting, and in a α-Toc/RM6 washout setting. MDA-MB-468 was treated with the α-Toc/RM6 combination for 72 hours, after which the α-Toc/RM6 combination was either washed (WO) or continued. 1nM of RM6 was subsequently added to the α-Toc/RM6 or α-Toc/RM6 WO groups, and signaling was assessed over the course of 2-48 hours. In the washout setting, RM6 was able to robustly suppress mTORC1 targets (**Figure 5.9D**). RM6 re-added to the α-Toc/RM6 combination was able to appreciably suppress mTORC1 targets, but this suppression was strikingly diminished, and less durable, compared to the WO setting. These data demonstrate that α-Toc persists in cells after an extended period of time, and that it's able to mediate interference towards newly added RM6 under these conditions.

To ascertain if this drug interference was mediated by any components of the cell culture media, MDA-MB-468 was treated with RM6 with or without α-Toc under conditions of serum free media, amino acid free media, and PBS for 4 hours. Under all conditions this drug interference was observed (**Figure 5.9E**). In the case of combined amino acid and serum starvation, the effect was dampened. This is likely due to the diminished activity of mTOR itself under these conditions, resulting from a lack of necessary stimuli that otherwise drives its function, compounded by RM6 mediated suppression. Cells in the PBS condition became completely detached due to loss of factors in the culture media that enable surface adhesion. While overexposure of the membrane was required, the drug interference was observed in this condition.

A

MDA-MB-468

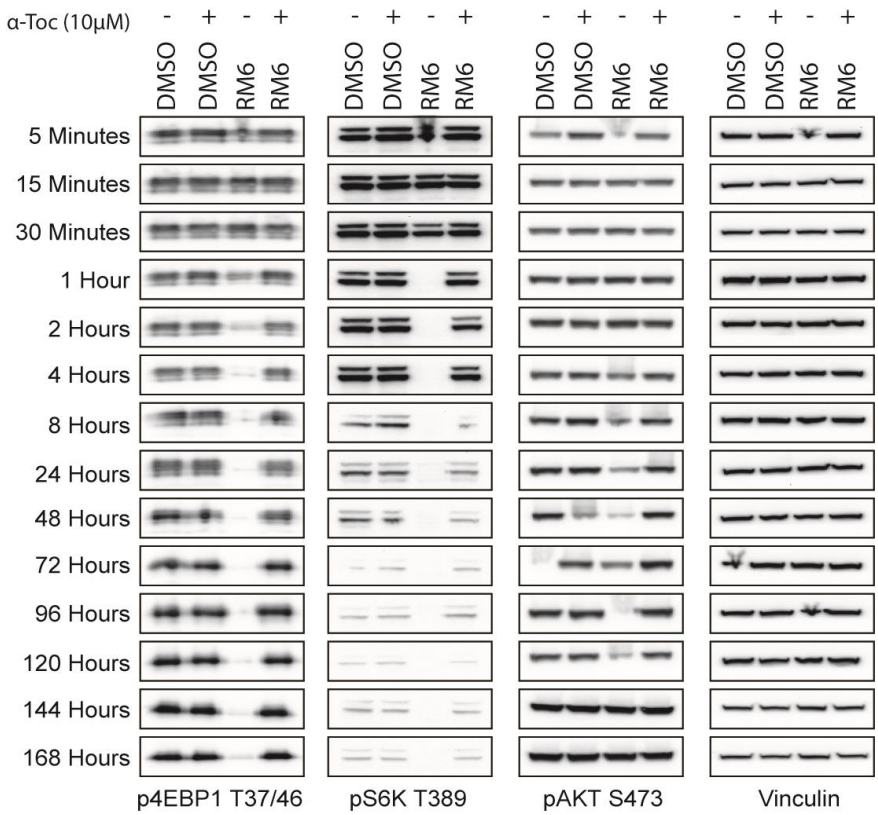

B

MDA-MB-468

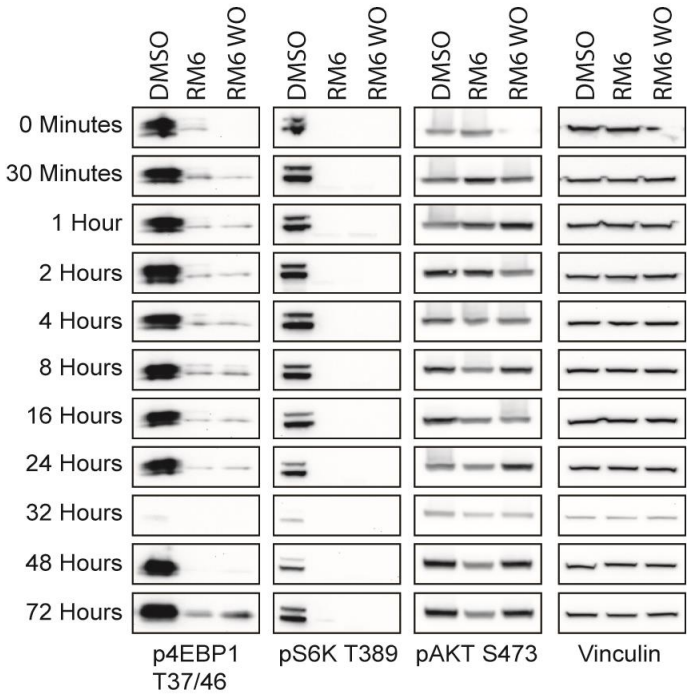

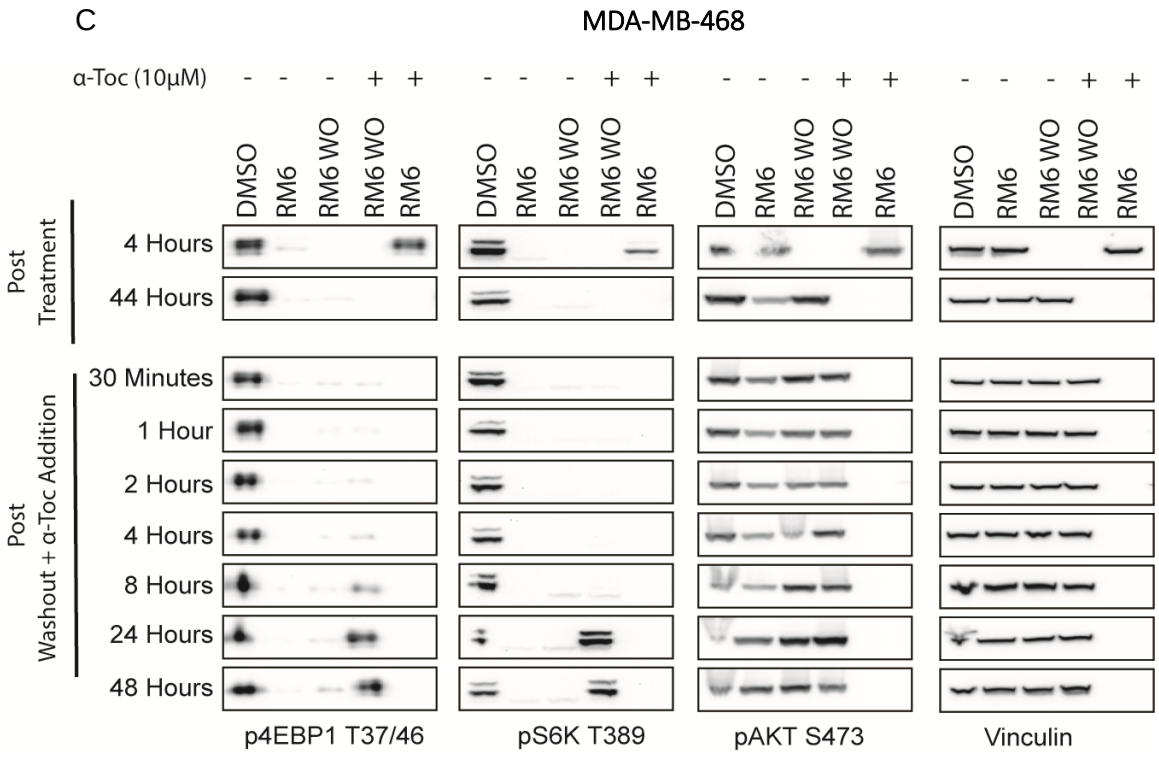
C
MDA-MB-468
α-Toc (10μM)
DMSO
RM6
RM6 WO
RM6 WO
RM6
Post Treatment
4 Hours
44 Hours
Post Washout + α-Toc Addition
30 Minutes
1 Hour
2 Hours
4 Hours
8 Hours
24 Hours
48 Hours
p4EBP1 T37/46
pS6K T389
pAKT S473
Vinculin

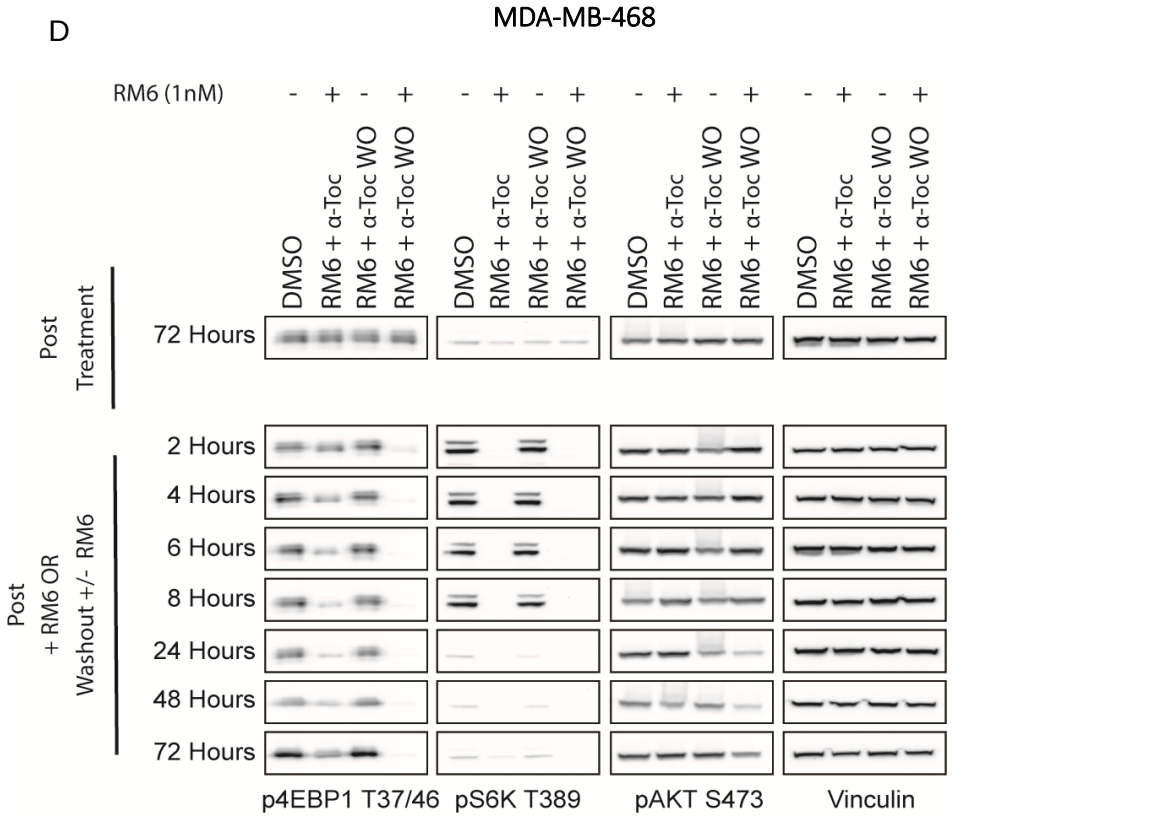
D
MDA-MB-468
RM6 (1nM)
DMSO
RM6 + α-Toc
RM6 + α-Toc WO
RM6 + α-Toc WO
Post Treatment
72 Hours
Post + RM6 OR Washout +/- RM6
2 Hours
4 Hours
6 Hours
8 Hours
24 Hours
48 Hours
72 Hours
p4EBP1 T37/46
pS6K T389
pAKT S473
Vinculin

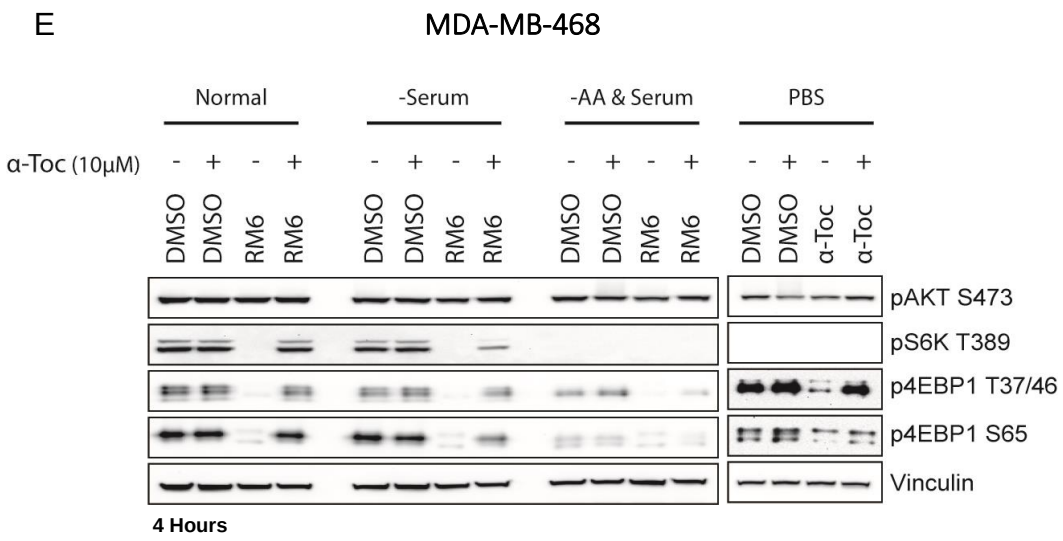

Figure 5.9 Kinetics and Dynamics of the α-Tocopherol/RM6 Drug Interference.

(A) MDA-MB-468 was treated with 1nM RM6 with or without 10μM α-Toc. Lysates were assessed at the indicated time points and probed with the indicated antibodies.

(B) MDA-MB-468 was treated with 1nM RM6 for 4 hours, followed by subsequent washout (media removal, PBS wash [3X], media replenishment - WO group) or continued treatment with no washout (RM6). Lysates were assessed at the indicated time points and probed with the indicated antibodies.

(C) MDA-MB-468 was treated with 1nM RM6 for 44 hours, followed by subsequent washout (media removal, PBS wash [3X], media replenishment – WO group) or continued treatment with no washout (RM6). 10μM α-Toc was added to the indicated RM6 WO group for 0.5-48 hours. Lysates were assessed at the indicated time points and probed with the indicated antibodies. Note that RM6 + 10μM α-Toc (rightmost lane) was only assessed at the 4-hour time point to highlight the early drug interference.

(D) MDA-MB-468 was treated with the combination of 1nM RM6 and 10μM α-Toc for 72 hours. After which the combination was washed out (media removal, PBS wash [3X], media replenishment – WO group) or treatment was continued with no washout (RM6 + α-Toc). 1nM RM6 was subsequently re-added to the indicated WO and RM6 + α-Toc continued treatment groups for 2-72 hours. Lysates were assessed at the indicated time points and probed with the indicated antibodies.

(E) MDA-MB-468 was treated with 1nM RM6 with or without 10μM α-Toc under conditions of normal media, serum free media, combined serum free and amino acid free media, and PBS for 4 hours. Lysates were probed with the indicated antibodies.

Preclinical Assessment of the α-Tocopherol/RM6 Drug Interference

Finally, we ascertained if this drug interference would occur *in vivo* using an H2122 CDX model. Mice were treated with 3mg/kg RM6 or vehicle (i.p.), and orally gavaged with either 100mg/kg α-Toc or 400mg/kg α-Toc once tumors reached ~100-150mm^3. Tumors were collected 4- and 24-hours post treatment, and tumor lysates probed with the indicated antibodies. Surprisingly, the 3mg/kg dose of RM6 did not suppress p4EBP1 (T37/46, S65) levels to any notable extent when compared to vehicle (**Figure 5.10A, B**). Levels of pS6K T389 and pAKT S473 were also variable and inconsistent between the treatment groups. In this same CDX model, a 6mg/kg dose of RM6 results in complete suppression of p4EBP1 S65 and induction of pAKT S473 by 24 hours (data not shown). Although we have not conducted any *in vivo* dosing experiments for RM6 in our NSCLC models, we anticipated the 3mg/kg dose would be effective since this dose readily suppresses mTORC1 targets in breast and endometrial cancer CDX and PDX models, and our NSCLC cell lines are similarly sensitive to RM6. While we cannot draw any conclusions as to the *in vivo* occurrence of this drug interference from our current data, we strongly suspect that it may occur in this setting given the striking *in vitro* data. Our future work will interrogate this hypothesis through a more rationally designed *in vivo* study.

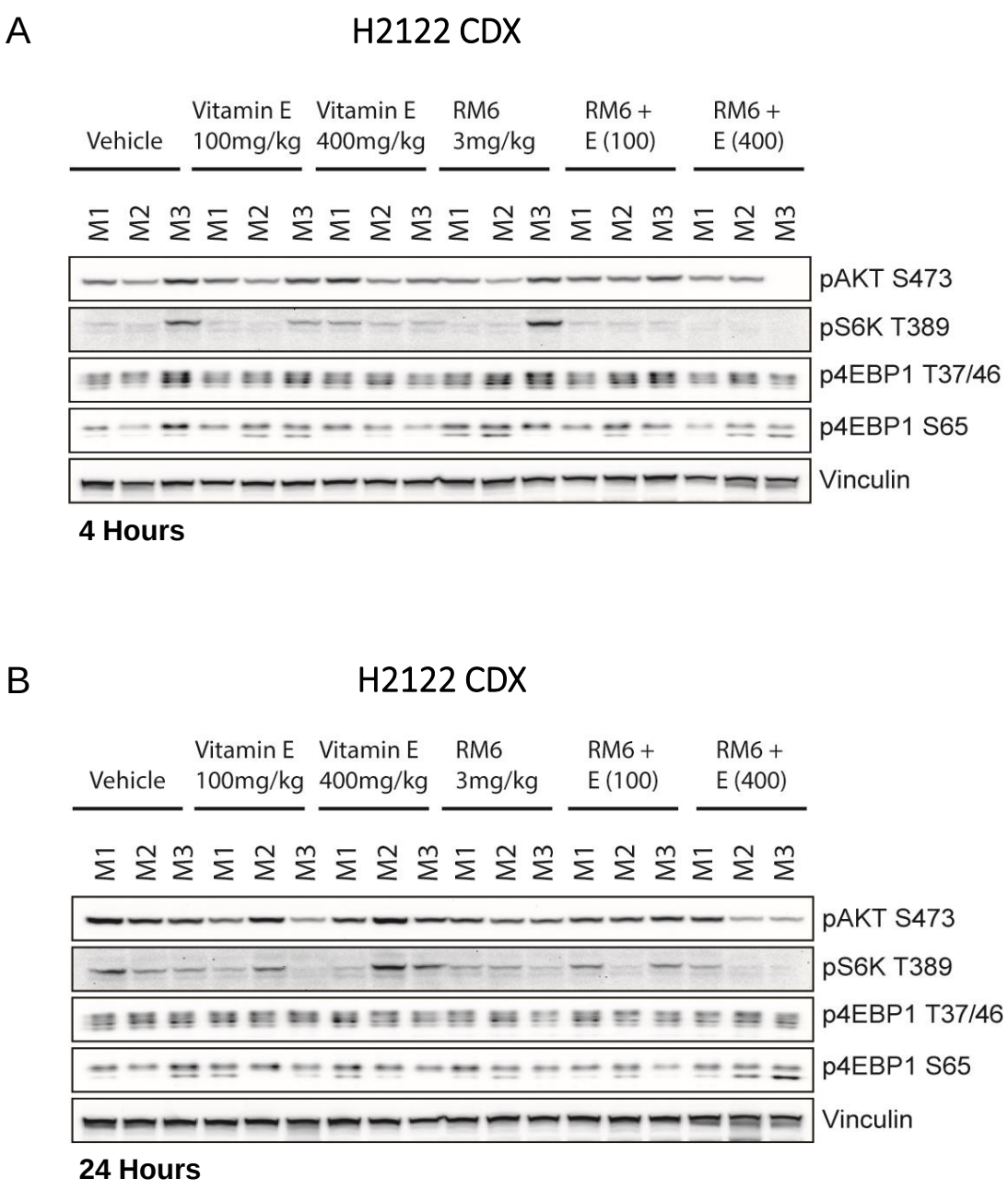

Figure 5.10 Preclinical Assessment of the α-Toc/RM6 Drug Interference.

(A), (B) An H2122 CDX model was treated with vehicle, 3mg/kg RM6 (i.p.), 100mg/kg or 400mg/kg α-Toc (oral gavage), or the combination of RM6 with both doses of α-Toc once tumors reached ~100-150mm^3. Tumors were collected 4- and 24- hours post single dose administration, and lysates probed with the indicated antibodies.

Chapter 6: Discussion

Conclusions

In the present study we have investigated the feasibility of using an mTORC1 selective inhibitor to enhance the efficacy of KRAS G12C inhibitors for the treatment of KRAS G12C mutant cancers, with a focus on NSCLC and CRC. We demonstrate that mTORC1 selective inhibitors enhance cell growth suppression and cell death induction mediated by KRAS G12C inhibition. The KRAS G12C/mTORC1 inhibitor combination also led to significant tumor regression in KRAS G12C mutant NSCLC CDX and PDX models. Furthermore, this drug combination did not induce hyperglycemia, a feature of AKT/mTORC2 inhibition that's limited the clinical efficacy of conventional PI3K, AKT, and mTOR inhibitors to date (Hanker et al. 2019, Castel et al. 2021).

At the molecular level, dual suppression of KRAS G12C and mTORC1 provoke synergistic modulation of a multiplicity of factors involved in regulating the cell cycle and survival. Among these targets are the cell cycle regulators Cyclin D1, pRB, p27, and claspin, the apoptosis regulator survivin, the extrinsic apoptosis factors TRAIL R1/DR4, TRAIL R2/DR5, and TNFR1, and the intrinsic apoptosis factors BIM, Bcl-xL, and Mcl-1. While the degree, necessity, and sufficiency to which each factor contributes to the growth suppressive and/or death inducing effects of the drug combination remain to be elucidated, these data highlight the vast synergy of the KRAS G12/mTORC1 inhibitor combination. Though not the focus of this report, we have gone on to demonstrate that the mTORC1 selective inhibitor RM6 enhances the efficacy of the KRAS G12C-GTP inhibitor RM18 by

translational inhibition of Cyclin D1 and Mcl-1, accounting for, at least in part, the synergistic growth suppression and cell death induction mediated by the combination.

We have also demonstrated that the drug combination dysregulates key elements of the ferroptosis network, resulting in suppression of GSH and induction of ROS and lipid peroxidation. Despite this, liproxstatin-1, a potent ferroptosis inhibitor, only modestly rescued cell death induced by the RM18/RM6 drug combination, while the iron chelator DFO, another agent used to block ferroptosis, failed to reduce cell death. Currently, there is no specific biomarker to detect ferroptosis, so it's usually confirmed by assessing whether cell death can be rescued by specific ferroptosis inhibitors (Liu et al. 2020). Since Lip-1 only modestly suppressed lipid peroxidation induced by the drug combination, we couldn't resolve whether its limited rescue of cell death reflected this metric, or if ferroptosis simply wasn't a mechanism contributing to treatment induced cell death in our models.

We attempted to better understand this by ascertaining the intrinsic sensitivity of our NSCL cell lines to well established ferroptosis inducers RSL3 (GPX4 inhibitor), Erastin (xCT inhibitor), and iFSP1 (FSP1 inhibitor). With the exception of H1373, H23, and H358, our models were resistant to RSL3 (3/10), while no evaluated cell line showed sensitivity to Erastin (7/7) or iFSP1 (4/4). Moreover, the combination of RSL3 and iFSP1 did not provoke synergistic killing in assessed models. Notably, Lip-1 completely rescued cell death induced by RS3L in sensitive cell lines, coincident with its more robust suppression of RSL3 induced lipid peroxidation. Collectively, these data suggest that dysregulation of the ferroptosis network will not inevitably result in ferroptotic cell death. This may stem from mechanisms that protect the cell from terminal ferroptosis in the

presence of perturbations that would otherwise cause it, and/or from an inherent absence, or lack of function, of yet unknown effectors that drive ferroptosis to completion.

In the final part of this study, we discovered that α-Tocopherol considerably impedes the activity of mTOR bi-steric inhibitors, inclusive of RapaLink-1 and the series of mTORC1 selective inhibitors RM1, RM2, RM3, and RM6, in addition to interfering with the activity of the KRAS G12C-GTP inhibitor RM18, and the KRAS G12D-GTP inhibitor RM44, although effects on these KRAS-GTP inhibitors were less durable compared to the mTOR bi-steric inhibitors. The initial impetus for investigating α-Toc stemmed from the underwhelming cell death rescue effects liproxstatin-1 demonstrated in the RM18/RM6 drug combination.

Lip-1, and the preceding ferrostatin-1 (Fer-1), were identified by high-throughput screens as potent inhibitors of ferroptosis - an activity ascribed to their ability to slow the accumulation of lipid hydroperoxides (Dixon et al. 2012, Friedmann Angeli et al. 2014). Zilka et al. later demonstrated that the ferroptosis suppressing activity of Fer-1 and Lip-1 likely derives from their reactivity as RTAs rather than inhibitors of lipoxygenases, which can enzymatically contribute to lipid peroxidation. In this study, the investigators determined that Fer-1 and Lip-1 inhibited autoxidations of styrene by peroxyl radicals roughly 10-fold more slowly than α-Tocopherol, the most biologically active form of vitamin E, and nature's premier lipid-soluble RTA (Burton and Ingold 1986, Zilka et al. 2017). However, Lip-1 and Fer-1 showed significantly more reactivity than α-Toc in phosphatidylcholine lipid bilayers. They further proposed that Lip-1 and Fer-1 had an increased radical-trapping capacity due to their ability to form end products that remain highly reactive to peroxyl radicals, consistent with previous reports by both the Conrad and

Stockwell groups demonstrating that Fer-1 and Lip-1 were more potent ferroptosis inhibitors than α-Toc (Friedmann Angeli et al. 2014, Skouta et al. 2014). Nevertheless, we speculated that in our models treated with these agents, preventing the initiation of lipid peroxidation would perhaps be key to attenuating the surmised ferroptosis, and α-Toc was demonstrated to be superior in this regard by Zilka et al. Hence, we evaluated α-Toc across our treatment groups, and obtained an extraordinary result.

α-Toc effectively rescued cell death mediated by the RM18/RM6 drug combination, almost completely in one of our NSCLC models, in addition to a recovery of cell growth suppression caused by the various treatment groups, while having negligible effects on the control. Subsequent assessment of signaling output revealed that α-Toc considerably and durably impeded the ability of RM6 to suppress mTORC1 targets pS6K and p4EBP1. The induction of pAKT S473 induced by RM6 was also diminished. This effect was demonstrated in several cancer models – NSCLC, breast cancer, CRC, and endometrial cancer – suggesting that it's inherent to α-Toc impeding RM6 activity, rather than a lineage specific phenomenon. α-Toc also interfered with the activity of RM18, leading to significant rescue/block of pERK at early time points, although the effects were less durable. We went on to show that this drug interference is specific to mTOR bi-steric inhibitors and KRAS-GTP (ON) inhibitors, as α-Toc did not interfere with the activity of several PI3K inhibitors (GDC0941, BYL719, AZD8186), an AKT inhibitor (MK2206), non-linked mTOR inhibitors (Rapamycin, MLN0128, AZD8055), an EGFR inhibitor (Cetuximab), KRAS G12C-GDP (OFF) inhibitors (MRTX849, AMG510, AZD8037), a MEK inhibitor (Trametinib), and an ERK inhibitor (SCH2277894).

Although the mechanism(s) of this nutrient/drug interference remains to be elucidated, for the KRAS-GTP (ON) inhibitors, we demonstrate that α-Toc disrupts the kinetics of drug binding to KRAS, detected by a reduction in the KRAS band shift, indicative of reduced drug binding. α-Toc did not affect binding of RM42, the pan RAS-GTP (ON) inhibitor, and it did not rescue/block suppression of pERK mediated by RM42. α-Toc also rescued/blocked pMEK suppression mediated by RM18 and RM44, with effects diminishing at later time points. Interestingly, α-Toc suppressed pMEK levels in the context of RM42 treatment, which on its own did not reduce pMEK. This may account for why pERK remained suppressed, rather than rescued, in the α-Toc/RM42 combination. These results demonstrate that α-Toc does have an effect on RM42, but that it presents differently to the effects observed for RM18 and RM44. We speculate that the α-Toc drug interference on these RAS-GTP inhibitors may stem from an effect on cyclophilin A, given that vitamin E has immunomodulatory properties. While RM42 also forms a binary complex with cyclophilin A, and its binding to KRAS was not perturbed by α-Toc, we cannot rule out a collective effect on RAS binding, as we did not evaluate pan RAS, NRAS, or HRAS in this experiment.

Likewise, we have not defined the mechanism by which α-Toc impedes the mTOR bi-steric inhibitors. However, we have made some important findings that suggest what factors may or may not play a role in mediating this inference. Notably, α-Toc does not affect the ability of mTOR to physiologically activate S6K upon amino acid starvation and subsequent re-stimulation. Additionally, α-Toc impedes the activity of RM6 in a variety of cancer cell lines, and at much lower doses than used by ferroptosis studies to rescue this mode of RCD. Collectively, these results suggest that α-Toc is directly impacting RM6

activity rather than factors that mediate or may influence its activity (i.e., its substrate mTOR, the genetic background and/or lineage of the cells). Furthermore NAC, an antioxidant that exhibited substantial suppression of ROS induced by the RM18/RM6 drug combination, failed to rescue cell death mediated by the same, implying that the antioxidant properties of α-Toc do not play a role in its cell death rescue effects. Rather, this activity was demonstrated to stem directly from its impediment of RM6 and, to a degree, RM18, such that these agents cannot efficiently suppress their targets. In the case of RM6, this interference is complete and durable, lasting for at least seven days – the longest time point assessed. NAC and Lip-1 did not share this feature with α-Toc, demonstrating no modulation of mTORC1 or RAS/ERK substrates in co-treatment experiments with these inhibitors (data not shown).

We also demonstrate that α-Toc impedes the entire class of evaluated mTOR bi-steric inhibitors, inclusive of RapaLink-1 and the series of mTORC1 selective inhibitors, albeit to varying degrees. For example, while 10μM of α-Toc considerably impedes the activity of RM3 and RM6, this dose is insufficient to preclude target suppression mediated by 10nM of RapaLink-1 or 10nM of RM1 (data not shown). Although bearing the same core constituents – Rapamycin, linker, active site inhibitor – these agents differ in their modulations to the Rapamycin core, the length and position of the chemical linker, and the active site inhibitor. The broad interference α-Toc exhibits towards these agents, compounded by the varying degrees to which α-Toc impedes each one, suggests that there's a chemical- and/or structural-based component to this effect that's influenced by the exact nature of the compound. As to what the chemical and/or overall structural

element(s) are that drive this susceptibility of the mTOR bi-steric inhibitors to α-Toc mediated interference remains to be determined.

Through dosing experiments, we demonstrate that there's an obvious stoichiometry to this drug interference, whereby certain doses of α-Toc can outcompete a given dose of RM6, leading to effective inhibition of its activity. Conversely, certain doses of RM6 can outcompete a given dose of α-Toc, permitting it to effectively suppress its target. At minimum there appears to be a 1000- to 10,000-fold order of magnitude to these effects, as 1μM of α-Toc can appreciably rescue/block suppression of p4EBP1 mediated by 1nM of RM6 (observed at early time points in the NSCLC cell line H2122 [**Figure 5.4A**] and the breast cancer cell line MDA-MB-468 [**Figure 5.8A**], and 10μM of α-Toc can durably rescue/block suppression of mTORC1 targets mediated by up to 10nM of RM6 (observed in CRC cell line SW837 [**Figure 5.4H**]. However, 100μM of α-Toc fails to impede the suppressive activity of 100nM+ of RM6, although an effect is still at play in this setting, demonstrated by the induction of pAKT S473 in the presence of higher RM6 doses (up to 10μM), an effect not observed with 10μM of α-Toc. Furthermore, 1mM of α-Toc can rescue/block suppression of mTORC1 targets mediated by 100nM of RM6. Interestingly, the pAKT S473 induction persists in several models, barring H2122. These data highlight the stoichiometry relationship between α-Toc and RM6, a key characteristic of this drug interference.

We have also shown that other analogues of the vitamin E family, namely the remaining 3 tocopherols and the 4 tocotrienols, also impede the activity of RM6, albeit to varying degrees. The tocotrienols – particularly β-TT, δ-TT, and γ-TT – exhibit a diminished drug interference profile compared to the tocopherols and α-TT. This reduced

activity trends with the loss of methyl groups on the chromanol ring among these unsaturated vitamin E analogues, suggesting that this structural feature may play a role in mediating this drug interference activity, in addition to saturation of the side chain. Other factors, including variability in uptake, transport, loss, and biological activity, may also account for the differential drug interference observed between the tocopherols and tocotrienols. The α-Toc derivatives acetate, phosphate, and hydrophobic tail lacking, water-soluble Trolox, did not precipitate any obvious impediment of RM6 activity. This further implies that the structural elements of vitamin E play a role in mediating this impediment, and that the acetate and phosphate groups of their respective derivatives preclude this interference, either by nature of changing the chemical structure as whole, or by losing the redox reactive hydroxyl moiety through complex with their functional groups. Additionally, these data suggest that that the fat solubility of α-Toc may be necessary to mediate its drug interference effects.

What's unique about this drug interference, at least in the case of the mTOR bi-steric inhibitors, is that it appears to be uninfluenced by the primary properties of vitamin E that have been demonstrated, or speculated, to affect other therapeutic agents. A literature search, along with a review of vitamin E's 273 potential drug interactions, broadly describes its possible interference on 4 classes of drugs: (1) anticoagulant/blood agents, (2) chemo-/radio-therapeutic agents, (3) iron supplementary agents, and (4) immunomodulators. Vitamin E may potentiate the effects of anticoagulants and platelet inhibitors since it's believed to inhibit the oxidation of reduced vitamin K and interfere with its dependent clotting factors. Additionally, *in vitro* and *ex vivo* human studies suggest that vitamin E can inhibit collagen-induced platelet activation and PKC-dependent platelet

aggregation. Although the potential effects of vitamin E on cancer chemo- and radio-therapy have not been fully established, at pharmacologic doses, the antioxidant properties of vitamin E could theoretically interfere with agents whose cytotoxic mechanism depends on generating ROS to damage DNA and proteins. Alternatively, vitamin E may help reduce oxidative stress associated with more aggressive cancers and protect non-cancer cells from oxidative damage. Limited data suggests that vitamin E may diminish the response to iron therapy in patients with anemia, although the mechanism has not been established. Finally, agents that are thought to have immunomodulatory properties, such as vitamin E, may antagonize the pharmacologic effects of immunosuppressants, although clinical cases of drug interactions have not been noted (drugs.com 2023).

Overall, the reported and speculated cases of vitamin E's drug interference profile are predominantly based on its antioxidant and purported immunomodulatory properties. However, in 2017, Uchihara et al. reported that α-Toc attenuated the effects of the anaplastic lymphoma kinase (ALK) inhibitor crizotinib independent of its antioxidant properties. In Ba/F3 cells expressing the fusion protein nucleophosmin-ALK (NPM-ALK), a common genetic alteration characterizing anaplastic large cell lymphomas (ALCL), α-Toc rescued/blocked crizotinib mediated suppression of NPM-ALK phosphorylation and phosphorylation of its downstream target STAT3. Moreover, α-Toc did not influence uptake of crizotinib by cells, and the drug interference was demonstrated to occur *in vivo* in a Ba/F3 NPM-ALK expressing CDX model (Uchihara et al. 2017).

In a subsequent report by the same group, these effects were observed in Ba/F3 cells transformed with EML4-ALK, a fusion protein harbored by a percentage of patients with NSCLC. α-Toc was demonstrated to impede the reduced phosphorylation of EML4-

ALK and its downstream targets STAT3 and ERK mediated by crizotinib (Uchihara et al. 2018). Notably, in both reports only α-Toc, and not other assessed tocopherol or tocotrienol analogues of vitamin E, provoked this drug interference. Hence, we've yet to come across any study that demonstrates a direct interference of the collective vitamin E family on a targeted pharmacological inhibitor such that we observe in the case of RM6. Although not yet assessed for the other mTOR bi-steric inhibitors, we anticipate a similar interference to occur with the remaining tocopherol and tocotrienol analogues.

Clinical Implications

The vitamin E drug interference towards mTOR bi-steric inhibitors and KRAS G12C-GTP inhibitors has two overt clinical implications: efficacy and toxicity mitigation. Regarding efficacy, while nutritional intake of vitamin E from food sources does not pose any drug interaction concerns (Podszun and Frank 2014), vitamin E is among the most commonly taken dietary supplements. Although the recommended dietary allowance (RDA) of vitamin E is 15mg for individuals 14+, most vitamin-E-only supplements provide ≥67 mg (100 IU) of the nutrient, with some supplying as much as 670 mg (1000 IU). Although these amounts are substantially higher than the RDAs, a high doses of vitamin E is very rarely toxic, although occasionally it can cause a risk of bleeding, as well as muscle weakness, fatigue, nausea, and diarrhea.

The bioavailability, metabolism, and biological activity of the various analogues of vitamin E should also be taken into account when considering efficacy concerns and their clinical applications. In a study conducted by Novotny et al., investigators modeled and quantified the kinetics, bioavailability, and metabolism of RRR-α-Tocopherol, the natural

stereoisomer of α-Toc produced by plants, in 12 healthy adults, 6 men and 6 women, aged 27 ± 6 years. Study participants ingested 1.81 nM of [5-$^{14}CH_3$]-RRR-α-Toc, with each dose containing 3.70 kBq of ^{14}C. Urine and feces were collected over the first 21 days from the start of dosing, and serial blood samples were drawn over the first 70 days, with all samples analyzed for RRR-α-Toc and ^{14}C by accelerator mass spectrometry. From these data, the investigators modeled and quantified the kinetics of RRR-α-Toc *in vivo* in humans (**Table 6.1**).

Tissue	Residence Time	Half-Life	Concentration
Plasma chylomicrons	22 Minutes	16 Minutes	120nM
Plasma lipoproteins	5 Hours	4 Hours	65µM
Rapidly absorbed plasma	3 Minutes	2 Minutes	
Plasma carboxyethyl hydroxychroman (CEHC)	-	-	460nM
Colon	-	-	9µM
Hepatocytes	-	-	820nM
HSC, brain, spleen, etc	2.42 Days	2 Days	392µM
Hepatocytes	2 Hours	2 Hours	25M
Adipose tissue	499 Days	184 Days	14µM
RBC extrinsic	14 Hours	9 Hours	25µM

Table 6.1 Modeled Residence Time, Half-Life, and Concentration of α-Toc Across Various Compartments in Humans.

Tabulated from Novotny, et al. *J Nutr*. (2012)

The bioavailability of RRR-α-Toc was determined to be 81 +/- 1%, and total body stores were estimated to be 220 μM (11 grams). Furthermore, the investigators found that a daily intake of 9.2 μM (4mg) of RRR-α-Toc maintained plasma RRR-α-Toc concentrations at 23 μM/L (Novotny et al. 2012). In terms of dietary supplements and fortified foods, α-Toc is more commonly provided in its acetate or succinate forms, given the enhanced stability of esterified vitamin E. This may seem problematic for potential efficacy concerns since the evaluated α-Toc derivatives failed to demonstrate any drug interference towards RM6. However, in the body α-Toc derivatives are readily hydrolyzed by intestinal and pancreatic enzymes to yield free α-Toc (Schmölz et al. 2016, Duncan and Suzuki 2017).

Compared to tocopherols, in the body tocotrienols have limited bioavailability, and are not sustained in the plasma for an adequate period of time, with concentrations peaking at 4-5 hours before complete loss by 24 hours. Of the tocotrienols, α-TT is the most abundant analogue circulated in plasma and lipoproteins (Fairus et al. 2006, Fairus et al. 2012). Despite their lower bioavailability, when compared to other analogues of the vitamin E family, δ-TT and γ-TT are considered to be more potent anti-cancer therapeutics, promoting a higher degree of cell death in preclinical cancer models of the cervix (Xu et al. 2017), lung (Zarogoulidis et al. 2013, Rajasinghe 2017), breast (Samant et al. 2010, Anwar et al. 2021, Ding et al. 2021, Grazier and Sylvester 2021, Sultana et al. 2021), colon (Wada et al. 2017, Yang et al. 2021), liver (Har and Keong 2005), skin (Chang et al. 2009), prostate (Yap et al. 2008, Jiang et al. 2012), blood (Sailo et al. 2018), pancreas (Husain et al. 2011), stomach (Manu et al. 2012), and brain (Abubakar et al. 2017), either alone or in combination with other agents. Collectively, between their limited bioavailability,

increased anti-tumor activity, and weaker drug interference activity observed *in vitro*, the tocotrienols would not be preferable for toxicity management application against mTORC1 selective inhibitors.

In our *in vitro* models, the α-Toc/RM6 drug interference occurs considerably at α-Toc doses of 5μM+ to 1nM of RM6. Cancer patients are among the many individuals who take vitamin E supplements, either alone or as part of a multivitamin regiment. Hence, at the excessive doses of vitamin E provided by these supplements, which will naturally reflect a higher concentration in serum and tissue, it's conceivable that the higher intake amount of vitamin E may negatively impact the clinical efficacy of these inhibitors. However, this also leads to the possibility of leveraging this drug interference to mitigate toxicity. Indeed, investigators have long since explored vitamin E and other antioxidants as a means to attenuate toxicity induced by chemo- and radio-therapeutic agents, although the clinical data has been variable (Donnelly et al. 2022). For example, in children with AML, vitamin E reduced chemo- and radio-therapy toxicity, indicated by a decreased occurrence of hepatitis and hematological complications (Al-Tonbary et al. 2009). Vitamin E was also demonstrated to attenuate cisplatin-induced neurotoxicity without compromising its antineoplastic efficacy (Pace et al. 2003), while no effect on doxorubicin-induced cardiotoxicity has been reported (Whittaker and Al-Ismail 1984).

In general, most mTOR inhibitors are well tolerated, but there are some common adverse effects including fatigue, rash, oral and gut mucositis, and metabolic complications such as increased risk of hyperglycemia, hypertriglyceridemia, and hypercholesterolemia (Hua et al. 2019). Oral mucositis in particular is a frequent complication, and a significant cause of dose reduction in the clinic. Vitamin E can potentially attenuate some of these

toxicities. While systemic administration may positively impact tumor cells, local application can potentially mitigate side effects such as oral mucositis, for example with a vitamin E mouth wash, and rashes, for example with a vitamin E topical cream.

Considering the clinical implications of this finding, we ascertained the extent and modulability of this drug interference. We observed that RM6 activity is durable, lasting for at least seven days [**Figure 5.9A**]. Even upon washout after 4 hours of treatment, the earliest time at which RM6 leads to maximal suppression of p4EBP1, owing to its 'sticky' nature, RM6 continues to robustly suppress mTORC1 substrates for up to 72 hours, the latest time point assessed [**Figure 5.9B**]. These data suggest that toxicity can build up in patients even during a drug holiday. We also demonstrated that the addition of α-Toc to cells after 44 hours of RM6 treatment, followed by drug washout, leads to a rapid rebound of mTORC1 substrates, with return of both p4EBP1 and pS6K to control levels by 24 hours [**Figure 5.9C**]. Thus, α-Toc can rapidly reverse the inhibitory activity of RM6. In the clinical setting, this suggests that we can potentially combat or prevent toxicity more rapidly by providing α-Toc during a drug break.

While systemic administration of α-Toc may reduce toxicity, it will also diminish antitumor activity. Therefore, we also evaluated if RM6 could suppress mTORC1 substrates if added to cells treated with the α-Toc/RM6 drug combination after an extended period of treatment. We showed that, after 72 hours of α-Toc/RM6 treatment, whereby mTORC1 substrates remained at control levels, supplemental RM6 was able to considerably suppress phosphorylation of 4EBP1 and S6K in the continued presence of the α-Toc/RM6 combination. When the α-Toc/RM6 combo was washed out, followed by RM6 addition, we observed a more significant and durable suppression of 4EBP1 and S6K

phosphorylation [**Figure 5.9D**]. These data demonstrate that supplemental RM6 can reverse the interference activity of α-Toc, suggesting that we can regain anti-tumor activity after causing systemic rescue.

In our *in vitro* models, α-Toc considerably impedes the activity of RM6 for a protracted period of time. However, in the body where drugs and nutrients are systemically cleared, it's possible that modulating dosing and timing of α-Toc treatment can abate toxicity while permitting the drug to be effective within a defined window. This can also be exploited in the combinatorial setting with KRAS G12C-GTP inhibitors. Collectively our date demonstrates that the α-Toc/RM6 drug interference is durable, reversible, and modulatable, highlighting the potential application of α-Toc to manage toxicity of mTOR bi-steric inhibitors given alone or in combination with other compounds, such as KRAS G12C inhibitors. Vitamin E may thus serve as a double-edged sword, potentially tempering both the clinical efficacy and the toxicity of these agents in the monotherapy and combination settings.

Future Work

Future work related to this study will focus on uncovering the mechanism by which vitamin E mediates this drug interference. Collectively, vitamin E has been demonstrated to (1) modulate the activity of signal transduction enzymes by directly binding to them, or by influencing their redox regulation, (2) modulate signal transduction by preventing the oxidation of lipids, or by adjusting the structure and composition of membrane lipid domains, such as lipid rafts, and (3) compete with lipid mediators for common binding sites within lipid transport proteins, thereby influencing their traffic, enzymatic conversion,

and signaling function (Zingg 2015, Ungurianu et al. 2021). Regarding RM6 and the class of mTOR bi-steric inhibitors, α-Toc may directly bind to these agents or a component of the mTOR complex, disrupt the composition and/or structure of relevant cell and/or organelle membranes where these agents mediate their effects, compete for uptake and/or transport molecules, and/or stimulate the degradation of these agents.

We have investigated the potential of mTOR complex interference through mTOR immunoprecipitation (IP) experiments. However, we observed no appreciable differences in the levels of mTOR complex components between mTOR immunoprecipitants from cells treated with RM6 alone or with the α-Toc/RM6 combination. Our initial attempt to determine if vitamin E interfered with the uptake of RM6 into cells was thwarted by an inability to detect RM6 by mass spectrometry at doses below 1μM, with our samples treated at the normal 1nM dose. Hence, more refined experiments will be required to determine the exact mechanism(s) driving the α-Toc-RM6 drug interference.

Notably, Rapamycin and mTOR kinase inhibitors (MLN0128, AZD8055), primary constituents of these mTOR bi-steric inhibitors complexed by an inert chemical linker, were unaffected by α-Toc. This suggests that the interference occurs by nature of the intact complex. Recently, Shokat and colleagues reported that interferon-induced transmembrane proteins (IFITMs) modulate the cell permeability of RapaLink-1 and other linked chemical agents that fall outside the traditional framework of low-molecular weight, nonpolar, rigid structures. In this study, IFITMs were demonstrated to facilitate uptake of RapaLink-1, validated by a profound reduction in the ability of RapaLink-1 to suppress mTORC1/2 targets upon collective sgRNA mediated knockdown of the highly homologous gene family members IFITM1, IFITM2, and IFITM3 (Lou et al. 2022). Whether these proteins also

facilitate uptake of the mTORC1 selective inhibitors, and whether vitamin E mediates its interference through modulating this interaction, will be the subject of future studies. However, through washout experiments we have shown that α-Toc can interfere with RM6 even after it's been taken up by cells and is no longer actively present in cell culture media. The de-inhibition of mTORC1 substrates occurs with relatively rapid kinetics, with modest, but appreciable detection by 4 hours [**Figure 5.9C**]. Hence, even if α-Toc can interfere with drug uptake at the plasma membrane through modulating potential uptake proteins, it can also mediate its interference after the drug has already entered the cell.

The washout experiments have also demonstrated that α-Toc cannot mediate its interference when removed from cell culture media before RM6 addition. This even occurs in the context wherein the α-Toc/RM6 combination is washed out after a 72-hour treatment period before RM6 re-addition, contrary to results whereby α-Toc can still diminish the activity of RM6 when RM6 is re-added to cells treated with the α-Toc/RM6 combination after this 72-hour period. These results may imply that α-Toc predominantly localizes to the plasma membrane to affect RM6 activity, and likely persists in a position whereby the mechanical disturbance and/or PBS buffer that constitutes cell washing can provoke its removal to a full or partial extent such that it cannot impede RM6 activity.

Vitamin E shows a propensity to associate with lipid rafts, and it can potentially modulate the local concentration of messenger lipids, their spatial clustering in membrane microdomains, or their transbilayer asymmetry, thus changing the ability of certain enzymes to interact with these membrane structures and, by extension, perform their functional roles (Bradford et al. 2003, Zingg 2015). This hypothesis would account for why an interference is not observed when α-Toc is removed by washout, and why its

interference activity is still retained, even after a protracted period of time (albeit in a diminished capacity), when cells are not subject to washout. This model of interference can also account for the ability of α-Toc to mediate its interference when added to cells after RM6 addition, whether RM6 remains in culture media or is removed by washout, as the added α-Toc may disrupt internal membrane bilayers where RM6 is already engage with its mTORC1 target, leading to disruption of RM6 engagement and subsequent de-inhibition of mTORC1 substrates.

Additionally, we will ascertain the feasibility of applying this drug interference clinically in the setting of toxicity management through a series of *in vivo* experiments. First, we must establish that the interference occurs in the preclinical mouse setting, as results from our initial experiment were inconclusive. We plan to repeat our pilot *in vivo* study utilizing either a breast cancer CDX model, where the effect of mTORC1 selective inhibitors has more published reports at this time (Lee et al. 2021, Burnett et al. 2023), or an endometrial cancer model, where we've already determined sensitivity and signaling dynamics across several doses. One obvious limitation to establishing the potential clinical application of this drug interference is conducting these experiments in the murine setting. While this can provide us with some measure as to the feasibility and timing of toxicity management, whether this drug interference and proposed toxicity management application will translate to humans in the clinical setting will require those assessments to take place in humans.

Bibliography

Abankwa, D., A. A. Gorfe, K. Inder and J. F. Hancock (2010). "Ras membrane orientation and nanodomain localization generate isoform diversity." Proc Natl Acad Sci U S A **107**(3): 1130-1135.

Abraham, A. G. and E. O'Neill (2014). "PI3K/Akt-mediated regulation of p53 in cancer." Biochem Soc Trans **42**(4): 798-803.

Abubakar, I. B., K. H. Lim, T. S. Kam and H. S. Loh (2017). "Enhancement of apoptotic activities on brain cancer cells via the combination of γ-tocotrienol and jerantinine A." Phytomedicine **30**: 74-84.

Adachi, Y., R. Kimura, K. Hirade and H. Ebi (2021). "Escaping KRAS: Gaining Autonomy and Resistance to KRAS Inhibition in KRAS Mutant Cancers." Cancers (Basel) **13**(20).

Ahmadian, M. R., P. Stege, K. Scheffzek and A. Wittinghofer (1997). "Confirmation of the arginine-finger hypothesis for the GAP-stimulated GTP-hydrolysis reaction of Ras." Nat Struct Biol **4**(9): 686-689.

Al-Tonbary, Y., M. Al-Haggar, R. El-Ashry, S. El-Dakroory, H. Azzam and A. Fouda (2009). "Vitamin e and N-acetylcysteine as antioxidant adjuvant therapy in children with acute lymphoblastic leukemia." Adv Hematol **2009**: 689639.

Algeciras-Schimnich, A., L. Shen, B. C. Barnhart, A. E. Murmann, J. K. Burkhardt and M. E. Peter (2002). "Molecular ordering of the initial signaling events of CD95." Mol Cell Biol **22**(1): 207-220.

Ali, E. S., K. Mitra, S. Akter, S. Ramproshad, B. Mondal, I. N. Khan, M. T. Islam, J. Sharifi-Rad, D. Calina and W. C. Cho (2022). "Recent advances and limitations of mTOR inhibitors in the treatment of cancer." Cancer Cell Int **22**(1): 284.

Allan, L. A., Clarke, P. R. (2009). "Apoptosis and autophagy: Regulation of caspase-9 by phosphorylation." Febs j **276**(21): 6063-6073.

Anderson, G. R., S. E. Wardell, M. Cakir, L. Crawford, J. C. Leeds, D. P. Nussbaum, P. S. Shankar, R. S. Soderquist, E. M. Stein, J. P. Tingley, P. S. Winter, E. K. Zieser-Misenheimer, H. M. Alley, A. Yllanes, V. Haney, K. L. Blackwell, S. J. McCall, D. P. McDonnell and K. C. Wood (2016). "PIK3CA mutations enable targeting of a breast tumor dependency through mTOR-mediated MCL-1 translation." Sci Transl Med **8**(369): 369ra175.

André, F., E. Ciruelos, G. Rubovszky, M. Campone, S. Loibl, H. S. Rugo, H. Iwata, P. Conte, I. A. Mayer, B. Kaufman, T. Yamashita, Y. S. Lu, K. Inoue, M. Takahashi, Z. Pápai, A. S. Longin, D. Mills, C. Wilke, S. Hirawat and D. Juric (2019). "Alpelisib for PIK3CA-Mutated, Hormone Receptor-Positive Advanced Breast Cancer." N Engl J Med **380**(20): 1929-1940.

Antonucci, L. A., J. V. Egger and N. A. Krucher (2014). "Phosphorylation of the Retinoblastoma protein (Rb) on serine-807 is required for association with Bax." Cell Cycle **13**(22): 3611-3617.

Anwar, M. R., A. K. M. N. Hossian, G. Matthaiolampakis and P. W. Sylvester (2021). "Abstract 2573: The anticancer effects of the vitamin E isoform, γ-tocotrienol, and vitamin D3 act synergistically to inhibit MDA-MB-231 triple negative breast cancer (TNBC) cell proliferation and viability in vitro." Cancer Research **81**(13_Supplement): 2573-2573.

Ashkenazi, A., W. J. Fairbrother, J. D. Leverson and A. J. Souers (2017). "From basic apoptosis discoveries to advanced selective BCL-2 family inhibitors." Nat Rev Drug Discov **16**(4): 273-284.

Astle, M. V., K. M. Hannan, P. Y. Ng, R. S. Lee, A. J. George, A. K. Hsu, Y. Haupt, R. D. Hannan and R. B. Pearson (2012). "AKT induces senescence in human cells via mTORC1 and p53 in the absence of DNA damage: implications for targeting mTOR during malignancy." Oncogene **31**(15): 1949-1962.

Austin, C. D., D. A. Lawrence, A. A. Peden, E. E. Varfolomeev, K. Totpal, A. M. De Mazière, J. Klumperman, D. Arnott, V. Pham, R. H. Scheller and A. Ashkenazi (2006). "Death-receptor activation halts clathrin-dependent endocytosis." Proc Natl Acad Sci U S A **103**(27): 10283-10288.

Averous, J., B. D. Fonseca and C. G. Proud (2008). "Regulation of cyclin D1 expression by mTORC1 signaling requires eukaryotic initiation factor 4E-binding protein 1." Oncogene **27**(8): 1106-1113.

Azenha, D., M. C. Lopes and T. C. Martins (2019). "Claspin: From replication stress and DNA damage responses to cancer therapy." Adv Protein Chem Struct Biol **115**: 203-246.

Babasaki, T., K. Sentani, Y. Sekino, G. Kobayashi, Q. Thang Pham, N. Katsuya, S. Akabane, D. Taniyama, T. Hayashi, M. Shiota, N. Oue, J. Teishima, A. Matsubara and W. Yasui (2021). "Overexpression of claspin promotes docetaxel resistance and is associated with prostate-specific antigen recurrence in prostate cancer." Cancer Med **10**(16): 5574-5588.

Bachawal, S. V., V. B. Wali and P. W. Sylvester (2010). "Enhanced antiproliferative and apoptotic response to combined treatment of gamma-tocotrienol with erlotinib or gefitinib in mammary tumor cells." BMC Cancer **10**: 84.

Baines, A. T., D. Xu and C. J. Der (2011). "Inhibition of Ras for cancer treatment: the search continues." Future Med Chem **3**(14): 1787-1808.

Banerjee, P., A. Basu, D. Datta, M. Gasser, A. M. Waaga-Gasser and S. Pal (2011). "The heme oxygenase-1 protein is overexpressed in human renal cancer cells following activation of the Ras-Raf-ERK pathway and mediates anti-apoptotic signal." J Biol Chem **286**(38): 33580-33590.

Bansal, R., Rakshit, S, Han, W, Kumar, K S (2022). "Modulation of Apoptosis Pathways in the Biology and Treatment of Multiple Myeloma." touchREVIEWS in Oncology & Haematology **17**(1): 48-54.

Bar-Peled, L., L. Chantranupong, A. D. Cherniack, W. W. Chen, K. A. Ottina, B. C. Grabiner, E. D. Spear, S. L. Carter, M. Meyerson and D. M. Sabatini (2013). "A Tumor suppressor complex with GAP activity for the Rag GTPases that signal amino acid sufficiency to mTORC1." Science **340**(6136): 1100-1106.

Battaglioni, S., D. Benjamin, M. Wälchli, T. Maier and M. N. Hall (2022). "mTOR substrate phosphorylation in growth control." Cell **185**(11): 1814-1836.

Ben-Sahra, I., J. J. Howell, J. M. Asara and B. D. Manning (2013). "Stimulation of de novo pyrimidine synthesis by growth signaling through mTOR and S6K1." Science **339**(6125): 1323-1328.

Ben-Sahra, I., G. Hoxhaj, S. J. H. Ricoult, J. M. Asara and B. D. Manning (2016). "mTORC1 induces purine synthesis through control of the mitochondrial tetrahydrofolate cycle." Science **351**(6274): 728-733.

Bendell, J. C., J. Rodon, H. A. Burris, M. de Jonge, J. Verweij, D. Birle, D. Demanse, S. S. De Buck, Q. C. Ru, M. Peters, M. Goldbrunner and J. Baselga (2012). "Phase I, dose-escalation study of BKM120, an oral pan-Class I PI3K inhibitor, in patients with advanced solid tumors." J Clin Oncol **30**(3): 282-290.

Bersuker, K., J. M. Hendricks, Z. Li, L. Magtanong, B. Ford, P. H. Tang, M. A. Roberts, B. Tong, T. J. Maimone, R. Zoncu, M. C. Bassik, D. K. Nomura, S. J. Dixon and J. A. Olzmann (2019). "The CoQ oxidoreductase FSP1 acts parallel to GPX4 to inhibit ferroptosis." Nature **575**(7784): 688-692.

Bertolio, R., F. Napoletano, M. Mano, S. Maurer-Stroh, M. Fantuz, A. Zannini, S. Bicciato, G. Sorrentino and G. Del Sal (2019). "Sterol regulatory element binding protein 1 couples mechanical cues and lipid metabolism." Nat Commun **10**(1): 1326.

Bianco, J. N., V. Bergoglio, Y. L. Lin, M. J. Pillaire, A. L. Schmitz, J. Gilhodes, A. Lusque, J. Mazières, M. Lacroix-Triki, T. I. Roumeliotis, J. Choudhary, J. Moreaux, J. S. Hoffmann, H. Tourrière and P. Pasero (2019). "Overexpression of Claspin and Timeless protects cancer cells from replication stress in a checkpoint-independent manner." Nat Commun **10**(1): 910.

Boriack-Sjodin, P. A., S. M. Margarit, D. Bar-Sagi and J. Kuriyan (1998). "The structural basis of the activation of Ras by Sos." Nature **394**(6691): 337-343.

Bos, J. L., H. Rehmann and A. Wittinghofer (2007). "GEFs and GAPs: critical elements in the control of small G proteins." Cell **129**(5): 865-877.

Bouillet, P., S. Cory, L. C. Zhang, A. Strasser and J. M. Adams (2001). "Degenerative disorders caused by Bcl-2 deficiency prevented by loss of its BH3-only antagonist Bim." Dev Cell **1**(5): 645-653.

Boulton, T. G., S. H. Nye, D. J. Robbins, N. Y. Ip, E. Radziejewska, S. D. Morgenbesser, R. A. DePinho, N. Panayotatos, M. H. Cobb and G. D. Yancopoulos (1991). "ERKs: a family of protein-serine/threonine kinases that are activated and tyrosine phosphorylated in response to insulin and NGF." Cell **65**(4): 663-675.

Boulton, T. G., G. D. Yancopoulos, J. S. Gregory, C. Slaughter, C. Moomaw, J. Hsu and M. H. Cobb (1990). "An insulin-stimulated protein kinase similar to yeast kinases involved in cell cycle control." Science **249**(4964): 64-67.

Bradford, A., J. Atkinson, N. Fuller and R. P. Rand (2003). "The effect of vitamin E on the structure of membrane lipid assemblies." J Lipid Res **44**(10): 1940-1945.

Briere, D. M., S. Li, A. Calinisan, N. Sudhakar, R. Aranda, L. Hargis, D. H. Peng, J. Deng, L. D. Engstrom, J. Hallin, S. Gatto, J. Fernandez-Banet, A. Pavlicek, K. K. Wong, J. G. Christensen and P. Olson (2021). "The KRAS(G12C) Inhibitor MRTX849 Reconditions the Tumor Immune Microenvironment and Sensitizes Tumors to Checkpoint Inhibitor Therapy." Mol Cancer Ther **20**(6): 975-985.

Brown, L. and S. Benchimol (2006). "The involvement of MAPK signaling pathways in determining the cellular response to p53 activation: cell cycle arrest or apoptosis." J Biol Chem **281**(7): 3832-3840.

Brunet, A., D. S. Weiss, T. J. Metzler, S. R. Best, T. C. Neylan, C. Rogers, J. Fagan and C. R. Marmar (2001). "The Peritraumatic Distress Inventory: a proposed measure of PTSD criterion A2." Am J Psychiatry **158**(9): 1480-1485.

Burnett, G. L., Y. C. Yang, J. B. Aggen, J. Pitzen, M. K. Gliedt, C. M. Semko, A. Marquez, J. W. Evans, G. Wang, W. S. Won, A. C. A. Tomlinson, G. Kiss, C. Tzitzilonis, A. P. Thottumkara, J. Cregg, K. T. Mellem, J. S. Choi, J. C. Lee, Y. Zhao, B. J. Lee, J. G. Meyerowitz, J. E. Knox, J. Jiang, Z. Wang, D. Wildes, Z. Wang, M. Singh, J. A. M. Smith and A. L. Gill (2023). "Discovery of RMC-5552, a Selective Bi-Steric Inhibitor of mTORC1, for the Treatment of mTORC1-Activated Tumors." J Med Chem **66**(1): 149-169.

Burton, G. W. and K. U. Ingold (1986). "Vitamin E: application of the principles of physical organic chemistry to the exploration of its structure and function." Accounts of Chemical Research **19**(7): 194-201.

Busserolles, J., J. Megías, M. C. Terencio and M. J. Alcaraz (2006). "Heme oxygenase-1 inhibits apoptosis in Caco-2 cells via activation of Akt pathway." Int J Biochem Cell Biol **38**(9): 1510-1517.

Byers, T. and G. Perry (1992). "Dietary carotenes, vitamin C, and vitamin E as protective antioxidants in human cancers." Annu Rev Nutr **12**: 139-159.

Cagnol, S. and J. C. Chambard (2010). "ERK and cell death: mechanisms of ERK-induced cell death--apoptosis, autophagy and senescence." Febs j **277**(1): 2-21.

Cagnol, S., E. Van Obberghen-Schilling and J. C. Chambard (2006). "Prolonged activation of ERK1,2 induces FADD-independent caspase 8 activation and cell death." Apoptosis **11**(3): 337-346.

Cameron, I. L., J. Munoz, C. J. Barnes and W. E. Hardman (2003). "High dietary level of synthetic vitamin E on lipid peroxidation, membrane fatty acid composition and cytotoxicity in breast cancer xenograft and in mouse host tissue." Cancer Cell Int **3**(1): 3.

Cancer Genome Atlas Research Network (2014). "Comprehensive molecular profiling of lung adenocarcinoma." Nature **511**(7511): 543-550.

Canon, J., K. Rex, A. Y. Saiki, C. Mohr, K. Cooke, D. Bagal, K. Gaida, T. Holt, C. G. Knutson, N. Koppada, B. A. Lanman, J. Werner, A. S. Rapaport, T. San Miguel, R. Ortiz, T. Osgood, J. R. Sun, X. Zhu, J. D. McCarter, L. P. Volak, B. E. Houk, M. G. Fakih, B. H. O'Neil, T. J. Price, G. S. Falchook, J. Desai, J. Kuo, R. Govindan, D. S. Hong, W. Ouyang, H. Henary, T. Arvedson, V. J. Cee and J. R. Lipford (2019). "The clinical KRAS(G12C) inhibitor AMG 510 drives anti-tumour immunity." Nature **575**(7781): 217-223.

Cantley, L. C. (2002). "The phosphoinositide 3-kinase pathway." Science **296**(5573): 1655-1657.

Caron, A., D. Richard and M. Laplante (2015). "The Roles of mTOR Complexes in Lipid Metabolism." Annu Rev Nutr **35**: 321-348.

Castel, P., E. Toska, J. A. Engelman and M. Scaltriti (2021). "The present and future of PI3K inhibitors for cancer therapy." Nat Cancer **2**(6): 587-597.

Chandarlapaty, S., A. Sawai, M. Scaltriti, V. Rodrik-Outmezguine, O. Grbovic-Huezo, V. Serra, P. K. Majumder, J. Baselga and N. Rosen (2011). "AKT inhibition relieves feedback suppression of receptor tyrosine kinase expression and activity." Cancer Cell **19**(1): 58-71.

Chang, L. C., S. K. Chiang, S. E. Chen, Y. L. Yu, R. H. Chou and W. C. Chang (2018). "Heme oxygenase-1 mediates BAY 11-7085 induced ferroptosis." Cancer Lett **416**: 124-137.

Chang, P. N., W. N. Yap, D. T. Lee, M. T. Ling, Y. C. Wong and Y. L. Yap (2009). "Evidence of gamma-tocotrienol as an apoptosis-inducing, invasion-suppressing, and chemotherapy drug-sensitizing agent in human melanoma cells." Nutr Cancer **61**(3): 357-366.

Chantranupong, L., S. M. Scaria, R. A. Saxton, M. P. Gygi, K. Shen, G. A. Wyant, T. Wang, J. W. Harper, S. P. Gygi and D. M. Sabatini (2016). "The CASTOR Proteins Are Arginine Sensors for the mTORC1 Pathway." Cell **165**(1): 153-164.

Chen, G. G., Z. M. Liu, A. C. Vlantis, G. M. Tse, B. C. Leung and C. A. van Hasselt (2004). "Heme oxygenase-1 protects against apoptosis induced by tumor necrosis factor-alpha and cycloheximide in papillary thyroid carcinoma cells." J Cell Biochem **92**(6): 1246-1256.

Coelho, M. A., S. de Carné Trécesson, S. Rana, D. Zecchin, C. Moore, M. Molina-Arcas, P. East, B. Spencer-Dene, E. Nye, K. Barnouin, A. P. Snijders, W. S. Lai, P. J. Blackshear and J. Downward (2017). "Oncogenic RAS Signaling Promotes Tumor Immunoresistance by Stabilizing PD-L1 mRNA." Immunity **47**(6): 1083-1099.e1086.

Coltorti, M., F. De Ritis and G. Giusti (1956). "[Enzymatic mechanisms of transsulfuration in biology and clinical practice]." G Clin Med **37**(3): 285-323.

Conradt, B. (2009). "Genetic control of programmed cell death during animal development." Annu Rev Genet **43**: 493-523.

Cook, M. G. and P. McNamara (1980). "Effect of dietary vitamin E on dimethylhydrazine-induced colonic tumors in mice." Cancer Res **40**(4): 1329-1331.

Corcoran, R. B., S. M. Rothenberg, A. N. Hata, A. C. Faber, A. Piris, R. M. Nazarian, R. D. Brown, J. T. Godfrey, D. Winokur, J. Walsh, M. Mino-Kenudson, S. Maheswaran, J. Settleman, J. A. Wargo, K. T. Flaherty, D. A. Haber and J. A. Engelman (2013). "TORC1 suppression predicts responsiveness to RAF and MEK inhibition in BRAF-mutant melanoma." Sci Transl Med **5**(196): 196ra198.

D'Mello, S. (2020). Chapter 11 - Programmed Cell Death Goodman's Medical Cell Biology. S. Goodman. United States, Academic Press 2020**:** 315-336.

Danielsen, S. A., P. W. Eide, A. Nesbakken, T. Guren, E. Leithe and R. A. Lothe (2015). "Portrait of the PI3K/AKT pathway in colorectal cancer." Biochim Biophys Acta **1855**(1): 104-121.

Datta, S. R., H. Dudek, X. Tao, S. Masters, H. Fu, Y. Gotoh and M. E. Greenberg (1997). "Akt phosphorylation of BAD couples survival signals to the cell-intrinsic death machinery." Cell **91**(2): 231-241.

Datta, S. R., A. M. Ranger, M. Z. Lin, J. F. Sturgill, Y. C. Ma, C. W. Cowan, P. Dikkes, S. J. Korsmeyer and M. E. Greenberg (2002). "Survival factor-mediated BAD phosphorylation raises the mitochondrial threshold for apoptosis." Dev Cell **3**(5): 631-643.

Dehan, E., F. Bassermann, D. Guardavaccaro, G. Vasiliver-Shamis, M. Cohen, K. N. Lowes, M. Dustin, D. C. Huang, J. Taunton and M. Pagano (2009). "betaTrCP- and Rsk1/2-mediated degradation of BimEL inhibits apoptosis." Mol Cell **33**(1): 109-116.

del Peso, L., M. González-García, C. Page, R. Herrera and G. Nuñez (1997). "Interleukin-3-induced phosphorylation of BAD through the protein kinase Akt." Science **278**(5338): 687-689.

DeNicola, G. M., F. A. Karreth, T. J. Humpton, A. Gopinathan, C. Wei, K. Frese, D. Mangal, K. H. Yu, C. J. Yeo, E. S. Calhoun, F. Scrimieri, J. M. Winter, R. H. Hruban, C. Iacobuzio-Donahue, S. E. Kern, I. A. Blair and D. A. Tuveson (2011). "Oncogene-induced Nrf2 transcription promotes ROS detoxification and tumorigenesis." Nature **475**(7354): 106-109.

Dibble, C. C. and L. C. Cantley (2015). "Regulation of mTORC1 by PI3K signaling." Trends Cell Biol **25**(9): 545-555.

Dijkers, P. F., R. H. Medema, J. W. Lammers, L. Koenderman and P. J. Coffer (2000). "Expression of the pro-apoptotic Bcl-2 family member Bim is regulated by the forkhead transcription factor FKHR-L1." Curr Biol **10**(19): 1201-1204.

Ding, Y., J. Fan, Z. Fan and K. Zhang (2021). "γ-Tocotrienol reverses multidrug resistance of breast cancer cells through the regulation of the γ-Tocotrienol-NF-κB-P-gp axis." J Steroid Biochem Mol Biol **209**: 105835.

Dixon, S. J., K. M. Lemberg, M. R. Lamprecht, R. Skouta, E. M. Zaitsev, C. E. Gleason, D. N. Patel, A. J. Bauer, A. M. Cantley, W. S. Yang, B. Morrison, 3rd and B. R. Stockwell (2012). "Ferroptosis: an iron-dependent form of nonapoptotic cell death." Cell **149**(5): 1060-1072.

Dixon, S. J., D. N. Patel, M. Welsch, R. Skouta, E. D. Lee, M. Hayano, A. G. Thomas, C. E. Gleason, N. P. Tatonetti, B. S. Slusher and B. R. Stockwell (2014). "Pharmacological inhibition of cystine-glutamate exchange induces endoplasmic reticulum stress and ferroptosis." Elife **3**: e02523.

Doll, S., F. P. Freitas, R. Shah, M. Aldrovandi, M. C. da Silva, I. Ingold, A. Goya Grocin, T. N. Xavier da Silva, E. Panzilius, C. H. Scheel, A. Mourão, K. Buday, M. Sato, J. Wanninger, T. Vignane, V. Mohana, M. Rehberg, A. Flatley, A. Schepers, A. Kurz, D. White, M. Sauer, M. Sattler, E. W. Tate, W. Schmitz, A. Schulze, V. O'Donnell, B. Proneth, G. M. Popowicz, D. A. Pratt, J. P. F. Angeli and M. Conrad (2019). "FSP1 is a glutathione-independent ferroptosis suppressor." Nature **575**(7784): 693-698.

Dolma, S., S. L. Lessnick, W. C. Hahn and B. R. Stockwell (2003). "Identification of genotype-selective antitumor agents using synthetic lethal chemical screening in engineered human tumor cells." Cancer Cell **3**(3): 285-296.

Donnelly, J., A. Appathurai, H. L. Yeoh, K. Driscoll and W. Faisal (2022). "Vitamin E in Cancer Treatment: A Review of Clinical Applications in Randomized Control Trials." Nutrients **14**(20).

Drosopoulos, K. G., M. L. Roberts, L. Cermak, T. Sasazuki, S. Shirasawa, L. Andera and A. Pintzas (2005). "Transformation by oncogenic RAS sensitizes human colon cells to TRAIL-induced apoptosis by up-regulating death receptor 4 and death receptor 5 through a MEK-dependent pathway." J Biol Chem **280**(24): 22856-22867.

Drosten, M., E. Y. Sum, C. G. Lechuga, L. Simón-Carrasco, H. K. Jacob, R. García-Medina, S. Huang, R. L. Beijersbergen, R. Bernards and M. Barbacid (2014). "Loss of p53 induces cell proliferation via Ras-independent activation of the Raf/Mek/Erk signaling pathway." Proc Natl Acad Sci U S A **111**(42): 15155-15160.

drugs.com. (2023). "Vitamin E Drug Interactions." Retrieved January 12, 2023, from https://www.drugs.com/drug-interactions/vitamin-e-index.html.

Drullinsky, P. R. and S. A. Hurvitz (2020). "Mechanistic basis for PI3K inhibitor antitumor activity and adverse reactions in advanced breast cancer." Breast Cancer Res Treat **181**(2): 233-248.

Duckworth, B. C. and L. C. Cantley (1997). "Conditional inhibition of the mitogen-activated protein kinase cascade by wortmannin. Dependence on signal strength." J Biol Chem **272**(44): 27665-27670.

Duncan, K. R. and Y. J. Suzuki (2017). "Vitamin E Nicotinate." Antioxidants (Basel) **6**(1).

Dyachok, J., S. Earnest, E. N. Iturraran, M. H. Cobb and E. M. Ross (2016). "Amino Acids Regulate mTORC1 by an Obligate Two-step Mechanism." J Biol Chem **291**(43): 22414-22426.

Eagle, H. (1955). "Nutrition needs of mammalian cells in tissue culture." Science **122**(3168): 501-514.

Eagle, H., K. A. Piez and V. I. Oyama (1961). "The biosynthesis of cystine in human cell cultures." J Biol Chem **236**: 1425-1428.

Ekoff, M., T. Kaufmann, M. Engström, N. Motoyama, A. Villunger, J. I. Jönsson, A. Strasser and G. Nilsson (2007). "The BH3-only protein Puma plays an essential role in cytokine deprivation induced apoptosis of mast cells." Blood **110**(9): 3209-3217.

El Hage, A. and O. Dormond (2021). "Combining mTOR Inhibitors and T Cell-Based Immunotherapies in Cancer Treatment." Cancers (Basel) **13**(6).

Fairus, S., R. M. Nor, H. M. Cheng and K. Sundram (2006). "Postprandial metabolic fate of tocotrienol-rich vitamin E differs significantly from that of alpha-tocopherol." Am J Clin Nutr **84**(4): 835-842.

Fairus, S., R. M. Nor, H. M. Cheng and K. Sundram (2012). "Alpha-tocotrienol is the most abundant tocotrienol isomer circulated in plasma and lipoproteins after postprandial tocotrienol-rich vitamin E supplementation." Nutr J **11**: 5.

Fan, B. Y., Y. L. Pang, W. X. Li, C. X. Zhao, Y. Zhang, X. Wang, G. Z. Ning, X. H. Kong, C. Liu, X. Yao and S. Q. Feng (2021). "Liproxstatin-1 is an effective inhibitor of oligodendrocyte ferroptosis induced by inhibition of glutathione peroxidase 4." Neural Regen Res **16**(3): 561-566.

Fan et al., Z., He, J., Fu, T., Lv, L., Wang, J. (2019). "Silencing of HMOX1 Enhances Apoptosis Caused by Arsenic Trioxide in HCC." International Journal of Clinical and Experimental Medicine **12**(8): :9858-9870.

Fan, Q., O. Aksoy, R. A. Wong, S. Ilkhanizadeh, C. J. Novotny, W. C. Gustafson, A. Y. Truong, G. Cayanan, E. F. Simonds, D. Haas-Kogan, J. J. Phillips, T. Nicolaides, M. Okaniwa, K. M. Shokat and W. A. Weiss (2017). "A Kinase Inhibitor Targeted to mTORC1 Drives Regression in Glioblastoma." Cancer Cell **31**(3): 424-435.

Fang, X., S. Yu, A. Eder, M. Mao, R. C. Bast, Jr., D. Boyd and G. B. Mills (1999). "Regulation of BAD phosphorylation at serine 112 by the Ras-mitogen-activated protein kinase pathway." Oncogene **18**(48): 6635-6640.

Feig, C., V. Tchikov, S. Schütze and M. E. Peter (2007). "Palmitoylation of CD95 facilitates formation of SDS-stable receptor aggregates that initiate apoptosis signaling." Embo j **26**(1): 221-231.

Fell, J. B., J. P. Fischer, B. R. Baer, J. F. Blake, K. Bouhana, D. M. Briere, K. D. Brown, L. E. Burgess, A. C. Burns, M. R. Burkard, H. Chiang, M. J. Chicarelli, A. W. Cook, J. J. Gaudino, J. Hallin, L. Hanson, D. P. Hartley, E. J. Hicken, G. P. Hingorani, R. J. Hinklin, M. J. Mejia, P. Olson, J. N. Otten, S. P. Rhodes, M. E. Rodriguez, P. Savechenkov, D. J. Smith, N. Sudhakar, F. X. Sullivan, T. P. Tang, G. P. Vigers, L. Wollenberg, J. G. Christensen and M. A. Marx (2020). "Identification of the Clinical Development Candidate MRTX849, a Covalent KRAS(G12C) Inhibitor for the Treatment of Cancer." J Med Chem **63**(13): 6679-6693.

Fernández, Y., M. Verhaegen, T. P. Miller, J. L. Rush, P. Steiner, A. W. Opipari, Jr., S. W. Lowe and M. S. Soengas (2005). "Differential regulation of noxa in normal melanocytes and melanoma cells by proteasome inhibition: therapeutic implications." Cancer Res **65**(14): 6294-6304.

Ferris, C. D., S. R. Jaffrey, A. Sawa, M. Takahashi, S. D. Brady, R. K. Barrow, S. A. Tysoe, H. Wolosker, D. E. Barañano, S. Doré, K. D. Poss and S. H. Snyder (1999). "Haem oxygenase-1 prevents cell death by regulating cellular iron." Nat Cell Biol **1**(3): 152-157.

Friedmann Angeli, J. P., M. Schneider, B. Proneth, Y. Y. Tyurina, V. A. Tyurin, V. J. Hammond, N. Herbach, M. Aichler, A. Walch, E. Eggenhofer, D. Basavarajappa, O. Rådmark, S. Kobayashi, T. Seibt, H. Beck, F. Neff, I. Esposito, R. Wanke, H. Förster, O. Yefremova, M. Heinrichmeyer, G. W. Bornkamm, E. K. Geissler, S. B. Thomas, B. R. Stockwell, V. B. O'Donnell, V. E. Kagan, J. A. Schick and M. Conrad (2014). "Inactivation of the ferroptosis regulator Gpx4 triggers acute renal failure in mice." Nat Cell Biol **16**(12): 1180-1191.

Fruman, D. A., H. Chiu, B. D. Hopkins, S. Bagrodia, L. C. Cantley and R. T. Abraham (2017). "The PI3K Pathway in Human Disease." Cell **170**(4): 605-635.

Fu, W. and M. N. Hall (2020). "Regulation of mTORC2 Signaling." Genes (Basel) **11**(9).

Fuchs, Y. and H. Steller (2011). "Programmed cell death in animal development and disease." Cell **147**(4): 742-758.

Galluzzi, L., I. Vitale, S. A. Aaronson, J. M. Abrams, D. Adam, P. Agostinis, E. S. Alnemri, L. Altucci, I. Amelio, D. W. Andrews, M. Annicchiarico-Petruzzelli, A. V. Antonov, E. Arama, E. H. Baehrecke, N. A. Barlev, N. G. Bazan, F. Bernassola, M. J. M. Bertrand, K. Bianchi, M. V. Blagosklonny, K. Blomgren, C. Borner, P. Boya, C. Brenner, M. Campanella, E. Candi, D. Carmona-Gutierrez, F. Cecconi, F. K. Chan, N. S. Chandel, E. H. Cheng, J. E. Chipuk, J. A. Cidlowski, A. Ciechanover, G. M. Cohen, M. Conrad, J. R. Cubillos-Ruiz, P. E. Czabotar, V. D'Angiolella, T. M. Dawson, V. L. Dawson, V. De Laurenzi, R. De Maria, K. M. Debatin, R. J. DeBerardinis, M. Deshmukh, N. Di Daniele, F. Di Virgilio, V. M. Dixit, S. J. Dixon, C. S. Duckett, B. D. Dynlacht, W. S. El-Deiry, J. W. Elrod, G. M. Fimia, S. Fulda, A. J. García-Sáez, A. D. Garg, C. Garrido, E. Gavathiotis, P. Golstein, E. Gottlieb, D. R. Green, L. A. Greene, H. Gronemeyer, A. Gross, G. Hajnoczky, J. M. Hardwick, I. S. Harris, M. O. Hengartner, C. Hetz, H. Ichijo, M. Jäättelä, B. Joseph, P. J. Jost, P. P. Juin, W. J. Kaiser, M. Karin, T. Kaufmann, O. Kepp, A. Kimchi, R. N. Kitsis, D. J. Klionsky, R. A. Knight, S. Kumar, S. W. Lee, J. J. Lemasters, B. Levine, A. Linkermann, S. A. Lipton, R. A. Lockshin, C. López-Otín, S. W. Lowe, T. Luedde, E. Lugli, M. MacFarlane, F. Madeo, M. Malewicz, W. Malorni, G. Manic, J. C. Marine, S. J. Martin, J. C. Martinou, J. P. Medema, P. Mehlen, P. Meier, S. Melino, E. A. Miao, J. D. Molkentin, U. M. Moll, C. Muñoz-Pinedo, S. Nagata, G. Nuñez, A. Oberst, M. Oren, M. Overholtzer, M. Pagano, T. Panaretakis, M. Pasparakis, J. M. Penninger, D. M. Pereira, S. Pervaiz, M. E. Peter, M. Piacentini, P. Pinton, J. H. M. Prehn, H. Puthalakath, G. A. Rabinovich, M. Rehm, R. Rizzuto, C. M. P. Rodrigues, D. C. Rubinsztein, T. Rudel, K. M. Ryan, E. Sayan, L. Scorrano, F. Shao, Y. Shi, J. Silke, H. U. Simon, A. Sistigu, B. R. Stockwell, A. Strasser, G. Szabadkai, S. W. G. Tait, D. Tang, N. Tavernarakis, A. Thorburn, Y. Tsujimoto, B. Turk, T. Vanden Berghe, P. Vandenabeele, M. G. Vander Heiden, A. Villunger, H. W. Virgin, K. H. Vousden, D. Vucic, E. F. Wagner, H. Walczak, D. Wallach, Y. Wang, J. A. Wells, W. Wood, J. Yuan, Z. Zakeri, B. Zhivotovsky, L. Zitvogel, G. Melino and G. Kroemer (2018). "Molecular mechanisms of cell death: recommendations of the Nomenclature Committee on Cell Death 2018." Cell Death Differ **25**(3): 486-541.

Gaschler, M. M. and B. R. Stockwell (2017). "Lipid peroxidation in cell death." Biochem Biophys Res Commun **482**(3): 419-425.

Gilley, J., P. J. Coffer and J. Ham (2003). "FOXO transcription factors directly activate bim gene expression and promote apoptosis in sympathetic neurons." J Cell Biol **162**(4): 613-622.

Gimple, R. C. and X. Wang (2019). "RAS: Striking at the Core of the Oncogenic Circuitry." Front Oncol **9**: 965.

Glauert, H. P., M. M. Beaty, T. D. Clark, W. S. Greenwell, V. Tatum, L. C. Chen, T. Borges, T. L. Clark, S. R. Srinivasan and C. K. Chow (1990). "Effect of dietary vitamin E on the development of altered hepatic foci and hepatic tumors induced by the peroxisome proliferator ciprofibrate." J Cancer Res Clin Oncol **116**(4): 351-356.

Grazier, J. J. and P. W. Sylvester (2021). "Abstract 2889: γ-Tocotrienol inhibition of metastatic phenotypic behavior is associated with a decrease in galectin-3 expression and distribution in the highly malignant mouse +SA & TS/A mammary tumor cells." Cancer Research **81**(13_Supplement): 2889-2889.

Green, D. R. and F. Llambi (2015). "Cell Death Signaling." Cold Spring Harb Perspect Biol **7**(12).

Guan, K. L., C. Figueroa, T. R. Brtva, T. Zhu, J. Taylor, T. D. Barber and A. B. Vojtek (2000). "Negative regulation of the serine/threonine kinase B-Raf by Akt." J Biol Chem **275**(35): 27354-27359.

Haas, B., V. Klinger, C. Keksel, V. Bonigut, D. Kiefer, J. Caspers, J. Walther, M. Wos-Maganga, S. Weickhardt, G. Röhn, M. Timmer, R. Frötschl and N. Eckstein (2018). "Inhibition of the PI3K but not the MEK/ERK pathway sensitizes human glioma cells to alkylating drugs." Cancer Cell Int **18**: 69.

Hahn, T., L. Szabo, M. Gold, L. Ramanathapuram, L. H. Hurley and E. T. Akporiaye (2006). "Dietary administration of the proapoptotic vitamin E analogue alpha-tocopheryloxyacetic acid inhibits metastatic murine breast cancer." Cancer Res **66**(19): 9374-9378.

Haigis, K. M., K. R. Kendall, Y. Wang, A. Cheung, M. C. Haigis, J. N. Glickman, M. Niwa-Kawakita, A. Sweet-Cordero, J. Sebolt-Leopold, K. M. Shannon, J. Settleman, M. Giovannini and T. Jacks (2008). "Differential effects of oncogenic K-Ras and N-Ras on proliferation, differentiation and tumor progression in the colon." Nat Genet **40**(5): 600-608.

Hall, B. E., D. Bar-Sagi and N. Nassar (2002). "The structural basis for the transition from Ras-GTP to Ras-GDP." Proc Natl Acad Sci U S A **99**(19): 12138-12142.

Hallin, J., L. D. Engstrom, L. Hargis, A. Calinisan, R. Aranda, D. M. Briere, N. Sudhakar, V. Bowcut, B. R. Baer, J. A. Ballard, M. R. Burkard, J. B. Fell, J. P. Fischer, G. P. Vigers, Y. Xue, S. Gatto, J. Fernandez-Banet, A. Pavlicek, K. Velastagui, R. C. Chao, J. Barton, M. Pierobon, E. Baldelli, E. F. Patricoin, 3rd, D. P. Cassidy, M. A. Marx, Rybkin, II, M. L. Johnson, S. I. Ou, P. Lito, K. P. Papadopoulos, P. A. Jänne, P. Olson and J. G. Christensen (2020). "The KRAS(G12C) Inhibitor MRTX849 Provides Insight toward Therapeutic Susceptibility of KRAS-Mutant Cancers in Mouse Models and Patients." Cancer Discov **10**(1): 54-71.

Hammond, D. E., C. J. Mageean, E. V. Rusilowicz, J. A. Wickenden, M. J. Clague and I. A. Prior (2015). "Differential reprogramming of isogenic colorectal cancer cells by distinct activating KRAS mutations." J Proteome Res **14**(3): 1535-1546.

Hanahan, D. and R. A. Weinberg (2011). "Hallmarks of cancer: the next generation." Cell **144**(5): 646-674.

Hanker, A. B., V. Kaklamani and C. L. Arteaga (2019). "Challenges for the Clinical Development of PI3K Inhibitors: Strategies to Improve Their Impact in Solid Tumors." Cancer Discov **9**(4): 482-491.

Har, C. H. and C. K. Keong (2005). "Effects of tocotrienols on cell viability and apoptosis in normal murine liver cells (BNL CL.2) and liver cancer cells (BNL 1ME A.7R.1), in vitro." Asia Pac J Clin Nutr **14**(4): 374-380.

Hara, K., Y. Maruki, X. Long, K. Yoshino, N. Oshiro, S. Hidayat, C. Tokunaga, J. Avruch and K. Yonezawa (2002). "Raptor, a binding partner of target of rapamycin (TOR), mediates TOR action." Cell **110**(2): 177-189.

Hara, K., K. Yonezawa, Q. P. Weng, M. T. Kozlowski, C. Belham and J. Avruch (1998). "Amino acid sufficiency and mTOR regulate p70 S6 kinase and eIF-4E BP1 through a common effector mechanism." J Biol Chem **273**(23): 14484-14494.

Harada, H., J. S. Andersen, M. Mann, N. Terada and S. J. Korsmeyer (2001). "p70S6 kinase signals cell survival as well as growth, inactivating the pro-apoptotic molecule BAD." Proc Natl Acad Sci U S A **98**(17): 9666-9670.

Hatzivassiliou, G., K. Song, I. Yen, B. J. Brandhuber, D. J. Anderson, R. Alvarado, M. J. Ludlam, D. Stokoe, S. L. Gloor, G. Vigers, T. Morales, I. Aliagas, B. Liu, S. Sideris, K. P. Hoeflich, B. S. Jaiswal, S. Seshagiri, H. Koeppen, M. Belvin, L. S. Friedman and S. Malek (2010). "RAF inhibitors prime wild-type RAF to activate the MAPK pathway and enhance growth." Nature **464**(7287): 431-435.

Hobbs, G. A., C. J. Der and K. L. Rossman (2016). "RAS isoforms and mutations in cancer at a glance." J Cell Sci **129**(7): 1287-1292.

Hofmann, M. H., M. Gmachl, J. Ramharter, F. Savarese, D. Gerlach, J. R. Marszalek, M. P. Sanderson, D. Kessler, F. Trapani, H. Arnhof, K. Rumpel, D. A. Botesteanu, P. Ettmayer, T. Gerstberger, C. Kofink, T. Wunberg, A. Zoephel, S. C. Fu, J. L. Teh, J. Böttcher, N. Pototschnig, F. Schachinger, K. Schipany, S. Lieb, C. P. Vellano, J. C. O'Connell, R. L. Mendes, J. Moll, M. Petronczki, T. P. Heffernan, M. Pearson, D. B. McConnell and N. Kraut (2021). "BI-3406, a Potent and Selective SOS1-KRAS Interaction Inhibitor, Is Effective in KRAS-Driven Cancers through Combined MEK Inhibition." Cancer Discov **11**(1): 142-157.

Holz, M. K., B. A. Ballif, S. P. Gygi and J. Blenis (2005). "mTOR and S6K1 mediate assembly of the translation preinitiation complex through dynamic protein interchange and ordered phosphorylation events." Cell **123**(4): 569-580.

Hong, D. S., M. G. Fakih, J. H. Strickler, J. Desai, G. A. Durm, G. I. Shapiro, G. S. Falchook, T. J. Price, A. Sacher, C. S. Denlinger, Y. J. Bang, G. K. Dy, J. C. Krauss, Y. Kuboki, J. C. Kuo, A. L. Coveler, K. Park, T. W. Kim, F. Barlesi, P. N. Munster, S. S. Ramalingam, T. F. Burns, F. Meric-Bernstam, H. Henary, J. Ngang, G. Ngarmchamnanrith, J. Kim, B. E. Houk, J. Canon, J. R. Lipford, G. Friberg, P. Lito, R.

Govindan and B. T. Li (2020). "KRAS(G12C) Inhibition with Sotorasib in Advanced Solid Tumors." N Engl J Med **383**(13): 1207-1217.

Hoshi, M., E. Nishida and H. Sakai (1988). "Activation of a Ca2+-inhibitable protein kinase that phosphorylates microtubule-associated protein 2 in vitro by growth factors, phorbol esters, and serum in quiescent cultured human fibroblasts." J Biol Chem **263**(11): 5396-5401.

Hu, J. L., L. Xiao, Z. Y. Li, Q. Wang, Y. Chang and Y. Jin (2013). "Upregulation of HO-1 is accompanied by activation of p38MAPK and mTOR in human oesophageal squamous carcinoma cells." Cell Biol Int **37**(6): 584-592.

Hu, K., K. Li, J. Lv, J. Feng, J. Chen, H. Wu, F. Cheng, W. Jiang, J. Wang, H. Pei, P. J. Chiao, Z. Cai, Y. Chen, M. Liu and X. Pang (2020). "Suppression of the SLC7A11/glutathione axis causes synthetic lethality in KRAS-mutant lung adenocarcinoma." J Clin Invest **130**(4): 1752-1766.

Hua, H., Q. Kong, H. Zhang, J. Wang, T. Luo and Y. Jiang (2019). "Targeting mTOR for cancer therapy." J Hematol Oncol **12**(1): 71.

Hübner, A., T. Barrett, R. A. Flavell and R. J. Davis (2008). "Multisite phosphorylation regulates Bim stability and apoptotic activity." Mol Cell **30**(4): 415-425.

Hunter, J. C., A. Manandhar, M. A. Carrasco, D. Gurbani, S. Gondi and K. D. Westover (2015). "Biochemical and Structural Analysis of Common Cancer-Associated KRAS Mutations." Mol Cancer Res **13**(9): 1325-1335.

Husain, K., R. A. Francois, T. Yamauchi, M. Perez, S. M. Sebti and M. P. Malafa (2011). "Vitamin E δ-tocotrienol augments the antitumor activity of gemcitabine and suppresses constitutive NF-κB activation in pancreatic cancer." Mol Cancer Ther **10**(12): 2363-2372.

Idriss, M., M. H. Hodroj, R. Fakhoury and S. Rizk (2020). "Beta-Tocotrienol Exhibits More Cytotoxic Effects than Gamma-Tocotrienol on Breast Cancer Cells by Promoting Apoptosis via a P53-Independent PI3-Kinase Dependent Pathway." Biomolecules **10**(4).

Ihle, N. T., L. A. Byers, E. S. Kim, P. Saintigny, J. J. Lee, G. R. Blumenschein, A. Tsao, S. Liu, J. E. Larsen, J. Wang, L. Diao, K. R. Coombes, L. Chen, S. Zhang, M. F. Abdelmelek, X. Tang, V. Papadimitrakopoulou, J. D. Minna, S. M. Lippman, W. K. Hong, R. S. Herbst, Wistuba, II, J. V. Heymach and G. Powis (2012). "Effect of KRAS oncogene substitutions on protein behavior: implications for signaling and clinical outcome." J Natl Cancer Inst **104**(3): 228-239.

Inguaggiato, P., L. Gonzalez-Michaca, A. J. Croatt, J. J. Haggard, J. Alam and K. A. Nath (2001). "Cellular overexpression of heme oxygenase-1 up-regulates p21 and confers resistance to apoptosis." Kidney Int **60**(6): 2181-2191.

Jaafar, F., A. Abdullah and S. Makpol (2018). "Cellular Uptake and Bioavailability of Tocotrienol-Rich Fraction in SIRT1-Inhibited Human Diploid Fibroblasts." Sci Rep **8**(1): 10471.

Janes, M. R., J. Zhang, L. S. Li, R. Hansen, U. Peters, X. Guo, Y. Chen, A. Babbar, S. J. Firdaus, L. Darjania, J. Feng, J. H. Chen, S. Li, S. Li, Y. O. Long, C. Thach, Y. Liu, A. Zarieh, T. Ely, J. M. Kucharski, L. V. Kessler, T. Wu, K. Yu, Y. Wang, Y. Yao, X. Deng, P. P. Zarrinkar, D. Brehmer, D. Dhanak, M. V. Lorenzi, D. Hu-Lowe, M. P. Patricelli, P. Ren and Y. Liu (2018). "Targeting KRAS Mutant Cancers with a Covalent G12C-Specific Inhibitor." Cell **172**(3): 578-589.e517.

Jeffers, J. R., E. Parganas, Y. Lee, C. Yang, J. Wang, J. Brennan, K. H. MacLean, J. Han, T. Chittenden, J. N. Ihle, P. J. McKinnon, J. L. Cleveland and G. P. Zambetti (2003). "Puma is an essential mediator of p53-dependent and -independent apoptotic pathways." Cancer Cell **4**(4): 321-328.

Jiang, Q. (2022). "Metabolism of natural forms of vitamin E and biological actions of vitamin E metabolites." Free Radic Biol Med **179**: 375-387.

Jiang, Q., X. Rao, C. Y. Kim, H. Freiser, Q. Zhang, Z. Jiang and G. Li (2012). "Gamma-tocotrienol induces apoptosis and autophagy in prostate cancer cells by increasing intracellular dihydrosphingosine and dihydroceramide." Int J Cancer **130**(3): 685-693.

Jiang, X., B. R. Stockwell and M. Conrad (2021). "Ferroptosis: mechanisms, biology and role in disease." Nat Rev Mol Cell Biol **22**(4): 266-282.

Jiao, D. and S. Yang (2020). "Overcoming Resistance to Drugs Targeting KRAS(G12C) Mutation." Innovation (Camb) **1**(2).

Jo, S. K., W. Y. Cho, S. A. Sung, H. K. Kim and N. H. Won (2005). "MEK inhibitor, U0126, attenuates cisplatin-induced renal injury by decreasing inflammation and apoptosis." Kidney Int **67**(2): 458-466.

Kang, S. A., M. E. Pacold, C. L. Cervantes, D. Lim, H. J. Lou, K. Ottina, N. S. Gray, B. E. Turk, M. B. Yaffe and D. M. Sabatini (2013). "mTORC1 phosphorylation sites encode their sensitivity to starvation and rapamycin." Science **341**(6144): 1236566.

Kang, T. H., J. Knoff, W. H. Yeh, B. Yang, C. Wang, Y. S. Kim, T. W. Kim, T. C. Wu and C. F. Hung (2014). "Treatment of tumors with vitamin E suppresses myeloid derived suppressor cells and enhances CD8+ T cell-mediated antitumor effects." PLoS One **9**(7): e103562.

Kaufman, J. M., J. M. Amann, K. Park, R. R. Arasada, H. Li, Y. Shyr and D. P. Carbone (2014). "LKB1 Loss induces characteristic patterns of gene expression in human tumors associated with NRF2 activation and attenuation of PI3K-AKT." J Thorac Oncol **9**(6): 794-804.

Kiel, C. and L. Serrano (2006). "The ubiquitin domain superfold: structure-based sequence alignments and characterization of binding epitopes." J Mol Biol **355**(4): 821-844.

Kim, D., J. Y. Xue and P. Lito (2020). "Targeting KRAS(G12C): From Inhibitory Mechanism to Modulation of Antitumor Effects in Patients." Cell **183**(4): 850-859.

Kim, D. H., D. D. Sarbassov, S. M. Ali, J. E. King, R. R. Latek, H. Erdjument-Bromage, P. Tempst and D. M. Sabatini (2002). "mTOR interacts with raptor to form a nutrient-sensitive complex that signals to the cell growth machinery." Cell **110**(2): 163-175.

Kim, J., M. Kundu, B. Viollet and K. L. Guan (2011). "AMPK and mTOR regulate autophagy through direct phosphorylation of Ulk1." Nat Cell Biol **13**(2): 132-141.

Kishimoto, M., Y. Yano, S. Yajima, S. Otani, T. Ichikawa and T. Yano (1998). "The inhibitory effect of vitamin E on 4-(methylnitrosamino)-1-(3-pyridyl)-1-butanone-induced lung tumorigenesis in mice based on the regulation of polyamine metabolism." Cancer Lett **126**(2): 173-178.

Kobayashi, G., K. Sentani, T. Babasaki, Y. Sekino, Y. Shigematsu, T. Hayashi, N. Oue, J. Teishima, A. Matsubara, N. Sasaki and W. Yasui (2020). "Claspin overexpression is associated with high-grade histology and poor prognosis in renal cell carcinoma." Cancer Sci **111**(3): 1020-1027.

Kohlhaas, S. L., A. Craxton, X. M. Sun, M. J. Pinkoski and G. M. Cohen (2007). "Receptor-mediated endocytosis is not required for tumor necrosis factor-related apoptosis-inducing ligand (TRAIL)-induced apoptosis." J Biol Chem **282**(17): 12831-12841.

Kolaja, K. L. and J. E. Klaunig (1997). "Vitamin E modulation of hepatic focal lesion growth in mice." Toxicol Appl Pharmacol **143**(2): 380-387.

Kuroshima, K., H. Yoshino, S. Okamura, M. Tsuruda, Y. Osako, T. Sakaguchi, S. Sugita, S. Tatarano, M. Nakagawa and H. Enokida (2020). "Potential new therapy of Rapalink-1, a new generation mammalian target of rapamycin inhibitor, against sunitinib-resistant renal cell carcinoma." Cancer Sci **111**(5): 1607-1618.

Kwan, A. K., G. A. Piazza, A. B. Keeton and C. A. Leite (2022). "The path to the clinic: a comprehensive review on direct KRAS(G12C) inhibitors." J Exp Clin Cancer Res **41**(1): 27.

Kwon, M. Y., E. Park, S. J. Lee and S. W. Chung (2015). "Heme oxygenase-1 accelerates erastin-induced ferroptotic cell death." Oncotarget **6**(27): 24393-24403.

Lang, D., S. Reuter, T. Buzescu, C. August and S. Heidenreich (2005). "Heme-induced heme oxygenase-1 (HO-1) in human monocytes inhibits apoptosis despite caspase-3 up-regulation." Int Immunol **17**(2): 155-165.

Lavoie, H., J. Gagnon and M. Therrien (2020). "ERK signalling: a master regulator of cell behaviour, life and fate." Nat Rev Mol Cell Biol **21**(10): 607-632.

Lavoie, H. and M. Therrien (2015). "Regulation of RAF protein kinases in ERK signalling." Nat Rev Mol Cell Biol **16**(5): 281-298.

Le Gal, K., M. X. Ibrahim, C. Wiel, V. I. Sayin, M. K. Akula, C. Karlsson, M. G. Dalin, L. M. Akyürek, P. Lindahl, J. Nilsson and M. O. Bergo (2015). "Antioxidants can increase melanoma metastasis in mice." Sci Transl Med **7**(308): 308re308.

Lee, B. J., J. A. Boyer, G. L. Burnett, A. P. Thottumkara, N. Tibrewal, S. L. Wilson, T. Hsieh, A. Marquez, E. G. Lorenzana, J. W. Evans, L. Hulea, G. Kiss, H. Liu, D. Lee, O. Larsson, S. McLaughlan, I. Topisirovic, Z. Wang, Z. Wang, Y. Zhao, D. Wildes, J. B. Aggen, M. Singh, A. L. Gill, J. A. M. Smith and N. Rosen (2021). "Selective inhibitors of mTORC1 activate 4EBP1 and suppress tumor growth." Nat Chem Biol **17**(10): 1065-1074.

Lee, K. H., C. Feig, V. Tchikov, R. Schickel, C. Hallas, S. Schütze, M. E. Peter and A. C. Chan (2006). "The role of receptor internalization in CD95 signaling." Embo j **25**(5): 1009-1023.

Lehr, S., J. Kotzka, H. Avci, A. Sickmann, H. E. Meyer, A. Herkner and D. Muller-Wieland (2004). "Identification of major ERK-related phosphorylation sites in Gab1." Biochemistry **43**(38): 12133-12140.

Ley, R., K. Balmanno, K. Hadfield, C. Weston and S. J. Cook (2003). "Activation of the ERK1/2 signaling pathway promotes phosphorylation and proteasome-dependent degradation of the BH3-only protein, Bim." J Biol Chem **278**(21): 18811-18816.

Li, G. X., M. J. Lee, A. B. Liu, Z. Yang, Y. Lin, W. J. Shih and C. S. Yang (2011). "δ-tocopherol is more active than α - or γ -tocopherol in inhibiting lung tumorigenesis in vivo." Cancer Prev Res (Phila) **4**(3): 404-413.

Li, X., D. Dai, B. Chen, H. Tang, X. Xie and W. Wei (2018). "Efficacy of PI3K/AKT/mTOR pathway inhibitors for the treatment of advanced solid cancers: A literature-based meta-analysis of 46 randomised control trials." PLoS One **13**(2): e0192464.

Liang, C., S. Shi, M. Liu, Y. Qin, Q. Meng, J. Hua, S. Ji, Y. Zhang, J. Yang, J. Xu, Q. Ni, M. Li and X. Yu (2019). "PIN1 Maintains Redox Balance via the c-Myc/NRF2 Axis to Counteract Kras-Induced Mitochondrial Respiratory Injury in Pancreatic Cancer Cells." Cancer Res **79**(1): 133-145.

Liao, W., Q. Xiao, V. Tchikov, K. Fujita, W. Yang, S. Wincovitch, S. Garfield, D. Conze, W. S. El-Deiry, S. Schütze and S. M. Srinivasula (2008). "CARP-2 is an endosome-associated ubiquitin ligase for RIP and regulates TNF-induced NF-kappaB activation." Curr Biol **18**(9): 641-649.

Lim, J. K. M., A. Delaidelli, S. W. Minaker, H. F. Zhang, M. Colovic, H. Yang, G. L. Negri, S. von Karstedt, W. W. Lockwood, P. Schaffer, G. Leprivier and P. H. Sorensen (2019). "Cystine/glutamate antiporter xCT (SLC7A11) facilitates oncogenic RAS transformation by preserving intracellular redox balance." Proc Natl Acad Sci U S A **116**(19): 9433-9442.

Lim, S. W., H. S. Loh, K. N. Ting, T. D. Bradshaw and N. A. Zeenathul (2014). "Cytotoxicity and apoptotic activities of alpha-, gamma- and delta-tocotrienol isomers on human cancer cells." BMC Complement Altern Med **14**: 469.

Lin, T., N. K. Mak and M. S. Yang (2008). "MAPK regulate p53-dependent cell death induced by benzo[a]pyrene: involvement of p53 phosphorylation and acetylation." Toxicology **247**(2-3): 145-153.

Lippman, S. M., E. A. Klein, P. J. Goodman, M. S. Lucia, I. M. Thompson, L. G. Ford, H. L. Parnes, L. M. Minasian, J. M. Gaziano, J. A. Hartline, J. K. Parsons, J. D. Bearden, 3rd, E. D. Crawford, G. E. Goodman, J. Claudio, E. Winquist, E. D. Cook, D. D. Karp, P. Walther, M. M. Lieber, A. R. Kristal, A. K. Darke, K. B. Arnold, P. A. Ganz, R. M. Santella, D. Albanes, P. R. Taylor, J. L. Probstfield, T. J. Jagpal, J. J. Crowley, F. L. Meyskens, Jr., L. H. Baker and C. A. Coltman, Jr. (2009). "Effect of selenium and vitamin E on risk of prostate cancer and other cancers: the Selenium and Vitamin E Cancer Prevention Trial (SELECT)." Jama **301**(1): 39-51.

Lito, P., N. Rosen and D. B. Solit (2013). "Tumor adaptation and resistance to RAF inhibitors." Nat Med **19**(11): 1401-1409.

Lito, P., M. Solomon, L. S. Li, R. Hansen and N. Rosen (2016). "Allele-specific inhibitors inactivate mutant KRAS G12C by a trapping mechanism." Science **351**(6273): 604-608.

Liu, F., X. Yang, M. Geng and M. Huang (2018). "Targeting ERK, an Achilles' Heel of the MAPK pathway, in cancer therapy." Acta Pharm Sin B **8**(4): 552-562.

Liu, J., W. Mao, B. Ding and C. S. Liang (2008). "ERKs/p53 signal transduction pathway is involved in doxorubicin-induced apoptosis in H9c2 cells and cardiomyocytes." Am J Physiol Heart Circ Physiol **295**(5): H1956-1965.

Liu, J., C. Zhang, J. Wang, W. Hu and Z. Feng (2020). "The Regulation of Ferroptosis by Tumor Suppressor p53 and its Pathway." Int J Mol Sci **21**(21).

Liu, K. Y. and Q. Jiang (2020). "Tocopherols and Tocotrienols Are Bioavailable in Rats and Primarily Excreted in Feces as the Intact Forms and 13'-Carboxychromanol Metabolites." J Nutr **150**(2): 222-230.

Liu, L., S. Das, W. Losert and C. A. Parent (2010). "mTORC2 regulates neutrophil chemotaxis in a cAMP- and RhoA-dependent fashion." Dev Cell **19**(6): 845-857.

Liu, P., W. Gan, Y. R. Chin, K. Ogura, J. Guo, J. Zhang, B. Wang, J. Blenis, L. C. Cantley, A. Toker, B. Su and W. Wei (2015). "PtdIns(3,4,5)P3-Dependent Activation of the mTORC2 Kinase Complex." Cancer Discov **5**(11): 1194-1209.

Liu, Z., P. Hou, M. Ji, H. Guan, K. Studeman, K. Jensen, V. Vasko, A. K. El-Naggar and M. Xing (2008). "Highly prevalent genetic alterations in receptor tyrosine kinases and phosphatidylinositol 3-kinase/akt and mitogen-activated protein kinase pathways in anaplastic and follicular thyroid cancers." J Clin Endocrinol Metab **93**(8): 3106-3116.

Liu, Z. M., G. G. Chen, E. K. Ng, W. K. Leung, J. J. Sung and S. C. Chung (2004). "Upregulation of heme oxygenase-1 and p21 confers resistance to apoptosis in human gastric cancer cells." Oncogene **23**(2): 503-513.

Loboda, A., M. Damulewicz, E. Pyza, A. Jozkowicz and J. Dulak (2016). "Role of Nrf2/HO-1 system in development, oxidative stress response and diseases: an evolutionarily conserved mechanism." Cell Mol Life Sci **73**(17): 3221-3247.

Lonn, E., J. Bosch, S. Yusuf, P. Sheridan, J. Pogue, J. M. Arnold, C. Ross, A. Arnold, P. Sleight, J. Probstfield and G. R. Dagenais (2005). "Effects of long-term vitamin E supplementation on cardiovascular events and cancer: a randomized controlled trial." Jama **293**(11): 1338-1347.

Lou, K., D. R. Wassarman, T. Yang, Y. Paung, Z. Zhang, T. A. O'Loughlin, M. K. Moore, R. K. Egan, P. Greninger, C. H. Benes, M. A. Seeliger, J. Taunton, L. A. Gilbert and K. M. Shokat (2022). "IFITM proteins assist cellular uptake of diverse linked chemotypes." Science **378**(6624): 1097-1104.

Ma, L., Z. Chen, H. Erdjument-Bromage, P. Tempst and P. P. Pandolfi (2005). "Phosphorylation and functional inactivation of TSC2 by Erk implications for tuberous sclerosis and cancer pathogenesis." Cell **121**(2): 179-193.

Ma, L., J. Teruya-Feldstein, P. Bonner, R. Bernardi, D. N. Franz, D. Witte, C. Cordon-Cardo and P. P. Pandolfi (2007). "Identification of S664 TSC2 phosphorylation as a marker for extracellular signal-regulated kinase mediated mTOR activation in tuberous sclerosis and human cancer." Cancer Res **67**(15): 7106-7112.

Magtanong, L., P. J. Ko, M. To, J. Y. Cao, G. C. Forcina, A. Tarangelo, C. C. Ward, K. Cho, G. J. Patti, D. K. Nomura, J. A. Olzmann and S. J. Dixon (2019). "Exogenous Monounsaturated Fatty Acids Promote a Ferroptosis-Resistant Cell State." Cell Chem Biol **26**(3): 420-432.e429.

Mahoney, C. L., B. Choudhury, H. Davies, S. Edkins, C. Greenman, G. Haaften, T. Mironenko, T. Santarius, C. Stevens, M. R. Stratton and P. A. Futreal (2009). "LKB1/KRAS mutant lung cancers constitute a genetic subset of NSCLC with increased sensitivity to MAPK and mTOR signalling inhibition." Br J Cancer **100**(2): 370-375.

Manning, B. D., A. R. Tee, M. N. Logsdon, J. Blenis and L. C. Cantley (2002). "Identification of the tuberous sclerosis complex-2 tumor suppressor gene product tuberin as a target of the phosphoinositide 3-kinase/akt pathway." Mol Cell **10**(1): 151-162.

Manning, B. D. and A. Toker (2017). "AKT/PKB Signaling: Navigating the Network." Cell **169**(3): 381-405.

Mantovani, F., L. Collavin and G. Del Sal (2019). "Mutant p53 as a guardian of the cancer cell." Cell Death Differ **26**(2): 199-212.

Manu, K. A., M. K. Shanmugam, L. Ramachandran, F. Li, C. W. Fong, A. P. Kumar, P. Tan and G. Sethi (2012). "First evidence that γ-tocotrienol inhibits the growth of human gastric cancer and chemosensitizes it to capecitabine in a xenograft mouse model through the modulation of NF-κB pathway." Clin Cancer Res **18**(8): 2220-2229.

Mao, B., Q. Zhang, L. Ma, D. S. Zhao, P. Zhao and P. Yan (2022). "Overview of Research into mTOR Inhibitors." Molecules **27**(16).

Martina, J. A., Y. Chen, M. Gucek and R. Puertollano (2012). "MTORC1 functions as a transcriptional regulator of autophagy by preventing nuclear transport of TFEB." Autophagy **8**(6): 903-914.

Matallanas, D., M. Birtwistle, D. Romano, A. Zebisch, J. Rauch, A. von Kriegsheim and W. Kolch (2011). "Raf family kinases: old dogs have learned new tricks." Genes Cancer **2**(3): 232-260.

McCain, J. (2013). "The MAPK (ERK) Pathway: Investigational Combinations for the Treatment Of BRAF-Mutated Metastatic Melanoma." P t **38**(2): 96-108.

Mellinghoff, I. K., M. Y. Wang, I. Vivanco, D. A. Haas-Kogan, S. Zhu, E. Q. Dia, K. V. Lu, K. Yoshimoto, J. H. Huang, D. J. Chute, B. L. Riggs, S. Horvath, L. M. Liau, W. K. Cavenee, P. N. Rao, R. Beroukhim, T. C. Peck, J. C. Lee, W. R. Sellers, D. Stokoe, M. Prados, T. F. Cloughesy, C. L. Sawyers and P. S. Mischel (2005). "Molecular determinants of the response of glioblastomas to EGFR kinase inhibitors." N Engl J Med **353**(19): 2012-2024.

Memmott, R. M. and P. A. Dennis (2009). "Akt-dependent and -independent mechanisms of mTOR regulation in cancer." Cell Signal **21**(5): 656-664.

Mendoza, M. C., E. E. Er and J. Blenis (2011). "The Ras-ERK and PI3K-mTOR pathways: cross-talk and compensation." Trends Biochem Sci **36**(6): 320-328.

Menon, S., C. C. Dibble, G. Talbott, G. Hoxhaj, A. J. Valvezan, H. Takahashi, L. C. Cantley and B. D. Manning (2014). "Spatial control of the TSC complex integrates insulin and nutrient regulation of mTORC1 at the lysosome." Cell **156**(4): 771-785.

Mikosz, C. A., D. R. Brickley, M. S. Sharkey, T. W. Moran and S. D. Conzen (2001). "Glucocorticoid receptor-mediated protection from apoptosis is associated with induction of the serine/threonine survival kinase gene, sgk-1." J Biol Chem **276**(20): 16649-16654.

Milburn, M. V., L. Tong, A. M. deVos, A. Brünger, Z. Yamaizumi, S. Nishimura and S. H. Kim (1990). "Molecular switch for signal transduction: structural differences between active and inactive forms of protooncogenic ras proteins." Science **247**(4945): 939-945.

Millis, S. Z., S. Ikeda, S. Reddy, Z. Gatalica and R. Kurzrock (2016). "Landscape of Phosphatidylinositol-3-Kinase Pathway Alterations Across 19 784 Diverse Solid Tumors." JAMA Oncol **2**(12): 1565-1573.

Mills, J. R., Y. Hippo, F. Robert, S. M. Chen, A. Malina, C. J. Lin, U. Trojahn, H. G. Wendel, A. Charest, R. T. Bronson, S. C. Kogan, R. Nadon, D. E. Housman, S. W. Lowe and J. Pelletier (2008). "mTORC1 promotes survival through translational control of Mcl-1." Proc Natl Acad Sci U S A **105**(31): 10853-10858.

Misale, S., J. P. Fatherree, E. Cortez, C. Li, S. Bilton, D. Timonina, D. T. Myers, D. Lee, M. Gomez-Caraballo, M. Greenberg, V. Nangia, P. Greninger, R. K. Egan, J. McClanaghan, G. T. Stein, E. Murchie, P. P. Zarrinkar, M. R. Janes, L. S. Li, Y. Liu, A. N. Hata and C. H. Benes (2019). "KRAS G12C NSCLC Models Are Sensitive to Direct Targeting of KRAS in Combination with PI3K Inhibition." Clin Cancer Res **25**(2): 796-807.

Mitchel, R. E. and R. McCann (1993). "Vitamin E is a complete tumor promoter in mouse skin." Carcinogenesis **14**(4): 659-662.

Mitchel, R. E. and R. A. McCann (2003). "Skin tumor promotion by Vitamin E in mice: amplification by ionizing radiation and Vitamin C." Cancer Detect Prev **27**(2): 102-108.

Miyazawa, T., G. C. Burdeos, M. Itaya, K. Nakagawa and T. Miyazawa (2019). "Vitamin E: Regulatory Redox Interactions." IUBMB Life **71**(4): 430-441.

Moelling, K., K. Schad, M. Bosse, S. Zimmermann and M. Schweneker (2002). "Regulation of Raf-Akt Cross-talk." J Biol Chem **277**(34): 31099-31106.

Moustafa-Kamal, M., T. J. Kucharski, W. El-Assaad, Y. M. Abbas, V. Gandin, B. Nagar, J. Pelletier, I. Topisirovic and J. G. Teodoro (2020). "The mTORC1/S6K/PDCD4/eIF4A Axis Determines Outcome of Mitotic Arrest." Cell Rep **33**(1): 108230.

Mugarza, E., F. van Maldegem, J. Boumelha, C. Moore, S. Rana, M. Llorian Sopena, P. East, R. Ambler, P. Anastasiou, P. Romero-Clavijo, K. Valand, M. Cole, M. Molina-Arcas and J. Downward (2022). "Therapeutic KRAS(G12C) inhibition drives effective interferon-mediated antitumor immunity in immunogenic lung cancers." Sci Adv **8**(29): eabm8780.

Mukherjee, R., K. G. Vanaja, J. A. Boyer, S. Gadal, H. Solomon, S. Chandarlapaty, A. Levchenko and N. Rosen (2021). "Regulation of PTEN translation by PI3K signaling maintains pathway homeostasis." Mol Cell **81**(4): 708-723.e705.

Murugan, A. K., M. Grieco and N. Tsuchida (2019). "RAS mutations in human cancers: Roles in precision medicine." Semin Cancer Biol **59**: 23-35.

Musa, J., M. F. Orth, M. Dallmayer, M. Baldauf, C. Pardo, B. Rotblat, T. Kirchner, G. Leprivier and T. G. Grünewald (2016). "Eukaryotic initiation factor 4E-binding protein 1 (4E-BP1): a master regulator of mRNA translation involved in tumorigenesis." Oncogene **35**(36): 4675-4688.

National Institutes of Health. (2021). "Vitamin E - Fact Sheet for Health Professionals." Retrieved January 12, 2023, from https://ods.od.nih.gov/factsheets/VitaminE-HealthProfessional/.

Nesterov, A., M. Nikrad, T. Johnson and A. S. Kraft (2004). "Oncogenic Ras sensitizes normal human cells to tumor necrosis factor-alpha-related apoptosis-inducing ligand-induced apoptosis." Cancer Res **64**(11): 3922-3927.

Nikiforov, M. A., M. Riblett, W. H. Tang, V. Gratchouck, D. Zhuang, Y. Fernandez, M. Verhaegen, S. Varambally, A. M. Chinnaiyan, A. J. Jakubowiak and M. S. Soengas (2007). "Tumor cell-selective regulation of NOXA by c-MYC in response to proteasome inhibition." Proc Natl Acad Sci U S A **104**(49): 19488-19493.

Novotny, J. A., J. G. Fadel, D. M. Holstege, H. C. Furr and A. J. Clifford (2012). "This kinetic, bioavailability, and metabolism study of RRR-α-tocopherol in healthy adults suggests lower intake requirements than previous estimates." J Nutr **142**(12): 2105-2111.

Odeleye, O. E., C. D. Eskelson, S. I. Mufti and R. R. Watson (1992). "Vitamin E protection against nitrosamine-induced esophageal tumor incidence in mice immunocompromised by retroviral infection." Carcinogenesis **13**(10): 1811-1816.

Ostrem, J. M., U. Peters, M. L. Sos, J. A. Wells and K. M. Shokat (2013). "K-Ras(G12C) inhibitors allosterically control GTP affinity and effector interactions." Nature **503**(7477): 548-551.

Pace, A., A. Savarese, M. Picardo, V. Maresca, U. Pacetti, G. Del Monte, A. Biroccio, C. Leonetti, B. Jandolo, F. Cognetti and L. Bove (2003). "Neuroprotective effect of vitamin E supplementation in patients treated with cisplatin chemotherapy." J Clin Oncol **21**(5): 927-931.

Pacold, M. E., S. Suire, O. Perisic, S. Lara-Gonzalez, C. T. Davis, E. H. Walker, P. T. Hawkins, L. Stephens, J. F. Eccleston and R. L. Williams (2000). "Crystal structure and functional analysis of Ras binding to its effector phosphoinositide 3-kinase gamma." Cell **103**(6): 931-943.

Pai, E. F., W. Kabsch, U. Krengel, K. C. Holmes, J. John and A. Wittinghofer (1989). "Structure of the guanine-nucleotide-binding domain of the Ha-ras oncogene product p21 in the triphosphate conformation." Nature **341**(6239): 209-214.

Palm, W., Y. Park, K. Wright, N. N. Pavlova, D. A. Tuveson and C. B. Thompson (2015). "The Utilization of Extracellular Proteins as Nutrients Is Suppressed by mTORC1." Cell **162**(2): 259-270.

Palm, W. and C. B. Thompson (2017). "Nutrient acquisition strategies of mammalian cells." Nature **546**(7657): 234-242.

Parlato, S., A. M. Giammarioli, M. Logozzi, F. Lozupone, P. Matarrese, F. Luciani, M. Falchi, W. Malorni and S. Fais (2000). "CD95 (APO-1/Fas) linkage to the actin cytoskeleton through ezrin in human T lymphocytes: a novel regulatory mechanism of the CD95 apoptotic pathway." Embo j **19**(19): 5123-5134.

Patricelli, M. P., M. R. Janes, L. S. Li, R. Hansen, U. Peters, L. V. Kessler, Y. Chen, J. M. Kucharski, J. Feng, T. Ely, J. H. Chen, S. J. Firdaus, A. Babbar, P. Ren and Y. Liu (2016). "Selective Inhibition of Oncogenic KRAS Output with Small Molecules Targeting the Inactive State." Cancer Discov **6**(3): 316-329.

Peh, H. Y., W. S. Tan, W. Liao and W. S. Wong (2016). "Vitamin E therapy beyond cancer: Tocopherol versus tocotrienol." Pharmacol Ther **162**: 152-169.

Peng, M., N. Yin and M. O. Li (2014). "Sestrins function as guanine nucleotide dissociation inhibitors for Rag GTPases to control mTORC1 signaling." Cell **159**(1): 122-133.

Persons, D. L., E. M. Yazlovitskaya and J. C. Pelling (2000). "Effect of extracellular signal-regulated kinase on p53 accumulation in response to cisplatin." J Biol Chem **275**(46): 35778-35785.

Peterson, T. R., S. S. Sengupta, T. E. Harris, A. E. Carmack, S. A. Kang, E. Balderas, D. A. Guertin, K. L. Madden, A. E. Carpenter, B. N. Finck and D. M. Sabatini (2011). "mTOR complex 1 regulates lipin 1 localization to control the SREBP pathway." Cell **146**(3): 408-420.

Petrache, I., L. E. Otterbein, J. Alam, G. W. Wiegand and A. M. Choi (2000). "Heme oxygenase-1 inhibits TNF-alpha-induced apoptosis in cultured fibroblasts." Am J Physiol Lung Cell Mol Physiol **278**(2): L312-319.

Pikor, L. A., V. R. Ramnarine, S. Lam and W. L. Lam (2013). "Genetic alterations defining NSCLC subtypes and their therapeutic implications." Lung Cancer **82**(2): 179-189.

Plotnikov, A., E. Zehorai, S. Procaccia and R. Seger (2011). "The MAPK cascades: signaling components, nuclear roles and mechanisms of nuclear translocation." Biochim Biophys Acta **1813**(9): 1619-1633.

Podszun, M. and J. Frank (2014). "Vitamin E-drug interactions: molecular basis and clinical relevance." Nutr Res Rev **27**(2): 215-231.

Polyak, K., J. Y. Kato, M. J. Solomon, C. J. Sherr, J. Massague, J. M. Roberts and A. Koff (1994). "p27Kip1, a cyclin-Cdk inhibitor, links transforming growth factor-beta and contact inhibition to cell cycle arrest." Genes Dev **8**(1): 9-22.

Potter, C. J., L. G. Pedraza and T. Xu (2002). "Akt regulates growth by directly phosphorylating Tsc2." Nat Cell Biol **4**(9): 658-665.

Poulikakos, P. I., C. Zhang, G. Bollag, K. M. Shokat and N. Rosen (2010). "RAF inhibitors transactivate RAF dimers and ERK signalling in cells with wild-type BRAF." Nature **464**(7287): 427-430.

Qie, S. and J. A. Diehl (2016). "Cyclin D1, cancer progression, and opportunities in cancer treatment." J Mol Med (Berl) **94**(12): 1313-1326.

Qin, J. Z., J. Ziffra, L. Stennett, B. Bodner, B. K. Bonish, V. Chaturvedi, F. Bennett, P. M. Pollock, J. M. Trent, M. J. Hendrix, P. Rizzo, L. Miele and B. J. Nickoloff (2005). "Proteasome inhibitors trigger NOXA-mediated apoptosis in melanoma and myeloma cells." Cancer Res **65**(14): 6282-6293.

Qin, X., B. Jiang and Y. Zhang (2016). "4E-BP1, a multifactor regulated multifunctional protein." Cell Cycle **15**(6): 781-786.

Quin, J., D. Engle, A. Litwiller, E. Peralta, A. Grasch, T. Boley and S. Hazelrigg (2005). "Vitamin E succinate decreases lung cancer tumor growth in mice." J Surg Res **127**(2): 139-143.

Rajasinghe, L. D., Gupta, S. V. (2017). "Tocotrienol-Rich Mixture Inhibits Cell Proliferation and Induces Apoptosis via Down-Regulation of the Notch-1/NF-κB Pathways in NSCLC Cells." Dove Press **2017**(9): 103-114.

Rajasinghe, L. D., R. H. Pindiprolu and S. V. Gupta (2018). "Delta-tocotrienol inhibits non-small-cell lung cancer cell invasion via the inhibition of NF-κB, uPA activator, and MMP-9." Onco Targets Ther **11**: 4301-4314.

Raman, M., W. Chen and M. H. Cobb (2007). "Differential regulation and properties of MAPKs." Oncogene **26**(22): 3100-3112.

Ranasinghe, R., M. Mathai and A. Zulli (2022). "Revisiting the therapeutic potential of tocotrienol." Biofactors **48**(4): 813-856.

Ray, L. B. and T. W. Sturgill (1987). "Rapid stimulation by insulin of a serine/threonine kinase in 3T3-L1 adipocytes that phosphorylates microtubule-associated protein 2 in vitro." Proc Natl Acad Sci U S A **84**(6): 1502-1506.

Razavipour, S. F., K. B. Harikumar and J. M. Slingerland (2020). "p27 as a Transcriptional Regulator: New Roles in Development and Cancer." Cancer Res **80**(17): 3451-3458.

Redza-Dutordoir, M. and D. A. Averill-Bates (2016). "Activation of apoptosis signalling pathways by reactive oxygen species." Biochim Biophys Acta **1863**(12): 2977-2992.

Revolution Medicines. (2023). "RAS(ON) Inhibitors " Retrieved January 12, 2023, from https://www.revmed.com/pipeline/rason-inhibitors.

Rodrik-Outmezguine, V. S., S. Chandarlapaty, N. C. Pagano, P. I. Poulikakos, M. Scaltriti, E. Moskatel, J. Baselga, S. Guichard and N. Rosen (2011). "mTOR kinase inhibition causes feedback-dependent biphasic regulation of AKT signaling." Cancer Discov **1**(3): 248-259.

Rodrik-Outmezguine, V. S., M. Okaniwa, Z. Yao, C. J. Novotny, C. McWhirter, A. Banaji, H. Won, W. Wong, M. Berger, E. de Stanchina, D. G. Barratt, S. Cosulich, T. Klinowska, N. Rosen and K. M. Shokat (2016). "Overcoming mTOR resistance mutations with a new-generation mTOR inhibitor." Nature **534**(7606): 272-276.

Roux, P. P. and I. Topisirovic (2018). "Signaling Pathways Involved in the Regulation of mRNA Translation." Mol Cell Biol **38**(12).

Ryter, S. W. (2021). "Heme Oxgenase-1, a Cardinal Modulator of Regulated Cell Death and Inflammation." Cells **10**(3).

Sailo, B. L., K. Banik, G. Padmavathi, M. Javadi, D. Bordoloi and A. B. Kunnumakkara (2018). "Tocotrienols: The promising analogues of vitamin E for cancer therapeutics." Pharmacol Res **130**: 259-272.

Samant, G. V., V. B. Wali and P. W. Sylvester (2010). "Anti-proliferative effects of gamma-tocotrienol on mammary tumour cells are associated with suppression of cell cycle progression." Cell Prolif **43**(1): 77-83.

Sancak, Y., L. Bar-Peled, R. Zoncu, A. L. Markhard, S. Nada and D. M. Sabatini (2010). "Ragulator-Rag complex targets mTORC1 to the lysosomal surface and is necessary for its activation by amino acids." Cell **141**(2): 290-303.

Sasaki, A. T., C. Janetopoulos, S. Lee, P. G. Charest, K. Takeda, L. W. Sundheimer, R. Meili, P. N. Devreotes and R. A. Firtel (2007). "G protein-independent Ras/PI3K/F-actin circuit regulates basic cell motility." J Cell Biol **178**(2): 185-191.

Saxton, R. A. and D. M. Sabatini (2017). "mTOR Signaling in Growth, Metabolism, and Disease." Cell **168**(6): 960-976.

Sayin, V. I., M. X. Ibrahim, E. Larsson, J. A. Nilsson, P. Lindahl and M. O. Bergo (2014). "Antioxidants accelerate lung cancer progression in mice." Sci Transl Med **6**(221): 221ra215.

Scheffler, M., M. A. Ihle, R. Hein, S. Merkelbach-Bruse, A. H. Scheel, J. Siemanowski, J. Brägelmann, A. Kron, N. Abedpour, F. Ueckeroth, M. Schüller, S. Koleczko, S. Michels, J. Fassunke, H. Pasternack, C. Heydt, M. Serke, R. Fischer, W. Schulte, U. Gerigk, L. Nogova, Y. D. Ko, D. S. Y. Abdulla, R. Riedel, K. O. Kambartel, J. Lorenz, I. Sauerland, W. Randerath, B. Kaminsky, L. Hagmeyer, C. Grohé, A. Eisert, R. Frank, L. Gogl, C. Schaepers, A. Holzem, M. Hellmich, R. K. Thomas, M. Peifer, M. L. Sos, R. Büttner and J. Wolf (2019). "K-ras Mutation Subtypes in NSCLC and Associated Co-occuring Mutations in Other Oncogenic Pathways." J Thorac Oncol **14**(4): 606-616.

Scheffzek, K., M. R. Ahmadian, W. Kabsch, L. Wiesmüller, A. Lautwein, F. Schmitz and A. Wittinghofer (1997). "The Ras-RasGAP complex: structural basis for GTPase activation and its loss in oncogenic Ras mutants." Science **277**(5324): 333-338.

Schmölz, L., M. Birringer, S. Lorkowski and M. Wallert (2016). "Complexity of vitamin E metabolism." World J Biol Chem **7**(1): 14-43.

Schneider-Brachert, W., U. Heigl and M. Ehrenschwender (2013). "Membrane trafficking of death receptors: implications on signalling." Int J Mol Sci **14**(7): 14475-14503.

Schneider-Brachert, W., V. Tchikov, O. Merkel, M. Jakob, C. Hallas, M. L. Kruse, P. Groitl, A. Lehn, E. Hildt, J. Held-Feindt, T. Dobner, D. Kabelitz, M. Krönke and S. Schütze (2006). "Inhibition of TNF receptor 1 internalization by adenovirus 14.7K as a novel immune escape mechanism." J Clin Invest **116**(11): 2901-2913.

Schneider-Brachert, W., V. Tchikov, J. Neumeyer, M. Jakob, S. Winoto-Morbach, J. Held-Feindt, M. Heinrich, O. Merkel, M. Ehrenschwender, D. Adam, R. Mentlein, D. Kabelitz and S. Schütze (2004). "Compartmentalization of TNF receptor 1 signaling: internalized TNF receptosomes as death signaling vesicles." Immunity **21**(3): 415-428.

She, Q. B., N. Chen and Z. Dong (2000). "ERKs and p38 kinase phosphorylate p53 protein at serine 15 in response to UV radiation." J Biol Chem **275**(27): 20444-20449.

She, Q. B., E. Halilovic, Q. Ye, W. Zhen, S. Shirasawa, T. Sasazuki, D. B. Solit and N. Rosen (2010). "4E-BP1 is a key effector of the oncogenic activation of the AKT and ERK signaling pathways that integrates their function in tumors." Cancer Cell **18**(1): 39-51.

Shenoy, K., Y. Wu and S. Pervaiz (2009). "LY303511 enhances TRAIL sensitivity of SHEP-1 neuroblastoma cells via hydrogen peroxide-mediated mitogen-activated protein kinase activation and up-regulation of death receptors." Cancer Res **69**(5): 1941-1950.

Sherr, C. J. and J. M. Roberts (1999). "CDK inhibitors: positive and negative regulators of G1-phase progression." Genes Dev **13**(12): 1501-1512.

Shih, A., F. B. Davis, H. Y. Lin and P. J. Davis (2002). "Resveratrol induces apoptosis in thyroid cancer cell lines via a MAPK- and p53-dependent mechanism." J Clin Endocrinol Metab **87**(3): 1223-1232.

Simanshu, D. K., D. V. Nissley and F. McCormick (2017). "RAS Proteins and Their Regulators in Human Disease." Cell **170**(1): 17-33.

Simi, L., N. Pratesi, M. Vignoli, R. Sestini, F. Cianchi, R. Valanzano, S. Nobili, E. Mini, M. Pazzagli and C. Orlando (2008). "High-resolution melting analysis for rapid detection of KRAS, BRAF, and PIK3CA gene mutations in colorectal cancer." Am J Clin Pathol **130**(2): 247-253.

Singh, G., N. Thakur and U. Kumar (2023). "RAS: Circuitry and therapeutic targeting." Cell Signal **101**: 110505.

Singh, S. and M. J. Smith (2020). "RAS GTPase signalling to alternative effector pathways." Biochem Soc Trans **48**(5): 2241-2252.

Skoulidis, F., B. T. Li, G. K. Dy, T. J. Price, G. S. Falchook, J. Wolf, A. Italiano, M. Schuler, H. Borghaei, F. Barlesi, T. Kato, A. Curioni-Fontecedro, A. Sacher, A. Spira, S. S. Ramalingam, T. Takahashi, B. Besse, A. Anderson, A. Ang, Q. Tran, O. Mather, H. Henary, G. Ngarmchamnanrith, G. Friberg, V. Velcheti and R. Govindan (2021). "Sotorasib for Lung Cancers with KRAS p.G12C Mutation." N Engl J Med **384**(25): 2371-2381.

Skouta, R., S. J. Dixon, J. Wang, D. E. Dunn, M. Orman, K. Shimada, P. A. Rosenberg, D. C. Lo, J. M. Weinberg, A. Linkermann and B. R. Stockwell (2014). "Ferrostatins inhibit oxidative lipid damage and cell death in diverse disease models." J Am Chem Soc **136**(12): 4551-4556.

Stephen, A. G., D. Esposito, R. K. Bagni and F. McCormick (2014). "Dragging ras back in the ring." Cancer Cell **25**(3): 272-281.

Stockwell, B. R., X. Jiang and W. Gu (2020). "Emerging Mechanisms and Disease Relevance of Ferroptosis." Trends Cell Biol **30**(6): 478-490.

Stolzenberg-Solomon, R. Z., S. Sheffler-Collins, S. Weinstein, D. H. Garabrant, S. Mannisto, P. Taylor, J. Virtamo and D. Albanes (2009). "Vitamin E intake, alpha-tocopherol status, and pancreatic cancer in a cohort of male smokers." Am J Clin Nutr **89**(2): 584-591.

Sultana, T. A., N. Aldabaan and P. W. Sylvester (2021). "Abstract 2572: γ-Tocotrienol inhibition of androgen receptor (AR) expression and activation in triple negative breast cancer (TNBC) MBA-MB-231 and MDA-MB-453 cells is associated with a reduction in proliferation, migration and epithelial-to-mesenchymal transition (EMT)." Cancer Research **81**(13_Supplement): 2572-2572.

Sun, W., Q. Wang, B. Chen, J. Liu, H. Liu and W. Xu (2008). "Gamma-tocotrienol-induced apoptosis in human gastric cancer SGC-7901 cells is associated with a suppression in mitogen-activated protein kinase signalling." Br J Nutr **99**(6): 1247-1254.

Sun, Z., S. Yin, C. Zhao, L. H. Fan and H. Hu (2022). "Involvement of PD-L1-mediated tumor-intrinsic signaling and immune suppression in tumorigenic effect of α-tocopherol." Carcinogenesis **43**(3): 243-253.

Szewczyk, K., A. Chojnacka and M. Górnicka (2021). "Tocopherols and Tocotrienols-Bioactive Dietary Compounds; What Is Certain, What Is Doubt?" Int J Mol Sci **22**(12).

Taguchi, K., N. Fujikawa, M. Komatsu, T. Ishii, M. Unno, T. Akaike, H. Motohashi and M. Yamamoto (2012). "Keap1 degradation by autophagy for the maintenance of redox homeostasis." Proc Natl Acad Sci U S A **109**(34): 13561-13566.

Tan, S., D. Schubert and P. Maher (2001). "Oxytosis: A novel form of programmed cell death." Curr Top Med Chem **1**(6): 497-506.

Tanaka, Y., S. Nakayamada, H. Fujimoto, Y. Okada, H. Umehara, T. Kataoka and Y. Minami (2002). "H-Ras/mitogen-activated protein kinase pathway inhibits integrin-mediated adhesion and induces apoptosis in osteoblasts." J Biol Chem **277**(24): 21446-21452.

Tesfay, L., B. T. Paul, A. Konstorum, Z. Deng, A. O. Cox, J. Lee, C. M. Furdui, P. Hegde, F. M. Torti and S. V. Torti (2019). "Stearoyl-CoA Desaturase 1 Protects Ovarian Cancer Cells from Ferroptotic Cell Death." Cancer Res **79**(20): 5355-5366.

Tewari, R., V. Sharma, N. Koul and E. Sen (2008). "Involvement of miltefosine-mediated ERK activation in glioma cell apoptosis through Fas regulation." J Neurochem **107**(3): 616-627.

Torrence, M. E., M. R. MacArthur, A. M. Hosios, A. J. Valvezan, J. M. Asara, J. R. Mitchell and B. D. Manning (2021). "The mTORC1-mediated activation of ATF4 promotes protein and glutathione synthesis downstream of growth signals." Elife **10**.

Toth, B. and K. Patil (1983). "Enhancing effect of vitamin E on murine intestinal tumorigenesis by 1,2-dimethylhydrazine dihydrochloride." J Natl Cancer Inst **70**(6): 1107-1111.

Troiani, T., S. Napolitano, C. M. Della Corte, G. Martini, E. Martinelli, F. Morgillo and F. Ciardiello (2016). "Therapeutic value of EGFR inhibition in CRC and NSCLC: 15 years of clinical evidence." ESMO Open **1**(5): e000088.

Tsao, H., V. Goel, H. Wu, G. Yang and F. G. Haluska (2004). "Genetic interaction between NRAS and BRAF mutations and PTEN/MMAC1 inactivation in melanoma." J Invest Dermatol **122**(2): 337-341.

Tsimaratou, K., D. Kletsas, N. G. Kastrinakis, P. K. Tsantoulis, K. Evangelou, M. Sideridou, M. Liontos, I. Poulias, M. Venere, M. Salmas, C. Kittas, T. D. Halazonetis and V. G. Gorgoulis (2007). "Evaluation of claspin as a proliferation marker in human cancer and normal tissues." J Pathol **211**(3): 331-339.

Turke, A. B., Y. Song, C. Costa, R. Cook, C. L. Arteaga, J. M. Asara and J. A. Engelman (2012). "MEK inhibition leads to PI3K/AKT activation by relieving a negative feedback on ERBB receptors." Cancer Res **72**(13): 3228-3237.

Uchihara, Y., T. Kidokoro, K. Tago, T. Mashino, H. Tamura and M. Funakoshi-Tago (2018). "A major component of vitamin E, α-tocopherol inhibits the anti-tumor activity of crizotinib against cells transformed by EML4-ALK." Eur J Pharmacol **825**: 1-9.

Uchihara, Y., F. Ueda, K. Tago, Y. Nakazawa, T. Ohe, T. Mashino, S. Yokota, T. Kasahara, H. Tamura and M. Funakoshi-Tago (2017). "Alpha-tocopherol attenuates the anti-tumor activity of crizotinib against cells transformed by NPM-ALK." PLoS One **12**(8): e0183003.

Ulisse, S., B. Cinque, G. Silvano, N. Rucci, L. Biordi, M. G. Cifone and M. D'Armiento (2000). "Erk-dependent cytosolic phospholipase A2 activity is induced by CD95 ligand cross-linking in the mouse derived Sertoli cell line TM4 and is required to trigger apoptosis in CD95 bearing cells." Cell Death Differ **7**(10): 916-924.

Ullah, R., Q. Yin, A. H. Snell and L. Wan (2022). "RAF-MEK-ERK pathway in cancer evolution and treatment." Semin Cancer Biol **85**: 123-154.

Ünal, E. B., F. Uhlitz and N. Blüthgen (2017). "A compendium of ERK targets." FEBS Lett **591**(17): 2607-2615.

Ungurianu, A., A. Zanfirescu, G. Nițulescu and D. Margină (2021). "Vitamin E beyond Its Antioxidant Label." Antioxidants (Basel) **10**(5).

Uprety, D. and A. A. Adjei (2020). "KRAS: From undruggable to a druggable Cancer Target." Cancer Treat Rev **89**: 102070.

Vanella, L., C. Di Giacomo, R. Acquaviva, I. Barbagallo, V. Cardile, D. H. Kim, N. G. Abraham and V. Sorrenti (2013). "Apoptotic markers in a prostate cancer cell line: effect of ellagic acid." Oncol Rep **30**(6): 2804-2810.

Vanhaesebroeck, B. and M. D. Waterfield (1999). "Signaling by distinct classes of phosphoinositide 3-kinases." Exp Cell Res **253**(1): 239-254.

Villanueva, J., Y. Yung, J. L. Walker and R. K. Assoian (2007). "ERK activity and G1 phase progression: identifying dispensable versus essential activities and primary versus secondary targets." Mol Biol Cell **18**(4): 1457-1463.

Villunger, A., E. M. Michalak, L. Coultas, F. Müllauer, G. Böck, M. J. Ausserlechner, J. M. Adams and A. Strasser (2003). "p53- and drug-induced apoptotic responses mediated by BH3-only proteins puma and noxa." Science **302**(5647): 1036-1038.

Wada, S., Y. Naito, Y. Matsushita, M. Nouchi, M. Kawai, E. Minami, W. Aoi, S. Ikeda, A. Higashi and T. Yoshikawa (2017). "δ-Tocotrienol suppresses tumorigenesis by inducing apoptosis and blocking the COX-2/PGE2 pathway that stimulates tumor–stromal interactions in colon cancer." Journal of Functional Foods **35**: 428-435.

Weber, J. D., D. M. Raben, P. J. Phillips and J. J. Baldassare (1997). "Sustained activation of extracellular-signal-regulated kinase 1 (ERK1) is required for the continued expression of cyclin D1 in G1 phase." Biochem J **326 (Pt 1)**(Pt 1): 61-68.

Wennström, S. and J. Downward (1999). "Role of phosphoinositide 3-kinase in activation of ras and mitogen-activated protein kinase by epidermal growth factor." Mol Cell Biol **19**(6): 4279-4288.

Westcott, P. M., K. D. Halliwill, M. D. To, M. Rashid, A. G. Rust, T. M. Keane, R. Delrosario, K. Y. Jen, K. E. Gurley, C. J. Kemp, E. Fredlund, D. A. Quigley, D. J. Adams and A. Balmain (2015). "The mutational landscapes of genetic and chemical models of Kras-driven lung cancer." Nature **517**(7535): 489-492.

Whittaker, J. A. and S. A. Al-Ismail (1984). "Effect of digoxin and vitamin E in preventing cardiac damage caused by doxorubicin in acute myeloid leukaemia." Br Med J (Clin Res Ed) **288**(6413): 283-284.

Will, M., A. C. Qin, W. Toy, Z. Yao, V. Rodrik-Outmezguine, C. Schneider, X. Huang, P. Monian, X. Jiang, E. de Stanchina, J. Baselga, N. Liu, S. Chandarlapaty and N. Rosen (2014). "Rapid induction of apoptosis by PI3K inhibitors is dependent upon their transient inhibition of RAS-ERK signaling." Cancer Discov **4**(3): 334-347.

Willis, S., C. L. Day, M. G. Hinds and D. C. Huang (2003). "The Bcl-2-regulated apoptotic pathway." J Cell Sci **116**(Pt 20): 4053-4056.

Wittinghofer, A., S. M. Franken, A. J. Scheidig, H. Rensland, A. Lautwein, E. F. Pai and R. S. Goody (1993). "Three-dimensional structure and properties of wild-type and mutant H-ras-encoded p21." Ciba Found Symp **176**: 6-21; discussion 21-27.

Woessmann, W., X. Chen and A. Borkhardt (2002). "Ras-mediated activation of ERK by cisplatin induces cell death independently of p53 in osteosarcoma and neuroblastoma cell lines." Cancer Chemother Pharmacol **50**(5): 397-404.

Wolfson, R. L., L. Chantranupong, R. A. Saxton, K. Shen, S. M. Scaria, J. R. Cantor and D. M. Sabatini (2016). "Sestrin2 is a leucine sensor for the mTORC1 pathway." Science **351**(6268): 43-48.

Wu, X., W. Xie, W. Xie, W. Wei and J. Guo (2022). "Beyond controlling cell size: functional analyses of S6K in tumorigenesis." Cell Death Dis **13**(7): 646.

Xu, W., Y. Mi, P. He, S. He and L. Niu (2017). "γ-Tocotrienol Inhibits Proliferation and Induces Apoptosis Via the Mitochondrial Pathway in Human Cervical Cancer HeLa Cells." Molecules **22**(8).

Yagoda, N., M. von Rechenberg, E. Zaganjor, A. J. Bauer, W. S. Yang, D. J. Fridman, A. J. Wolpaw, I. Smukste, J. M. Peltier, J. J. Boniface, R. Smith, S. L. Lessnick, S. Sahasrabudhe and B. R. Stockwell (2007). "RAS-RAF-MEK-dependent oxidative cell death involving voltage-dependent anion channels." Nature **447**(7146): 864-868.

Yang, C., Y. Zhao, S. Im, C. Nakatsu, Y. Jones-Hall and Q. Jiang (2021). "Vitamin E delta-tocotrienol and metabolite 13'-carboxychromanol inhibit colitis-associated colon tumorigenesis and modulate gut microbiota in mice." J Nutr Biochem **89**: 108567.

Yang, H., D. G. Rudge, J. D. Koos, B. Vaidialingam, H. J. Yang and N. P. Pavletich (2013). "mTOR kinase structure, mechanism and regulation." Nature **497**(7448): 217-223.

Yang, W. S., R. SriRamaratnam, M. E. Welsch, K. Shimada, R. Skouta, V. S. Viswanathan, J. H. Cheah, P. A. Clemons, A. F. Shamji, C. B. Clish, L. M. Brown, A. W. Girotti, V. W. Cornish, S. L. Schreiber and B. R. Stockwell (2014). "Regulation of ferroptotic cancer cell death by GPX4." Cell **156**(1-2): 317-331.

Yang, W. S. and B. R. Stockwell (2008). "Synthetic lethal screening identifies compounds activating iron-dependent, nonapoptotic cell death in oncogenic-RAS-harboring cancer cells." Chem Biol **15**(3): 234-245.

Yano, T., Y. Obata, Y. Yano, S. Otani and T. Ichikawa (1994). "Vitamin E acts as a useful chemopreventive agent to reduce spontaneous lung tumorigenesis in mice." Cancer Lett **87**(2): 205-210.

Yano, T., S. Yajima, K. Hagiwara, I. Kumadaki, Y. Yano, S. Otani, M. Uchida and T. Ichikawa (2000). "Vitamin E inhibits cell proliferation and the activation of extracellular signal-regulated kinase during the promotion phase of lung tumorigenesis irrespective of antioxidative effect." Carcinogenesis **21**(11): 2129-2133.

Yano, Y., T. Yano, M. Uchida, A. Murakami, M. Ogita, T. Ichikawa, S. Otani and K. Hagiwara (1997). "The inhibitory effect of vitamin E on pulmonary polyamine biosynthesis, cell proliferation and carcinogenesis in mice." Biochim Biophys Acta **1356**(1): 35-42.

Yao, W., Y. T. Oh, J. Deng, P. Yue, L. Deng, H. Huang, W. Zhou and S. Y. Sun (2016). "Expression of Death Receptor 4 Is Positively Regulated by MEK/ERK/AP-1 Signaling and Suppressed upon MEK Inhibition." J Biol Chem **291**(41): 21694-21702.

Yao, X., Y. Zhang, J. Hao, H. Q. Duan, C. X. Zhao, C. Sun, B. Li, B. Y. Fan, X. Wang, W. X. Li, X. H. Fu, Y. Hu, C. Liu, X. H. Kong and S. Q. Feng (2019). "Deferoxamine promotes recovery of traumatic spinal cord injury by inhibiting ferroptosis." Neural Regen Res **14**(3): 532-541.

Yap, W. N., P. N. Chang, H. Y. Han, D. T. Lee, M. T. Ling, Y. C. Wong and Y. L. Yap (2008). "Gamma-tocotrienol suppresses prostate cancer cell proliferation and invasion through multiple-signalling pathways." Br J Cancer **99**(11): 1832-1841.

Yart, A., M. Laffargue, P. Mayeux, S. Chretien, C. Peres, N. Tonks, S. Roche, B. Payrastre, H. Chap and P. Raynal (2001). "A critical role for phosphoinositide 3-kinase upstream of Gab1 and SHP2 in the activation of ras and mitogen-activated protein kinases by epidermal growth factor." J Biol Chem **276**(12): 8856-8864.

Ye, Q., W. Cai, Y. Zheng, B. M. Evers and Q. B. She (2014). "ERK and AKT signaling cooperate to translationally regulate survivin expression for metastatic progression of colorectal cancer." Oncogene **33**(14): 1828-1839.

Yi, J., J. Zhu, J. Wu, C. B. Thompson and X. Jiang (2020). "Oncogenic activation of PI3K-AKT-mTOR signaling suppresses ferroptosis via SREBP-mediated lipogenesis." Proc Natl Acad Sci U S A **117**(49): 31189-31197.

You, H., M. Pellegrini, K. Tsuchihara, K. Yamamoto, G. Hacker, M. Erlacher, A. Villunger and T. W. Mak (2006). "FOXO3a-dependent regulation of Puma in response to cytokine/growth factor withdrawal." J Exp Med **203**(7): 1657-1663.

Yu, J., Y. Zhang, J. McIlroy, T. Rordorf-Nikolic, G. A. Orr and J. M. Backer (1998). "Regulation of the p85/p110 phosphatidylinositol 3'-kinase: stabilization and inhibition of the p110alpha catalytic subunit by the p85 regulatory subunit." Mol Cell Biol **18**(3): 1379-1387.

Yuan, X., Y. Duan, Y. Xiao, K. Sun, Y. Qi, Y. Zhang, Z. Ahmed, D. Moiani, J. Yao, H. Li, L. Zhang, A. E. Yuzhalin, P. Li, C. Zhang, A. Badu-Nkansah, Y. Saito, X. Liu, W. L. Kuo, H. Ying, S. C. Sun, J. C. Chang, J. A. Tainer and D. Yu (2022). "Vitamin E Enhances Cancer Immunotherapy by Reinvigorating Dendritic Cells via Targeting Checkpoint SHP1." Cancer Discov **12**(7): 1742-1759.

Zahedi, B., H. J. Goo, N. Beaulieu, G. Tazmini, R. J. Kay and R. B. Cornell (2011). "Phosphoinositide 3-kinase regulates plasma membrane targeting of the Ras-specific exchange factor RasGRP1." J Biol Chem **286**(14): 12712-12723.

Zarogoulidis, P., A. Cheva, K. Zarampouka, H. Huang, C. Li, Y. Huang, N. Katsikogiannis and K. Zarogoulidis (2013). "Tocopherols and tocotrienols as anticancer treatment for lung cancer: future nutrition." J Thorac Dis **5**(3): 349-352.

Zha, J., H. Harada, E. Yang, J. Jockel and S. J. Korsmeyer (1996). "Serine phosphorylation of death agonist BAD in response to survival factor results in binding to 14-3-3 not BCL-X(L)." Cell **87**(4): 619-628.

Zhang, Y., R. V. Swanda, L. Nie, X. Liu, C. Wang, H. Lee, G. Lei, C. Mao, P. Koppula, W. Cheng, J. Zhang, Z. Xiao, L. Zhuang, B. Fang, J. Chen, S. B. Qian and B. Gan (2021). "mTORC1 couples cyst(e)ine availability with GPX4 protein synthesis and ferroptosis regulation." Nat Commun **12**(1): 1589.

Zhang, Y. H., K. Ma, J. R. Liu, H. X. Wang, W. X. Tian, Y. H. Tu and W. G. Sun (2018). "γ-tocotrienol inhibits the invasion and migration of human gastric cancer cells through downregulation of cyclooxygenase-2 expression." Oncol Rep **40**(2): 999-1007.

Zhu, G., L. Pei, H. Xia, Q. Tang and F. Bi (2021). "Role of oncogenic KRAS in the prognosis, diagnosis and treatment of colorectal cancer." Mol Cancer **20**(1): 143.

Zhu, X. F., W. Li, J. Y. Ma, N. Shao, Y. J. Zhang, R. M. Liu, W. B. Wu, Y. Lin and S. M. Wang (2015). "Knockdown of heme oxygenase-1 promotes apoptosis and autophagy and enhances the cytotoxicity of doxorubicin in breast cancer cells." Oncol Lett **10**(5): 2974-2980.

Zilka, O., R. Shah, B. Li, J. P. Friedmann Angeli, M. Griesser, M. Conrad and D. A. Pratt (2017). "On the Mechanism of Cytoprotection by Ferrostatin-1 and Liproxstatin-1 and the Role of Lipid Peroxidation in Ferroptotic Cell Death." ACS Cent Sci **3**(3): 232-243.

Zimmermann, S. and K. Moelling (1999). "Phosphorylation and regulation of Raf by Akt (protein kinase B)." Science **286**(5445): 1741-1744.

Zingg, J. M. (2015). "Vitamin E: A Role in Signal Transduction." Annu Rev Nutr **35**: 135-173.

Zuberi, M., I. Khan and J. P. O'Bryan (2020). "Inhibition of RAS: proven and potential vulnerabilities." Biochem Soc Trans **48**(5): 1831-1841.